

https://dspace.org/

Development of mixed matrix membrane for desulfurization of sulfur rich petroleum stream

Burla, Swathi

2022

https://hdl.handle.net/10539/34379

Downloaded from a DSpace repository. https://dspace.org/



DEVELOPMENT OF MIXED MATRIX MEMBRANE FOR DESULFURIZATION OF SULFUR RICH PETROLEUM STREAM

SWATHI BURLA (1195116)

The Faculty of Engineering and the Built Environment, University of the Witwatersrand, Johannesburg. In fulfilment of the requirements for the degree of Doctor of Philosophy

Supervisors: Prof. Diakanua Bavon Nkazi and Dr. Manoko Maubane-Nkadimeng

PhD Thesis, December, 2021

DECLARATION

I declare that this research thesis, "*Development Of Mixed Matrix Membrane For Desulfurization Of Sulfur Rich Petroleum Stream",* is my own, unaided work and that each source of information used has been acknowledged by means of a complete refence in each chapter. This thesis is being submitted for the degree of Doctor of Philosophy in the University of Witwatersrand, Johannesburg. It has not been submitted before for any degree or any other research work or examination in any University.



_____

(Signature of PhD candidate)

_____28_____ day of_____December_____2021

DEDICATION

This research work is dedicated to:

My loving family for supporting and encouraging me throughout this journey.

My family is my strength.

ACKNOWLEDGMENT

To begin, I want to express my gratitude to my supervisor, Prof. Diakunua Bavon Nkazi, for his dedication, encouragement, and assistance in my research as well as obtaining financial support for the project. Without his help and encouragement, the project would not have been completed. I'd like to express my gratitude to the National Research Foundation (NRF) and the University of Witwatersrand for their financial support in the form of NRF Scholarship and Post Graduate Merit Awards (PMA).

I'd like to also express my gratitude to Dr. Manoko Maubane-Nkadimeng of the School of Chemistry for co-supervising and sharing her expertise and assisting me with nano carbon material synthesis. I am grateful to the School of Chemical and Metallurgical Engineering (CHMT) for providing me with the opportunity to complete the project there. I also appreciate the assistance and support provided by the School of Chemistry and the Microscopy and Microanalysis Unit (MMU) and their staff in providing laboratory and analytical facilities.

This research was conducted successfully with the support of Mr. Motlatsi Phali (CHMT), Mrs. Petra Dinham (CHMT), and Prof. Alexander Ziegler (MMU) for assistance in analysis and my fellow postgraduate students for their encouragement.

ABSTRACT

The presented study focused on the methods of synthesizing the hexagonal boron nitride (h-BN), carbon dots (C-dots) and carbon dot doped boron nitride (CBN) nano materials for applications in dibenzothiophene (DBT) desulfurization. The synthesized materials were characterized using different analytical techniques such as transmission electron microscopy (TEM), scanning electron microscope (SEM), X-ray diffraction (XRD) and fourier transform infra-red (FTIR) to confirm the synthesis of the desired products. H-BN was synthesized using chemical vapor deposition (CVD) and heat treatment furnace (HTF) methods, with CVD producing better h-BN product at 900 ^{o}C calcination temperature and HTF products forming with high impurities. FTIR analysis of h-BN CVD (900 ^{o}C) showed two characteristic peaks at 1369 cm^{-1} and 787 cm^{-1} confirming the formation of h-BN. An extra peak at 3250 cm^{-1} of hydroxyl (-OH) vibration, indicates the presence of small amount of -OH on h-BN on all the products. The -OH peak intensity was decreased with increased calcination temperature, as shown from the FTIR spectra of different h-BN products calcined at 3 different temperatures. The TEM analysis observed several stacked parallel line-like structures (layers) with multiple layered disordered structures of h-BN flakes. The SEM image displayed an unevenly distributed grained powder of h-BN microstructure. XRD peaks of h-BN synthesized via CVD method reveals a strong peak of the crystallographic (002) plane at $2\theta = 27.17$ ° with some broadening, indicating low crystalline nature of h-BN. The C-dots were successfully synthesized using hydrothermal carbonization of chitosan raw material in an autoclave. The existence of various functional groups in C-dots was confirmed by the FTIR spectroscopy. TEM images clearly showed a nearly spherical shaped C-dots with diameter of 5-10 nm. XRD analysis showed a broad diffraction peak at $2\theta = 21.07$ ° indicating the presence of amorphous carbon.

The synthesis of novel CBN material was successfully carried out by adapting a method from the literature. The FTIR analysis shows that the h-BN was not modified by C-dot addition. TEM image of CBN confirms the doping of nano sized C-dots into the h-BN lateral layers. The SEM images reveal porous microstructure of the CBN nanomaterial indicating the doping of C-dots induced some structural defects into the h-BN that resulted in reduction of the crystalline nature of CBN. XRD analysis of CBN revealed a slight shift in main peak as a result of amorphous C-dot doping on h-BN.

Mixed matrix membrane (MMM) membranes based on polyphenylsulfone (PPSU) embedded with the synthesized h-BN and CBN were developed and analysed for the desulfurization of DBT-hexane model fuel. The FTIR analysis of the membranes revealed that there was no change in the PPSU functionalities except for the additional peak at 3233 cm^{-1} for PPSU-CBN membrane. This indicates the presence of -OH group which might result in the interaction between CBN and PPSU of the MMM membranes. The SEM images of both pristine PPSU and PPSU MMM membranes revealed the porous nature of the developed membranes. The PPSU membrane showed less pores compared to the MMMs. The adsorption studies at varying parameters show that PPSU-CBN membranes were performing better than the PPSU-h-BN membranes. The addition of C-dots is believed to have increased the adsorption sites in the CBN during synthesis which enhanced the adsorption of DBT on membranes. The temperature variation had more influence on the adsorption capacity of the membranes which can be observed from the adsorption isotherm studies. The kinetic models of the adsorption are studied for the PPSU-CBN membrane adsorption system. The models show that the diffusion of adsorbate into the pore of the adsorbent and the interaction of adsorbate-adsorbent are favoured at room temperature. The results indicate a multi mechanism occurring at 309.15 K where the reaction rate was considered as a controlling factor. Based on the R^2 values, it can be concluded that the removal of sulfur using a polymeric membrane embedded with CBN involved various

mechanisms and the diffusion film models confirmed that the adsorption was controlled by the membrane-pore diffusion mechanism.

TABLE OF CONTENTS

DECLARATION i

DEDICATION ii

ACKNOWLEDGMENT iii

ABSTRACT iv

TABLE OF CONTENTS vii

LIST OF FIGURES xiii

LIST OF TABLES xx

NOMENCLATURE xxi

1. CHAPTER ONE: INTRODUCTION 1

1.1 Introduction 1

1.2 Research Background and Motivation 2

1.3 Problem Statement 4

1.4 Research Aim and Objectives 6

1.5 Thesis Outline 7

1.6 Conclusion 8

1.7 References 9

2. CHAPTER TWO: LITERATURE REVIEW 12

2.1 Introduction 12

2.2 The State of Oil Sector, Desulfurization and Emission Policies across the Globe 15

2.2.1 World Oil Reserves 15

2.2.2 World Oil Demand 18
2.2.3 Crude Oil Refinery Process 22
2.2.4 Global Emission Standards 28
2.2.5 SOx Regulations and Policies 33
2.2.6 Africa's stand towards Low Sulphur Fuels 41
2.3 Desulfurization of Crude Oil Products 45
2.4 Desulfurization Techniques 46
2.4.1 Conventional Desulfurization Techniques 46
2.4.1.1 Hydrodesulfurization (HDS) 46
2.4.2 Alternative/Non-conventional Desulfurization Techniques 49
2.4.2.1 Oxidative Desulfurization 49
2.4.2.2 Extractive Desulfurization 51
2.4.2.3 Biodesulfurization 52
2.4.2.4 Adsorptive Desulfurization 54
2.5 Membrane technology 56
2.5.1 Membrane technology for desulfurization process 57
2.5.2 Benefits of using mixed matrix membrane for desulfurization techniques 58
2.5.3 Process description and requirements for membrane desulfurization 59
2.5.3.1 Pervaporation (PV) 59
2.5.3.2 Pervaporation process 61
2.5.3.3 Adsorption 62
2.5.4 Adsorption Kinetics and Adsorption Isotherms 65
2.5.4.1 Adsorption capacity 65
2.5.4.2 Adsorption kinetics 66
2.5.4.3 Equilibrium of adsorption 67

2.5.4.4 Activation energy 70
2.5.4.5 Thermodynamic parameters 71
2.5.5 Properties of Membranes 72
2.5.5.1 Morphology 72
2.5.5.2 Interfacial compatibility 73
2.5.5.3 Interfacial voids 74
2.5.5.4 Crosslinking 76
2.5.5.5 Thermal stability 77
2.5.5.6 Mechanical properties of MMMs adsorbents 77
2.5.5.7 Filler content 78
2.5.6 Chemistry of the sulfur removal process using Membranes/Mixed matrix membrane 79
2.5.6.1 Facilitated Transport Carriers 79
2.5.6.2 π type complex 81
2.5.7 Choice of embedded and polymeric materials 82
2.5.7.1 Porous materials 82
2.6 Boron Nitride 83
2.6.1 BN Synthesis 84
2.6.2 BN in desulfurization 86
2.6.3 BN Structure 87
2.6.4 BN Allotropes 88
2.6.5 h-BN functionalization 89
2.7 Carbon dots (C-dots) 89
2.8 Conclusion 92
2.9 References 93

3. CHAPTER THREE: DEVELOPMENT OF BORON NITRIDE AND CARBON DOT SYSTEM 121

3.1 Introduction 121

3.2 Graphical representation of Methodology 121

3.2.1 Overview of h-BN synthesis 122

3.2.2 Overview of C-dot synthesis 123

3.2.3 Overview of C-dot doped on h-BN 124

3.3 Methods 125

3.3.1 Synthesis of Boron Nitride 125

3.3.2 Carbon Dot (C-dots) 130

3.3.3 Carbon dot doped on h-Boron nitride (CBN) 131

3.4 Analytical Techniques 132

3.5 Results and Discussion 134

3.5.1 Hexagonal Boron Nitride 134

3.5.2 Carbon Dot 144

3.5.3 Carbon dot doped on Boron nitride (CBN) 148

3.6 Conclusion 152

3.7 References 153

4. CHAPTER FOUR: DEVELOPMENT OF PPSU MEMBRANES EMBEDDED WITH H-BN AND CBN 157

4.1 Introduction 158

4.2 Methods 158

4.2.1 PPSU membrane preparation 158

4.2.2 Synthesis of PPSU Mixed Matrix Membranes (MMM) embedded with h-BN and CBN nanofillers 159

4.2.3 Overview of the membrane development....160
4.3 Membrane desulfurization process....161
4.4 Analytical Techniques....161
4.5 Results and Discussions....161
4.6 Conclusion....170
4.7 References....171
5. CHAPTER FIVE: DESULPHURISATION PROCESS OF MIXED MATRIX MEMBRANES....172
5.1 Introduction....172
5.2 Methods....172
5.3 Desulfurization process....174
5.3.1 Effect of contact time....174
5.3.2 Effect of amount of adsorbent....175
5.3.3 Effect of temperature....175
5.4 Analytical Techniques....175
5.5 Results and Discussion....176
5.5.1 Adsorption capacity behaviour....186
5.5.2 Effect of temperature on the adsorption capacity of PPSU-CBN membrane 190
5.6 Conclusion....191
5.7 References....193
6. CHAPTER SIX: ADSORPTION BEHAVIOUR AND KINETIC MODELS....196
6.1 Introduction....196
6.2 Adsorption isotherms for single component equilibria....196

6.2.1 Linear adsorption isotherm equation 196
6.2.2 Freundlich adsorption equation 198
6.2.3 Langmuir adsorption Equation 199
6.2.4 Temkin Adsorption Equation 200
6.2.5 Multi-isotherms behaviour 202
6.3 Adsorption Kinetics 203
6.3.1 Adsorption Reaction Models 204
6.3.1.1 Pseudo First Order Reaction model 204
6.3.1.2 Pseudo Second Order Reaction model 205
6.3.1.3 Elovich's equation 207
6.3.1.4 Langmuir-Hinshelwood Kinetics 208
6.3.2 Adsorption Diffusion Models 209
6.3.2.1 Linear driving force diffusion model 209
6.3.2.2 Film diffusion model 211
6.3.2.3 Spahn and Schlunder film diffusion model 212
6.3.2.4 Weber-Morris model 213
6.4 Conclusion 215
6.5 References 216
7. CHAPTER SEVEN: CONCLUSION AND RECOMMENDATIONS 217
7.1 Conclusion 217
7.2 Recommendation 219
Appendix A: Development of hexagonal boron nitride (h-BN) and carbon dot system 220
Appendix B: Development of PPSU MMM 225
Appendix C: Adsorption studies 229

LIST OF FIGURES

Figure 1.1 World Energy Demand....2

Figure 2.1 World Energy Consumption 13

Figure 2.2 World Oil Reserves 16

Figure 2.3 World Energy Demand 2021 - 2025 18

Figure 2.4 World Oil Demand by Region 2021 - 2025 19

Figure 2.5 World Oil Demand by Road Transportation 2021 - 2025....20

Figure 2.6 Passenger Cars in the World 2021 - 2025 21

Figure 2.7 Commercial Cars in the World 2021 - 2025 21

Figure 2.8 Basic Refinery Operations....24

Figure 2.9 Crude oil sulfur compounds (R=alkyl)....26

Figure 2.10 Complex Refinery Operations....27

Figure 2.11 Global SO_2 in Atmosphere 29

Figure 2.12 Top Countries emitting SO_2 32

Figure 2.13 Sources of SO_2 emissions....33

Figure 2.14 Maximum Sulfur Limits in Gasoline in 2021....37

Figure 2.15 Maximum Sulfur Limits in On-Road Diesel in 2021....37

Figure 2.16 Maximum Sulfur Limits in Gasoline in 2025.....39

Figure 2.17 Maximum Sulfur Limits in On-Road Diesel in 2025.....39

Figure 2.18 Worldwide Emission Standards 40

Figure 2.19 Fuel Imports and Exports in Africa.....42

Figure 2.20 Regional Map within Africa.....43

Figure 2.21 Reactivity of various sulfur compounds in hydrodesulfurization versus their ring sizes and positions of alky substitutions on the ring.....48

Figure 2.22 (a) Universal Oil Products (UOP)/Eni Oxidative Desulfurization Process (Ron et al., 2004); (b) Oxidation of DBT to corresponding Sulfone.....50

Figure 2.23 General process flow of extractive desulfurization. 52

Figure 2.24 Biodesulfurization Process Operations.....53

Figure 2.25 Simplified adsorptive desulfurization flow process 55

Figure 2.26 FESEM images of cross-sections of raw PI and zeolites/PI MMMs adsorbents: (1) 0 wt.%, (2) 18 wt.%, (3) 40 wt.%, and (4) 50 wt.% 73

Figure 2.27 Image of various structures at the polymer/filler interface region 74

Figure 2.28 Facilitated transport of Thiophnic compounds through Pebax MMM.....80

Figure 2.29 Images shows C-dot core and possible functionalities on C-dots 90

Figure 3.1 The flow diagram of h-BN synthesis and its characterization 122

Figure 3.2 The flow diagram of C-dot synthesis and its characterization 123

Figure 3.3 The flow diagram of C-dot doped on h-BN and its characterization 124

Figure 3.4 Methods used for the development of adsorptive materials.....125

Figure 3.5 Water bath set up for precursor preparation 128

Figure 3.6 Horizontal CVD method for h-BN synthesis 130

Figure 3.7 Hydrothermal synthesis of Carbon dots 131

Figure 3.8 (a) Precursor formed from Boric acid and urea reaction mixture, (b) h-BN product after heating in a CVD reactor, and (c) h-BN from HTF.....134

Figure 3.9 (a) FTIR spectra of h-BN from the precursors prepared at (a) 120 N_2 flowrate, (b) 60 N_2 flowrate and (c) 90 N_2 flowrate 137

Figure 3.10 FTIR spectra of h-BN synthesized using CVD method at different temperatures 138

Figure 3.11 The FTIR spectra of precursor formed from urea, boric acid before heat treatment and final h-BN product from CVD and HTF methods heated at 900 ^oC.....139

Figure 3.12 TEM images of h-BN CVD (900 ^oC) (a) showing stacked layer like structures, and (b) h-BN with multiple crippled layers.....141

Figure 3.13 SEM image showing h-BN aggregates from CVD (900 ^oC).....142

Figure 3.14 Image showing XRD peaks of precursor, synthesized h-BN by CVD (900 ^oC) method and HTF (900 ^oC) method.....143

Figure 3.15 TEM images (a) C-dots (200nm) and (b) C-dots (100nm).....145

Figure 3.16 XRD spectra of C-dots 146

Figure 3.17 FTIR of synthesized C-dots.....147

Figure 3.18 TEM image of C-dots doped onto h-BN.....148

Figure 3.19 SEM images of (a) CBN porous microstructure, and (b) Porous bulk solids and some flakes of hexagonal layers.....150

Figure 3.20 Comparison of FTIR spectra of h-BN CVD (900^{o}C) and CBN.....150

Figure 3.21 XRD image of CBN and h-BN CVD.....151

Figure 4.1 Development ofPPSU MMM with CBN nanoparticles.....160

Figure 4.2 FTIR spectra of PPSU, PPSU-CBN and PPSU-h-BN membranes.....162

Figure 4.3 SEM images of (a) PPSU membrane with surface layer and inner pores (b) PPSU-CBN (0.2wt.%) membrane, (c) PPSU-h-BN (0.2wt.%) membrane, (d), PPSU-CBN (0.4wt.%) membrane and (e) PPSU-h-BN (0.4 wt.%) membrane.....165

Figure 4.4 (a) PPSU membrane surface (b) cross section of PPSU membrnae, (c) cross section of PPSU-CBN (1.2 wt.%) membrane, (d), PPSU-CBN (1.2 wt.%) membrane surface showing surface layer thickness and (e) porous network channels of PPSU-CBN (0.8 wt.%) membrane 168

Figure 5.1 Batch adsorption process set-up for sulfur removal using MMM embedded with h-BN and CBN.....174

Figure 5.2 Desulfurisation behaviour with time.....176

Figure 5.3 Desulfurisation behaviour with adsorbent amount.....178

Figure 5.4 Desulfurisation behaviour with temperature.....179

Figure 5.5 Graphs showing adsorption behaviour for varying contact time at (a) rapid phase and (b) slow phase 182

Figure 5.6 Graphs showing adsorption behaviour for varying adsorbent amount at (a) rapid phase and (b) slow phase 183

Figure 5.7 Graphs showing adsorption behaviour for varying temperature at (a) rapid phase and (b) slow phase 184

Figure 5.8 Linear adsorption isotherm (for effect of varying contact time) of PPSU-h-BN and PPSU-CBN membranes 186

Figure 5.9 Adsorption isotherms.....187

Figure 5.10 Linear adsorption isotherms of PPSU-h-BN and PPSU-CBN membranes for varying (a) temperature and (b) amount of adsorbents.....189

Figure 5.11 Effect of temperature on PPSU-CBN membrane adsorption capacity.....191

Figure 6.1 Linear adsorption isotherm.....197

Figure 6.2 Freundlich adsorption isotherm.....199

Figure 6.3 Langmuir adsorption isotherm 200

Figure 6.4 Temkin adsorption isotherm.....202

Figure 6.5 Pseudo First Order reaction.....205

Figure 6.6 Pseudo Second Order reaction.....207

Figure 6.7 Elovich's kinetic model.....208

Figure 6.8 Langmuir-Hinshelwood Kinetic model 209

Figure 6.9 Linear driving force diffusion model 210

Figure 6.10 Linear driving force diffusion behaviour (a) at 309.15K and (b) 299.15K 211

Figure 6.11 Film diffusion model 212

Figure 6.12 Spahn and Schlunder film diffusion model 213

Figure 6.13 Weber-Morris model 214

Figure A.1 XRD of h-BN synthesized by HTF method calcined at 700 ^{o}C 220

Figure A.2 XRD of h-BN synthesized by HTF method calcined at 800 ^{o}C 220

Figure A.3 XRD of h-BN synthesized by CVD method calcined at 700 ^{o}C 221

Figure A.4 XRD of h-BN synthesized by CVD calcined at 800 ^{o}C 221

Figure A.5 TEM image of h-BN calcined by HTF (800 ^{o}C) 222

Figure A.6 TEM image of h-BN calcined by CVD (800 ^{o}C) 222

Figure A.7 TEM image of h-BN calcined by CVD (900 ^{o}C) 223

Figure A.8 TEM image of C-dots 223

Figure A.9 TEM image of CBN 224

Figure B.1 SEM image of PPSU membrane 225

Figure B.2 SEM image of PPSU-h-BN (0.6wt.%) membrane 225

Figure B.3 SEM image of PPSU-CBN (0.6wt.%) membrane 226

Figure B.4 SEM image of PPSU-h-BN (0.8wt.%) membrane 226

Figure B.5 SEM image of PPSU-CBN (0.8wt.%) membrane 227

Figure B.6 SEM image of CBN material.....227

Figure B.7 FTIR spectra of PPSU, PPSU-h-BN and PPSU-CBN membranes 228

LIST OF TABLES

Table 2.1 Difference between Physical and Chemical Adsorption (Karge and Weitkamp, 2008) 63

Table 2.2 r-values and their relative isotherm type.....69

Table 5.1 R^2 values of h-BN and CBN systems at different parameters at slow phase.....185

Table 6.1 Temkin adsorption constants 201

Table 6.2 Coefficient of determination (R^2) 203

Table 6.3 Pseudo second order reaction constants.....206

Table C.1 Sulfur removal capacity of PPSU-h-BN and PPSU-CBN membranes with varying time 229

Table C.2 Sulfur removal capacity of PPSU-h-BN and PPSU-CBN membranes with varying amount od adsorbent material in PPSU 229

Table C.3 Sulfur removal capacity of PPSU-h-BN and PPSU-CBN membranes with varying temperature 230

NOMENCLATURE

AgNP	Ag Nanoparticles
Au/Pd	Gold Palladium
BDS	Biodesulfurization
BN	Boron Nitride
BNNFs	Boron Nitride Nanofibers
BNNSs	Boron Nitride Nanosheets
BNNTs	Boron Nitride Nanotubes
BP	British Petroleum
BT	Benzothiophene
CBN	Carbon Dot Doped Boron Nitride
CCAC	Climate And Clean Air Coalition
C-dots	Carbon Dots
CH_4	Methane
CNT	Carbon Nanotubes
CO	Carbon Monoxide
CO_2	Carbon Dioxide
COVID	Coronavirus Disease
CREA	Centre for Research on Energy and Clean Air
CVD	Chemical Vapor Deposition
DBT	Dibenzothiophene
EAC	East African Community
ECOWAS	Economic Community of West African States
EGCS	Exhaust Gas Cleaning System

FESEM	Field-Emission Scanning Electron Microscope
FGD	Flue Gas Desulphurisation System
FTIR	Fourier Transform Infra-Red
GDP	Gross Domestic Product
GHG	Green House Gases
GNS	Graphene Nanosheets
h-BN	Hexagonal Boron Nitride
HDDI	Heavy Duty Diesel Initiative
HDS	Hydrodesulfurization
H_2S	Hydrogen Sulfide
HPLC	High Performance Liquid Chromatography
HSAB	Hard And Soft Acids and Bases
HSFO	High-Sulfur Fuel Oil
HTF	Heat Treatment Furnace
IEA	International Energy Association
IMO	International Maritime Organisation
$J\ mol^{-1}\ K^{-1}$	Joule Per Mole Kelvin
K	Kelvin
KCN	Potassium Cyanide
$kg\ m^{-3}$	Kilogram Per Cubic Metre
LNG	Liquefied Natural Gas
LPG	Liquified Petroleum Gas
mboe/d	Thousand Barrels of Oil Equivalent Per Day
mb/d	Thousand Barrels Per Day

MEROX	Mercaptan Oxidation
mg/km	Milligram/Kilogram
MMM	Mixed Matrix Membrane
MOF	Metal Organic Framework
MPa	Megapascal
MoS_2	Molybdenum Disulfide
$MMtCO_2e$	Million Metric Tons of CO_2 Equivalent
NASA	National Aeronautics and Space Administration
NDC	Nationally Determined Contribution
NH_3	Ammonia
NH_4HS	Ammonium Bi-sulfide
NMP	N-Methyl-2-Pyrrolidone
N_2O	Nitrous Oxide
NOx	Nitrogen Oxides
OECD	Organisation For Economic Co-Operation and Development
OPEC	Organization of the Petroleum Exporting Countries
PA	Polyamide
PDA	Polydopamine
PDMS	Polydimethylsiloxane
Pebax	Poly- Ether-Block-Amide
PES	Polyethersulfone
PI	Polyimide
$PM_{2.5}$	Particulate Matter Less Than 2.5 Micrometres
ppm	Parts Per Million

PPSU	Polyphenylsulfone
SADC	Southern African Development Community
SALEDS	South African Low Emission Development Strategy
SBA	Santa Barbara Amorphous
SECA	Sulfur Emission Control Areas
SEM	Scanning Electron Microscope
SO_2	Sulfur Dioxide
SO_3	Sulfur Trioxide
SO_x	Sulfur Dioxides
TEM	Transmission Electron Microscopy
ULSD	Ultra-Low Sulfur Diesel
VLSFO	Very-Low Sulfur Fuel Oil
VMT	Vehicle Miles Travelled
WHO	World Health Organization
XRD	X-Ray Diffraction

1. CHAPTER ONE: INTRODUCTION

1.1 Introduction

Sulfur and its compounds are naturally present in crude oil and shale gas (Samokhvalov and Tatarchuk, 2010). The removal of sulfur is significant at various stages of petroleum refining due to its toxicity; corrosive nature and; its presence in transportation fuels can result in SO_2 emissions leading to several environmental problems (Martinie et al., 2010). According to the latest environmental regulations, the sulfur content in the transportation fuel must be reduced to ultra-low levels of 30-50 ppm for gasoline and diesel (Babich and Moulijin, 2003; Samokhvalov and Tatarchuk, 2010). The implication of these regulations produces cleaner fuels besides producing large quantities of petroleum streams concentrated with sulfur compounds. The concentrated sulfur streams also contain a mixture of other organic and inorganic compounds which are extremely alkaline, odiferous and toxic because of chemical treatments to remove sulfur (Martinie et al., 2010).

Such streams cannot be released into the sea or land directly due to the possibility of contamination and thus require significant processing that allows a safe disposal and recovery of possible chemical compounds. The current regulations on industries for environmental protection emphasize on upgrading technologies to minimize the sulfur content from fuels that are toxic to environment. As a result, ultra-deep desulfurization of liquid fuels is important, and this has attracted a lot of attention in recent years. In order to meet the much anticipated zero sulfur emission standards in the future, significant attempts have been made to develop innovative sulfur reduction methods and also new materials for high efficiency desulfurization of hydrocarbon fuels.

1.2 Research Background and Motivation

South Africa invests huge amounts in importing crude oil along with other industrial minerals including sulfur due to the rapid growth of product demand. About 80% of the world's energy, as shown in Figure 1.1 based on latest amounts, is produced from fossil fuels, over half of which comes from petroleum (Srivastava, 2012). Several processes which include petroleum refining and other material synthesis require expensive methods to efficiently obtain high yields of valuable products. This dependency of energy supply on hydrocarbons (crude oil products) due to growing demand has become a major concern for the country in terms of affordability (imports) and climate change. As per Energy Master Plan of Liquid Fuels, the country strongly promotes energy efficiency in all energy consuming sectors for sustainable development to reduce emissions and meet product demand (Bergh, 2012; DME- RSA, 2008).

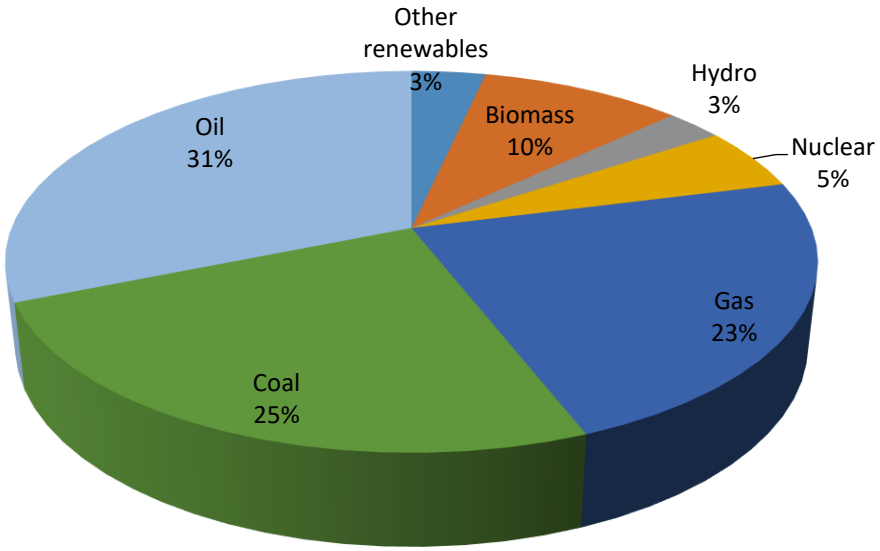


Figure 1.1 World Energy Demand (IEA, 2021)

In light of the above concerns, the South African government has devised a sustainable development strategy aimed at encouraging energy conservation, reducing the negative effect of energy use on the environment, and lowering economic costs, all of which can contribute to the country's social, economic, and environmental sustainability. Therefore, government encourages the academia and industries to not only develop new technologies and methodologies that are energy efficient and environmentally beneficial but also provides an opportunity to recover possible chemical compounds that can be used in appropriate applications.

Several physical and chemical techniques such as hydrodesulfurization (HDS); amine gas treatment; catalytic and non-catalytic adsorption; conversions such as oxidation, alkylation; and membrane separation are employed for desulfurization of crude oil products which in turn are highly expensive and involve complex technical operation (Kumari and Sengupta, 2021). While several such methods for sulfur removal in industries have been successfully introduced, developing new devices or optimizing existing technologies will increase product output and minimize material consumption during oil refining. (Lin et al., 2010). Membrane technology is one such method that can be considered efficient in removal of sulfur compounds from petrochemical industrial streams. As a result, the production of membranes for desulfurization has the ability to save energy because the separation process occurs without phase transfer, and it can deliver quick, with low capital and operating costs, and is simple to operate when compared to traditional techniques. The advantages of such technology also include easier scale up and high selectivity (Asghar et al., 2021).

1.3 Problem Statement

Sulfur removal from petroleum products has always been essential, and it continues to be so today due to environmental concerns (Martinie et al., 2010). Increasing pollution has resulted in continuing worldwide effort to impose strict regulations on petroleum industries to adhere to maintaining ultra-low sulfur levels in the products to significantly reduce sulfur toxicity in environment (Gawande and Kaware, 2014). The combustion of fuel by automobile engines results in SOx emission causing major air pollution. As a result, to lessen the detrimental health and environmental effects of automobile exhaust emissions, the sulfur content of motor fuels must be reduced (Babich and Moulijin, 2003).

There are many physical and chemical separation techniques as well as the more recent biological separation techniques available in the market and in the literature for sulfur removal from the fuel. As desulfurization technology efficiency becomes a critical factor, only a few are considered successful since most of these methods are inefficient at the industrial level. Conventional methods such as hydrodesulfurization have been widely used commercially for sulfur removal. However, the products obtained suffer from loss of octane number and the method is highly expensive (Kong et al., 2007). Other concerns requiring attention include capital-operation cost, low feed flexibility, short process cycle, technical complexity and overall refiner value (Ito and Van Veen, 2006). As a result, it is important to improve the current desulfurization process in order to increase sulfur removal efficiency while also reducing costs and reusing waste to create useful goods (Lin et al., 2010). This research on membrane separation can possibly address the issues of sulfur removal from sulfur rich petroleum streams. Use of this membrane technology is attractive as the material is inexpensive, does not require pre-treatment techniques, and has longevity and is simple in operation. Therefore, the scope of

the project will be on the membrane design and optimization to maximize selectivity for sulfur species.

Polydimethylsiloxane (PDMS) is a polymer and because of its low cost, exceptional permeability to small molecules, good durability, and processability, PDMS is the most common polymer for desulfurization. However, high flexibility of its molecular chains results in low mechanical strength. Other polymers like polyimide, poly (ethylene-glycol), polyurethane, etc., are prevalent in the field of desulfurization (Fihri et al., 2016). Polyethersulfone (PES) is a member of polyarylsulfone which has been used widely in separation techniques due to its excellent chemical, thermal, hydrolytic stability and good mechanical property with a considerable research on its modifications. The sulfone group in the core of the main polymer chain distinguishes polyaryl sulfones from other polymers (Mark, 1969). The main disadvantage of PES is its rigidity which results in low selectivity and high energy demand. Therefore, the recently introduced polyphenylsulfone (PPSU) polymer of polyarylsulfones can be a stronger candidate for membrane preparation due to its thermal stability, higher acid/base hydrolysis resistance, chemical resistance and compatibility, plasticization resistance, and mechanical resilience (Darvishmanesh et al., 2011; Hwang et al., 2011).

By integrating nanomaterials into the membrane matrix, high flux and selectivity for sulfur species can be achieved. Boron nitride (BN) and its composites have recently been used as adsorbents for adsorptive desulfurization and as catalysts for oxidative desulfurization to separate refractive sulfur compounds like dibenzothiophene (DBT) from liquid fuels. Previous studies found numerous mechanisms including low coordinated atom construction (Xiong et al., 2016), carbon doping (Xiong et al., 2015), oxygen doping (Dai et al., 2020) or surfactant control (Xiong et al., 2017) to control the local atomic and electronic structure of

BN in order to improve the efficiency of hexagonal BN (h-BN) for desulfurization. Owing to being inexpensive and metal-free, with low toxicity and high efficiency, h-BN nanomaterials with high adsorption performance for DBT are preferable (Rajendran et al., 2020). However, the use of BN is still in its infancy stage for potential applications. Hence, it is important to apply suitable strategies that will further enhance the efficiency of adsorptive desulfurization to reach potential industrial applications.

Latest developments in desulfurization using h-BN as an adsorbent has motivated the use of h-BN material as adsorbent and fillers in the polymer matrix in the present study. To increase overall selectivity and permeability of the membrane against sulfur compounds, carbon dot doped boron nitride (CBN) were integrated with the polymer. Small amounts of these CBN particles added to the membrane are intended to increase the membrane's overall efficiency for separating sulfur species.

1.4 Research Aim and Objectives

The primary aim of this research work is to develop a polymeric mixed matrix membrane based on PPSU embedded with nano materials such as h-BN and CBN, and design a desulfurization system for sulfur rich streams. To achieve the aims of this project, objectives below were investigated

a) Synthesis and characterization of h-BN and carbon dots (C-dots) as nano filler for PPSU membrane for removal of dibenzothiophene (DBT) from model fuel;
b) Doping of C-dots onto h-BN to synthesize CBN and their characterization to use as nanofillers in PPSU to produce mixed matrix membranes for desulfurization;
c) Development and characterization of PPSU-based mixed matrix membranes (MMM) with h-BN and CBN as nanofillers, and investigation of the chemical and mechanical

properties of the PPSU membranes when different weight ratios of nano materials are used.

d) Performance evaluation of the synthesized h-BN and CBN filled PPSU membranes for removal of sulfur-containing compounds.
e) Investigation of the nano material concentration, operating temperature, and time on the adsorption capacities of the the developed PPSU-h-BN and PPSU-CBN membranes.
f) Evaluation and comparison of the obtained results with the existing adsorption models.

1.5 Thesis Outline

Chapter one briefly describes the research introduction, background and motivation for this study and also includes the problem statement and the aim and objectives of the current study. A brief summary on the significance on sulfur removal from fuels and the limitations of existing desulfurization technologies is also given.

Chapter two, presents the overview of the refinery industry and background information on existing and future emission policies, existing sulfur removal methods, advantages and the current challenges faced in the petroleum industry and possible solutions needed to address the problems.

Chapter three gives a graphical representation and a brief description on the methodologies involved in the study including the synthesis and characterization of h-BN, carbon dots, and doping of carbon dots on h-BN (CBN).

Chapter four describes tha development of mixed matrix membranes (MMM) and their charecterization and the methods used for desulfurization tests.

Chapter five investigates the adsorptive desulfurization efficiency of the synthesized PPSU membranes embedded with h-BN and CBN materials by varying the operating conditions. The operating conditions considered for this research work include temperature, time, and adsorbent filler concentration. Chapters six compares the membrane adsorption capacities with the existing adsorption models and explains the adsorption kinetics from the results obtained. The seventh chapter ends with overall conclusion of the study's key results and recommendations for future studies.

1.6 Conclusion

This chapter briefly introduces the research work and related topics which will be elaborated in further chapters starting with the literature review. The primary aim of this research work is to develop a polymeric mixed matrix membrane based on PPSU embedded with materials such as h-BN and CBN, and design a desulfurization system for sulfur rich streams. The process of achieving this goal follows a set list of objectives with a relevant and distinctive methodological processes elaborated in their respective chapters.

1.7 References

Asghar, U. et al., 2021. Review of the Progress in Emission Control Technologies for the Abatement of CO_2, SO_x and NO_x from Fuel Combustion. Journal of Environmental Chemical Engineering, p. 106064.

Babich, I.V. and Moulijn, J.A., 2003. Science and technology of novel processes for deep desulfurization of oil refinery streams: a review☆. Fuel, 82(6), pp.607-631

Bergh, C., 2012. Energy efficiency in the South Africa crude oil refining industry drivers, barriers and opportunities (Doctoral dissertation, University of Cape Town).

Dai, L., Wei, Y., Xu, X., Wu, P., Zhang, M., Wang, C., Li, H., Zhang, Q., Li, H. and Zhu, W., 2020. Boron and Nitride Dual vacancies on Metal-Free Oxygen Doping Boron Nitride as Initiating Sites for Deep Aerobic Oxidative Desulfurization. ChemCatChem, 12(6), pp.1734-1742.

Darvishmanesh, S., Jansen, J.C., Tasselli, F., Tocci, E., Luis, P., Degrève, J., Drioli, E. and Van der Bruggen, B., 2011. Novel polyphenylsulfone membrane for potential use in solvent nanofiltration. Journal of Membrane Science, 379(1-2), pp.60-68.

DME - RSA 2008. National Energy Efficiency Strategy of the Republic of South Africa, First Review. Department of Minerals and Energy.

Fihri, A., Mahfouz, R., Shahrani, A., Taie, I. and Alabedi, G., 2016. Pervaporative desulfurization of gasoline: a review. Chemical Engineering and Processing: Process Intensification, 107, pp.94-105.

Gawande, P.R. and Kaware, J., 2014. Desulphurization Techniques for Liquid Fuel: A Review. Int. J. Eng. Technol. Manag. Appl. Sci, 2, pp.121-127.

Hwang, L.L., Tseng, H.H. and Chen, J.C., 2011. Fabrication of polyphenylsulfone/polyetherimide blend membranes for ultrafiltration applications: The effects of blending ratio on membrane properties and humic acid removal performance. Journal of membrane science, 384(1-2), pp.72-81.

Ito, E. and Van Veen, J.R., 2006. On novel processes for removing sulphur from refinery streams. Catalysis today, 116(4), pp.446-460.

Kong, Y., Lin, L., Yang, J., Shi, D., Qu, H., Xie, K. and Li, L., 2007. FCC gasoline desulfurization by pervaporation: Effects of gasoline components. Journal of Membrane Science, 293(1-2), pp.36-43.

Kumari, S. and Sengupta, S., 2021. Non-hydrogen processes for simultaneous desulfurization and denitrogenation of light petroleum fuels—an elaborative review. Environmental Science and Pollution Research, pp. 1-35.

Lin, L., Hong, L., Jianhua, Q. and Jinjuan, X., 2010. Progress in the technology for desulfurization of crude oil. China Petrol. Process. Petrochem. Technol, 12, pp.1-6.

Mark, H.F., 1969. Encyclopedia of Polymer Science and Technology: Phenolic resins to Polyelectrolytes (Vol. 10). Interscience Publishers.

Martinie, G.D., Al-Shahrani, F.M. and Dabbousi, B.O., Saudi Arabian Oil Co, 2010. Process for treating a sulfur-containing spent caustic refinery stream using a membrane electrolyzer powered by a fuel cell. U.S. Patent 7,713,399.

Oil 2021, 2021.International Energy Agency, IEA

Rajendran, A., Fan, H.X., Feng, J. and Li, W.Y., 2020. Desulfurization on boron nitride and boron nitride-based materials. Chemistry–An Asian Journal, 15(14), pp.2038-2059.

Samokhvalov, A. and Tatarchuk, B.J., 2010. Review of experimental characterization of active sites and determination of molecular mechanisms of adsorption, desorption and regeneration of the deep and ultradeep desulfurization sorbents for liquid fuels. Catalysis Reviews, 52(3), pp.381-410.

Srivastava, V.C., 2012. An evaluation of desulfurization technologies for sulfur removal from liquid fuels. Rsc Advances, 2(3), pp.759-783.

Xiong, J., Li, H., Yang, L., Luo, J., Chao, Y., Pang, J. and Zhu, W., 2017. Metal-free boron nitride adsorbent for ultra-deep desulfurization. AIChE Journal, 63(8), pp.3463-3469.

Xiong, J., Yang, L., Chao, Y., Pang, J., Wu, P., Zhang, M., Zhu, W. and Li, H., 2016. A large number of low coordinated atoms in boron nitride for outstanding adsorptive desulfurization performance. Green Chemistry, 18(10), pp.3040-3047.

Xiong, J., Zhu, W., Li, H., Yang, L., Chao, Y., Wu, P., Xun, S., Jiang, W., Zhang, M. and Li, H., 2015. Carbon-doped porous boron nitride: metal-free adsorbents for sulfur removal from fuels. Journal of Materials Chemistry A, 3(24), pp.12738-12747.

2. CHAPTER TWO: LITERATURE REVIEW

2.1 Introduction

The energy sector constituting of companies that involve in producing and supplying energy is a dynamic industry. According to various sources, about 80% of the world's energy over the last decade, is produced from fossil fuels, over half of which comes from petroleum (BP, 2021). Since its first production in 1859 crude oil has been the most sought after energy source considering its usage in transporation, heating, electricity generation as well in the production of plastics (Soeder, 2021). However, this finite naturally occurring resource is a finite entity and the world is looking into energy transitions from non-renewable to more efficient and renewable energy. There are quite a few organizations across the world that track global energy transitions, collect-prepare-analyse-publish data, perform insights and market analysis even considering COVID-19 effects. These entities work and report on the energy sector for organizations to develop appropriate responses and make informed decision.

By various source reports published during the course of 2021, concerning the world's primary energy consumption stats, oil is the most reliable fuel at 31.2%, as shown in Figure 2.1. Coal is the second largest fuel accounting for 27.2%. Natural Gas accounts for 24.7% and is third in line. Several processes which include oil refining and other material synthesis require expensive methods to efficiently obtain high yields of energy and valuable products from them (BP, 2021).

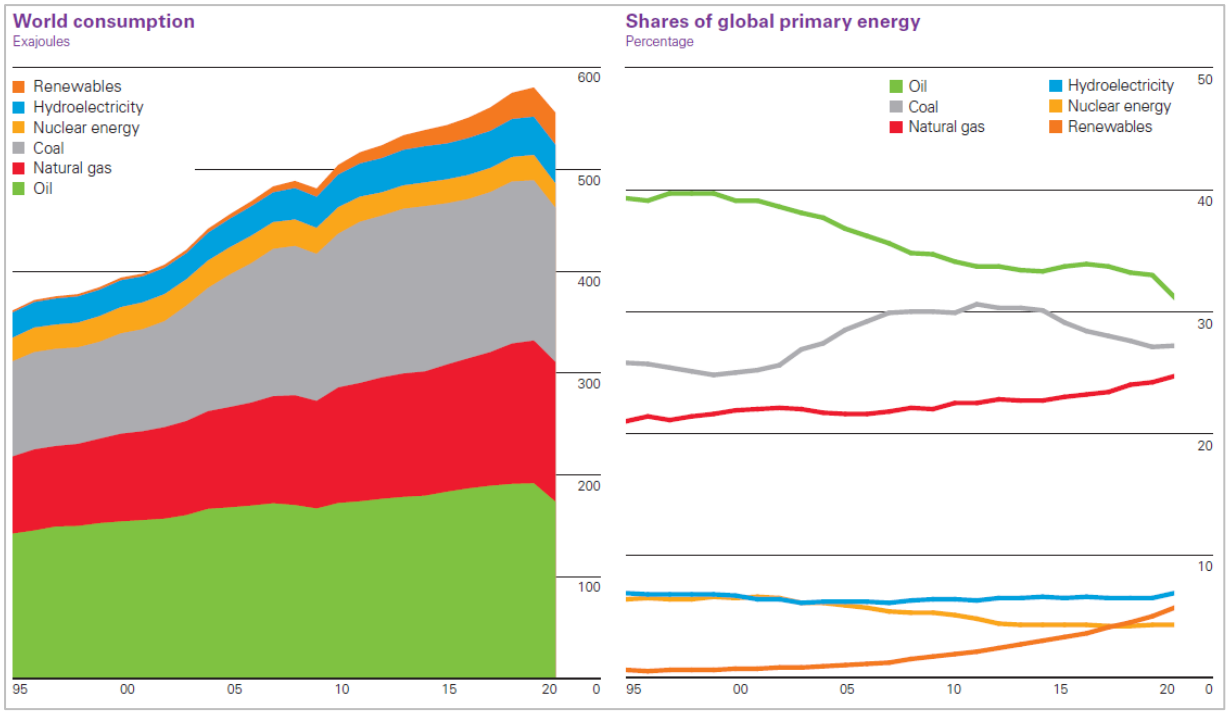


Figure 2.1 World Energy Consumption (BP, 2021) (reproduced with permission from BP)

Africa as a continent heavily relies on crude oil (Boateng et al., 2021). South Africa lacks domestic oil resources and invests huge amounts in importing crude oil along with other industrial minerals including sulfur due to the rapid growth of product demand (Akinbami et al., 2021). On average South Africa's total crude oil demand annually is 26.3 million tons with the total imports and exports accounting for nearly 50% of the Gross Domestic Product (GDP) composed of also agricultural and mineral products (Su et al., 2021). This dependency of energy supply on crude oil products due to growing demand has become a major concern for the country, as with the rest of the world, in terms of import affordability and climate change. As per the National Development Plan 2030, the country strongly promotes energy efficiency in all energy consuming sectors for sustainable development to reduce emissions and meet product demand (Field, 2021).

Crude oil is a complex yellowish-black liquid mixture made up of a vast number of hydrocarbon compounds as well as small amounts of metals and organic compounds containing sulfur, oxygen, nitrogen (Grimmer et al., 2021). It comes from different parts of the world found in geological formations beneath the earth's surface with different physical and chemical characteristics. Sulfur content in crude oils, for example, ranges from 0.05 to more than 10 weight percent with some commercially produced crude oils exceeding 4% sulfur (Jatoi et al., 2021). Crude oil and other hydrocarbon products naturally contain sulfur in minor quantities as inorganic or organic forms (Shi and Wu, 2021).

Sulfur must be reduced or eliminated to considerable levels as its presence in petroleum products generally results in equipment corrosion which includes pipelines, pumping, and refining equipment, and the production of harmful emissions due to combustion. The primary cause for the formation of soot or particulate in the atmosphere from diesel combustion is the presence of trace amounts of sulfur in the black exhaust fumes. It also contaminates the oxidation catalyst in the emission control system, making the oxidation of harmful Carbon Monoxide (CO), hydrocarbons, and volatile organic compounds less efficient (Rochard et al., 2021). Adding to the aforementioned issues, new environmental legislation in many countries mandated an ultra-low level of sulfur in transportation fuels of 10–15 parts per million (ppm) to further reduce the negative effects of sulfur compounds (Roman et al., 2021). The success of ultra-deep desulfurization depends on various factors such as process parameters, feedstock source, and quality, the reactivity of sulfur compounds in the feed stream, etc. (Lima, 2021) Consequently, petroleum industries should aspire to not only produce clean fuels but also effluents that are safe for disposal.

2.2 The State of Oil Sector, Desulfurization and Emission Policies across the Globe

Based on the extensive research data and energy sector information available as of the last quarter of 2021, the following sections briefly delve into the oil and gas energy sector providing an overview of oil reserves and their demand globally especially in road transportation, the refinery industry, desulfurization and related background information on existing and future emission policies, particularly on SOx compounds.

The following sections also selectively leverages, reviews, reproduces, and summarizes certain aspects of the energy industry that are free for use or provided by organisations such as Stratas Advisors, International Energy Agency (IEA), and British Petroleum (BP) p.l.c amongst others with due acknowledgement or permission. Briefly, Stratas Advisors is an energy sector consultancy firm helping provide insights on periodic data across the oil and gas value chain (Stratas Advisors, 2021). IEA is an intergovernmental organisation that works with countries around the world to shape energy policies across countries (IEA, 2021). British Petroleum p.l.c. is a multinational oil and gas company that periodically reviews world energy data (BP, 2021). The Organization of the Petroleum Exporting Countries (OPEC) is also another intergovernmental organisation shaping energy policies across its member countries (OPEC, 2021).

2.2.1 World Oil Reserves

Between 1860 and 2019, the world consumed just about 1.5 trillion barrels of oil and as of the year 2021, there is an estimate of almost 1.5 trillion barrels of oil left in the world (Davies and Simmons, 2021) (World Oil Projections , 2021). At the current rate of extraction, oil is expected to last for another 53.3 years (Dolah et al., 2022). The continent of Africa is home to an

abundance of energy resources, including about 10% of the world's oil reserves, however, it still has difficulty in harnessing these precious resources to meet its energy demand (OPEC, 2021). The map shown in Figure 2.2 depicts proven oil reserves as of 2021. Venezuela being the top in the list, is estimated to have almost 300 billion barrels of reserves and 18.2% of the world oil share. South Africa on the other hand is ranked 86 with estimated oil reserves of 15 million barrels with 0.0009% world share (Landgeist, 2021) (Stratas Advisors, 2021).

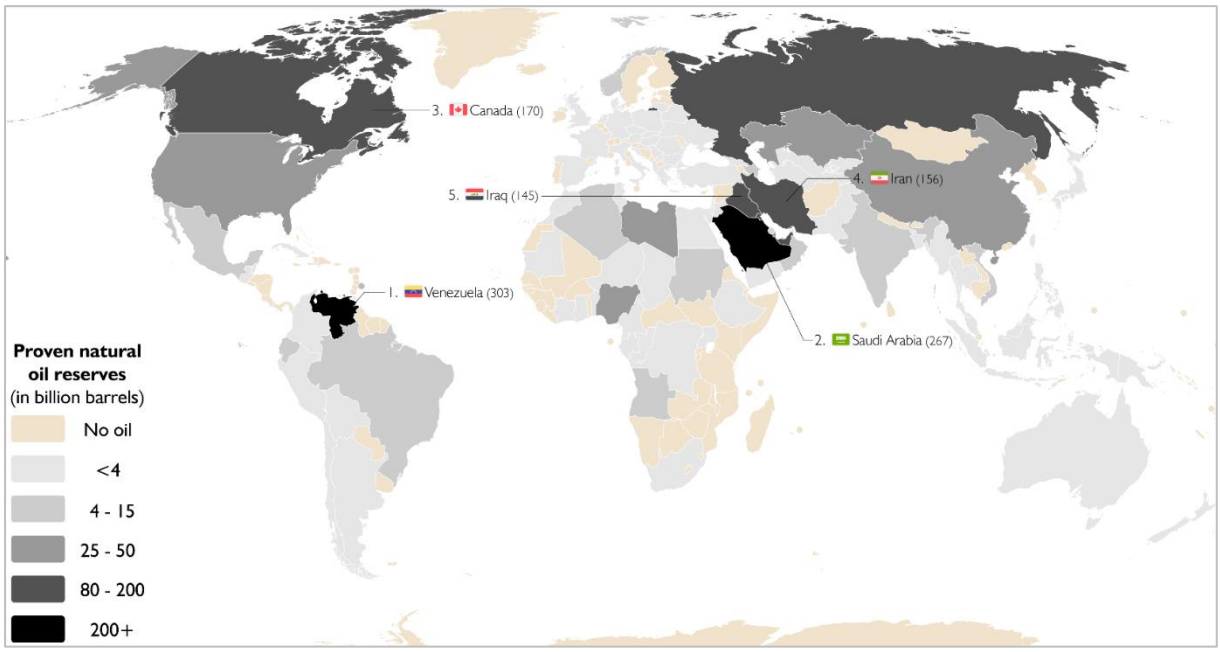


Figure 2.2 World Oil Reserves (Landgeist, 2021) (Stratas Advisors, 2021)

Oil will continue to play an important role in daily life since it has proven to be a key necessity. Based on current industry stats, one of the most important industries of the global economy is petroleum refining (Hashmi, 2021). It continues to play a critical role in global industrialization and urbanization, processing more goods greater than any other sector partaking in the day-to-day lives of the current 7.9 billion population (Rees, 2021). Thanks to crude oil and its refining process, the demand for transportation fuel, electricity, and various consumer goods such as

plastics is expected to only rise with projected population growth to about 8.2 billion by 2025 (Kumar, 2021) (World Population Projections, 2021).

Hydrocarbons, as well as other minerals and trace elements, make up crude oil. Alkanes, cycloalkanes, aromatics, polycyclic aromatics, sulfur-containing compounds, and other compounds make up the bulk of crude oil. Most studies focus on refineries environment issues and CO_2 failing to concentrate on other Green House Gases (GHG) such as CH_4, N_2O, and SO_2 emissions including liquid and solid waste (Abdussalam et al., 2021). Sulfur being the most abundant element next to carbon and hydrogen, and followed by nitrogen, are typically concentrated in the crude oil's higher boiling fractions (Shi and Wu, 2021). Sulfur compounds cause refining facilities to corrode and catalysts to poison, necessitating processing considerations such as desulfurization (Larraz, 2021). Additionally, nitrogen-compounds have a direct effect on the refining processes by poisoning cracking catalysts leading to the inhibition of the hydrodesulfurization catalysts (Bello et al., 2021).

Furthermore, there are negative environmental consequences due to sulfur and nitrogen oxide emission and it is important to remove them during the refining process. Sulfur and nitrogen when removed, protects the machinery and the atmosphere while also making the process more reliable and cost-effective (Zehra et al., 2022). Refiners will gain a lot of money by improving the design and operation of these facilities. Instead of constructing wholly new plants, businesses are investing billions of dollars in the research and development of novel procedures that can save time and money while also being safer for the environment. Besides, the oil and gas industry is under tremendous pressure to provide safe working conditions while also optimizing the refining process due to economic, regulatory, and environmental concerns (Bathrinath et al., 2021).

2.2.2 World Oil Demand

Despite the COVID pandemic, the long-term energy trends globally and the world primary energy demand is set to increase to 303 thousand barrels of oil equivalent per day (mboe/d) in 2025 when compared to 275.4 mboe/d as shown in Figure 2.3, majorly from the developing countries (OPEC, 2021). Further, the energy demand additions from the developing countries comes from its promising economic and population growth, and increased urbanization.

On the other hand, the low population growth in the Organisation for Economic Co-operation and Development (OECD) region with 38 member countries, improving efficiency in all principal energy sectors and a shift towards renewable energy, with lower transformation losses compared to conventional electricity generation, are main precursors to declining primary energy demand in the region (Paramati et al., 2022).

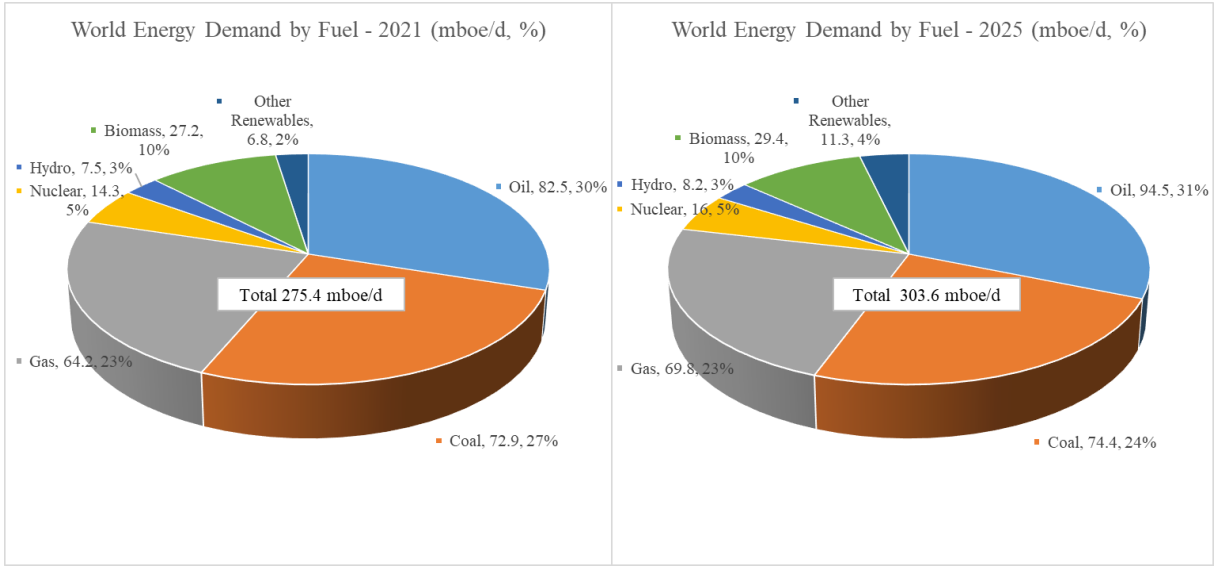


Figure 2.3 World Energy Demand 2021 - 2025 (OPEC, 2021)

There is a stark contrast in trends between expected developments in the OECD and non-OECD countries. Future oil demand growth globally will be almost exclusively driven by non-OECD countries in which demand will increase to 94.4 mboe/d in 2025 from about 82.5 mboe/d at the start of 2021 as shown in Figure 2.4.

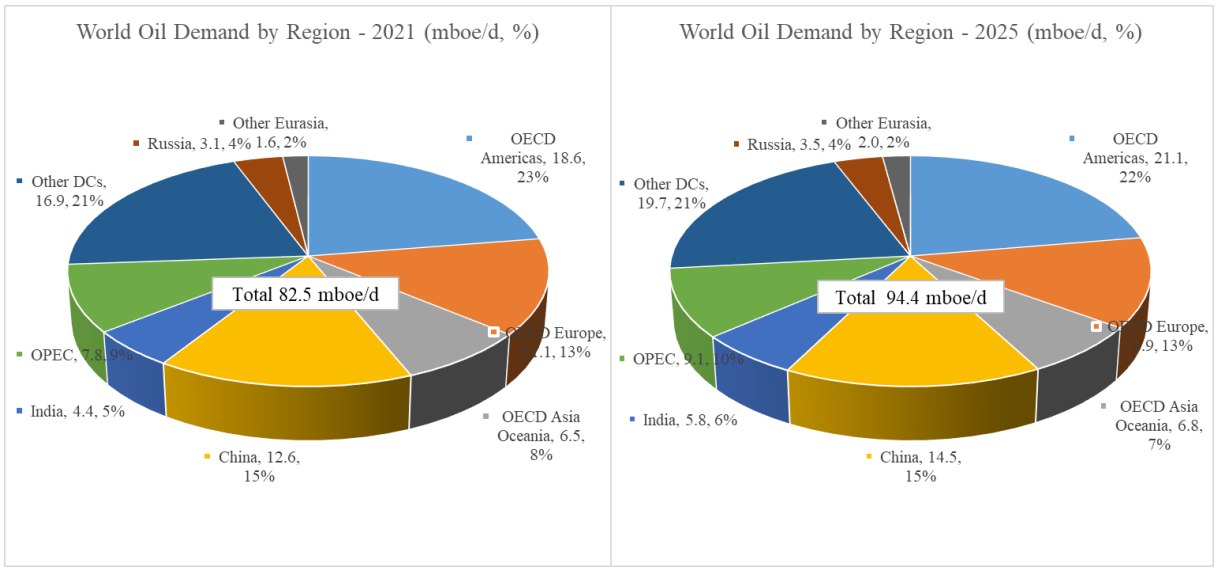


Figure 2.4 World Oil Demand by Region 2021 - 2025 (OPEC, 2021)

The COVID-19 pandemic during the first half of 2020 had unprecedented implications for the road transportation sector in particular. The otherwise busy streets of large cities became empty and quiet. Car sales alone plunged by more than half in many countries over the course of several months. Oil demand in this sector collapsed. Bearing in mind many such uncertainties and assuming a gradual demand recovery during the next few years, oil demand in the automobile sector itself is projected to reach around 46.3 thousand barrels per day (mb/d) in 2025 as shown in Figure 2.5. Taking into account the projected regional developments in the size of the vehicle fleet, its composition, and fuel economy and vehicle miles travelled (VMT), this is an increase from about 40.0 mb/d at the start of 2021, apart from shipping, aviation, and other sectors (OPEC, 2021) (IEA, 2021). Future oil demand in this sector will heavily depend on developments in global vehicle stocks in terms of their size and composition.

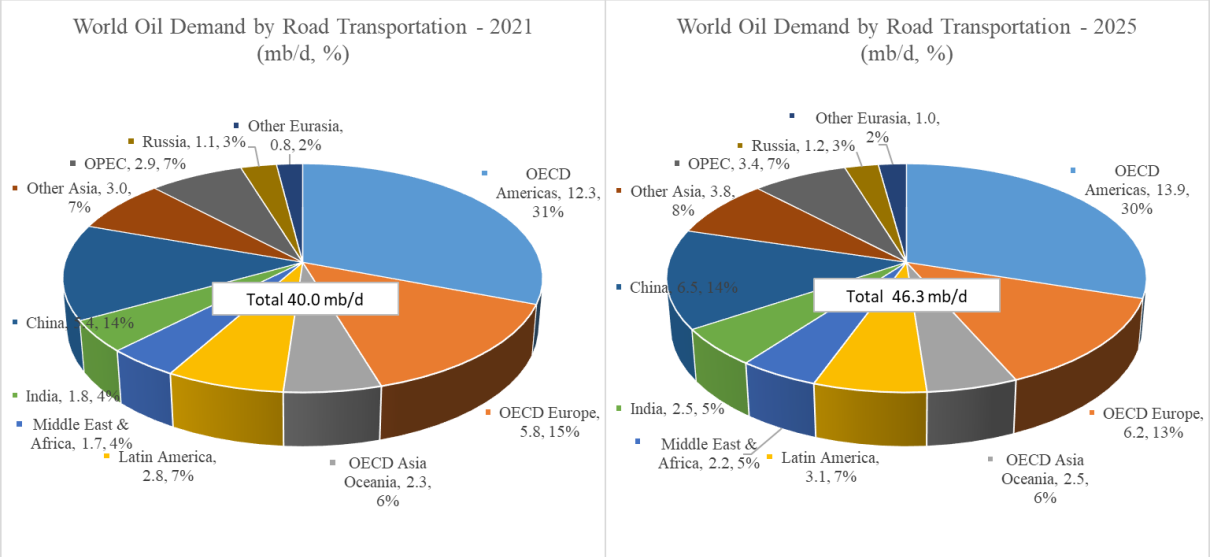


Figure 2.5 World Oil Demand by Road Transportation 2021 - 2025 (OPEC, 2021)

Standards for fuel efficiency vehicles are set to be tightened globally. Many African countries have national energy strategies, albeit with differing time horizons. For example, the South African government has approved a Low Emission Development Strategy (SALEDS) intending to achieve net-zero emissions by 2050. It plans to achieve this goal with Nationally Determined Contribution (NDC) target emissions of 398-510 million metric tons of CO_2 equivalent ($MMtCO_2e$) from 2021-2025 (Lawrence and Ballard, 2020).

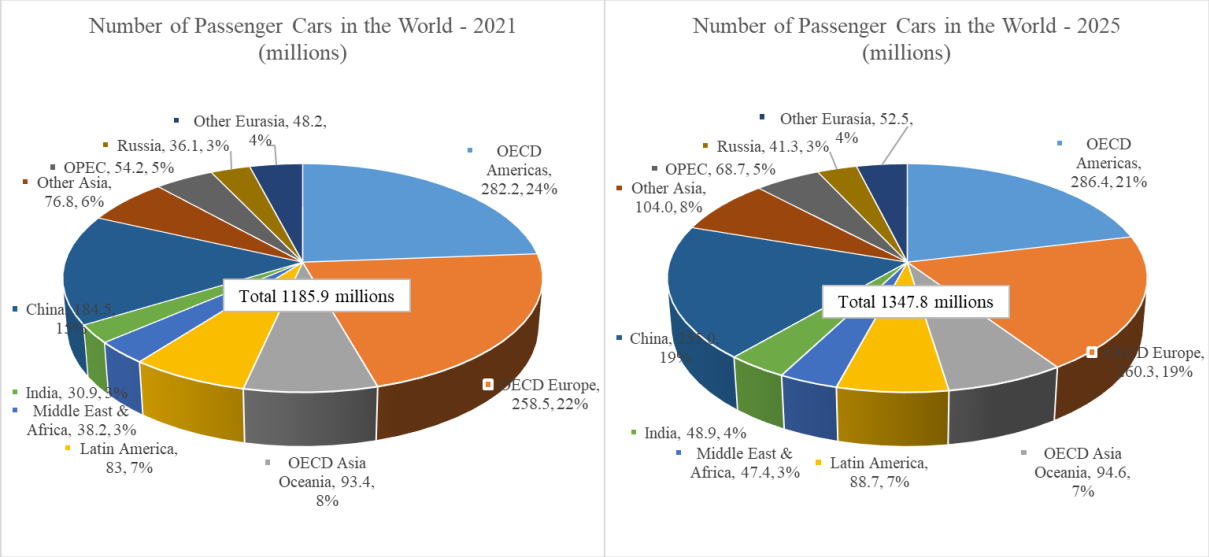


Figure 2.6 Passenger Cars in the World 2021 - 2025 (OPEC, 2021)

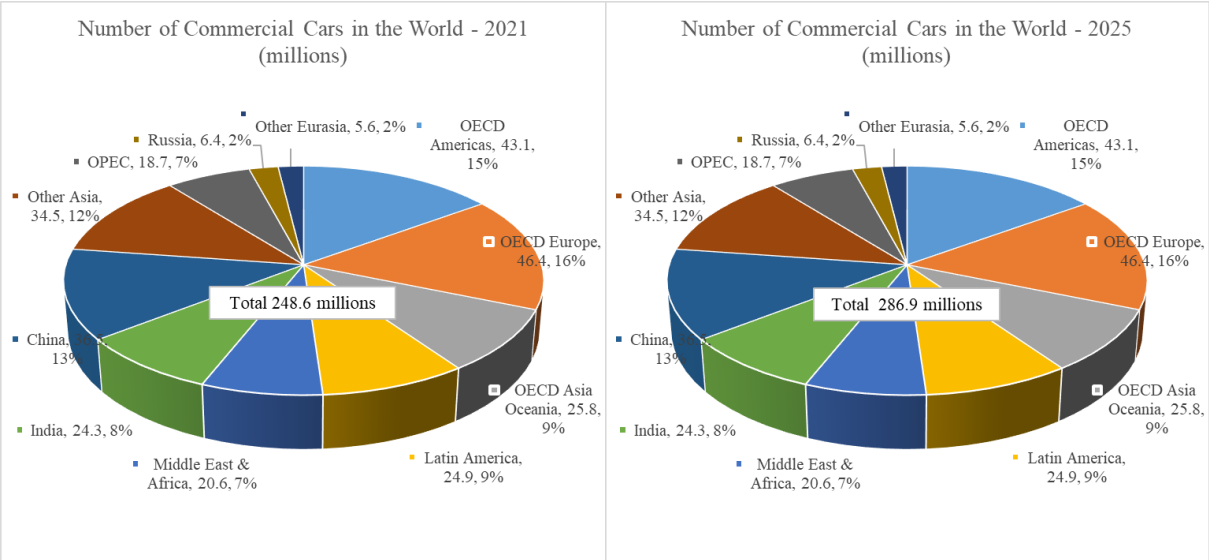


Figure 2.7 Commercial Cars in the World 2021 - 2025 (OPEC, 2021)

Taking into account the projected regional developments in the size of the vehicle fleet, its composition, and fuel economy and VMT, vehicle fleets continue to expand in developing countries due to economic and population growth, and urbanization. Globally, the number of passenger cars is expected to reach 1.35 billion in 2025 from 1.19 billion at the start of 2021,

and commercial vehicles are projected to increase to 287 million in 2025 from about 249 million at the start of 2021 as shown in Figure 2.6 and Figure 2.7 respectively (OPEC, 2021) (IEA, 2021).

2.2.3 Crude Oil Refinery Process

In a nutshell, an oil refinery is an industrial crude oil processing plant that converts crude oil into items like naphtha, kerosene, diesel fuel, and liquified petroleum gas (LPG). Petroleum refining is a dynamic industry and the price of oil can have a significant impact on inflation as oil serves as a key production input to firms for the manufacturing of various goods and services (Babuga and Naseem, 2021). The petroleum refining and process engineering industries are always evolving. Although no new refineries are being built, corporations throughout the world continue to expand or repurpose large portions of their existing refineries year after year.

Crude oil is separated into different fractions through the process of boiling, which give this process the term fractional distillation. This is the main process in petroleum refining. During the crude oil boiling process, the lighter, more volatile components of crude oil rise to the top of the boiling column, while the heavier fractions with the greatest boiling points remain at the bottom (Kanaboshi et al., 2021). Thermal cracking of the heavy bottom fractions produces more usable light materials (Aljamali and Salih, 2021). Sulfur is a non-metallic yellowish material that is also known as ‘brimstone’ (Torres et al., 2020). Many fossil fuels contain it in different concentrations, and their combustion releases sulfur compounds that are hazardous to the atmosphere. The sulfur content of some of the more widely used fossil fuels is classified, with lower sulfur fuels typically being higher-priced (Huang et al., 2020).

No. 2 Distillate, which is a petroleum distillate that can be used as either diesel fuel or fuel oil, is currently estimated to have a sulfur level of 0.05 % or less for on-highway vehicle use and a sulfur level of greater than 0.05 % for off-highway use, home heating oil, commercial and industrial uses. The distillation temperature for the No. 2 Diesel Fuel group of the No. 2 Distillate is 640 degrees Fahrenheit at the 90% recovery stage (Liu and McMillan, 2020). It is used in high-speed diesel engines like those used in locomotives, trucks, and cars. This involves the necessity for Ultra-Low Sulfur Diesel (ULSD) with a sulfur level of less than 15 ppm. Residual fuel is graded as containing no more than 1% sulfur, regardless of its use. Coal can also be graded as low-sulfur if it contains less than 1% sulfur or high-sulfur if it contains more than 1% sulfur (Koech et al., 2021).

Because of its many and varied parts, as well as the wide variety of products that can be made from it, crude oil processing is extremely complicated. Oil is continually pumped via the heat exchanger device and into the vaporizer section of the topping unit's multiple-draw fractioning tower through the tube still. Cracking produces cracking-still gas, pressure distillate, cracked gasoline, and pressure-still tars, among other things (He et al., 2021).

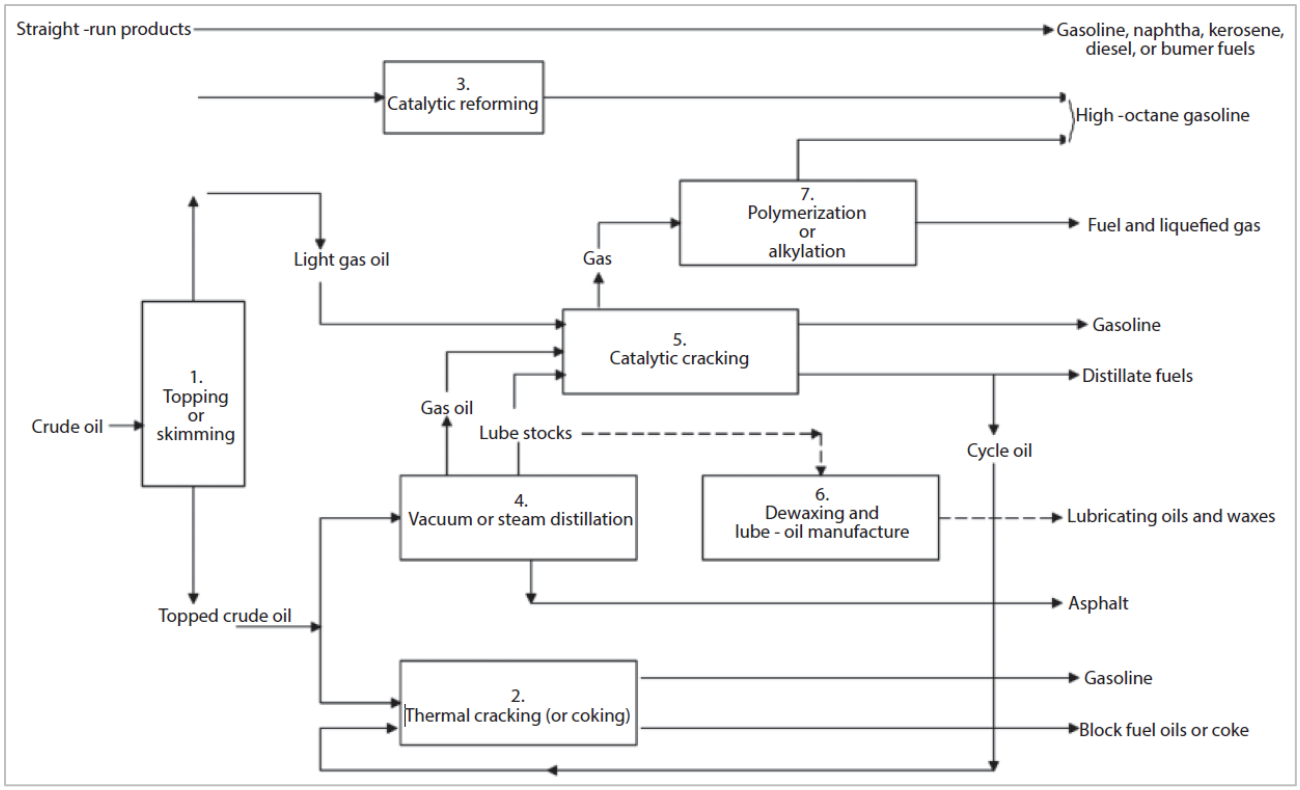


Figure 2.8 Basic Refinery Operations (Coker, 2021)

Oil refineries are complex facilities, but they are well-established and well-integrated. The basic crude oil refinery process is depicted in Figure 2.8, which includes topping, thermal cracking, catalytic reforming, vacuum distillation, and catalytic cracking. Some individual refinery processes at the unit level are common to all refineries. Some of the basic refinery products include Gasoline, Diesel, Kerosene, Naphtha, Fuel oils etc. and are used in both industrial and domestic sectors (Aljamali and Salih, 2021).

Sulfur and its compounds are naturally present in crude oil and shale gas (Katasonova et al., 2021). The removal of sulfur is significant at various stages of petroleum refining due to its toxicity, corrosive nature, and its presence in transportation fuels can result in SO_2 emissions leading to several environmental problems (Randrianarisoa and Gillen, 2021). The amount of sulfur in the oil and air is measured in parts per million (ppm). According to the environmental

regulations in the last decade, the sulfur content in the transportation fuel must be reduced to ultra-low levels on an average in the range of 10-50 ppm for gasoline and diesel (Roman et al., 2021)

The implication of these regulations produces cleaner fuels besides producing large quantities of petroleum streams concentrated with sulfur compounds. The concentrated sulfur streams also contain a mixture of other organic and inorganic compounds which are extremely alkaline, odiferous, and toxic because of chemical treatment to remove sulfur (Katasonova et al., 2021).

Such streams cannot be released into the sea or land directly due to the possibility of contamination and thus require significant processing that allows safe disposal and recovery of possible chemical compounds. The current regulations on industries for environmental protection emphasize on upgrading technologies to minimize the sulfur content from fuels that are toxic to the environment. Hence, ultra-deep desulfurization of liquid fuels is critical, and it has gotten a lot of media coverage in recent years. Significant efforts have been made to create innovative sulfur reduction strategies to fulfill the greatly anticipated zero sulfur emission regulations in the second half of this century as per the Paris Agreement as well as new materials for high efficiency desulfurization of hydrocarbon fuels (Kanaboshi et al., 2021).

The removal of sulfur compounds is completely dependent on the boiling point range of the oil and this is directly related to the structure or nature and concentration of sulfur species. As a result, the amount of sulfur compounds in the distillation fraction increases with boiling points ranges, and the heavy distillate contains the most refractory sulfur compounds (Javadli and De Klerk, 2012). In crude oil, there are many important groups of sulfur-containing compounds as shown in Figure 2.9.

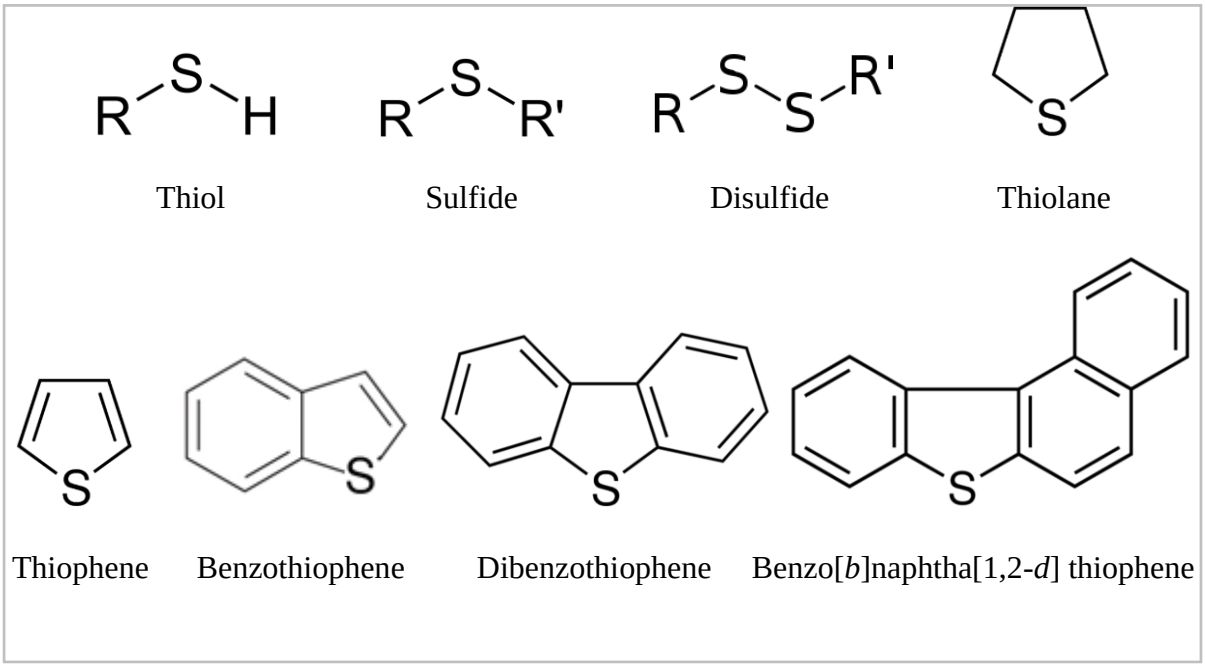


Figure 2.9 Crude oil sulfur compounds (R=alkyl) (Javadli and De Klerk, 2012)

Sulfur is removed from petroleum oil, molten metals, and flue gases during desulfurization through the Flue Gas Desulphurisation System (FGD) processes based on the absorption of sulfur dioxide. During the refining process, petroleum desulfurization extracts sulfur and its compounds from different sources. Catalytic hydrotreating is used in the desulfurization process apart from other chemical or physical processes, such as the adsorption process. The amount of sulfur extracted and the type of stream treated to determine the desulfurization method.

Hydroprocessing is a conventional refining process in which hydrocarbons react with hydrogen using methods such as hydrotreating, hydrocracking, and hydrogenation (Prajapati et al., 2021). Figure 2.10 depicts a typical but complex refinery unit's process flow diagram, which includes not only the three primary processes of separation, conversion, and treating, but also additional processing (Coker, 2021).

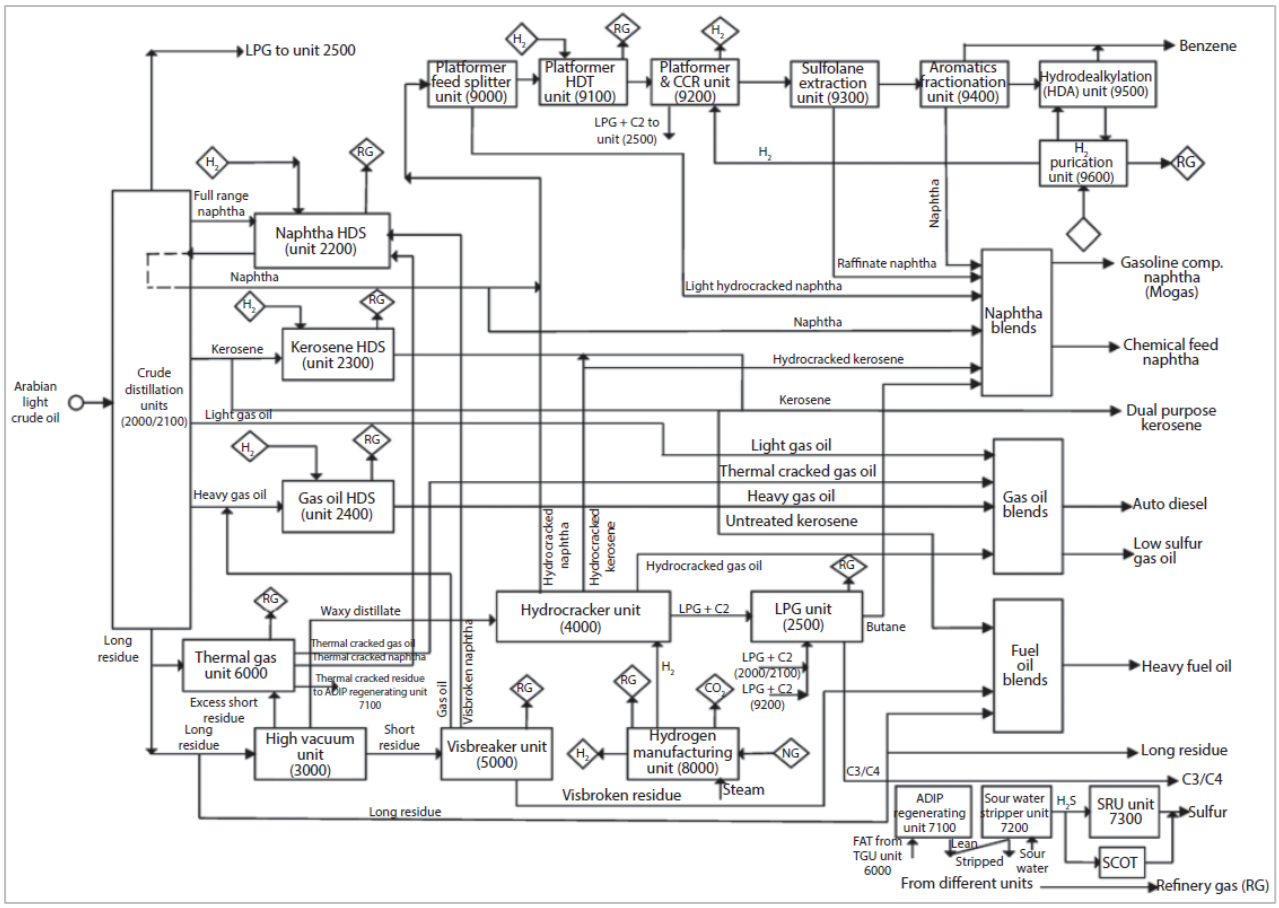


Figure 2.10 Complex Refinery Operations (Coker, 2021)

Since crude oil prices are unpredictable, refiners are dealing with a competitive business climate. For example, the demand for oil in road transport and aviation was hit the hardest as mobility ground to a halt during the COVID-19 lockdowns. With less demand for heavy, high-sulfur, and acidic crudes, demand for lighter products is growing, and product regulations and emission standards are tightening. On the other hand, transportation fuel demand continues to rise.

2.2.4 Global Emission Standards

Sulfur removal from petroleum products has always been essential, and it continues to be so today due to environmental concerns. Increasing pollution has resulted in continuing worldwide efforts to impose strict regulations on petroleum industries to control Green House Gas (GHG) emissions and maintain ultra-low sulfur levels in the products to significantly reduce sulfur toxicity in the environment. Sulfur compounds are acidic in nature which are not only toxic but are also highly reactive when forming SO_2 resulting in major air pollution apart from CO_2 (Kanaboshi et al., 2021). Countries globally have pledged to reduce emissions and make this transition secure, affordable and fair to all citizens. Protocols are in place globally to ensure that relevant laws, such as risk communication, pollution, and waste minimization, are followed.

In addition to pure hydrocarbons and carbon monoxide, there are sulfur oxides (SOx), nitrogen oxides (NOx), ammonia (NH_3), hydrogen sulfide (H_2S), particulates, as well as toxic and volatile organic compounds are all present in crude oil. Sulfur, which is also the focus of this research, is the most critical of these from the viewpoint of air pollution and environmental problems such as acid rain. High levels of sulfur in the refinery streams can cause refinery equipment to corrode and result in sulfur compounds being released into the atmosphere (Coker, 2021).

A few years earlier, climate change and fuel quality legislation were addressed separately, but today, any industry that uses fuel oil has stringent policies in place to improve air quality and mitigate global warming. This section aims to briefly evaluate the emission standards, regulations, and policies associated with reviving refineries and desulfurization. Even though the COVID-19 pandemic has temporarily disrupted the energy sector and suppressed emissions due to the economic downturn but the low economic growth is not to be mistaken as the low-

emission strategy. Perhaps faster systemic improvements in the way we generate and use energy, as well as policies implemented by countries around the world, will permanently reverse the pollution trend.

Governments have the power and duty to accelerate renewable energy transformations and bring the planet on track to meet our climate targets, including net-zero emissions. The map shown in Figure 2.11 shows the November 2021 SO_2 emissions data across the world provided by NASA. SO_2 Climatology derived from satellite instruments depicts a global image of SO_2 column mass, which is the cumulative amount of SO_2 present in the Earth's atmosphere's lowest layer (NASA, 2021).

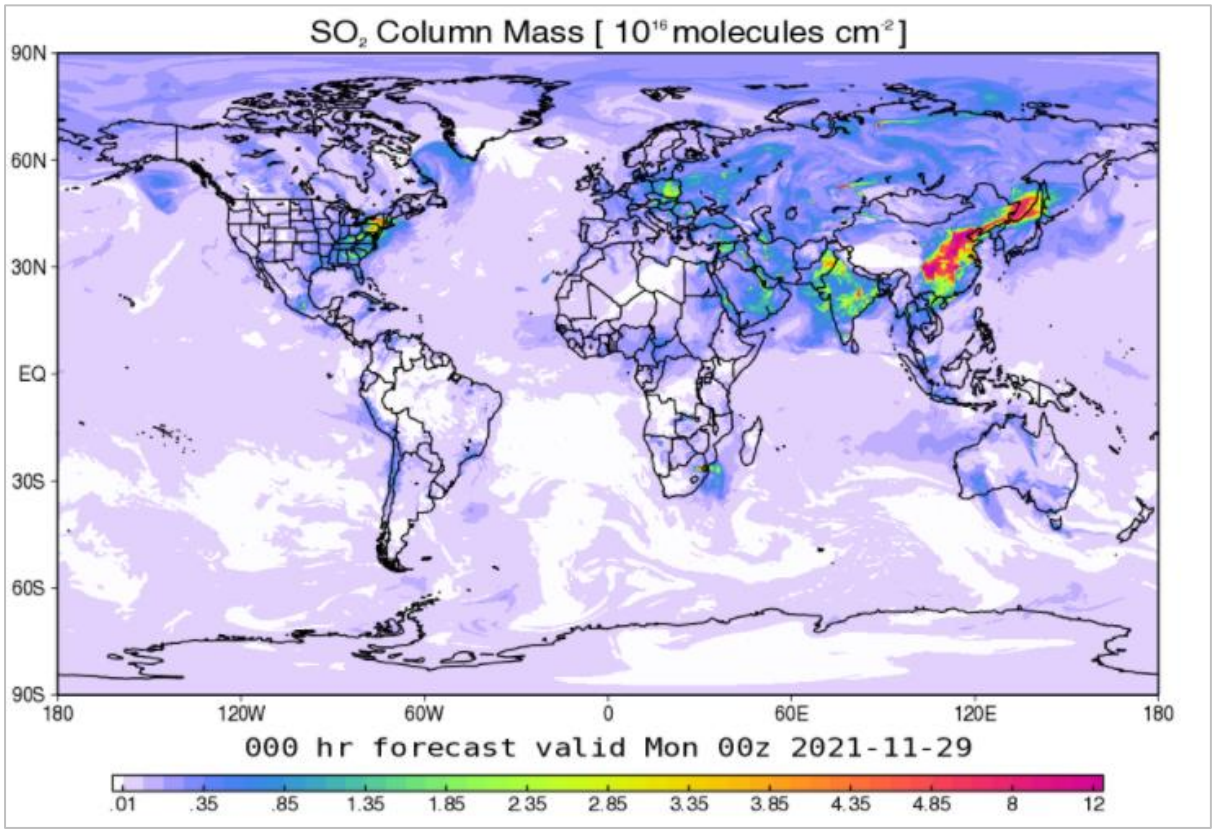


Figure 2.11 Global SO2 in Atmosphere (NASA, 2021)

Non-GHGs such as sulfur oxides (SO_x) and nitrogen oxides (NO_x), are responsible for poor air quality, and Green House Gases (GHGs) such as carbon dioxide (CO_2) and methane (CH_4), are responsible for climate change. These are the two major types of gases emitted by fuel oil. The combustion process oxidizes the sulfur content of the fuel, converting it to sulfur dioxide (SO_2) and sulfur trioxide (SO_3) molecules, resulting in SO_x emissions. Even though the co-benefits of sulfur and carbon reduction are unclear, SO_x emissions cause a cooling effect on the atmospheric particles and clouds. Therefore, this has also led to studies expressing concerns that reducing SOx emissions would reduce the cooling impact and may result in net warming (Haywood, 2021).

Crude oils include sulfur heteroatoms. Hydrogen sulfide (H_2S) which is contained in crude oils in the dissolved state (< 50 ppm by weight) is a toxic gas. Crude oils are classified as corrosive (sour) or non-corrosive (sweet) in simple terms based on the H_2S concentration within them. Sour crude is described as crude that contains more than 6 ppm of dissolved H_2S. Such sulfur compounds react with the iron and steel used in the refining process corroding the machinery, the container tanks, and the piping resulting in pyrophoric iron sulfide (Lang, et al., 2021).

As mentioned earlier sulfuric acid and sulfur dioxide are generated when petroleum products containing sulfur compounds are burned. Hydrodesulfurization and other catalytic hydrotreating processes strip the sulfur compounds from the refinery product streams. In the case of mercaptans, sweetening processes either eliminate the obnoxious sulfur compounds or turn them into odourless disulfides. When a crude's total sulfur content is assessed and if it exceeds 1%, it is characterized as corrosive or sour or heavy and less than 1% its sweet or light crude (Kikasu, 2021).

To avoid damage to pollution control systems in Euro 4/IV and above vehicles, low sulfur fuels with a ppm of less than 50 are required. The most efficient emissions control systems, such as diesel particulate filters, require maximum sulfur levels of 10 to 15 ppm. This is ultra-low sulfur fuel required to achieve the emission reductions needed to meet filter-forcing requirements (Zhai and Wolff, 2021). According to recent reports, while cleaner fuels will minimize SOx related premature mortality and morbidity, policymakers must weigh trade-offs that could result in climate change consequences. Sulfur Dioxide (SO_2) is a colorless, odorless air pollutant that is widely distributed and dangerous to breathe. However, calculating pollution can be done in a variety of ways. The simplest way to calculate transportation emissions is to multiply the amount of energy or fuel consumed by an appropriate "emissions factor," which is the ratio of emissions emitted per unit of energy or fuel consumed (Akpan and Fuls, 2021).

SO_2 accounts for 98% of SO_x emissions. The type of fuel used and, more specifically, the amount of sulfur in the fuel has an impact on sulfur dioxide (SO_2) emissions. To compute SO_2 emissions, calculate the total bunker intake (in tonnes) by the percentage of sulfur present in the fuel and then by the exact factor of 0.02 (in tonnes). For example, when burning marine fuel with a sulfur content of 2.5%, the acceptable emissions factor is equivalent to 50 kg SO_2 per tonne of fuel. The factor of 0.02 is exact and is derived from sulfur-oxygen chemical reactions (Kontovas, 2014).

The top ten countries that released the most anthropogenic SO_2 for 2019 - 2020, are shown in Figure 2.12. Anthropogenic refers to something that occurs as a direct or indirect consequence of human activity. India is the world's largest SO_2 emitter, accounting for over 21% of global anthropogenic SO_2 emissions, led by Russia and China. South Africa's SO_2 emissions, which are ranked seventh on the list, are also entirely anthropogenic (GreenPeace, 2021). The South African government relaxed SO_2 emission regulations for coal power plants in April 2020,

more than doubling the allowed emission rate. This call was in support of the country's power utility companies, which considered compliance with SO_2 regulations expensive to the economy. In 2021, South Africa's coal-reliant power utility, Eskom, has become the world's biggest emitter of SO_2 according to the Centre for Research on Energy and Clean Air (CREA). Eskom, on the other hand, has stated that it has begun a program to convert retiring coal-fired power plants to renewable energy sources (CREA, 2021)

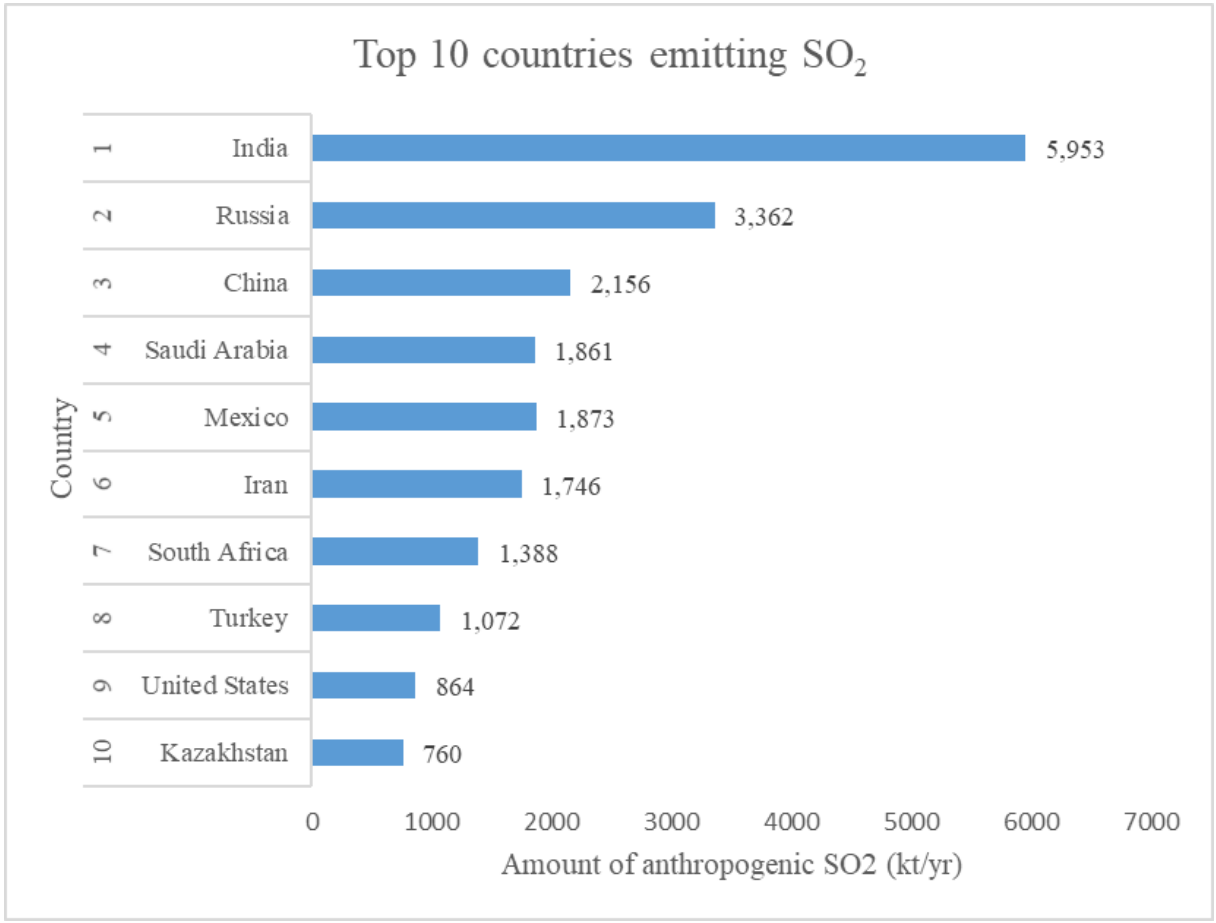


Figure 2.12 Top Countries emitting SO2 (GreenPeace, 2021)

2.2.5 SOx Regulations and Policies

Given the dangers of SOx emissions globally, there are regulations in place for all industrial sectors including transportation to adhere to across the world. The chart shown in Figure 2.13 depicts the global contribution of major industry sectors and natural sources to overall SO_2 emissions, expressed in kilotonnes per year (GreenPeace, 2021). Environmental organizations continually encourage policymakers to suspend investments in fossil fuels and move to cleaner energy sources, but they must also improve emissions standards and mandate the use of fuel gas pollution reduction technologies at power plants and other industrial SO_2 emitters, as well as switching to renewable energy sources.

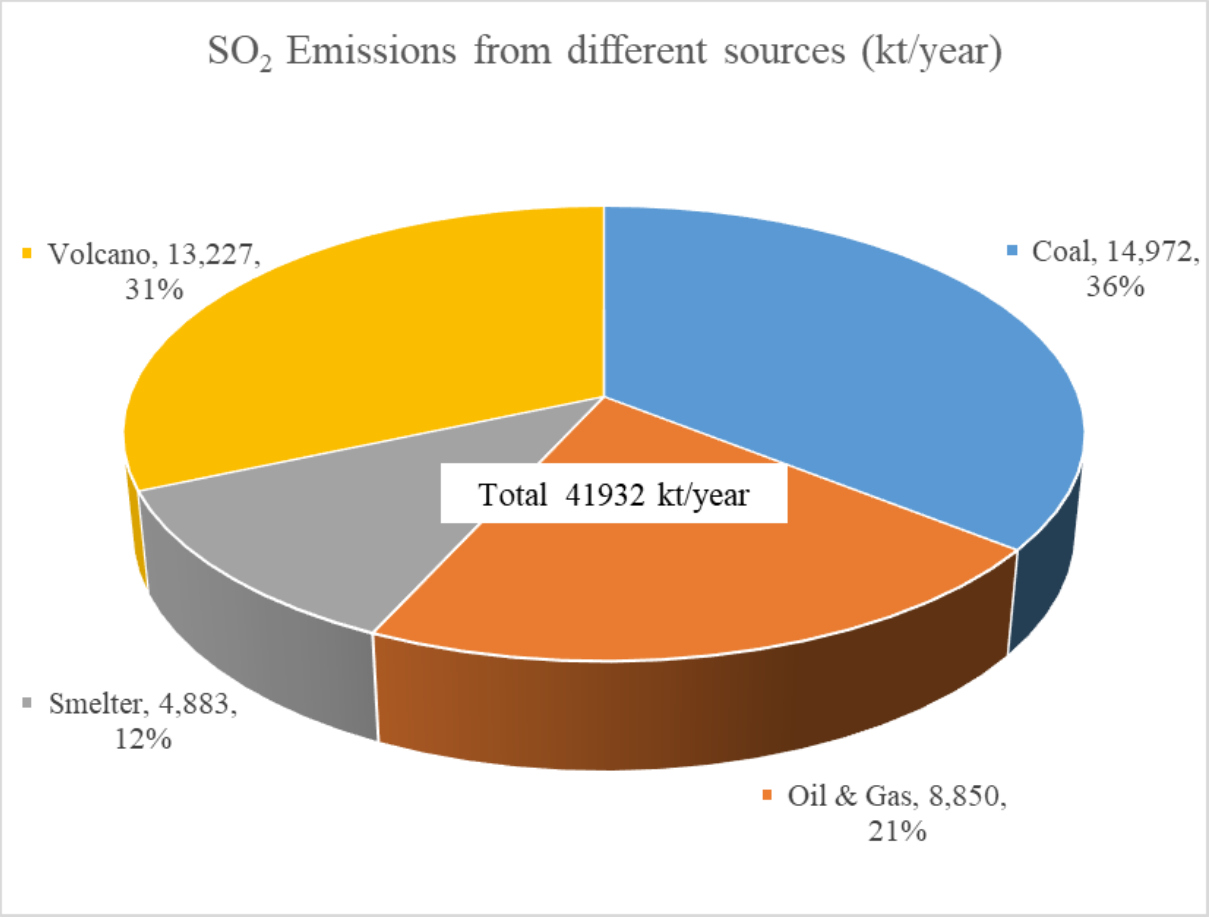


Figure 2.13 Sources of SO2 emissions (GreenPeace, 2021)

The Heavy Duty Diesel Initiative (HDDI) of the Climate and Clean Air Coalition (CCAC) is a global initiative to introduce low-sulfur fuels and cleaner diesel cars. It is a key output of the CCAC and HDDI, which has been funded and built to direct efforts in the years to follow to nearly eliminate fine particles and black carbon emissions from new and current heavy-duty vehicles and engines. This policy also serves as an invitation to join the HDDI and CCAC in its worldwide desulfurization campaign, directing the efforts of agencies, governments, and specialists concerned with the environmental and clean air benefits of low sulfur fuels and greener technology (CCAC, 2021).

Many strategies have been established based on the oil and diesel fuel demand that looked at global oil flows in terms of quantity and quality, as well as refinery studies that looked at various refinery upgrades which allowed for the development of low sulfur diesel fuels. As part of this strategy, several case studies in various regions were examined, and the health benefits of moving to low sulfur fuels and cleaner diesel vehicles were modelled. This does not include countries that have already implemented a minimum of 50 ppm fuel sulfur requirements and related Euro 4/IV equivalent vehicle emissions standards. It's worth noting that there are significant additional environmental requirements for ultra-low-sulfur fuels and related standards, as well as the possibility of additional benefits from increased compliance and enforcement initiatives (CCAC, 2021).

According to the World Health Organization (WHO), air pollution is responsible for one out of every eight deaths worldwide, making it the world's single most serious environmental threat. Diesel engines provide 85% of all road transportation. Diesel engine exhaust is inherently carcinogenic to humans, polluting the environment and causing premature death. Fine inhalable particles that are 2.5 micrometers and smaller called Particulate Matter ($PM_{2.5}$) are to blame. Sulfur-rich fuel can also harm structures that control nitrogen oxides, a pollutant

that promotes smog and the formation of more $PM_{2.5}$. By 2030, there will be an immediate need to reduce short-lived climate pollution by introducing low-sulfur fuels and related vehicle emission standards.

High-sulfur fuels are still used in more than half of the world's countries. This is necessitating a revised list of fuel quality requirements as well as a rapid transition to low-sulfur fuel production at their refineries. The total mass of $PM_{2.5}$ produced by an engine in general is made up of several components amongst which three main components are listed below (Attia et al., 2022):

- Sulfate Fragments, which include sulfuric acid and absorbed water
- Solid Fraction, which includes black carbon and ash
- Soluble Organic Fraction, which includes unburned gasoline and oil

Depending on the engine technology, engine load, and gasoline sulfur concentration, the amount of each of these components varies dramatically. The mass of sulfates formed increases as the sulfur content of the fuel increases, resulting in an increase in total $PM_{2.5}$. To reduce these contaminants, the planet follows two principles, which are (El-Dorghamy et al., 2021):

- Filter-Forcing Vehicle Standard
- Fuel Policy Package

European fuel rules establish a maximum of 10 ppm sulfur diesel to comply with Euro 6/VI vehicle emissions requirements. In the United States, where heavy-duty vehicle emission rules from 2007 and 2010 and the newer Tier-3 passenger vehicle emission standards have led to the introduction of diesel particulate filters, the overall diesel sulfur level is 15 ppm. Chile and Canada are both in the same boat. All refining countries are obliged to strive for 10/ 15 ppm

diesel production to achieve universal adoption of diesel particulate filters in the vehicle fleet .

Reducing the sulfur content of refined fuels necessitated the installation of specialized refining units since sulfur can be found in all crude oils as an impurtity. This does cost hundreds of millions of dollars. Distillate hydrotreating is the most popular method for reducing sulfur in diesel fuel. To reduce the sulfur content of diesel generated at a refinery, existing distillate hydrotreating capacity must be replaced, expanded, or retrofitted, and hydrogen supply must be increased. To reap the benefits of desulfurization, in some developing countries such as Kenya, additional criteria which include age limits, emission limits, and effective compliance and enforcement methods, have been adopted.

Fuel specifications and emission standards are different for different fuel types as well as differ from country to country. The global maximum limits in on-road diesel sulfur vary from 10 ppm in the most developed regions to 12,000 ppm in developing countries, whereas gasoline varies widely from 10 ppm to 2500 ppm. However, over the last few years, there appears to be a continuous good trend toward decreased sulfur content in diesel.

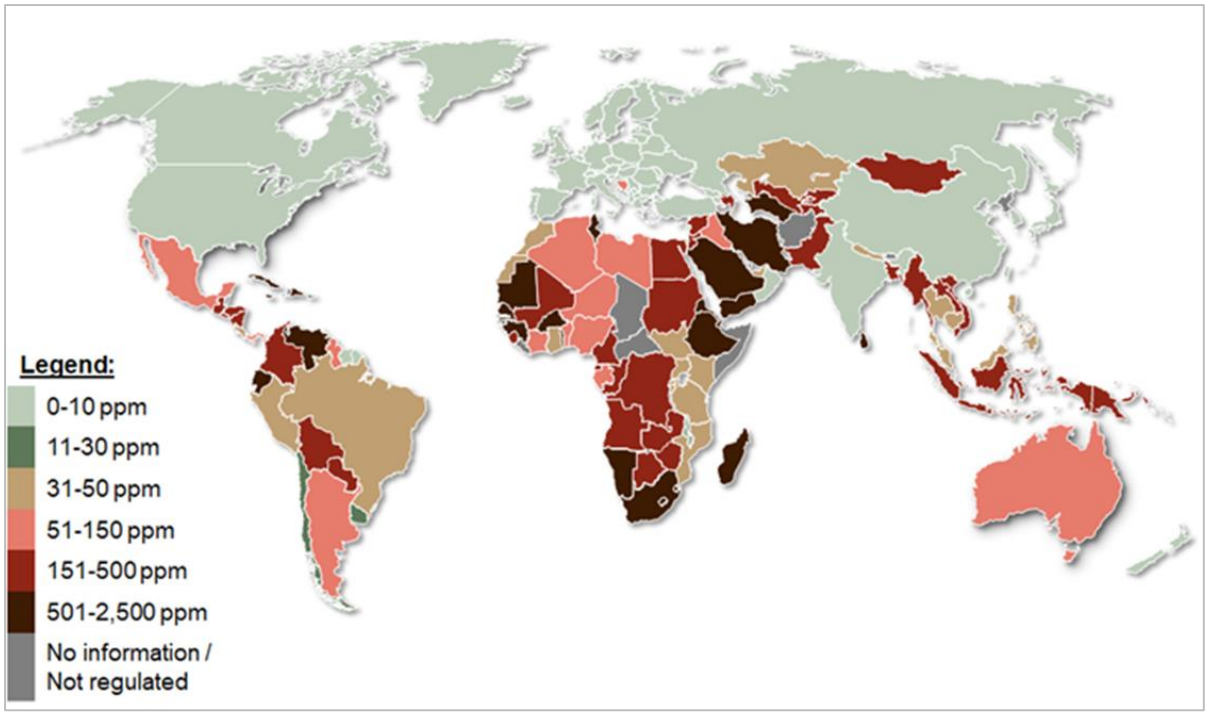


Figure 2.14 Maximum Sulfur Limits in Gasoline in 2021 (Stratas Advisors, 2021)

(reproduced with permission from Stratas Advisors)

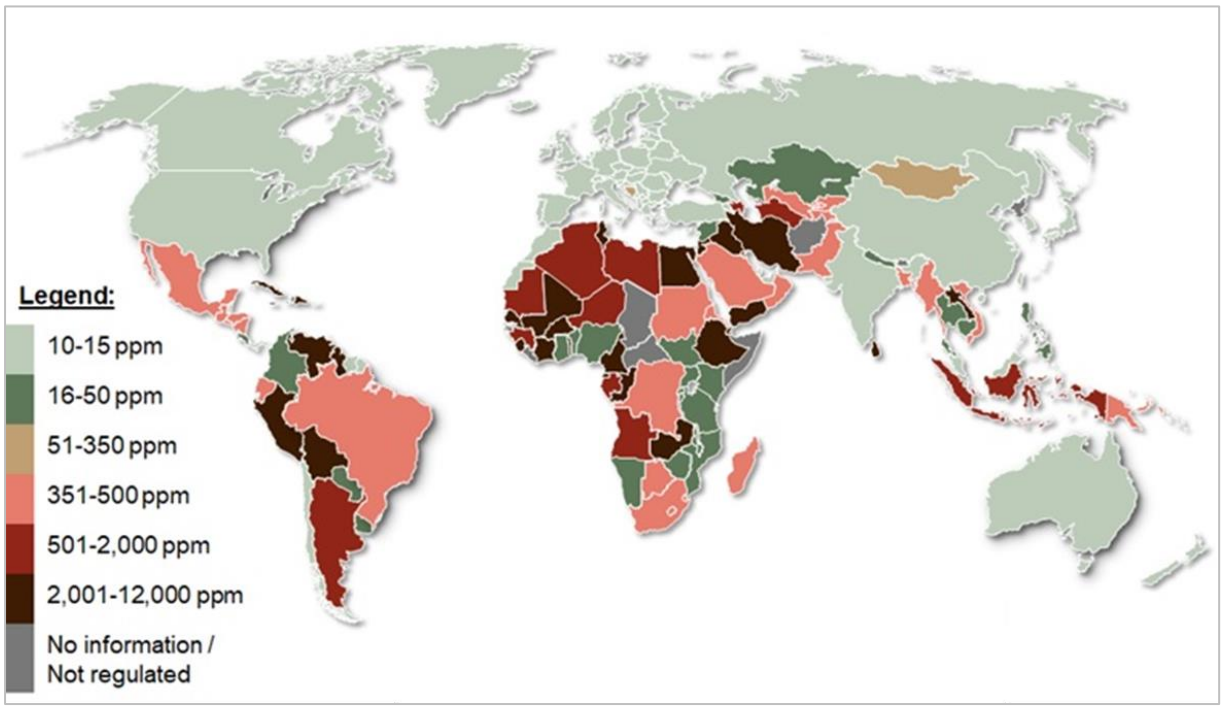


Figure 2.15 Maximum Sulfur Limits in On-Road Diesel in 2021 (Stratas Advisors, 2021)

(reproduced with permission from Stratas Advisors)

Global energy transition, and oil and gas consulting firms such as Stratas Advisors are confident that many countries have embarked on a journey to position themselves and achieve progress in achieving low SOx emissions shortly through governmental measures. Figure 2.14 and Figure 2.15 show the maximum sulfur limits in Gasoline and On-Road Diesel for 2021. Although, governments and automakers continue to delay the implementation of low sulphur fuel standards owing to COVID, poor market strategy, lapsed engine technology and many other uncertainties at the local, regional and global level (Stratas Advisors, 2021).

Figure 2.16 and Figure 2.17 show the expected maximum sulfur limits in gasoline and on-road diesel by the year 2025. Four key parameters are considered year after year to determine the list of countries positioning themselves towards low sulfur content in fuel (Stratas Advisors, 2021):

- Maximum permissible limits in national guidelines and regulations
- Year of implementation for sulfur limits as required by legislation
- Restrictions imposed by local or regional requirements
- Market levels to measure countries that have the same legislated cap

In te order of significance, the first parameter is the priority criteria to map the countries. Along with this and the other three parameters are used in ranking the countries implementing emission controls. Although, rapid shifts in consumer behavior as a result of the pandemic, as well as a stronger push by policymakers towards a low-carbon future, have resulted in a sharp drop in oil demand expectations.

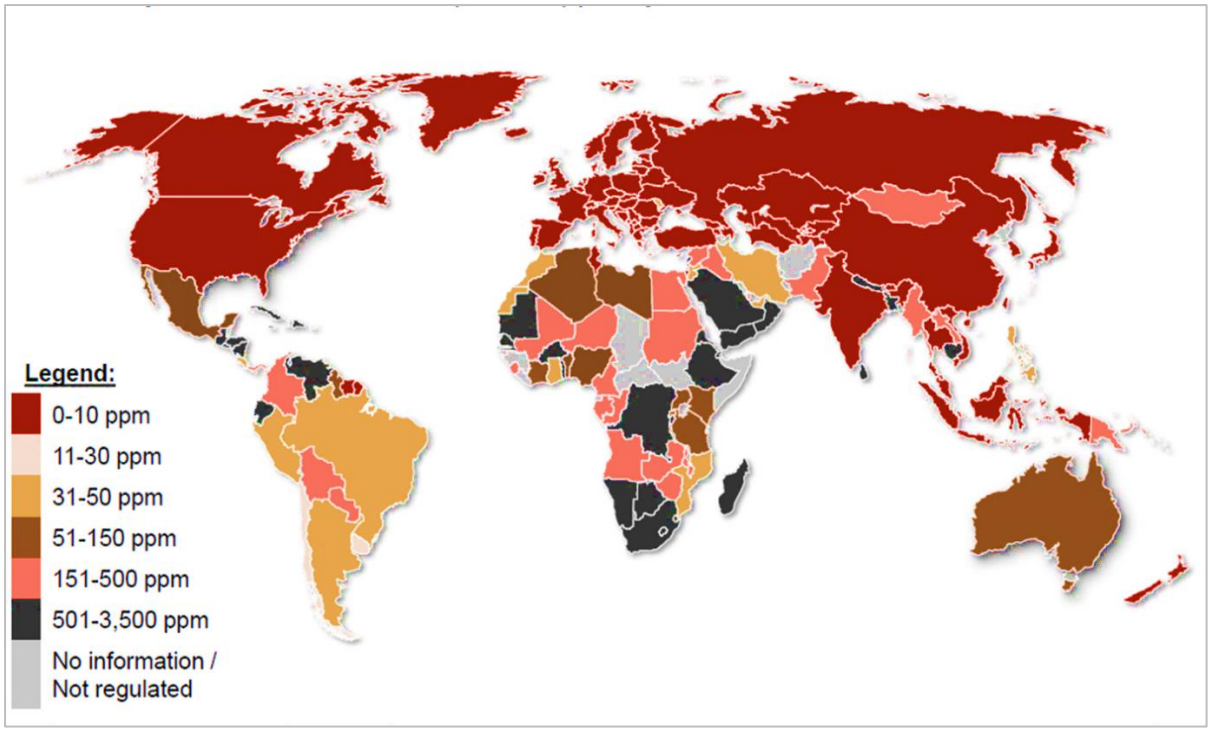


Figure 2.16 Maximum Sulfur Limits in Gasoline in 2025 (Stratas Advisors, 2021)

(reproduced with permission from Stratas Advisors)

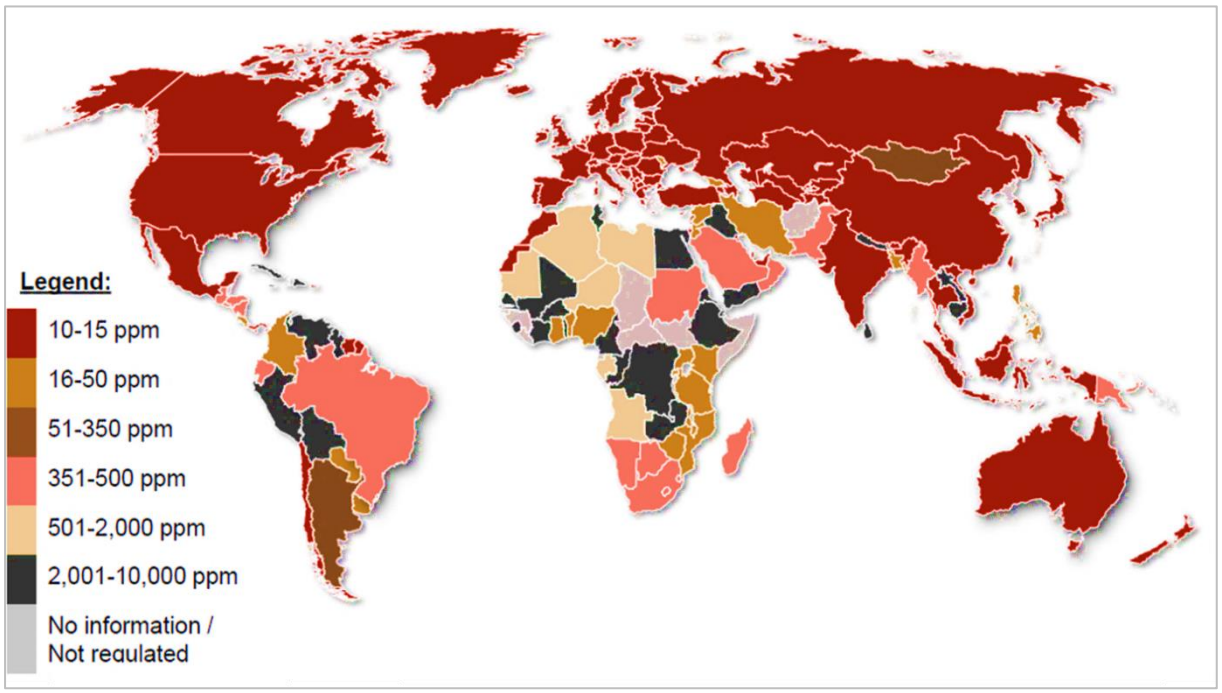


Figure 2.17 Maximum Sulfur Limits in On-Road Diesel in 2025 (Stratas Advisors, 2021)

(reproduced with permission from Stratas Advisors)

According to the IEA, the global total oil demand was 91.0 mb/d at the end of 2020, while supply was 93.9 mb/d. This includes inland deliveries, foreign marine bunkers, refining fuel, crude for direct burning, oil from non-conventional sources, and other sources of supply. Other middle distillates and diesel are becoming more common as transportation fuels. Additionally, there is also progress worldwide in the area of clean-fuel vehicles using biodiesel, hydrogen, electricity, ethanol, Liquefied natural gas (LNG), LPG, and natural gas, etc., focusing on cleaner energy technologies. To meet ambitious mid-century targets for net-zero emissions, a far stronger shift toward a cleaner energy future would be needed. More clear government policies and legislative action, as well as significant behavioral improvements, would be needed (IEA, 2021). Figure 18 shows the global emission legislation by world region regulated by different legislation packages. All regulations limit the maximum emissions in milligram/kilogram (mg/km) for each vehicle sold (Continental Automotive, 2019) (Revo, 2021).

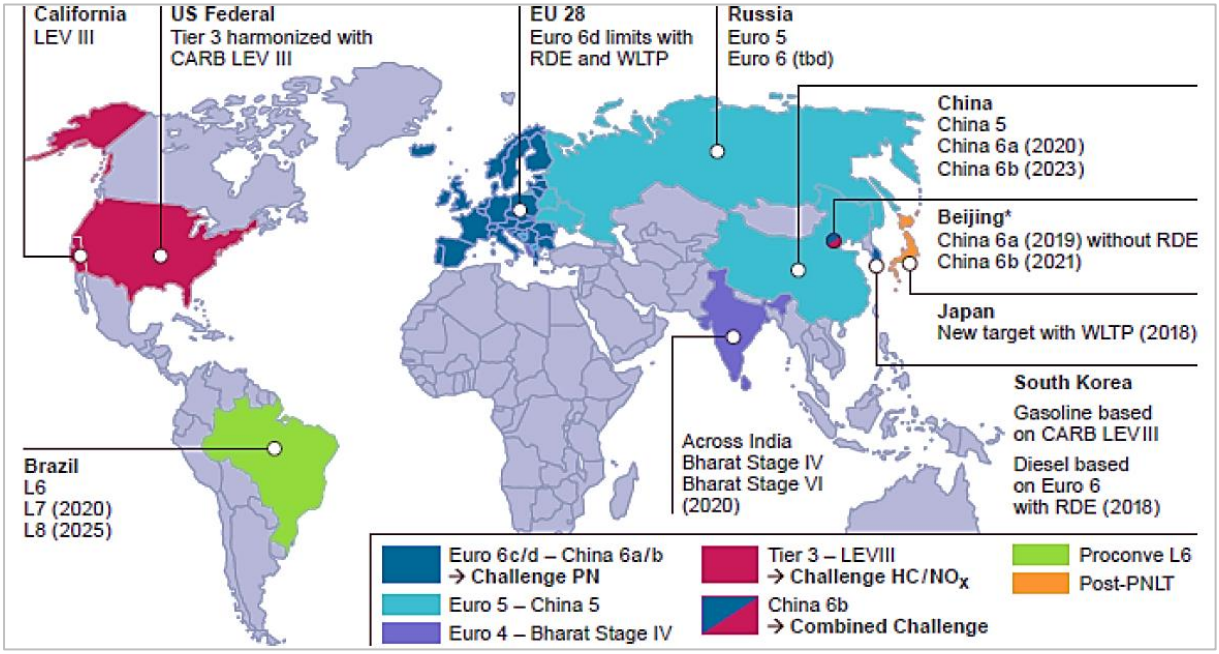


Figure 2.18 Worldwide Emission Standards (Continental Automotive, 2019) (Revo, 2021)

Not just the road transport and coal consumption, the maritime industry also is affected by sulfur emission control regulations. Currently, stricter limits on sulfur (SOx) emissions are already in place with 0.10% in Sulfur Emission Control Areas (SECA), however, the International Maritime Organisation (IMO) has set the sulfur limits in fuel oil from 3.50% to 0.50% by mass (0.50% m/m is 5000 ppm) global sulfur cap in January 2020 requiring the use of Very-Low Sulfur Fuel Oil (VLSFO) or compliant fuel blends. Unless the ship is equipped with an Exhaust Gas Cleaning System (EGCS) or scrubbers that enable the use of High-Sulfur Fuel Oil (HSFO) as an alternative, the cap regulation applies. (DNV, 2021).

2.2.6 Africa's stand towards Low Sulphur Fuels

The oil industry plays a strategic role in enabling the African economy, however, rapid urbanization and motorization in Africa in increasing air pollution from vehicle emissions. Africa is a large continent with 54 sovereign countries recognized by the United Nations. Some countries such as Nigeria, Libya, and Algeria have significant crude oil reserves and others such as Egypt, Nigeria, and South Africa, have several refineries. However, many of these countries do not have updated refineries or are not operating at full capacity. The rest of Africa have no oil reserves or refineries and is completely reliant on imports. There is growing awareness of the necessity to reduce fuel sulphur levels in Africa and that it will be easier and more efficient to do so under regional cooperation (Adeola et al., 2021).

Morocco was the first country to introduce the lowest limit of 10 ppm on the African continent even though it is fully dependent on fuel imports as of now. South Africa is expected to supply across the continent 10 ppm sulfur fuels as well by the end of 2023. Regulations relating to

climate change are causing a move away from traditional fuels. To meet the new regulations, several of South Africa's oil refineries will need to modernize their equipment. The plan in West Africa to reduce sulfur in fuel imports and to upgrade refineries is an encouraging effort. The harmonization of 50 ppm in Southern Africa will positively affect the landlocked countries of the region and is heavily dependent on South Africa's capability to implement its Clean Fuels 2 Program (CF2) by 2025 which require South African gasoline and diesel to contain no more than 10 ppm sulfur, among other provisions (Dane et al., 2019).



Figure 2.19 Fuel Imports and Exports in Africa (Stratas Advisors, 2021) (reproduced with permission from Stratas Advisors)

For several countries worldwide, sulfur reduction in fuels within the next five years is expected to be either 50 ppm or 10 ppm. Africa on the other hand has a different story to tell. The continent is divided by a) oil producing countries with refineries, b) non-oil producing countries with refineries, and c) non-oil producing countries without refineries that are fully dependent on imports as shown in Figure 2.19 (Stratas Advisors, 2021). So to speak, no country in Africa is self-sufficient in fuels. Out of the 54 recognized countries, 17 are landlocked and are heavily reliant on coastal countries on fuel quality and regulations, therefore, cannot impose their regulations (Sarpong and Bein, 2020).

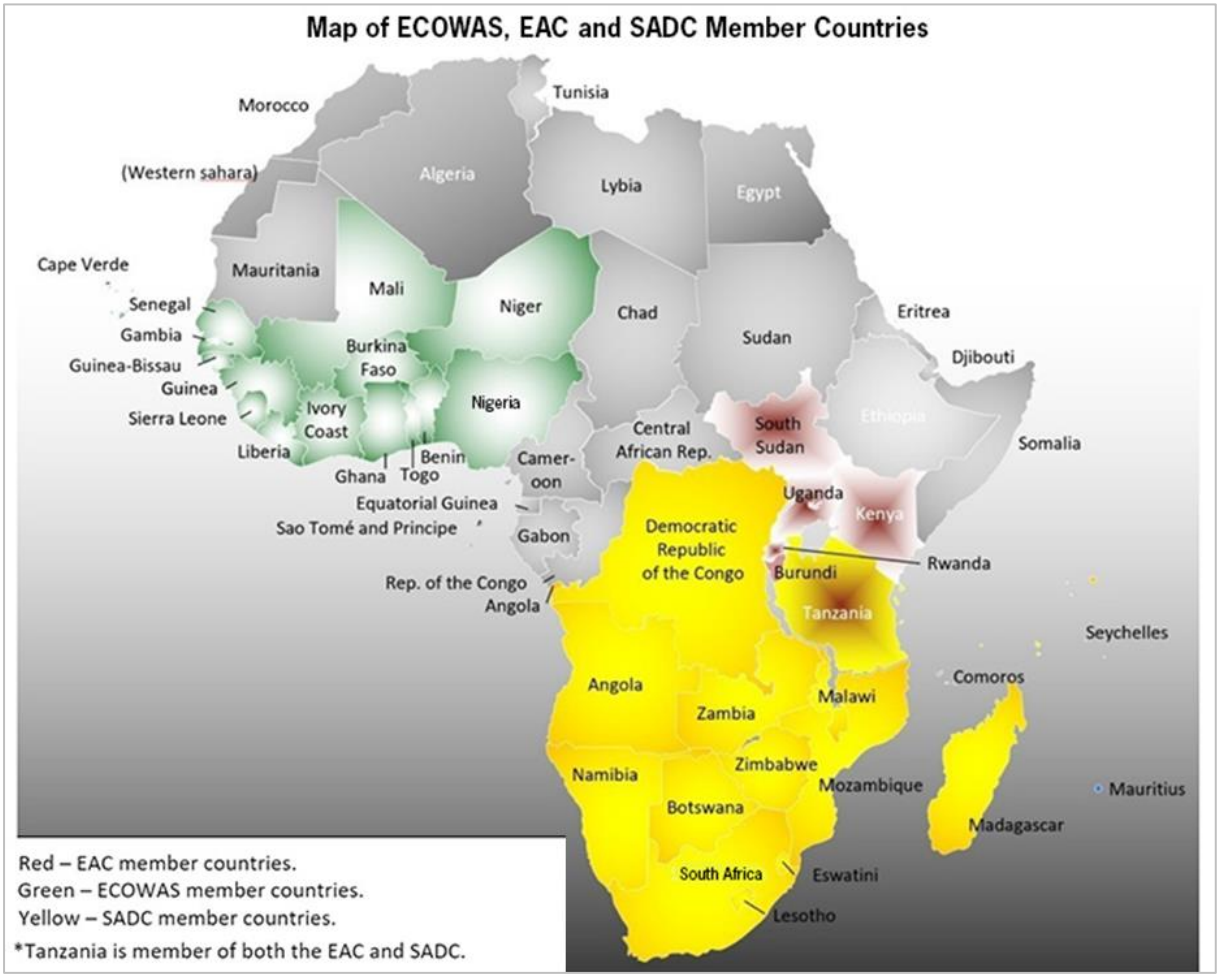


Figure 2.20 Regional Map within Africa (Stratas Advisors, 2021) (reproduced with permission from Stratas Advisors)

Regionally as well, Africa is divided as shown in Figure 2.20 with member countries of the continent associating themselves with region based strategic and political endeavours. In East African Community (EAC), the penetration of 10 ppm is occurring in the market by way of imports through Kenya and the new standards for 10 ppm sulfur fuels are expected to be drafted by 2022. The latest plan in the Economic Community of West African States (ECOWAS) is to import 50 ppm sulfur fuels by January 2021 and stop its regional production of higher than 50 ppm by January 2025. Southern African Development Community (SADC) agreed to reduce sulfur levels in fuels to 50 ppm or less by end of 2022 for importing countries and by 2025 for countries with refineries. Furthermore, the plan is to eventually reduce to 10 ppm between 2025 and 2030 for all countries in the region (Stratas Advisors, 2021). However, the majority of the issue in the continent continues to lie in upgrading the local refineries. For now, the move of sulfur reduction in Africa would not be followed by the implementation of stricter vehicle emission standards in many countries. Furthermore, old vehicles will continue to be imported from Europe and Asia, as border control is not efficient in the majority of the countries in Africa.

Major African economies like South Africa are still grappling with sluggish economic development, high unemployment levels, poverty, and a fossil-fuel-based economy, despite decades of democratic governance. The share of imports in the country's fuel consumption will likely increase, however, with the South African government's announcement regarding a major modernization of aging refineries in 2021 there seems to be a positive political sign (Rempel and Gupta, 2021). As of now, turning to imports will nevertheless allow a smoother transition to the supply of lower sulfur fuels in South Africa and its neighbors.

2.3 Desulfurization of Crude Oil Products

As mentioned in the previous sections crude oil is a complex mixture primarily consisting of hydrocarbons along with other minor constituents such as sulfur. The presence of elemental sulfur, mercaptans (RSH), and sulfides including polysulfides (RSnR) in crude oil convert to H_2S called sulfidation leading to corrosion along with ammonium bi-sulfide (NH_4HS) amongst other corrosions in the oil refinery (Subramanian, 2021). The recovery of pure hydrocarbon products from refineries is highly desirable as the presence of impurities results in undesirable effects.

The removal of minor constituents especially sulfur involves in various processes such as hydrogen treatment, MEROX process (mercaptan oxidation) and chemical treatment of the refinery distillates at various stages. As a result, the final streams (effluent) from petroleum plants contain a mixture of acidic and sulfur compounds that must be reduced to concentrations low enough to decrease acidity, odour and other harmful effects resulting mainly from sulfur impurities (Achaw and Danso-Boateng, 2021).

Elemental sulfur, Hydrogen sulfide (H_2S), and pyrite are the inorganic forms present in dissolved forms in minor quantities. Sulfides, thiols, and thiophenic compounds are the organic forms that are present majorly in crude oil. Other sulfur compounds that are simple to eliminate include cyclic sulfides (thiolanes) and aliphatic acyclic sulfides (thioethers); and aromatic sulfur compounds like benzonaphthothiophene that are difficult to remove using traditional Hydrodesulfurization (HDS) or thermal techniques due to their complex structures (Rezvani and Aghmasheh, 2021).

Refineries produce large volumes (up to 150 gallons per hour) of spent caustic streams (effluent) because of using aqueous Sodium Hydroxide to treat crude oil and its distillates.

These effluents have a variety of compounds such as phenols, carboxylates, naphthenates, carbonates, sulfides, bisulfides, sulfates, thiosulfate, sulfonic acids and other sulfurous, organic and inorganic compounds (Onojake and Waka, 2021). Discharge of these effluents to surface waters or sewage treatment without proper processing is prohibited due to extreme toxicity and alkalinity. Consequently, petroleum industries should aspire to not only produce clean fuels but also effluents that are safe for disposal.

2.4 Desulfurization Techniques

Several techniques are available for the reduction or removal of sulfur compounds from crude oil and its distillates. The classification of desulfurization techniques described by Babich and Moulijn (2003) can be based on three factors such as: (i) conversion of organosulfur compounds during desulfurization, (ii) role of hydrogen and (iii) the type of process used.

2.4.1 Conventional Desulfurization Techniques

Hydrodesulfurization (HDS) along with other carbon rejection technologies such as coking and catalytic cracking (FCC) are traditionally used to remove sulfur and its derivatives from fuel (Javadli and De Klerk, 2012). Among them, the widely used conventional catalytic method for sulfur reduction is HDS which operates in presence of hydrogen and catalysts under severe conditions (Srivastava, 2012).

2.4.1.1 Hydrodesulfurization (HDS)

HDS is the most common method which is extensively used for desulfurization of crude oil and other refinery streams (Javadli and De Klerk, 2012). The process involves in the conversion

of organosulfur compounds to Hydrogen sulfide (H_2S) in a fixed bed reactor with a suitable catalyst, where an oil stream and hydrogen are co-fed under elevated temperature and pressure (Babich and Moulijin, 2003). The resultant H_2S removed from HDS can be converted to elemental sulfur by Clause process (Song, 2002). Many catalysts are available for HDS process but the standard catalysts being used are $NiMo/Al_2O_3$ and $CoMo/Al_2O_3$ with reactor conditions ranging from temperature 200 to 425 ^oC and pressure from 1 to 18 megapascal (MPa). The reactor design and its conditions such as temperature, pressure, and selection of catalyst depend on the application, nature and concentration of the Sulfur compounds in the feed stream (Babich and Moulijin, 2003). HDS process can efficiently remove aliphatic organosulfur compounds from low boiling point oil fractions such as sulfides, disulfides, thiols and mercaptans as they are highly reactive. Organosulfur compounds from high boiling point fractions contain thiophene, benzothiophene and their alkyl derivatives along with other polynuclear Sulfur species which are least reactive and cannot be removed by HDS (Babich and Moulijin, 2003).

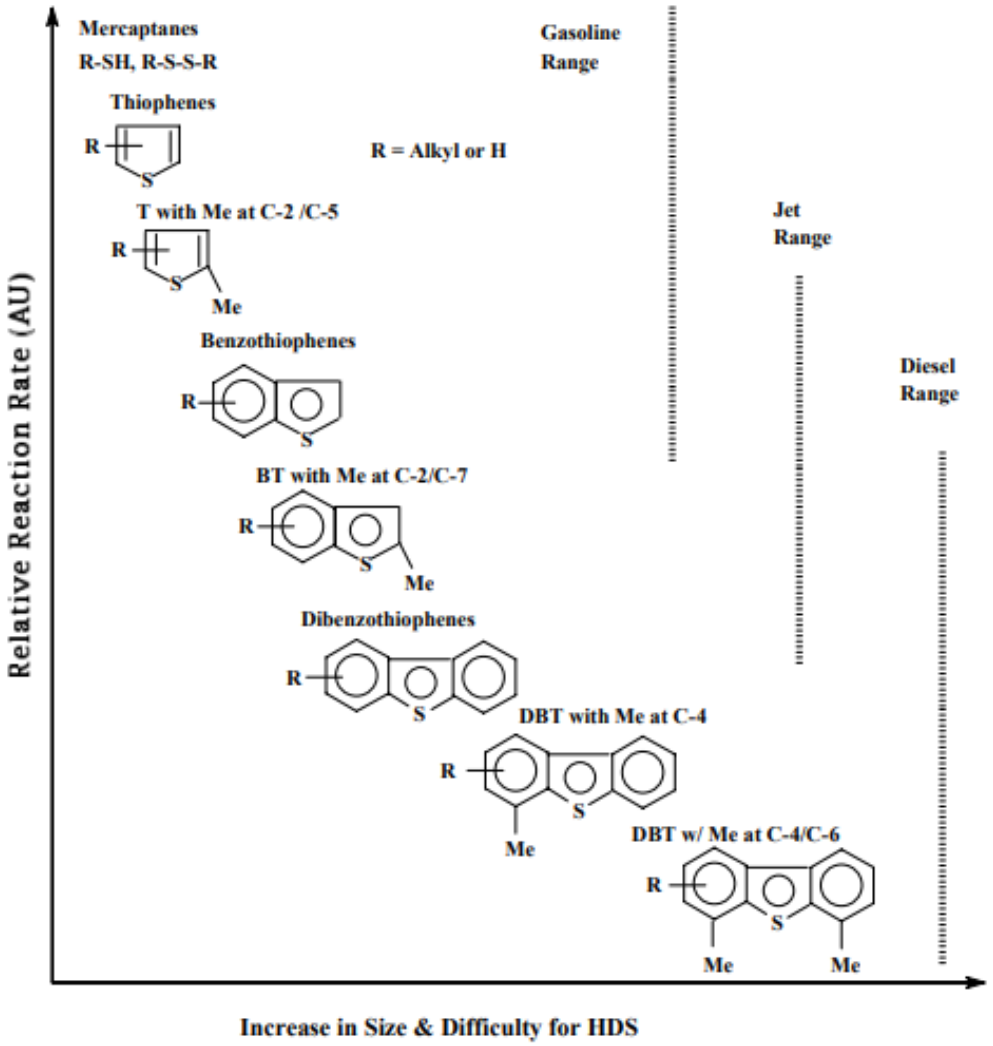


Figure 2.21 Reactivity of various sulfur compounds in hydrodesulfurization versus their ring sizes and positions of alky substitutions on the ring (Song, 2002)

Although HDS is widely used for desulfurization, the requirement of regular H_2 supply besides high temperature and pressure makes it economically undesirable (Lin et al., 2010). It may also result in unwanted side reactions such as coke formation, decrease in the octane number and catalytic deactivation due to severe operating conditions (Aitani et al., 2000). Furthermore, deep desulfurization of feed streams to remove refractory (less reactive) sulfur compounds may not be effective using HDS (Srivastava, 2012).

2.4.2 Alternative/Non-conventional Desulfurization Techniques

Methods that do not require hydrogen for sulfur reduction are generally categorized under non-conventional or non HDS based desulfurization techniques as most of them operate without hydrogen (Babich and Moulijin, 2003). Though, traditional techniques are effective in desulfurization, the methods involve in expensive processing and their carbon footprint is substantial (Javadli and De Klerk, 2012). Therefore, alternative desulfurization techniques based on oxidation, extraction, adsorption, biodesulfurization or their combinations have gained much significance over traditional methods.

2.4.2.1 Oxidative Desulfurization

Oxidative desulfurization is a process in which a chemical reaction between organic sulfur compound and an oxidant results in the oxidation of sulfur compound to sulfones which can be easily separated from hydrocarbons liquid fuels due to their higher polarity (Javadli and De Klerk, 2012; Srivastava, 2012). This method is advantageous over conventional HDS method as it can be performed in the liquid phase under very mild operating conditions of near room temperature and atmospheric pressure (Agarwal and Sharma, 2009). The refractory sulfur species such as dibenzothiophenes (DBT) can also be easily oxidized under low temperature and pressure which is not possible in HDS unless the severity of the conditions is increased (Ron et al., 2004). Various oxidizing agents such as nitrogen oxides, nitric acid, hydrogen peroxide, per acids, ozone, t-BuOOH, oxygen, air etc can be used (Agarwal and Sharma, 2009). Generally, oxidation in combination with other separation methods such as solvent extraction, adsorption, distillation or decomposition can be used in oxidative desulfurization in order to separate or remove the oxidized sulfones from hydrocarbon fuel.

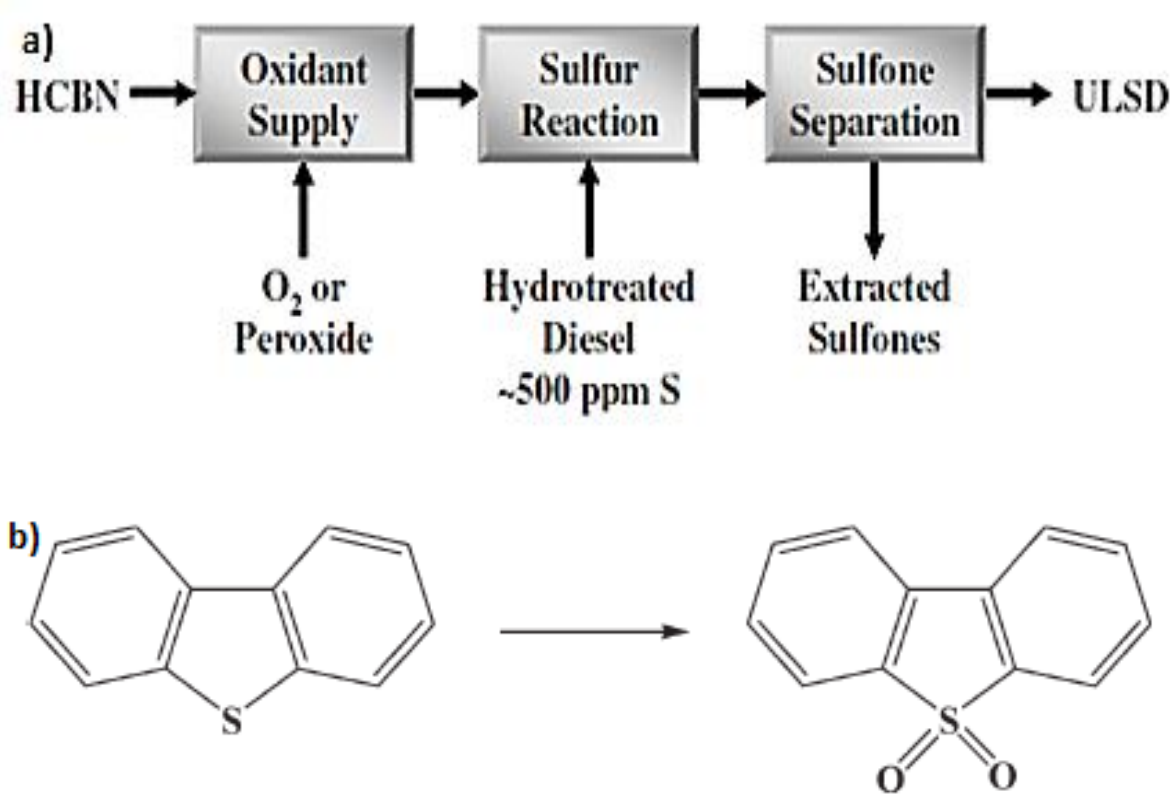


Figure 2.22 (a) Universal Oil Products (UOP)/Eni Oxidative Desulfurization Process (Ron et al., 2004); (b) Oxidation of DBT to corresponding Sulfone (Srivastava, 2012).

Desulfurization based on oxidation can achieve up to 85% of sulfur removal but the use of many oxidants might result in oxygen incorporation into the treated oil, dehydrogenation, condensation and polymerization. In oxidation reactions where Nitrogen Oxides (NO) are used as oxidants, use of 1 to 20 v% of NO's is recommended as higher concentrations of NO's with petroleum vapors within the reactor might form dangerous explosive mixtures (Aitani et al., 2000). Additionally, the sulfone waste management at the end of the process and increase in operation cost due to increased sulfur feed requiring higher oxidant consumption are the other disadvantages of this process (Ito and Van Veen, 2006).

2.4.2.2 Extractive Desulfurization

Extraction of sulfur compounds from refinery streams depends on the solubility difference of sulfur compounds and the hydrocarbons in selected solvents. As organo sulfur compounds have higher solubility than hydrocarbons, they are extracted into the solvent and the sulfur rich solvent is separated from the hydrocarbon stream (Gawande and Kaware, 2014). Extractive desulfurization is a liquid/liquid separation process with two liquids (feed stream and solvent) being immiscible. Different solvents such as acetone, ethanol, polyethylene glycols, nitrogen containing solvents and several ionic liquids have been tried with 50-90% of sulfur extraction from the hydrocarbon strems (Babich and Moulijin, 2003).

According to Babich and Moulijin, (2003), the process flow consists of a mixing tank where the feed stream is mixed with appropriate solvent for the sulfur compounds to be extracted into the solvent. The mixture is then transferred into a separator to separate hydrocarbon stream (which can be processed further) from the sulfur rich solvent. This solvent mixture is further distilled to remove sulfur compounds from solvent. The solvent is recycled and sent to the mixing tank. The process is attractive due to: low temperature and pressure requirements for operating which avoid the chemical conversion of feedstock; not requiring H_2 resulting in energy saving and; the process being purely physical resulting in easy separation.

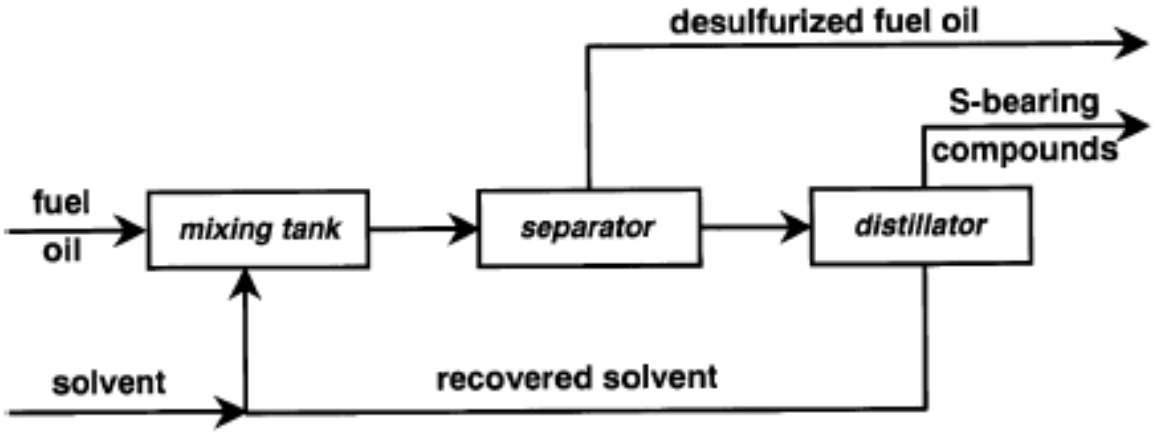


Figure 2.23 General process flow of extractive desulfurization (Babich and Moulijin, 2003).

The productivity of this method is limited by the solubility of the organosulfur compounds in the solvent (Babich and Moulijin, 2003). The viscosity of the feed stream and solvent should be low and different boiling point of solvent and sulfur compounds are preferred to enhance mixing and extraction (Javadli and De Klerk, 2012). Sometimes, the separation of sulfur compounds can be poor, and the recovered solvent might contain compounds extracted from feed stream that are difficult to remove by distillation which can affect quality of both hydrocarbon stream and solvent recovered.

2.4.2.3 Biodesulfurization

Biodesulfurization (BDS) is an alternate technology based on biological activity and processes that could remove sulfur from oil. The process captures on microorganisms' requirement of sulfur as a growth factor and as important element for their physiological activities, which in a possible approach in decreasing fuel acidity (Boniek et al. 2015). It is a complementary method

used with HDSand highly advantageous for removal of sulfur in fossil fuel. This process allows the removal of the sulfur atom at moderate temperatures and pressures. In addition, it may also be considered more advantageous than the HDS, since it retains more energy (Gray et al. 2003).

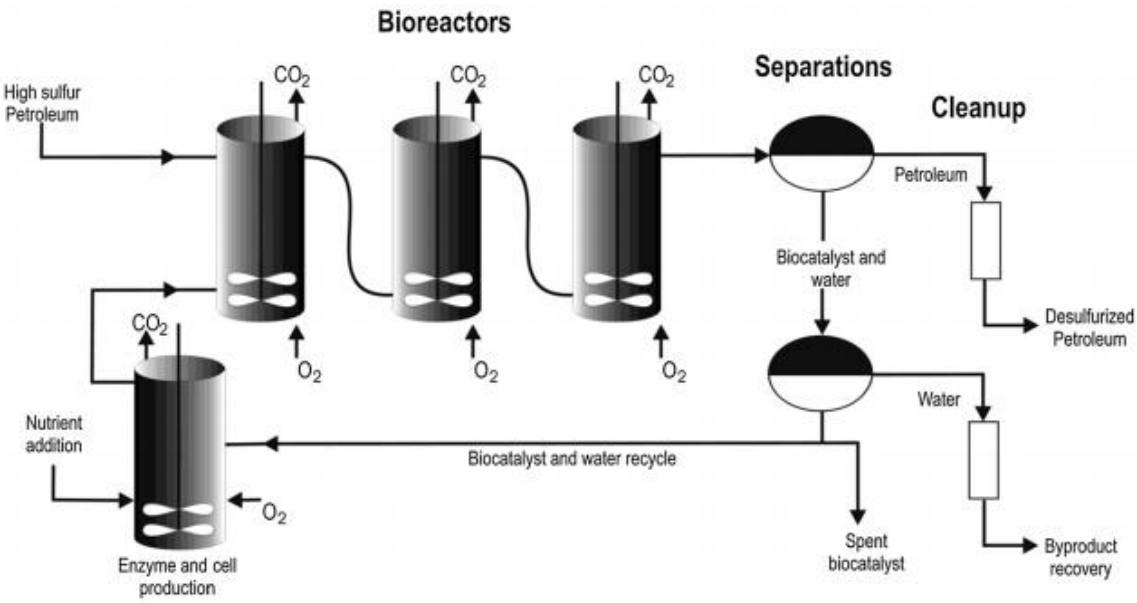


Figure 2.24 Biodesulfurization Process Operations (Boniek et al. 2015)

Biodesulfurization typically takes place in a continuous stirred tank reactor containing biocatalyst slurry, high-sulfur petroleum feedstock, and oxygen as shown in the Figure 2.24. The process then separates desulfurized petroleum from the aqueous biocatalyst output stream.

Aside from the obvious advantages of biodesulfurization, the industry has new legislation in place for which businesses can spend literally tens, if not hundreds, of billions of dollars over the next decade or longer to comply. As feedstock to refineries change, there must be an accompanying change in refinery technology. This means a movement from conventional means of refining heavy feedstock typically using coking technologies to more innovative processes that will coax the last drips of liquid fuels from the feedstock.

2.4.2.4 Adsorptive Desulfurization

Adsorptive desulfurization is a simple and economically feasible method based on the adsorption of sulfur compounds onto the solid sorbent material (Agarwal and Sharma, 2009). It can be classified into two: physical adsorptive desulfurization where sulfur compounds are physically adsorbed without being chemically converted and reactive adsorptive desulfurization where organic sulfur compounds chemically bound with adsorbent as sulfide. Depending on the process and feedstock used, the adsorbent can be regenerated thermally or by flushing with a desorbent, and the condensed sulfur can be removed as H_2S, SOx, or elemental sulfur (Javadli and De Klerk, 2012).

Several adsorbent materials based on carbon materials, metal oxides, metal sulfides, reduced metals, zeolite based materials have been used to desulfurize different petroleum fractions (Kim et al., 2006).

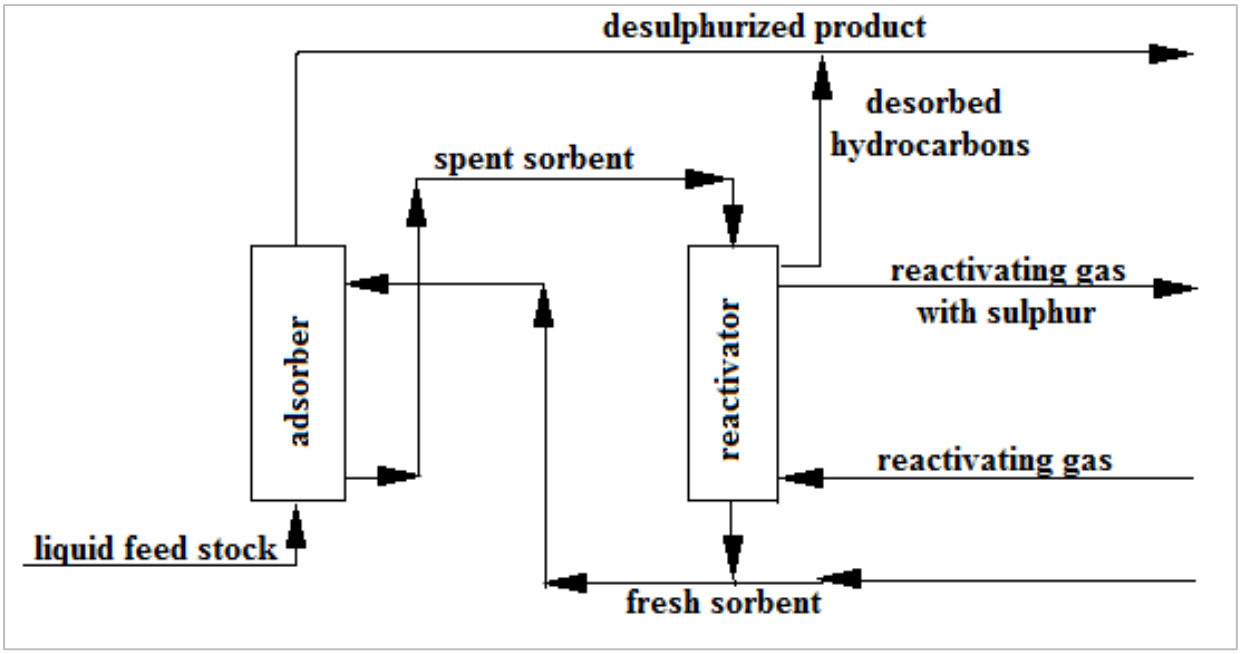


Figure 2.25 Simplified adsorptive desulfurization flow process (Babich and Moulijin, 2003)

The efficiency of adsorbent material primarily depends on its adsorption capacity, selectivity for sulfur species, durability and regenerability (Babich and Moulijin, 2003). Many adsorbents that have been developed for adsorption have acceptable levels of desulfurization but are inefficient to be used at industrial level (Javadli and De Klerk, 2012; Agarwal and Sharma, 2009). A detailed discussion on adsorptive desulfurization will be included in membrane technology section of this chapter.

Although there are many physical and chemical separation techniques as well as the more recent biological separation techniques available in the market and various published literature. The biological technology known as Biodesulfurization (BDS) captures microorganisms' requirement of sulfur as a growth factor and as an important element for their physiological activities, which is a plausible approach in decreasing fuel acidity (Jatoi et al., 2021). Only a

few of the desulfurization methods mentioned in this section are considered successful since most of these are inefficient at the industrial level as of today but research on scalable processes is still in progress. To a large extend conventional methods such as hydrodesulfurization have been widely used commercially for sulfur removal.

2.5 Membrane technology

The world demand for fuel is rapidly growing due to rapid growth of automobile industry and increased product demand. Higher yields of valuable products from petroleum industry requires refining and methods that are expensive. This reliance has been a significant source of concern as the exhaust gas from fuel combustion is becoming a threat to the environment. The present situation of the world strongly prompts energy efficiency in all energy consuming sectors for sustainable development to reduce emission and meet the product demand. The world should comply with constant change and tightening of the fuel standards and regulations to reduce vehicle pollution and greenhouse gas emissions (Seddon and Zhang, 2018). The renewable energy has become a global trend with many countries focussing on solar, wind, nuclear power and bio-fuel sources to replace fossil fuels. However, renewable sources could take many generations to compete or replace the cheaper conventional fuels in order to cope with growing energy demand (Nehlsen, 2006).

Membrane technology is a promising substitution over traditional separation processes with waste minimization and zero discharge. Through the combination of energy supplies and diverse technologies, as well as the recovery and recycling of useful materials from waste streams, current industries are focusing on a clean and sustainable future (Singha et al., 2017; Singha et al., 2013). They are crucial for various commercial applications in petrochemical,

chemical, food, pharmaceutical, semiconductor, biotechnological, and environmental industries as they play a significant role in minimizing the environmental impact and lowering the operating costs owing to their efficiency, high stability and ease of operation, adaptability to changes in process streams and simple control schemes (Vinh-Thang and Kaliaguine, 2013; Zhao et al., 2004).

Membrane is a selective barrier that allows certain components to pass through it (permeate) and retains non selective species (retentate or concentrate) in the liquid or gas mixture. Currently, some industrially significant membrane separation processes are already implemented at commercial scale while some others are at more or less advanced development stage, and some to be desirably developed (Vinh-Thang and Kaliaguine, 2013).

2.5.1 Membrane technology for desulfurization process

Desulfurization of crude oil products is accomplished using a variety of physical and chemical approaches, which are expensive and time-consuming processes. (Ito and Van Veen, 2006). Membrane technology is one such approach that may be regarded efficient in the removal of sulfur compounds from petrochemical industrial streams. . The development of membranes for desulfurization is potentially energy saving, as the separation process takes place without phase transition and compared to the conventional techniques, it can offer simple, low capital and operating cost and is fully automated with no moving parts. (Fihri et al., 2016).

Sulfur removal has traditionally been accomplished using conventional technologies such as hydrodesulfurization. However, the obtained products lose octane number, and the procedure

is quite costly (Kong et al., 2007). Capital-operations costs, poor feed flexibility, a short process cycle, technical complexity, and overall refiner value are among the other issues that need to be addressed (Ito and Van Veen, 2006). The membrane desulfurization technology is a non HDS method that has gained increased attention from researchers and refiners worldwide due to its low cost, easy operation and environmental friendliness with no reduction in the cetane number of fuels.

2.5.2 Benefits of using mixed matrix membrane for desulfurization techniques

Technical reports on membrane separation process of sulfur containing compounds are confined mostly to patents/patent applications for companies like W.R.Grac, ExxonMobil and Engineering Company and Marathon Oil Company (Lin et al., 2006). Effective implementation of a membrane-based separation technique at both laboratory and industrial scale is determined significantly on the appropriate chemical, mechanical, and permeation properties of membranes. Latest developments of membrane materials have apparently reached a limit in trade-off between selectivity and permeability (Vinh-Thang and Kaliaguine, 2013). Hence, the research emphasis has been shifted towards the development of mixed matrix membranes (MMM), with an effective approach to tune the structure and improve the performance of the extensively used polymeric membranes with the addition of nanofillers/inorganic fillers (Li et al., 2017; Low et al., 2018).

Pure membranes are very effective; nevertheless, there is a need for modification to enhance the membrane activity by functionality as the membranes suffer from a major trade-off between separation flux and enrichment factor in most situations, i.e. higher separation flux is followed by lower enrichment factor and vice versa (Yang et al., 2013). Modification helps to manipulate

the selectivity of a membrane by either enhancing or diminishing its selectivity depending on what the membrane is meant to achieve. These can be achieved by either changing the pore size, hydrophobicity/hydrophilicity, surface roughness, thickness or composition of the membrane (Kiani et al., 2015). Modification of such factors are considered by comprehensively taking into account the available relevant literature and reports.

Two main approaches such as membrane material selection and enhancement of membrane efficiency by physical and chemical modification, like filling (Qi et al., 2007), copolymerization (Sha et al., 2018), blending (Baheri et al., 2017), and crosslinking (Lin et al., 2006) are existing in the membrane modification for desulfurization.

The discussion of the following physical and chemical factors are essential to strategize the possible approaches in order to overcome the trade-off relationship and achieve substantial desulfurization efficiency by membrane technology.

2.5.3 Process description and requirements for membrane desulfurization

Separation processes such as distillation, pervaporation and adsorption are energy-intensive procedures that allow the separation by size exclusion or chemical affinity by physisorption (Sholl and Lively 2016). Pervaporation and adsorption are the two main membrane desulfurization processes. This section focuses on the description of recently developed mixed matrix membranes for adsorptive and pervaporative desulfurization.

2.5.3.1 Pervaporation (PV)

Separation processes dealing with organic liquid mixtures play an important and indispensable role in the fields of energy and the environment. Organic liquid separation, unlike gas

separation methods, poses considerable problems and obstacles due to greater interactions between various organic molecules (Yu et al., 2016). Even though, distillation is commonly used, it suffers from many disadvantages associated with: higher energy usage; difficult to deal with azeotropic and close azeotropic mixtures; uneconomic when the amount of a major component is considerably higher or lower than that of other components in the mixture (Cai et al., 2020). Pervaporation, a membrane separation method, is energy-efficient and environmentally friendly separation technique that has tremendous potential to resolve certain distillation drawbacks or even eliminate distillation in certain situations. It has adjustable working conditions for the separation of close-boiling or azeotropic liquid mixtures (Yang et al., 2014). Different methods of desulfurization were already developed to date, which were introduced in previous sections. Pervaporation in deep desulfurization has been widely investigated as a newly emerging unit operation for its simpler handling, less energy usage, simpler scale-up, etc. (Yang et al., 2013). The membrane plays a significant role in a pervaporation process and influences whether this process can be industrially useful.

Pervaporation can be used as a promising alternative technology to desulfurize liquid hydrocarbon streams (Amaral et al., 2014; Cao et al., 2011). When compared with the traditional naphtha hydrodesulfurization process, pervaporation makes it possible to extract compounds of organic sulfur with a much lower loss of octane rating. In addition, it functions with mild conditions with no requirement for hydrogen and catalysts involvement, contributing to lower operating costs as a result (Lin et al., 2009). The effectiveness of pervaporation desulfurization is correlated to membrane affinity with sulfur compounds (Amaral et al., 2014).

Generally, pervaporation membranes can be classified depending on the nature of the membrane material into polymer-based membranes and inorganic material-based membranes. Polymer-based membranes are more frequently used compared to inorganic material-based

membranes due to the inherent attributes such as simple processability, large-scale processing and comparatively low cost (Vinh-Thang and Kaliaguine, 2013; Li et al., 2013).

Using various material types, including polydimethylsiloxane (PDMS) (Wang et al., 2018; Qi et al., 2006; Cao et al., 2011), polyethylene glycol (PEG) (Lin et al., 2006; Gao et al., 2018), polyimides (PI) (Yuen et al., 2007; Wang et al., 2006), and polyethersulfone (PES) (Li et al., 2009;) etc.,different membranes for deep desulfurization have been established to date.

Since the membrane-based S-Brane method was reported and developed by W.R. Grace&Co., CT, USA, in 2002, much of the research efforts have centred on incorporating PV technology to fuel desulfurization (Lin et al., 2009). The published literature were mainly from Grace Davison Group, ExxonMobil Research and Engineering Company, Marathon Oil Company, Trans Ionics Company and some universities. The technique used by S-Brane, is a well-known pervaporation-based industry-scale procedure for selective removal of sulfur-containing hydrocarbon molecules. It concentrates the sulfur in the stream of the permeate (~30% of the total volume), which will then be processed in the HDS process (Cao et al., 2011).

2.5.3.2 Pervaporation process

Lin et al., (2009) conducted the pervaporation experiments on a membrane which was placed in the pervaporation cell. Under ambient pressure, the sulfur rich feed blend was fed into the upstream side and the vacuum on the downstream side was maintained at certain rate using a vacuum pump. Permeate sample was captured in a cold trap of liquid nitrogen, weighed and evaluated. The total flux of permeate J was measured by dividing the weight of permeate accumulated in the cold trap by time and the membrane's surface area. The flux of permeation (J, kg/(m^2 h)) has been described as:

$$J = \frac{Q}{A \times t} \qquad (2.a)$$

Where, Q (kg) is the total amount of the permeate collected during the experimental period (t, h), and A (m^2) was the effective membrane area. Furthermore, the flux was adjusted according to the membrane thickness, which was determined based on the cast thickness and the degree of swelling. The normalized flux was denoted as J_N (kg μm/m^2 h), $J_N = J \times l$, where the thickness of the membrane in the swollen state was denoted by l (μm).

Gas chromatography is used to assess the feed and permeate compositions fitted with a capillary column and flame ionization detector. The injector, detector and oven temperatures were set at 200 ^oC, 250 ^oC and 80 ^oC, respectively. The membrane's separation selectivity was given by the enrichment factor of Thiophene (β), defined as:

$$\beta = \frac{\omega^P}{\omega^F} \qquad (2.b)$$

Where, ω^F and ω^P are denoted as the weight fractions of thiophene in the feed and permeate, respectively (Cao et al., 2011).

2.5.3.3 Adsorption

Adsorbents have wide surface area that can effectively adsorb and hold liquid or gas molecules on their surface. They have shown great promise in a wide range of applications, including water and air purification, catalysis, and many others (Jiuhui, 2008; Choi et al., 2009). The adsorption process is one of the separation methods that involves in the adhering of certain materials to another material's surface through physical attraction (physisorption) or chemical

bond formation (chemisorption) (Rouquerol et al., 2013). Adsorbents have wide surface area that can effectively adsorb and hold liquid or gas molecules on their surface. They have shown great promise in a wide range of applications, including water and air purification, catalysis, and many others (Jiuhui, 2008; Choi et al., 2009).

Chemisorption involves in a single layer of adsorbate molecules being adsorbed, and recovery of the adsorbent demands a greater amount of heat due to the chemical bond formation. Physisorption, on the other hand, can entail the formation of multiple layers of adsorbed molecules. Furthermore, since physisorption is not energetically enabled, thermodynamic equilibrium is easily achieved, and the rate of increase is rapid (Rouquerol et al., 2013). As elaborated in the Table 2.1, chemisorption is extremely complex compared to physical adsorption, as chemisorption usually needs an activation energy, so achieving thermodynamic equilibrium can be slow and higher temperatures will lead to improved adsorption (Karge and Weitkamp, 2008).

Table 2.1 Difference between Physical and Chemical Adsorption (Karge and Weitkamp, 2008)

Physical Adsorption	**Chemical Adsorption**
Low heat of adsorption (< 2 or 3 times latent heat of evaporation)	High heat of adsorption (> 2 or 3 times latent heat of evaporation)
Monolayer or Multilayer	Monolayer only

No dissociation of adsorbed species	May involve dissociation of adsorbed species
No electron transfer, although polarization of sorbate may occur	Electron transfer leading to bond formation between sorbate and surface
Non-activated, rapid and reversible	Activated, may be slow and irreversible
Non-Specific	Highly Specific
Only significant at relatively low temperature	Possible over a wide range of temperatures

Adsorption is favoured approach among the most energy-efficient processes for deep desulfurization as it has flexibility, selectivity, and involves minimal costs since the process is applied under mild conditions (Yin et al., 2012; Wang et al., 2008). The adsorbent's properties, such as preference for organosulfur compounds over hydrocarbons, retention capability, endurance, and reactivation, all contribute to the process' effectiveness (Javadli & Klerk, 2012).

Molecular sieves (Sentorun-Shalaby et al., 2011), metal-based compounds (Ahmed and Jhung, 2016), zeolites (Barzamini et al, 2014), and carbon-based sorbents (Shi et al, 2015) have been utilized as adsorbents for desulfurization. Since adsorption is a surface process, effective adsorbent materials must have large surface areas and well-defined pore structures in order to adsorb particular target molecules selectively. As a result, in-depth analysis is needed.

The characteristics of adsorbent materials must include, a high specific surface area to absorb as much adsorbate as possible; a well-defined pore structure to selectively absorb the adsorbate

and improve adsorption; chemical, thermal, and mechanical stability to allow them to be reproduced without losing their properties or efficacy.

2.5.4 Adsorption Kinetics and Adsorption Isotherms

2.5.4.1 Adsorption capacity

The interaction between different properties such as contact time, temperature, and adsorbent quantity can be used to calculate the adsorption capacity by maintaining one of the parameters constant. . The adsorption isotherm where temperature is kept constant, is given as a plot of the adsorbed sulfur concentration at equilibrium, C_e, versus the adsorption capacity in equilibrium, q_e. The formulation of a mathematical model for an adsorption process is influenced by the equilibrium behaviour of the process (Weber & Smith, 1987). Adsorption equilibrium data is used to evaluate adsorption processes and, in particular, for the selection of a suitable adsorbent, and the design of an appropriate adsorber in a proposed adsorbate/adsorbent system.

The adsorption potential at any time and in equilibrium are given by the equations 2.1 and 2.2 (Jiwalak et al., 2010).

$$q_t = (C_o - C_t)\, V/W \qquad (2.1)$$

$$q_e = (C_o - C_e)\, V/W \qquad (2.2)$$

Where **q** represents the amount of sulfur compounds adsorbed per gram of adsorbent at any time **(q_t)** and at equilibrium **(q_e)**, **Co** represents the initial concentration (**mg/l**), **C_t** represents

the concentration at time **t (mg/l)**, **V** represents the volume of a solution **(l)**, and **W** represents the weight of the adsorbent used **(g)**.

The following equation can be used to measure the sulfur removal efficiency, **SR (%)**:

$$\mathbf{SR} = ((\boldsymbol{C_o} - \boldsymbol{C_t}) / \boldsymbol{C_0}) \times \mathbf{100} \quad (2.3)$$

2.5.4.2 Adsorption kinetics

The study of adsorption kinetics aids in determining the time taken to reach equilibrium during the adsorption process, as well as the regulating mechanisms of the adsorption process such as mass transfer and rate of the chemical reaction (Mittal et al., 2006; Kumar and Kirthika, 2009). The kinetics of sulfur adsorption can be analysed using pseudo-first-order and pseudo-second-order equations. Based on the linear regression correlation coefficient, or R^2, the best fit model is chosen (Jiwalak et al., 2010).

The pseudo-first-order rate proposed by Lagergren (1989) is given below (Jiwalak et al., 2010).

$$\boldsymbol{dq_t/d_t} = \boldsymbol{k_1}\ (\boldsymbol{q_e} - \boldsymbol{q_t}) \quad (2.4)$$

Where $\boldsymbol{k_1}$ is the pseudo-first-order adsorption rate constant **(min^{-1})**.

The following equation is obtained by integrating this equation and applying the initial conditions of $\mathbf{q_t = 0}$ at **t = 0** and $\mathbf{q = q_t}$ at **t=t**:

$$\mathbf{ln}\ (\boldsymbol{q_e} - \boldsymbol{q_t}) = \mathbf{ln}\ \boldsymbol{q_e} - \boldsymbol{k_1 t} \quad (2.5)$$

A linear relationship of **ln ($q_e - q_t$)** versus **t (min)** implies that this model is applicable to fit the experimental data. The **k_1 value** can be calculated from the plots of **ln ($q_e - q_t$)** versus **t** (Darwish, 2015).

Applying the boundary condition q_t (t=0)=0 as well as integrating gives the following equation. (Lakshmi *et al*., 2009).

$$\log (q_e - q_t) = \log q_e - ((k_1 / 2.303)\, t) \quad (2.6)$$

The following is the pseudo-second-order kinetic model (Lakshmi *et al*., 2009):

$$dq_t/dt = k_2 (q_e - q_t)^2 \quad (2.7)$$

Where k_2 is the pseudo-second-order adsorption rate constant **(g/mg.min)**.

The following equation is obtained by integrating the equation and applying the applying boundary conditions (t = 0 and $q_t = q_e$ to $t = t$ and $q_t = q_t$).

$$t / q_t = (1 / k_2 q_e^2) + (t / q_e) \quad (2.8)$$

q_e and k_2 values can be obtained from the slope and intercept of the plot of t/q_t versus t/q_e

2.5.4.3 Equilibrium of adsorption

Adsorption is the deposition of particles on an interfacial layer, which is usually described using adsorption isotherms. At constant temperature, an adsorption isotherm is a mathematical model that describes the relationship between the amount of a substance adsorbed and its equilibrium concentration in the solution (Foo and Hameed, 2010). It depicts the distribution of adsorption molecules between the liquid and solid phases during equilibrium. These

isotherms are based on assumptions about the adsorbents' homogeneity/heterogeneity, the type of coverage, and the potential interaction between the adsorbate species (Kumar and Kirthika, 2009). The Langmuir and Freundlich models are the two most commonly used models.

Adsorption occurs at specific homogeneous locations on the surface, according to Langmuir Isotherm model (Jiwalak et al., 2010). Furthermore, it is assumed that once an adsorbate has occupied a site, no further adsorption can occur at that location. This isotherm's theoretical equation is shown below (Hameed et al., 2008).

$$q_e = Q_m K C_e / (1 + K C_e) \quad (2.9)$$

Where $\mathbf{Q}_m$ is the maximum amount of adsorbate per unit weight adsorbent needed to form complete monolayer coverage on the surface bound, and **K** is a Langmuir constant related to binding site affinity **(l/mg)**.

As shown below, the above equation can be rearranged into a linear form:

$$C_e/q_e = (1/Q_m K) + ((1/Q_m) \times C_e) \quad (2.10)$$

$$1/q_e = (1/Q_m) + (1/Q_m K C_e) \quad (2.11)$$

The Langmuir constants Q_m and K, can be determined from the intercepts and slopes of a plot of $\mathbf{(1/q_e)}$ versus **(1/Ce)**. The separation factor can be determined using the following equation to analyse the progression of the adsorption dimensionless constant. (Weber & Chakravorti, 1974).

$$r = 1 / (1 + K C_o) \quad (2.12)$$

The form of an isotherm is determined by the value of **r**. The fact that the r-value decreases as the temperature rises suggests that the adsorption process is more favorable at higher temperatures (Mittal et al., 2006). At constant temperature, equilibrium adsorption isotherms illustrate the correlations between the adsorbate's equilibrium concentration in the solid and liquid phases. Single component adsorption isotherms are usually interpreted by the curves/shapes such as linear, favorable, very favorable, irreversible, and unfavorable (Barros et al., 2013). The r-values and relative isotherm types are shown in the Table 2.2.

Table 2.2 r-values and their relative isotherm type

Values of r	**Type of isotherm**
$0 < r < 1$	Favourable
$r = 0$	Irreversible
$r = 1$	Linear
$r > 0$	Unfavourable

The adsorption equilibrium on heterogeneous surfaces is defined by Freundlich Isotherm. It is based on the premise that adsorption occurs at various locations with a variety of adsorption energies (Kumar and Kirthika, 2009). It does not assume a monolayer capacity, unlike the

Langmuir Isotherm (Jiwalak et al., 2010). This isotherm's theoretical equation is shown below (Hameed et al., 2008).

$$q_e = K_f C_e^{1/n} \quad (2.13)$$

Where K_f represents adsorption potential **(mg/g)** and **1/n** represents adsorption strength **(l/mg)**.

This equation is written in linear form as:

$$\log q_e = \log K_f + (1/n) \log C_e \quad (2.14)$$

The slopes and intercepts of a plot of **log q_e** versus **log C_e** can be used to calculate the Freundlich constants K_f and **1/n**. The n-value indicates the adsorption process's favourability, with **n > 1** implying that the adsorption process is favourable under the specified conditions (Chiou and Li, 2002).

2.5.4.4 Activation energy

The empirical Van 't Hoff and Arrhenius equation, as shown below, can be used to measure the process' activation energy (Jiwalak et al., 2010).

$$k = Ae^{-E_a/RT} \quad (2.15)$$

Where **A** is the pre-exponential component, **Ea** is the activation energy **(KJ/mol)**, **R** is the gas constant **(8.314 J/mol.K)**, **k** is either the pseudo-first-order rate constant or the second-order rate constant depending on **R^2** value, and **T** is the temperature in **Kelvins**.

This equation is written in logarithmic form as follows:

$$\ln k = \ln A - (E_a/RT) \quad (2.16)$$

The activation energy is calculated using an Arrhenius plot of **ln k** versus **1/T**. Whether the process is physical adsorption or chemical adsorption is determined by the magnitude of this activation energy. The activation energy for physical adsorption processes is normally between **5** and **40 KJ/mol** (Nollet et al., 2003). This is due to poor intermolecular forces and, as a result, a low energy requirement for bond breaking. Due to the much stronger bonds involved in chemical adsorption processes, the activation energy usually varies from **40** to **800 KJ/mol** (Nollet et al., 2003; Jiwalak et al., 2010).

2.5.4.5 Thermodynamic parameters

The Gibbs free energy **(ΔG°)**, enthalpy **(ΔH°)** and entropy **(ΔS°)** are the thermodynamic parameters studied in this review. The following equations were used to calculate them.

$$K_c = C_{ads,} / C_e \quad (2.17)$$

$$\Delta G^0 = -RT \ln K_c \quad (2.18)$$

$$\ln K_c = (\Delta S^0/ R) - (\Delta H^0/RT) \quad (2.19)$$

$$\Delta G^0 = \Delta H^0 - T\Delta S^0 \quad (2.20)$$

Where $\mathbf{K_c}$ represents the equilibrium constant, $\mathbf{C_{ads,e}}$ represents the sulfur concentration adsorbed at equilibrium **(mg/l)**, $\mathbf{C_e}$ represents the sulfur concentration remaining in diesel at equilibrium **(mg/l)**, **R** represents the gas constant **(8.314 J/mol.K)**, and **T** represents the temperature in **Kelvin**. (Jiwalak et al., 2010). From the experimental results, the equilibrium constant, **Kc**, was determined. The Equation for ΔG^o was used to measure the Gibbs free

energy. A Van 't Hoff plot of **ln K_c** versus **1/T** was generated, and the entropy and enthalpy were calculated using the intercept and slope of the chart.

2.5.5 Properties of Membranes

The performance of the membranes is greatly influenced by their chemical and mechanical properties. The following sections will discuss various properties and conditions used in the recent developments of membrane desulfurization. Since, the current study focuses on developing MMM using adsorptive material for sulfur removal, this section will focus on discussing membrane modifications using different fillers to improve the efficiency of the membrane.

2.5.5.1 Morphology

The distribution of filler particles into three-dimensional network structures of MMMs adsorbents is a critical consideration for achieving excellent separation properties. The membrane adsorption mechanism demonstrates that morphology has a major impact on the transport properties of small molecules in MMMs adsorbents. The images from the field-emission scanning electron microscope (FESEM) in Figure 2.26 show that raw polyimide (PI) membranes, as well as zeolites/PI MMMs, have numerous finger-like and sponge-like pores, suggesting a good mechanism to ensure contact between the integrated zeolites and liquid fuel flowing through them. (Lin et al., 2012).

The zeolites particles are dispersed and embedded in the polymer matrix, and as the loading quantity of zeolites is increased, the particles appear to be reagglomerated. The variations by

increasing the zeolite content to 50% in the zeolites/PI MMMs images, are clearly visible indicating that the finger-like pores become less and much more irregular. Part of the molecular interface and network between the polymer and particles are disrupted at 50% of zeolite loading, with defects emerged, indicating poor mechanical strength and practical applicability. It is inferred from FESEM photos that MMMs have favorable conditions for MMMs adsorbents with 40% zeolite material (Lin et al., 2012).

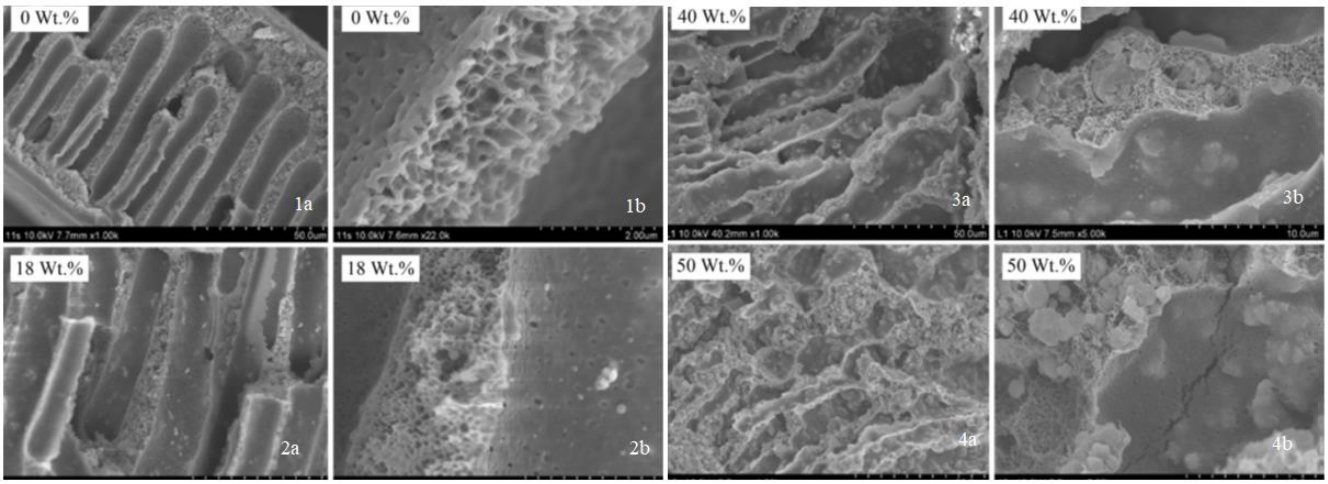


Figure 2.26 FESEM images of cross-sections of raw PI and zeolites/PI MMMs adsorbents: (1) 0 wt.%, (2) 18 wt.%, (3) 40 wt.%, and (4) 50 wt.% (Lin et al., 2012)

2.5.5.2 Interfacial compatibility

The polymer matrix plays a prominent part in permeability, and the inorganic filler has a control factor for the selectivity of the separation process. Consequently, interfacial compatibility between the two phases has a substantial influence on the efficiency of separation for such membranes (Maghami and Abdelrasoul, 2018).

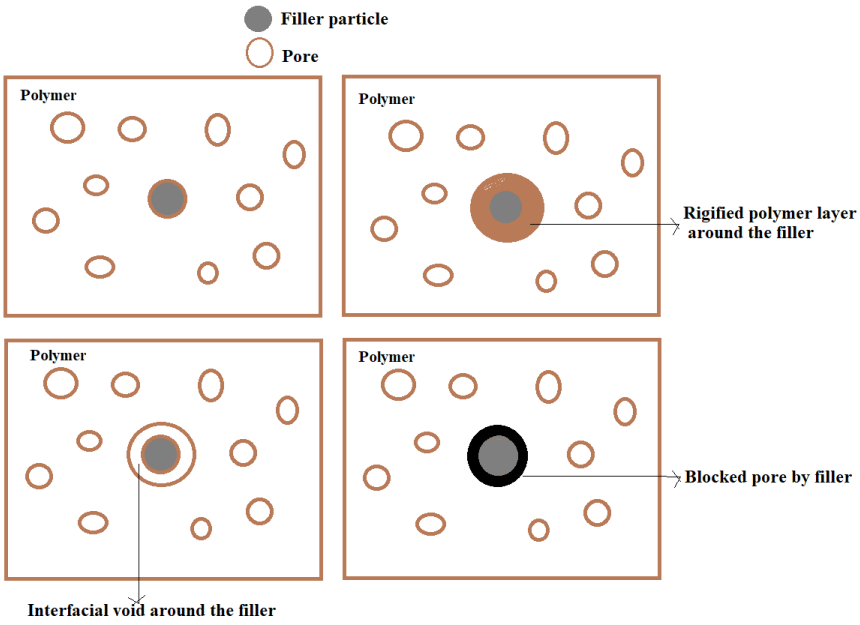


Figure 2.27 Image of various structures at the polymer/filler interface region (Moore and Koros, 2005)

2.5.5.3 Interfacial voids

The inclusion of fillers has a substantial impact on the overall efficiency of the produced MMMs. Two significant factors, namely, the interaction between the polymer process and the filler, and the stress induced during preparation, are responsible for the formation of interfacial voids (Aroon et al., 2010; Yong et al., 2001). Additional channels that enable the solvent to flow through the membrane are produced by the formation of interfacial voids (Alpatova et al., 2015). However, the mechanical strength and rejection rate are also impacted by the density of the channel (Chung et al., 2007).

Dense membranes consist of two types of cavities: the network cavity, which refers to the interstitial cavities in the cross-linked site; the other is the aggregate cavity, which refers to the cavities within the network clusters and at the polymer-filler interfaces in hybrid membranes

(Yang et al., 2015). The feature of aggregate cavities shows the effect of the fillers on the membrane interface structure. It is well known that the selectivity of hybrid membranes reduces if the polymer-filler interface is greater than the network clusters, otherwise the permeability will decrease (Liu et al., 2014).

It is commonly considered that incorporating impermeable fillers to a polymer matrix contributes to the decline in the molecule transport, thereby improving the barrier property of the membrane. Nevertheless, it is observed that the some fillers can serve as the nanospacer stopping polymer chains from compact packaging (Merkel et al., 2002). Although, if fillers are only bound by the weak force vander Waals, they are likely to break off (Yu et al., 2016). Stronger interaction at the interface is thus helpful to overcome this issue.

Yu et al., (2016), developed adhesion based filler materials by adhesing nanoparticles with graphene nanosheets (GNS) using dopamine, since dopamine is an adhesive with a wide variety of applications and can bind well to both nanoparticles and GNS. In this study, polydopamine (PDA) coated GNS was used to load Ag nanoparticles (AgNP), then fabricated into poly- ether-block-amide (Pebax) polymer matrix.

The PDA/GNS and Ag-PDA/GNS composites were interfering with the stacking of the polyamide (PA) segments of Pebax polymer, consequently destructing the PA segments thereby enhancing the membrane permeability. The increase in the filler content reduced the radius and intensity of free volume cavity signifying the stronger interaction between Pebax chain and composite interface owing to the adhesive effect of PDA. Dopamine coating and AgNP loading may inhibit agglomeration of GNS, whilst GNS may avoid agglomeration of AgNPs. AgNPs can serve a facilitated transport role towards thiophene in model gasoline and improve the efficiency of membrane separation. Besides that, the membrane showed increased

resistance to swelling due to the multiple interactions between the Pebax matrix and the Ag-PDA/GNS at the interface.

Usually, poor interfacial interaction produces non-selective voids at the interface and then results in the lack of selectivity. Several experiments were carried out to improve the interfacial interaction between the polymer and metal organic framework (MOF) by functionalizing the polymer matrix and/or MOF fillers (Li et al., 2016; Venna et al., 2015). In spite of these elaborate works, it is still important to choose MOFs that have stronger interfacial interaction with polymer matrix, such as hydrogen bonds, to eliminate non-selective interfacial voids and simplify the process of preparation (Yu et al., 2018).

2.5.5.4 Crosslinking

By crosslinking the polymer backbone, rigidity is enhanced thereby improving the swelling resistance, but with reduced diffusivity and permeation flux (Stafie et al., 2005). The copolymer, which connects various monomeric units together, is beneficial in integrating both the swelling resistance of rigid chains and the high permeability of flexible polymer (Rychlewska et al., 2017). Pebax, a widely used copolymers has the rigid PA segments acting as a "bone" that contributes to mechanical strength and swelling resistance, whereas the flexible polyether segments function like a "mussel" that contributes to increased permeability (Yu et al., 2018).

2.5.5.5 Thermal stability

The study of MMM with zeolite particles proved that thermal decomposition temperatures for MMMs adsorbents (with the exception of 50 wt. percent zeolite content membranes) are greater than those of the raw polyimide (PI) membrane due to the addition of the zeolite fillers. The interaction of organic PI substrate with inorganic zeolites limits the thermal movement of the polymer and increases the energy required for the movement and segmentation of the polymer chains, thus improving the thermal stability of the membranes.

MMMs adsorbents with 50 wt. percent of zeolite content, nevertheless, have lower decomposition temperatures than raw PI and other MMM adsorbents (Lin et al., 2012). This was attributed to higer concentration of inorganic particles in polymer that appear to agglomerate, which cannot promise successful interfacial inorganic/organic binding.

In another study of MMM thermal stability, it was shown that compared to pristine PDMS membrane, the weight loss rate of PDMS–GNS hybrid membranes is slower no more than 0.2 % ;although it becomes faster when the GNS content is 0.5 %, which could be caused by the agglomeration of GNS (Yang et al., 2015).

2.5.5.6 Mechanical properties of MMMs adsorbents

Lin et al., (2012), studied the influence of the embedded zeolite material on the tensile strength of the MMMs adsorbents. It was noticed that both the tensile strength and the modulus of the MMMs adsorbents first improved and then reduced with the increasing content of the embedded particles. The inclusion of inorganic particles clearly increased the mechanical strength of the MMMs adsorbents within a certain range. The efficiency of the MMMs

adsorbents, however, dropped dramatically when the embedded particle content is 50 %. The polymer will be the main structure component of the hybrid membrane if the embedded particle content is at a lower level. And the zeolite particles can be integrated into the polymer membrane matrix quite well, ensuring the inorganic/organic phase's thorough interfacial behaviour. When the content of the embedded particles is increased beyond a certain concentration, the interfacial defects formed between inorganic particles had a significant detrimental effect on the tensile strength of the prepared MMMs.
In particular, 40 wt. % of MMM adsorbents displayed enhanced morphology, thermal and me -chanical properties (Lin et al,2012).

2.5.5.7 Filler content

The filler content is crucial for the interactions between the polymer and the fillers to resolve the issues arising from the mechanical and thermal instability of the membranes. Beigbeder et al., (2008), studied the membrane properties of PDMS based membranes embedded with carbon nanotubes (CNT). It wa observed that the aggregate cavity of PDMS-CNT membranes is almost unaffected, suggesting that the CH–π interactions between the methyl groups of PDMS and the π-electron-rich surface of CNT resulting in a desirable interfacial composition. Although, when the filler content exceeds 0.5wt percent, the aggregate cavity intensity decreases after the agglomeration of filler particles reduces interfacial region (Cao et al, 2014).

The dependency of the thermal stability of MMM on the filler content was already known. The rate of flux too is affected by the filler content where, 0.2 weight percent of GNS in PDMS showed superior permeation flux when the content was varied from 0 to 0.5 weight percent. It

was believed that due the high aspect ratio of GNS, a larger polymer-filler interfacial area is enhanced by introducing GNS into the PDMS matrix (Yang et al., 2015)

The porous nature of zeolite (fillers) has a huge effect on permeable molecule transport. In the membranes, the available free volume among polymeric chains, interface voids between polymeric chains and inorganic filler, and macro and mesopores in zeolite offer greater diffusion for small molecules than unfilled membranes. The larger the polymer matrix, the more permeation is reached subsequently. With increasing zeolite content, the sulfur enrichment factor first increased, then decreased. Under low zeolite content (9 weight percent), the change in sulfur enrichment factor was not significant. The sulfur enrichment factor and flux are both higher at 9 weight percent of CuY content (Lin et al, 2010). The steady increase in filler content, on the other hand, resulted in a major reduction in the sulfur enrichment factor. The outcomes ought to be due to two contributory factors. The size screening effect and the complexation force between CuY and thiophenes, for instance, will facilitate thiophene sorption in membranes and enhance the sulfur enrichment factor. On the other hand, there is a trade-off between flux and selectivity during the PV process (Kariduraganavar et al, 2004).

2.5.6 Chemistry of the sulfur removal process using Membranes/Mixed matrix membrane

2.5.6.1 Facilitated Transport Carriers

Facilitated transport membranes are studied by researchers, inspired by protein mediated facilitated diffusion in cytomembranes in order to bind/release certain molecules across membranes. In most cases, transition metal ions cannot be directly combined with the polymer matrix because, owing to their limited size and poor contact with polymer chains, leakage of

metal ions is extreme (Yang et al., 2014). The recommended method for the preparation of facilitated transport membranes is to immobilize transition metal ions on engineered carriers and then combine them with polymers.

Generally, the facilitated transportation within membranes is attained through the effective hopping of small molecules from one carrier to another. Pan et al., (2018) analysed the performance of molybdenum disulfide (MoS_2) incorporated PEBAX membranes on removal of thiophene from n-octane-thiophene mixture. The basal plane of MoS_2 nanosheets can serve as a facilitated transport carrier for thiophene molecules as their interaction (binding energy of thiophene on the MoS_2 nanosheet basal plane is 0.42 eV) remains within the scope of reversible chemical complexing (Salmeron et al., 1982; King, 1987). Thiophene hops continuously from one carrier to another as MoS_2 provides large and clean surface which also enhances transport rate thereby leading to higher diffusion selectivity by hybrid membrane.

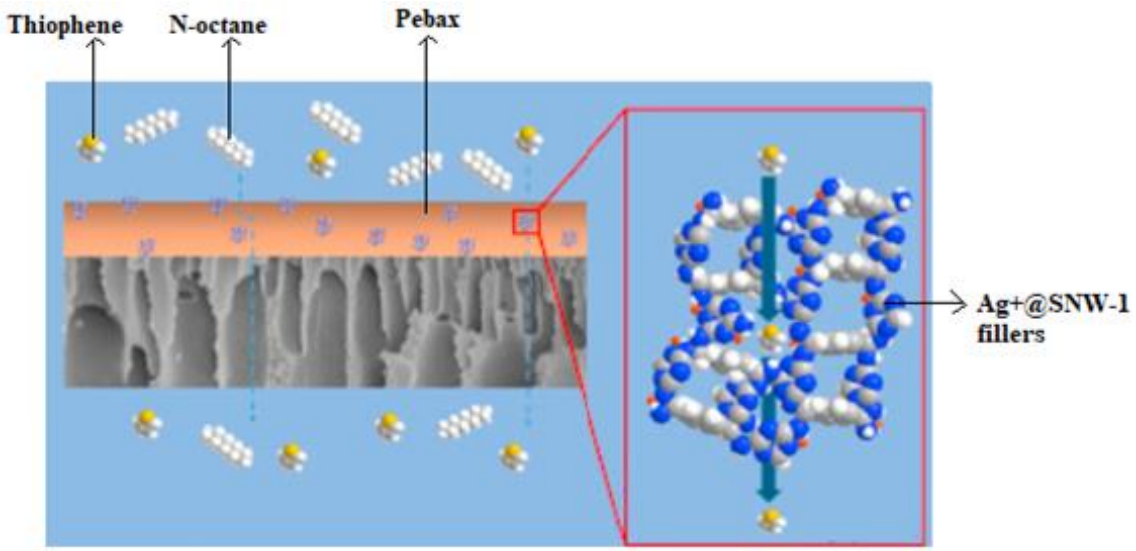


Figure 2.28 Facilitated transport of Thiophnic compounds through Pebax MMM (Pan et al., 2018)

2.5.6.2 π type complex

A set of transition-metal ion-exchanged Y zeolites (with Cu, Ni, Pd, and Ag ions) for sulfur removal were reported by Takahashi et al., (2002) and Velu et al., (2003). For the separation of thiophenes from model oil, Qi et al., (2007) prepared PDMS–AgY zeolite mixed matrix membranes. The trade-off effect of filling on the selectivity and flux was discussed. Li et al., (2008), developed PDMS–Ni^{2+}Y zeolite hybrid membranes for thiophene removal from model gasoline systems through pervaporation. The distinct adsorption performance of MMM adsorbents with different functional zeolites was significantly correlated with the binding force between the functional particles and the sulfur compounds. For NaY, desulfurization depends on physical adsorption of zeolite pore channels that bind through weak Van der Waals force to sulfur (Lin et al., 2012). This poor binding yields low selectivity of adsorption for sulfur, hence low desulfurization performance. Besides that, the adsorption process is different for ion-exchange modified AgY and CeY zeolites.

Several research studies have shown that transition metal ions of inorganic materials (e.g., Ag, Cu, Ni, Ce and Pd) can interact through π-complexation with non-benzene aromatic compounds such as thiophene to facilitate the separation performance of hybrid membranes (Yang et al., 2014; Cao et al., 2011). In fact, sulfur atom in thiophene has two lone pairs of electrons: one pair situated in the plane of the ring that can be donated (n type donor) to form direct S-M 'σ' with the adsorbent (Ce^{+}) or the other pair on the six-electron π system of the aromatic ring which can form a (π type) complex with the metal ions. The former sigma type can be seen in Ce^{+} and later pi type complexes in Ag^{+} ions. However, the bonding strength of sigma is greater than that of the pi complex. This also indicates that desorption in pi is easier than that of sigma which implies that pi type complexes are easier, energy saving when compared to sigma.

It can be inferred that graphene is a possible material for effectively controlling the polymer matrix framework. Besides the mentioned materials in this section, the sulfur-containing heterocyclic aromatic compounds (such as thiophene and dibenzothiophene) in gasoline can effectively be adsorbed onto graphene by π-π interactions due to the abundant free π-bonds of sp^2 atoms in graphene (Yang et al., 2015).

The facilitated transport feature of AgNP can influence the membrane through chain rigidification, and could further improve the selectivity of the Pebax-Ag-PDA/GNS (6 weight percent) membrane (Yu et al., 2016). Ag^0 and Ag^+ can synergistically promote the transport of thiophene in the gasoline model. Ag^0 is a Lewisacid, whereas thiophene is a Lewisbase, which according to the principle of hard and soft acids and bases (HSAB) (Li et al., 2015), can have affinity towards each other; while the interaction of π-π stacking occurs between Ag^+ and thiophene, as indicated by the Dewar-Chatt model (Safarik and Eldridge, 1998).

The π-complexation was once proposed between thiophene molecules and silver ions as the theory indicates that lone electron pairs would be donated by sulfur in thiophene, and silver ions have empty d orbit as receptors (Takahashi et al., 2002). The role carried by metallic ions, such as AgS, Cu_2S, or Pb_2S, is seldom seen for metallic ions incorporated into MMM. Consequently, an increase in permeation flux and selectivity may be likely to be due to the facilitated mass transfer of silver ions (Yang et al., 2014).

2.5.7 Choice of embedded and polymeric materials

2.5.7.1 Porous materials

A proper configuration of the pore channel will reduce the resistance to mass transfer. The selectivity will be further increased through molecular sieving if the pore size lies between the penetrants. In addition, to prevent the formation of interfacial defects, carriers must be well

compatible with polymers (Li et al., 2015; Yu et al., 2016). It has been shown that a good way to increase membrane performance is to add suitable fillers. MMMs have therefore been developed by doping various inorganic particles in the development of novel hybrid membranes for sulfur removal (Zhang et al., 2020). Zhang et al, (2020), used Santa Barbara Amorphous 15 (SBA-15) with a hierarchical porous structure as multi-functional additives. The SBA-15 has dual-pore architecture with hexagonally organized mesopores and micropores (Vattipalli et al., 2016). The cylindrical mesopores have molecular transport expressways to decrease the resistance to mass transfer and ensure enhanced permeability, while the molecular sieving effects of micropores on the wall are vital for increasing permselectivity of Thiophene. Additionally, SBA 15's high density silanol groups (SiOH) have strong polymer adherence for longterm membra ne stability (Tseng et al., 2013).

With high hydrophobicity, ZIF-8 porous fillers can have an effective pore structure to selectively recover organic compounds, benefiting from its flexible pore structure. Embedding ZIF-8 into PDMS induced a layer capable of introducing passable diffusion channels that eliminated the physical incorporation barrier of porous materials (Li et al., 2020).

2.6 Boron Nitride

Hexagonal BN (h-BN), also known as white graphene, is a two-dimension (2D) material, structurally similar to graphene as it has the same honeycomb structure, but varies in chemical and electronic properties of graphene (Liu et al., 2019). Contrary to graphene, h-BN shows ionic feature and strong interaction due to the different electronegativities between N and B (Ouyang and Long, 2021). It resists oxidation to higher temperatures than graphite. Thus, it is a multipurpose ceramic material with excellent properties that attracts a wide area of industrial applications. As a result of its unique properties such as reducing thermal expansions and

friction coefficients, increasing thermal conductivity, its utilization in composite materials has increased tremendously in the last few decades (Haubner et al., 2002; Kempfer, 1990). As compared to graphite, h-BN has a larger band gap showing exceptional properties, such as electrical insulation, high oxidation resistance and outstanding chemical stability (Singhal et al., 2008; Zheng et al., 2018). The polarity of the B–N bond, in specific, has been proven to effectively facilitate adsorption ability (Lei et al., 2013).

2.6.1 BN Synthesis

BN is a chemical compound formed from an equivalent number of atoms of boron (B) and nitrogen (N). By using the reaction between molten H_3BO_3 and potassium cyanide (KCN) Balmain, (1842), first illustrated BN synthesis. Since then, the preparation of numerous BN nanostructures, including boron nitride nanotubes (BNNTs) (Wu and Yin, 2011), boron nitride nanosheets (BNNSs) (Cai et al., 2016), boron nitride nanofibers (BNNFs) (Qiu et al., 2009), three dimensional boron nitride nanoflowers (Lian et al., 2011) etc., have been extensively investigated.

It's worth mentioning that the essential properties of BN, such as diameter, defects, morphology, surface area, and edge structures, can all be significantly affected by the synthetic routes used (Zheng et al., 2018). As a result, selecting an appropriate synthetic method for designing highly productive BN materials for any specification is critical.

To date, different conventional methodologies have been developed for the production of h-BN, which include chemical vapor deposition (CVD), solvo-thermal process, and solid-state reaction (Lei et al., 2013; Lian et al., 2013; Tang et al., 2008). In the high-temperature reaction furnace, the CVD is commonly used to produce h-BN (Lei et al., 2013). The solvo-thermal

synthesis will speed up the reaction by heating the sealed reactor to provide a high-pressure reaction atmosphere (Lian et al., 2013). In most cases, h-BN is made using the solid-state reaction process in presence of N_2 atmosphere. Continuous N_2 supply will assure that the reaction remains in the planned course and also acts as a protecting gas in the synthesis process. The solid-state reaction is a challenging process because of the high reaction temperatures (higher than 900 °C) and low heating rates (Tang et al., 2008).

However, the frequently utilized method for BN synthesis is the controlled chemical synthesis that was mostly used for desulfurization. It should be noted that the variables such as reactant ratios, temperature, and solvent may have a considerable effect on the properties and desulfurization of BN (Rajendran et al., 2020).

For BN synthesis, various experimental procedures using a combination of reactants containing boron and nitrogen precursors have been studied in the literature (Singhal et al., 2008). Each process is unique due to the various parameters that influence the reaction rate, time, distance, form, number of layers, and h-BN yield (Li et al., 2011)

In this process, low-cost B and N-containing precursors such as boric acid, boron oxide, urea, and melamine are widely used (Marchesini et al., 2019). This process is capable of developing extremely porous structures of h-BNNS because gaseous products such as CO_2, CO, and NH_3 are produced during the thermal treatment (Wu et al., 2016). Furthermore, the materials produced by this process are mostly fine powders, which are ideal for a variety of applications.

2.6.2 BN in desulfurization

Graphene-like BN or h-BN has excellent chemical, thermal and mechanical stabilities, due to which it has recently been proposed as one of the prominent topics of material science (Lee et al., 2010; Song et al., 2013). The adsorption efficiency of BN has garnered a lot of attention recently. As a novel adsorbent for promising applications like hydrogen storage (Lian et al., 2012) and water treatment (Lei et al., 2013), the use of BN with high specific surface area and additional active reaction sites allow them to demonstrate outstanding efficiency for adsorption of metal ions and organic pollutants (Yan et al., 2017). Besides that, BN can be synthesized through a low-cost and environmentally friendly process (Abdikheibari et al., 2018).

The traditional adsorbents often used in adsorptive desulfurization, include zeolites (Yang et al., 2003), mesoporous silica (Gu et al., 2014), supported metals (Wang et al., 2009) and activated carbon (Xiao et al., 2012; Ania and Bandosz, 2005). Although, several other new desulfurization adsorbents have been investigated in recent years, they have several shortcomings such as low stability or inadequate adsorption capacity or environmental harmfulness (Xiong et al., 2018) and expensive synthesis and reaction process (Yan et al., 2017). Thus, the production of an efficient and cost effective adsorbent for adsorptive desulfurization is extremely desirable.

To separate refractive sulfur compounds like dibenzothiophene (DBT) from liquid fuels, BN and its composites have lately been utilized as adsorbents for adsorptive desulfurization and as catalysts for oxidative desulfurization. Studies have shown that a variety of mechanisms for controlling the local atomic and electronic structure of h-BN, could improve the effectiveness for sulfur separation.

The use of BN material as an adsorbent and fillers in the polymer matrix in the current work was inspired by recent developments in desulfurization utilizing BN as an adsorbent. It has a host of outstanding features, including mechanical strength, thermal stability and non-toxicity that can be advantageous in a wide range of membrane applications, from pressure driven filtration to temperature driven operation, where membrane mechanical strength as well as chemical and thermal stability are crucial for the long life of the membrane (Golberg et al., 2010; Wang et al., 2013; Camacho et al., 2013). Moreover, the polar B-N bonds are useful for selective desulfurization which is an additional benefit for desulfurization adsorbent from fuels (Yan et al., 2017).

According to earlier studies, the principle of hard and soft acids and bases (HSAB) plays an incredibly significant role in the adsorption process (Xiao et al., 2008; Li et al., 2016). Soft acid is prone to react with soft base, which is very well known, and hard acid is likely to interfere with hard base. BN will exhibit certain Lewis acidity as it is electron-deficient and have a certain electron-attracting capacity due to the presence of virtual orbitals in boron atoms. Experimental findings indicate that commonly discussed aromatic sulfur compound DBT is classified as a soft base (Li et al., 2016).

2.6.3 BN Structure

h-BN is a group III (B)–V(N) compound composed of layers of alternating sp^2-hybridised boron and nitrogen atoms in a honeycomb lattice (Shen et al., 2019). h-BN nanosheets (h-BNNS) are also known as "white graphene" because they are isostructural to graphene. The atomic layers are stacked on top of each other by van der Waals forces, with alternate boron and nitrogen atoms bonded together by strong covalent bonds within the atomic layers (Pakdel et al., 2014).

2.6.4 BN Allotropes

BN usually occurs in its most stable crystallographic form, i.e. hexagonal boron nitride (h-BN) under standard conditions (Kubota et al., 2007). Contrasting to majority of carbon allotropes, BN should be synthesized from B and N precursors. There are six boron nitride crystalline allotropic phases, namely, hexagonal (h-BN, as graphite), cubic (c-BN or zinc blend form, as diamond) is known for its excellent hardness, wurtzite (w-BN, as hexagonal diamond), rhombohedral (r-BN), fullerene-like BN, single and multi-walled nanotubes. In particular, most of them are isoelectronic and structurally identical to their carbon equivalents (Tian et al., 2013; Arenal and Lopez-Bezanilla, 2009).

The structure of both c-BN and w-BN is made up of of sp^3-hybridized B and N atoms, but the difference in both is that w-BN has BN_3 or NB_3 tetrahedrons positioned at a different angle (Soma et al., 1974). h-BN has a layered configuration similar to graphite. The 2 dimensional (2D) layer has alternating B and N atoms joined by strong covalent bonds, while the 2D layers are bound together by weak van der Waals forces. The interlayer spacing between h-BN layers is found to be 3.30~3.34 Å whereas graphite displays a spacing of 3.33~3.35 Å (Hassan et al., 2020).

Although h-BN has structural similarity to that of graphene, the electron distribution in both is differed. Unlike C-C bonds of graphite layers, where the electrons are similarly contributed and uniformly dispersed, the electron pairs in sp^2-hybridized B–N bonds are more restricted to the N atoms owing to their higher electronegativity. Moreover, the lone pair of electrons in the N p_z orbital is only partly delocalized with the B p_z orbital (Weng et al., 2016).

2.6.5 h-BN functionalization

Chemical functionalization of h-BN is a concern because of its high chemical stability. Water-assisted exfoliated h-BN flakes have been identified to contain a limited number of functional oxygen groups (Lin et al., 2011). However, studies indicate that the degree of functionalization is marginal, so that effective cross-linking of individual sheets using external cross-linking agents is nearly impossible (Sudeep et al., 2015). Other non-covalent functionalization methods of h-BN nanostructures were also explored (Zhi et al., 2005; Wang et al., 2008). The resulting linkages are due to pi-pi interactions as well as boron-nitrogen interactions.

A significant number of recently developed published methods of desulfurization using less explored BN material in sulfur removal research are available in scientific journals. Although being new in the sulfur removal technology, BN has shown some exceptional properties in reducing the sulfur levels in the liquid fuels.

2.7 Carbon dots (C-dots)

Carbon based nanomaterials are very fascinating and have drawn considerable attention in the last few years (Song et al., 2018). Carbon dots (C-dotss) are an interesting and unique class of carbon nanostructures with dimensions below 10 nm, that are being explored for different applications because of their beneficial optical stability, low toxicity, biocompatibility, and ease of functionalization (Jahanbakhshi and Habibi, 2016; Chen et al., 2016).

Considerable attention has been paid to the design, manufacture and use of C-dot based hybrids, composites and doped nanomaterials as the components of C-dots have many benefits, such as low toxicity, water solubility, superior physicochemical stability (Jahanbakhshi and Habibi, 2016). Surface modification flexibility as well as abundant functional groups (-OH,-

COOH, etc.) on the C-dot surface offer several desirable sites for the development of different nanomaterials based on C-dots. In addition, some analysis shows that the photo-excited C-dots can act as remarkable electron donor species (Wang et al., 2009). The photo-excited C-dots have high electron-donating potential that enables the reduction of metal ions to metal nanoparticles on their surface to make various metallic and metallic oxide nanomaterial hybrids and composites.

Because of the low-temperature processability of the synthesis procedures and good hydrophilicity, the C-dots are compatible with large-area, roll-to-roll mass production techniques (Choi et al., 2013). Consequently, the electron transfer properties along with high stability, abundant surface functionnal groups, and high surface area of C-dots present these nanostructures as the suitable electrocatalysts, sensor materials (Huang et al., 2014; Zhu et al., 2013)

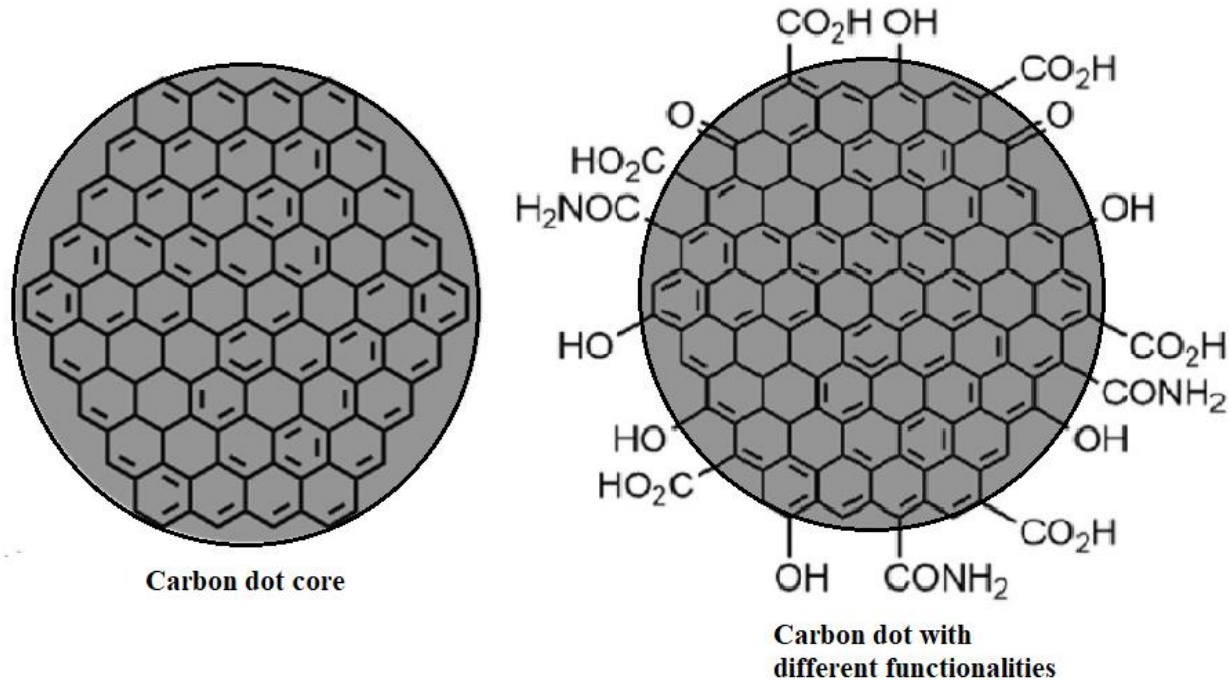


Figure 2.29 Images shows C-dot core and possible functionalities on C-dots (Barman and Patra, 2018)

Numerous raw materials have been used in C-dot synthesis, namely graphite oxide (Wang et al., 2011), citric acid (Ludmerczki et al., 2019), glycerol, coffee grounds (Crista et al., 2020) and grass (Sabet and Mahdavi, 2019).

Lignin was utilized as a raw material, which is an extensively available natural organic polymer to synthesize C-dots (Fu et al., 2013; Ragan and Megonnell, 2011). However, owing to strong carbon to carbon linkages in their molecular structure, it is very challenging to degrade lignin and its derivatives. It is still feasible, however, to efficiently synthesize high-quality C-dots with low-cost and easily obtainable starting materials in a simple and environmentally safe process.

Chitosan is a linear polysaccharide that includes -OH and-NH_2 groups. It is the second most available natural biopolymer, non-hazardous, biodegradable and relatively economical. Furthermore, Chitosan has long been discarded in the form of seafood waste. In this study, with chitosan as the carbon source, water-soluble and reductive C-dots were synthesized through the hydrothermal process (Song et al., 2018).

Several synthesis processes were subsequently identified for the preparation of C-dots, such as pyrolysis, acidic oxidation, hydrothermal treatments, laser ablation, electrochemical carbonization, combustion, microwave methods. The hydrothermal carbonization method was used as an efficient technique for the synthesis of novel carbon-based materials, particularly C-dots, among different techniques (Titirici et al., 2008). Due to the cost efficiency, and being quick and single step process, hydrothermal procedure using an appropriate precursor is known as one of the efficient and low-cost methods with high selectivity and increased yield (Atienzar et al., 2013 ; Niu et al., 2015).

BN nanostructures can be functionalized for them to be potential nanofillers in membrane desulfurization. That being said, this particular work with PPSU-CBN MMM as an adsorbent for the removal of sulfur compounds from fuels has not been reported to the best of our knowledge. The prepared membranes were extensively studied to examine the influence of the addition of h-BN and C-dot doped h-BN on the membrane's physicochemical properties. The performance of the fabricated membranes in separating DBT from model fuel was also investigated.

2.8 Conclusion

This chapter is an elaborate and comprehensive list of literature reviewed for this research work. It provides an outline of all the functional aspects of the crude oil production including an overview of the the latest information connected with the refinery processes as well as policies associated with the production and consumption of crude oil products. It also consists of all the relevant concepts related to the conventional and non conventional desulfurization techniques including the required membrane properties for the design of MMM for the current research study.

2.9 References

Abdikheibari, S., Lei, W., Dumée, L.F., Milne, N. and Baskaran, K., 2018. Thin film nanocomposite nanofiltration membranes from amine functionalized-boron nitride/polypiperazine amide with enhanced flux and fouling resistance. Journal of Materials Chemistry A, 6(25), pp.12066-12081.

Abdussalam, O., Trochu, J., Fello, N. & Chaabane, A., 2021. Recent advances and opportunities in planning green petroleum supply chains: a model-oriented review. International Journal of Sustainable Development & World Ecology, pp. 1-16.

Achaw, O. and Danso-Boateng, E., 2021. Crude Oil Refinery and Refinery Products. Chemical and Process Industries, pp. 235-265.

Adeola, A.O., Akingboye, A.S., Ore, O.T., Oluwajana, O.A., Adewole, A.H., Olawade, D.B. and Ogunyele, A.C., 2021. Crude oil exploration in Africa: socio-economic implications, environmental impacts, and mitigation strategies. Environment Systems and Decisions, pp.1-25.

Agarwal, P. and Sharma, D.K., 2009. Comparative studies on the bio-desulfurization of crude oil with other desulfurization techniques and deep desulfurization through integrated processes. Energy & Fuels, 24(1), pp.518-524.

Ahmed, I. and Jhung, S.H., 2016. Adsorptive desulfurization and denitrogenation using metal-organic frameworks. Journal of Hazardous materials, 301, pp.259-276.

Aitani, A.M., Ali, M.F. and Al-Ali, H.H., 2000. A review of non-conventional methods for the desulfurization of residual fuel oil. Petroleum Science and Technology, 18(5-6), pp.537-553.

Akinbami, O., Oke, S. & Bodunrin, M., 2021. The state of renewable energy development in South Africa: An overview. Alexandria Engineering Journal, 60(6), pp. 5077-5093.

Akpan, P. and Fuls, W., 2021. Cycling of coal fired power plants: A generic CO_2 emissions factor model for predicting CO_2 emissions. Energy, Volume 214, p. 119026.

Aljamali, N. and Salih, N., 2021. Review on Chemical Separation of Crude Oil and Analysis of Its Components. Journal of Petroleum Engineering & Technology, 11(2), pp. 35-49p.

Alpatova, A., Meshref, M., McPhedran, K.N. and El-Din, M.G., 2015. Composite polyvinylidene fluoride (PVDF) membrane impregnated with Fe_2O_3 nanoparticles and multiwalled carbon nanotubes for catalytic degradation of organic contaminants. Journal of membrane science, 490, pp.227-235.

Amaral, R.A., Habert, A.C. and Borges, C.P., 2014. Activated carbon polyurethane membrane for a model fuel desulfurization by pervaporation. Materials Letters, 137, pp.468-470.

Arenal, R. and Lopez-Bezanilla, A., 2015. Boron nitride materials: an overview from 0D to 3D (nano) structures. Wiley Interdisciplinary Reviews: Computational Molecular Science, 5(4), pp.299-309.

Aroon, M.A., Ismail, A.F., Matsuura, T. and Montazer-Rahmati, M.M., 2010. Performance studies of mixed matrix membranes for gas separation: A review. Separation and purification Technology, 75(3), pp.229-242.

Atienzar, P., Primo, A., Lavorato, C., Molinari, R. and García, H., 2013. Preparation of graphene quantum dots from pyrolyzed alginate. Langmuir, 29(20), pp.6141-6146.

Attia, A.M., Kulchitskiy, A.R., Nour, M., El-Seesy, A.I. and Nada, S.A., 2022. The influence of castor biodiesel blending ratio on engine performance including the determined diesel particulate matters composition. Energy, 239, p.121951.

Babich, I.V. and Moulijn, J.A., 2003. Science and technology of novel processes for deep desulfurization of oil refinery streams: a review☆. Fuel, 82(6), pp.607-631.

Babuga, U. and Naseem, N., 2021. Asymmetric Effect of Oil Price Change on Inflation: Evidence from Sub Saharan Africa Countries. International Journal of Energy Economics and Policy, 11(1), p. 448.

Baheri, B. and Mohammadi, T., 2017. Sorption, diffusion and pervaporation study of thiophene/n-heptane mixture through self-support PU/PEG blend membrane. Separation and Purification Technology, 185, pp.112-119.

Barman, M.K. and Patra, A., 2018. Current status and prospects on chemical structure driven photoluminescence behaviour of carbon dots. Journal of Photochemistry and Photobiology C: Photochemistry Reviews, 37, pp.1-22.

Barros, M. A. S. D., Arroyo, P. A., & Silva, E. A. (2013). General Aspects of Aqueous Sorption Process in Fixed Beds. Mass Transfer—Advances in Sustainable Energy and Environment Oriented Numerical Modeling, InTech, Rijeka: 361-3.

Barzamini, R., Falamaki, C. and Mahmoudi, R., 2014. Adsorption of ethyl, iso-propyl, n-butyl and iso-butyl mercaptans on AgX zeolite: Equilibrium and kinetic study. Fuel, 130, pp.46-53.

Bathrinath, S., Abuthakir, N., Koppiahraj, K., Saravanasankar, S., Rajpradeesh, T. and Manikandan, R., 2021. An initiative towards sustainability in the petroleum industry: A review. Materials Today: Proceedings.

Beigbeder, A., Linares, M., Devalckenaere, M., Degée, P., Claes, M., Beljonne, D., Lazzaroni, R. and Dubois, P., 2008. CH-π Interactions as the Driving Force for Silicone-Based Nanocomposites with Exceptional Properties. Advanced materials, 20(5), pp.1003-1007.

Bello, S.S., Wang, C., Zhang, M., Gao, H., Han, Z., Shi, L., Su, F. and Xu, G., 2021. A Review on the Reaction Mechanism of Hydrodesulfurization and Hydrodenitrogenation in Heavy Oil Upgrading. Energy & Fuels, 35(14), pp.10998-11016.

Boateng, E., Adam, A. & Junior, P., 2021. Modelling the heterogeneous relationship between the crude oil implied volatility index and African stocks in the coronavirus pandemic. Resources Policy, Volume 74, p. 102389.

Boniek, D., Figueiredo, D., dos Santos, A.F.B. and de Resende Stoianoff, M.A., 2015. Biodesulfurization: a mini review about the immediate search for the future technology. Clean Technologies and Environmental Policy, 17(1), pp.29-37.

BP, 2021. BP Statistical Review of World Energy 2021, London: British Petroleum plc.

Cai, C., Fan, X., Han, X., Li, J. and Vardhan, H., 2020. Improved desulfurization performance of polyethyleneglycol membrane by incorporating metal organic framework CuBTC. Polymers, 12(2), p.414.

Cai, Q., Mateti, S., Watanabe, K., Taniguchi, T., Huang, S., Chen, Y. and Li, L.H., 2016. Boron nitride nanosheet-veiled gold nanoparticles for surface-enhanced Raman scattering. ACS applied materials & interfaces, 8(24), pp.15630-15636.

Camacho, L.M., Dumée, L., Zhang, J., Li, J.D., Duke, M., Gomez, J. and Gray, S., 2013. Advances in membrane distillation for water desalination and purification applications. Water, 5(1), pp.94-196.

Cao, K., Jiang, Z., Zhao, J., Zhao, C., Gao, C., Pan, F., Wang, B., Cao, X. and Yang, J., 2014. Enhanced water permeation through sodium alginate membranes by incorporating graphene oxides. Journal of membrane science, 469, pp.272-283.

Cao, R., Zhang, X., Wu, H., Wang, J., Liu, X. and Jiang, Z., 2011. Enhanced pervaporative desulfurization by polydimethylsiloxane membranes embedded with silver/silica core–shell microspheres. Journal of hazardous materials, 187(1-3), pp.324-332.

CCAC, 2021. Reducing Emissions from Heavy-Duty Vehicles and Fuels, s.l.: Climate and Clean Air Coalition (CCAC).

Chen, W., Hu, C., Yang, Y., Cui, J. and Liu, Y., 2016. Rapid synthesis of carbon dots by hydrothermal treatment of lignin. Materials, 9(3), p.184.

Chiou, M.S. and Li, H.Y., 2002. Equilibrium and kinetic modeling of adsorption of reactive dye on cross-linked chitosan beads. Journal of hazardous materials, 93(2), pp.233-248.

Choi, H., Ko, S.J., Choi, Y., Joo, P., Kim, T., Lee, B.R., Jung, J.W., Choi, H.J., Cha, M., Jeong, J.R. and Hwang, I.W., 2013. Versatile surface plasmon resonance of carbon-dot-supported silver nanoparticles in polymer optoelectronic devices. Nature Photonics, 7(9), pp.732-738.

Choi, S., Drese, J.H. and Jones, C.W., 2009. Adsorbent materials for carbon dioxide capture from large anthropogenic point sources. ChemSusChem: Chemistry & Sustainability Energy & Materials, 2(9), pp.796-854.

Chung, T.S., Jiang, L.Y., Li, Y. and Kulprathipanja, S., 2007. Mixed matrix membranes (MMMs) comprising organic polymers with dispersed inorganic fillers for gas separation. Progress in polymer science, 32(4), pp.483-507.

Coker, A. K., 2021. Petroleum Refining Design and Applications Handbook. s.l.:John Wiley & Sons.

Continental Automotive, 2019. Worldwide Emission Standards and Related Regulations, s.l.: Continental Automotive.

CREA, 2021. Eskom is now the world's most polluting power company, s.l.: Centre for Research on Energy and Clean Air (CREA).

Crista, D., El Mragui, A., Algarra, M., Esteves da Silva, J.C., Luque, R. and Pinto da Silva, L., 2020. Turning Spent Coffee Grounds into Sustainable Precursors for the Fabrication of Carbon Dots. Nanomaterials, 10(6), p.1209.

Dane, A., Wright, D. and Montmasson-Clair, G., 2019. Exploring the Policy Impacts of a Transition To Electric Vehicles in South Africa. Pretoria: Trade & Industrial Policy Strategies.

Darwish, N.N., 2015. Adsorption study of desulfurization of diesel oil using activated charcoal (Doctoral dissertation).

Davies, A. and Simmons, M., 2021. Demand for 'advantaged'hydrocarbons during the 21st century energy transition. Energy Reports, Volume 7, pp. 4483-4497.

DNV, 2021. Global Sulphur Cap 2020, s.l.: DNV Group.

Dolah, R., Zafar, S. and Hassan, M., 2022. Alternative jet fuels: biojet fuels' challenges and opportunities. Value-Chain of Biofuels, pp. 181-194.

El-Dorghamy, A., Attia, M. and Allam, H., 2021. Low-Emission Zones (LEZs) and Prerequisites for Sustainable Cities and Clean Air in Egypt. Center for Environment and Development for the Arab Region and Europe.

Field, T., 2021. A Just Energy Transition and Functional Federalism: The Case of South Africa. Transnational Environmental Law, 10(2), pp. 237-261.

Fihri, A., Mahfouz, R., Shahrani, A., Taie, I. and Alabedi, G., 2016. Pervaporative desulfurization of gasoline: a review. Chemical Engineering and Processing: Process Intensification, 107, pp.94-105.

Foo, K.Y. and Hameed, B.H., 2010. Insights into the modeling of adsorption isotherm systems. Chemical engineering journal, 156(1), pp.2-10.

Fu, K., Yue, Q., Gao, B., Sun, Y. and Zhu, L., 2013. Preparation, characterization and application of lignin-based activated carbon from black liquor lignin by steam activation. Chemical Engineering Journal, 228, pp.1074-1082.

Gao, J., Zhu, S., Dai, Y., Xiong, C., Li, C., Yang, W. and Jiang, X., 2018. Performance and mechanism for extractive desulfurization of fuel oil using modified polyethylene glycol. Fuel, 233, pp.704-713.

Gawande, P.R. and Kaware, J., 2014. Desulphurization Techniques for Liquid Fuel: A Review. Int. J. Eng. Technol. Manag. Appl. Sci, 2, pp.121-127.

Golberg, D., Bando, Y., Huang, Y., Terao, T., Mitome, M., Tang, C. and Zhi, C., 2010. Boron nitride nanotubes and nanosheets. ACS nano, 4(6), pp.2979-2993.

Gray, K.A., Mrachko, G.T. and Squires, C.H., 2003. Biodesulfurization of fossil fuels. Current opinion in microbiology, 6(3), pp.229-235.

GreenPeace, 2021. Ranking the World's Sulfur Dioxide (SO_2) Hotspots: 2019-2020, s.l.: GreenPeace and CREA.

Grimmer, C., Rüger, C., Streibel, T. & Cuoq, F., 2021. Description of Steam Cracker Fouling and Coking Residues by Thermal. Energy Fuels, 33(11), pp. 11592-11602.

Gu, Q., Zhu, W., Xun, S., Chang, Y., Xiong, J., Zhang, M., Jiang, W., Zhu, F. and Li, H., 2014. Preparation of highly dispersed tungsten species within mesoporous silica by ionic liquid and their enhanced catalytic activity for oxidative desulfurization. Fuel, 117, pp.667-673.

Hameed, B.H., Mahmoud, D.K. and Ahmad, A.L., 2008. Equilibrium modeling and kinetic studies on the adsorption of basic dye by a low-cost adsorbent: Coconut (Cocos nucifera) bunch waste. Journal of hazardous materials, 158(1), pp.65-72.

Hashmi, N., 2021. Evolutionary analysis of global oil and gas sector and its impact on global economy. International Journal of Management, 12(2), pp. 773-779.

Hassan, J., Ikram, M., Ul-Hamid, A., Imran, M., Aqeel, M. and Ali, S., 2020. Application of chemically exfoliated boron nitride nanosheets doped with co to remove organic pollutants rapidly from textile water. Nanoscale research letters, 15, pp.1-13.

Haubner, R., Wilhelm, M., Weissenbacher, R. and Lux, B., 2002. Boron nitrides—properties, synthesis and applications. High Performance Non-Oxide Ceramics II, pp.1-45.

Haywood, J., 2021. Atmospheric aerosols and their role in climate change. Climate change, pp. 645-659.

He, M., Wang, Z., Moldowan, J. and Peters, K., 2021. Insights into catalytic effects of clay minerals on hydrocarbon composition of generated liquid products during oil cracking from laboratory pyrolysis experiments. Organic Geochemistry, p. 104331.

Huang, D., Hua, Y., Loughney, S., Blanco-Davis, E. and Wang, J., 2020. Lifespan cost analysis of alternatives to global sulphur emission limit with uncertainties. Proceedings of the Institution of Mechanical Engineers, Part M: Journal of Engineering for the Maritime Environment, 235(4), pp. 921-930.

Huang, Q., Zhang, H., Hu, S., Li, F., Weng, W., Chen, J., Wang, Q., He, Y., Zhang, W. and Bao, X., 2014. A sensitive and reliable dopamine biosensor was developed based on the Au@ carbon dots–chitosan composite film. Biosensors and Bioelectronics, 52, pp.277-280.

IEA, 2021. World Energy Outlook 2021, s.l.: International Energy Agency.

Ito, E. and Van Veen, J.R., 2006. On novel processes for removing sulphur from refinery streams. Catalysis today, 116(4), pp.446-460.

Jahanbakhshi, M. and Habibi, B., 2016. A novel and facile synthesis of carbon quantum dots via salep hydrothermal treatment as the silver nanoparticles support: Application to electroanalytical determination of H_2O_2 in fetal bovine serum. Biosensors and Bioelectronics, 81, pp.143-150.

Jatoi, A. et al., 2021. Overview of bioelectrochemical approaches for sulfur reduction: current and future perspectives. Biomass Conversion and Biorefinery, pp. 1-16.

Javadli, R. and De Klerk, A., 2012. Desulfurization of heavy oil. Applied petrochemical research, 1(1), pp. 3-19.

Jiuhui, Q.U., 2008. Research progress of novel adsorption processes in water purification: a review. Journal of environmental sciences, 20(1), pp.1-13.

Jiwalak, N., Rattanaphani, S., Bremner, J.B. and Rattanaphani, V., 2010. Equilibrium and kinetic modeling of the adsorption of indigo carmine onto silk. Fibers and Polymers, 11(4), pp.572-579.

Kanaboshi, H., Sano, F., Oda, J., Akimoto, K. and Onishi, N., 2021. Cost-efficient measures in the oil refinery and petrochemical sectors for the reduction of CO_2 emissions under the Paris Agreement and air pollution under the MARPOL Convention. Energy and Climate Change, 2, p.100027.

Karge, H.G. and Weitkamp, J. eds., 2008. Adsorption and diffusion (Vol. 7). Springer Science & Business Media.

Kariduraganavar, M.Y., Kittur, A.A., Kulkarni, S.S. and Ramesh, K., 2004. Development of novel pervaporation membranes for the separation of water–isopropanol mixtures using sodium alginate and NaY zeolite. Journal of membrane science, 238(1-2), pp.165-175.

Katasonova, O., Savonina, E. & Maryutina, T., 2021. Extraction Methods for Removing Sulfur and Its Compounds from Crude Oil and Petroleum Products. Russian Journal of Applied Chemistry, 94(4), pp. 411-436.

Kempfer, L., 1990. The many faces of boron nitride. Materials engineering, 107(11), pp.41-44.

Kiani, S., Mousavi, S.M., Shahtahmassebi, N. and Saljoughi, E., 2015. Hydrophilicity improvement in polyphenylsulfone nanofibrous filtration membranes through addition of polyethylene glycol. Applied Surface Science, 359, pp.252-258.

Kikasu, E., 2021. The dr congo's petroleum industry: confusion and misperception over the real physical density of crude oil produced in the kongo central province of DRC. Academy of Strategic Management Journal, 20(5), pp. 1-24.

Kim, J.H., Ma, X., Zhou, A. and Song, C., 2006. Ultra-deep desulfurization and denitrogenation of diesel fuel by selective adsorption over three different adsorbents: A study on adsorptive selectivity and mechanism. Catalysis Today, 111(1-2), pp.74-83.

King, C.J., 1987. Separation processes based on reversible chemical complexation. Handbook of separation process technology, pp.760-774.

Koech, L., Rutto, H., Lerotholi, L., Everson, R.C., Neomagus, H., Branken, D. and Moganelwa, A., 2021. Spray drying absorption for desulphurization: a review of recent developments. Clean Technologies and Environmental Policy, pp.1-22.

Kong, Y., Lin, L., Yang, J., Shi, D., Qu, H., Xie, K. and Li, L., 2007. FCC gasoline desulfurization by pervaporation: Effects of gasoline components. Journal of Membrane Science, 293(1-2), pp.36-43.

Kontovas, C., 2014. The green ship routing and scheduling problem (GSRSP): a conceptual approach. Transportation Research Part D: Transport and Environment, Volume 31, pp. 61-69.

Kubota, Y., Watanabe, K., Tsuda, O. and Taniguchi, T., 2007. Deep ultraviolet light-emitting hexagonal boron nitride synthesized at atmospheric pressure. Science, 317(5840), pp.932-934.

Kumar, M., 2021. Increasing population and decreasing environment. Ecology Research, Volume 2, p. 36. Landgeist, 2021. Oil Reserves. [Online] Available at: https://landgeist.com/2021/05/15/oil-reserves/.

Kumar, P.S. and Kirthika, K., 2009. Equilibrium and kinetic study of adsorption of nickel from aqueous solution onto bael tree leaf powder. Journal of Engineering Science and Technology, 4(4), pp.351-363.

Lakshmi, U.R., Srivastava, V.C., Mall, I.D. and Lataye, D.H., 2009. Rice husk ash as an effective adsorbent: Evaluation of adsorptive characteristics for Indigo Carmine dye. Journal of Environmental Management, 90(2), pp.710-720.

Lang, Z., Wang, D., Liu, H. and Gou, X., 2021. Mapping the knowledge domains of research on corrosion of petrochemical equipment: An informetrics analysis-based study. Engineering Failure Analysis, Volume 129, p. 105716.

Larraz, R., 2021. A Brief History of Oil Refining. Substantia, 5(2), pp. 129-152.

Lawrence, A. and Ballard, 2020. South Africa's Energy Transition. s.l.:Palgrave Macmillan.

Lee, C., Li, Q., Kalb, W., Liu, X.Z., Berger, H., Carpick, R.W. and Hone, J., 2010. Frictional characteristics of atomically thin sheets. science, 328(5974), pp.76-80.

Lei, W., Portehault, D., Liu, D., Qin, S. and Chen, Y., 2013. Porous boron nitride nanosheets for effective water cleaning. Nature communications, 4(1), pp.1-7.

Li, B., Xu, D., Jiang, Z., Zhang, X., Liu, W. and Dong, X., 2008. Pervaporation performance of PDMS-Ni2+ Y zeolite hybrid membranes in the desulfurization of gasoline. Journal of Membrane Science, 322(2), pp.293-301.

Li, G., Si, Z., Cai, D., Wang, Z., Qin, P. and Tan, T., 2020. The in-situ synthesis of a high-flux ZIF-8/polydimethylsiloxane mixed matrix membrane for n-butanol pervaporation. Separation and Purification Technology, 236, p.116263

Li, H., Tuo, L., Yang, K., Jeong, H.K., Dai, Y., He, G. and Zhao, W., 2016. Simultaneous enhancement of mechanical properties and CO_2 selectivity of ZIF-8 mixed matrix membranes: Interfacial toughening effect of ionic liquid. Journal of Membrane Science, 511, pp.130-142.

Li, H., Zhu, W., Zhu, S., Xia, J., Chang, Y., Jiang, W., Zhang, M., Zhou, Y. and Li, H., 2016. The selectivity for sulfur removal from oils: an insight from conceptual density functional theory. AIChE Journal, 62(6), pp.2087-2100.

Li, L.H., Chen, Y., Behan, G., Zhang, H., Petravic, M. and Glushenkov, A.M., 2011. Large-scale mechanical peeling of boron nitride nanosheets by low-energy ball milling. Journal of materials chemistry, 21(32), pp.11862-11866.

Li, W., Pan, F., Song, Y., Wang, M., Wang, H., Walker, S., Wu, H. and Jiang, Z., 2017. Construction of molecule-selective mixed matrix membranes with confined mass transfer structure. Chinese journal of chemical engineering, 25(11), pp.1563-1580.

Li, Y., He, G., Wang, S., Yu, S., Pan, F., Wu, H. and Jiang, Z., 2013. Recent advances in the fabrication of advanced composite membranes. Journal of Materials Chemistry A, 1(35), pp.10058-10077.

Li, Y., Wang, S., He, G., Wu, H., Pan, F. and Jiang, Z., 2015. Facilitated transport of small molecules and ions for energy-efficient membranes. Chemical Society Reviews, 44(1), pp.103-118.

Lian, G., Zhang, X., Si, H., Wang, J., Cui, D. and Wang, Q., 2013. Boron nitride ultrathin fibrous nanonets: one-step synthesis and applications for ultrafast adsorption for water treatment and selective filtration of nanoparticles. ACS applied materials & interfaces, 5(24), pp.12773-12778.

Lian, G., Zhang, X., Tan, M., Zhang, S., Cui, D. and Wang, Q., 2011. Facile synthesis of 3D boron nitride nanoflowers composed of vertically aligned nanoflakes and fabrication of graphene-like BN by exfoliation. Journal of Materials Chemistry, 21(25), pp.9201-9207.

Lian, G., Zhang, X., Zhang, S., Liu, D., Cui, D. and Wang, Q., 2012. Controlled fabrication of ultrathin-shell BN hollow spheres with excellent performance in hydrogen storage and wastewater treatment. Energy & Environmental Science, 5(5), pp.7072-7080.

Lima, F., Branco, L., Silvestre, A. & Marrucho, I., 2021. Deep desulfurization of fuels: Are deep eutectic solvents the alternative for ionic liquids?. Fuel, Volume 293, p. 120297.

Lin, L., Hong, L., Jianhua, Q. and Jinjuan, X., 2010. Progress in the technology for desulfurization of crude oil. China Petrol. Process. Petrochem. Technol, 12, pp.1-6.

Lin, L., Kong, Y., Wang, G., Qu, H., Yang, J. and Shi, D., 2006. Selection and crosslinking modification of membrane material for FCC gasoline desulfurization. Journal of Membrane Science, 285(1-2), pp.144-151.

Lin, L., Wang, A., Dong, M., Zhang, Y., He, B. and Li, H., 2012. Sulfur removal from fuel using zeolites/polyimide mixed matrix membrane adsorbents. Journal of Hazardous materials, 203, pp.204-212.

Lin, L., Wang, G., Qu, H., Yang, J., Wang, Y., Shi, D. and Kong, Y., 2006. Pervaporation performance of crosslinked polyethylene glycol membranes for deep desulfurization of FCC gasoline. Journal of membrane science, 280(1-2), pp.651-658.

Lin, L., Zhang, Y. and Kong, Y., 2009. Recent advances in sulfur removal from gasoline by pervaporation. Fuel, 88(10), pp.1799-1809.

Lin, L., Zhang, Y. and Li, H., 2010. Pervaporation and sorption behavior of zeolite-filled polyethylene glycol hybrid membranes for the removal of thiophene species. Journal of colloid and interface science, 350(1), pp.355-360.

Lin, Y., Williams, T.V., Xu, T.B., Cao, W., Elsayed-Ali, H.E. and Connell, J.W., 2011. Aqueous dispersions of few-layered and monolayered hexagonal boron nitride nanosheets from sonication-assisted hydrolysis: critical role of water. The Journal of Physical Chemistry C, 115(6), pp.2679-2685.

Liu, F., Nattestad, A., Naficy, S., Han, R., Casillas, G., Angeloski, A., Sun, X. and Huang, Z., 2019. Fluorescent Carbon-and Oxygen-Doped Hexagonal Boron Nitride Powders as Printing Ink for Anticounterfeit Applications. Advanced Optical Materials, 7(24), p.1901380.

Liu, W., Hu, S., Liu, G., Pan, F., Wu, H., Jiang, Z., Wang, B., Li, Z. and Cao, X., 2014. Creation of hierarchical structures within membranes by incorporating mesoporous microcapsules for enhanced separation performance and stability. Journal of Materials Chemistry A, 2(15), pp.5267-5279.

Liu, Y. and McMillan, C.A., 2020. 2018 Industrial Energy Data Book (No. NREL/BK-6A20-73901; DOE/GO-102020-5178). National Renewable Energy Lab.(NREL), Golden, CO (United States).

Low, Z.X., Ji, J., Blumenstock, D., Chew, Y.M., Wolverson, D. and Mattia, D., 2018. Fouling resistant 2D boron nitride nanosheet–PES nanofiltration membranes. Journal of Membrane Science, 563, pp.949-956.

Ludmerczki, R., Mura, S., Carbonaro, C.M., Mandity, I.M., Carraro, M., Senes, N., Garroni, S., Granozzi, G., Calvillo, L., Marras, S. and Malfatti, L., 2019. Carbon dots from citric acid

and its intermediates formed by thermal decomposition. Chemistry–A European Journal, 25(51), pp.11963-11974.

Maghami, M. and Abdelrasoul, A., 2018. Zeolite mixed matrix membranes (Zeolite-Mmms) for sustainable engineering. Zeolites and Their Applications; BoD–Books on Demand: Norderstedt, Germany, p.115.

Marchesini, S., Wang, X. and Petit, C., 2019. Porous Boron Nitride Materials: Influence of Structure, Chemistry and Stability on the Adsorption of Organics. Frontiers in chemistry, 7, p.160.

Merkel, T.C., Freeman, B.D., Spontak, R.J., He, Z., Pinnau, I., Meakin, P. and Hill, A.J., 2002. Ultrapermeable, reverse-selective nanocomposite membranes. Science, 296(5567), pp.519-522.

Mittal, A., Mittal, J. and Kurup, L., 2006. Adsorption isotherms, kinetics and column operations for the removal of hazardous dye, Tartrazine from aqueous solutions using waste materials—Bottom Ash and De-Oiled Soya, as adsorbents. Journal of hazardous materials, 136(3), pp.567-578.

Moore, T.T. and Koros, W.J., 2005. Non-ideal effects in organic–inorganic materials for gas separation membranes. Journal of Molecular Structure, 739(1-3), pp.87-98.

NASA, 2021. Global Sulfur Dioxide Monitoring Home Page. [Online] Available at: https://so2.gsfc.nasa.gov/.

Nehlsen, J.P., 2006. Developing clean fuels: Novel techniques for desulfurization (Doctoral dissertation, Princeton University).

Niu, W.J., Li, Y., Zhu, R.H., Shan, D., Fan, Y.R. and Zhang, X.J., 2015. Ethylenediamine-assisted hydrothermal synthesis of nitrogen-doped carbon quantum dots as fluorescent probes for sensitive biosensing and bioimaging. Sensors and Actuators B: Chemical, 218, pp.229-236.

Nollet, H., Roels, M., Lutgen, P., Van der Meeren, P. and Verstraete, W., 2003. Removal of PCBs from wastewater using fly ash. Chemosphere, 53(6), pp.655-665.

Onojake, M. and Waka, T., 2021. Review of Oilfield Chemicals Used in Oil and Gas Industry. Asian Journal of Physical and Chemical Sciences, pp. 8-24.

OPEC, 2021. World Oil Outlook 2021, s.l.: Organization of the Petroleum Exporting Countries.

Ouyang, H., Li, W. and Long, Y., 2021. Carbon-doped h-BN for the enhanced electrochemical determination of dopamine. Electrochimica Acta, 369, p.137682.

Pakdel, A., Bando, Y. and Golberg, D., 2014. Nano boron nitride flatland. Chemical Society Reviews, 43(3), pp.934-959.

Pan, F., Ding, H., Li, W., Song, Y., Yang, H., Wu, H., Jiang, Z., Wang, B. and Cao, X., 2018. Constructing facilitated transport pathway in hybrid membranes by incorporating MoS2 nanosheets. Journal of Membrane Science, 545, pp.29-37.

Paramati, S., Shahzad, U. and Dogan, B., 2022. The role of environmental technology for energy demand and energy efficiency: Evidence from OECD countries. Renewable and Sustainable Energy Reviews, Volume 153, p. 111735.

Prajapati, R., Kohli, K. and Maity, S., 2021. Slurry phase hydrocracking of heavy oil and residue to produce lighter fuels: An experimental review. Fuel, Volume 288, p. 119686.

Qi, R., Wang, Y., Chen, J., Li, J. and Zhu, S., 2007. Pervaporative desulfurization of model gasoline with Ag_2O-filled PDMS membranes. Separation and Purification Technology, 57(1), pp.170-175.

Qi, R., Wang, Y., Chen, J., Li, J. and Zhu, S., 2007. Removing thiophenes from n-octane using PDMS–AgY zeolite mixed matrix membranes. Journal of membrane science, 295(1-2), pp.114-120.

Qi, R., Wang, Y., Li, J., Zhao, C. and Zhu, S., 2006. Pervaporation separation of alkane/thiophene mixtures with PDMS membrane. Journal of Membrane Science, 280(1-2), pp.545-552

Qiu, Y., Yu, J., Rafique, J., Yin, J., Bai, X. and Wang, E., 2009. Large-scale production of aligned long boron nitride nanofibers by multijet/multicollector electrospinning. The Journal of Physical Chemistry C, 113(26), pp.11228-11234.

Ragan, S. and Megonnell, N., 2011. Activated carbon from renewable resources—Lignin. Cellulose Chemistry and Technology, 45(7), p.527.

Randrianarisoa, L. and Gillen, D., 2021. Reducing emissions in international transport: A supply chain perspective. Transportation Research Part D: Transport and Environment, p. 103074.

Rees, W., 2021. Growth through contraction: conceiving an eco-economy. Real-world Econ Rev, Volume 96, pp. 98-118.

Rempel, A. and Gupta, J., 2021. Fossil fuels, stranded assets and COVID-19: Imagining an inclusive & transformative recovery. World Development, Volume 146, p. 105608.

Revo, 2021. GPF (GASOLINE PARTICULATE FILTER) – WHAT IS IT AND WHAT DOES IT DO?, s.l.: Revo.

Rezvani, M. and Aghmasheh, M., 2021. Synthesis of t-B. PWFe/NiO nanocomposite as an efficient and heterogeneous green nanocatalyst for catalytic oxidative-extractive desulfurization of gasoline. Environmental Progress & Sustainable Energy, p. e13616.

Rochard, G., Olivet, L., Tannous, M., Poupin, C., Siffert, S. and Cousin, R., 2021. Recent Advances in the Catalytic Treatment of Volatile Organic Compounds: A Review Based on the Mixture Effect. Catalysts, 11(10), p.1218.

Roman, F.F., Díaz de Tuesta, J.L., Silva, A.M., Faria, J.L. and Gomes, H.T., 2021. Carbon-based materials for oxidative desulfurization and denitrogenation of fuels: a review. Catalysts, 11(10), p.1239.

Ron, G., Paul, B. and Visnja, G., 2004. Oxidative desulfurization: a newtechnology for ULSD. Prepr Pap Am Chem Soc, Div Fuel Chem, 49(2), pp.577-579.

Rouquerol, J., Rouquerol, F., Llewellyn, P., Maurin, G. and Sing, K.S., 2013. Adsorption by powders and porous solids: principles, methodology and applications. Academic press.

Rychlewska, K., Kujawski, W. and Konieczny, K., 2017. Pervaporative performance of PEBA and PDMS based commercial membranes in thiophene removal from its binary mixtures with hydrocarbons. Fuel Processing Technology, 165, pp.9-18.

Sabet, M. and Mahdavi, K., 2019. Green synthesis of high photoluminescence nitrogen-doped carbon quantum dots from grass via a simple hydrothermal method for removing organic and inorganic water pollutions. Applied Surface Science, 463, pp.283-291.

Safarik, D.J. and Eldridge, R.B., 1998. Olefin/paraffin separations by reactive absorption: a review. Industrial & engineering chemistry research, 37(7), pp.2571-2581.

Salmeron, M., Somorjai, G.A., Wold, A., Chianelli, R. and Liang, K.S., 1982. The adsorption and binding of thiophene, butene and H2S on the basal plane of MoS_2 single crystals. Chemical Physics Letters, 90(2), pp.105-107.

Sarpong, S. and Bein, M., 2020. The relationship between good governance and CO_2 emissions in oil-and non-oil-producing countries: a dynamic panel study of sub-Saharan Africa. Environmental Science and Pollution Research, 27(17), pp. 21986-22003.

Seddon, D. and Zhang, B. eds., 2018. Hydroprocessing catalysts and processes: the challenges for biofuels production (Vol. 17). World Scientific.

Sentorun-Shalaby, C., Saha, S.K., Ma, X. and Song, C., 2011. Mesoporous-molecular-sieve-supported nickel sorbents for adsorptive desulfurization of commercial ultra-low-sulfur diesel fuel. Applied Catalysis B: Environmental, 101(3-4), pp.718-726.

Sha, S., Zhang, X.L., Wang, L.M., Li, Y.M., Lin, L.G. and Zhang, Y.Z., 2018. Effect of synthetic conditions on the morphology and gasoline desulfurization performance of microphase-separated membranes. Cellulose, 25(6), pp.3487-3497.

Shen, T., Liu, S., Yan, W. and Wang, J., 2019. Highly efficient preparation of hexagonal boron nitride by direct microwave heating for dye removal. Journal of Materials Science, 54(12), pp.8852-8859.

Shi, Q. and Wu, J., 2021. Review on Sulfur Compounds in Petroleum and Its Products: State-of-the-Art and Perspectives. Energy & Fuels, 35(18), pp. 14445-14461.

Shi, Y., Zhang, X. and Liu, G., 2015. Activated carbons derived from hydrothermally carbonized sucrose: remarkable adsorbents for adsorptive desulfurization. ACS Sustainable Chemistry & Engineering, 3(9), pp.2237-2246.

Sholl, D.S. and Lively, R.P., 2016. Seven chemical separations to change the world. Nature News, 532(7600), p.435.

Singha, N.R., Das, P. and Ray, S.K., 2013. Recovery of pyridine from water by pervaporation using filled and crosslinked EPDM membranes. Journal of Industrial and Engineering Chemistry, 19(6), pp.2034-2045.

Singha, N.R., Karmakar, M., Mahapatra, M., Mondal, H., Dutta, A., Roy, C. and Chattopadhyay, P.K., 2017. Systematic synthesis of pectin-g-(sodium acrylate-co-N-isopropylacrylamide) interpenetrating polymer network for superadsorption of dyes/M (II): Determination of physicochemical changes in loaded hydrogels. Polymer Chemistry, 8(20), pp.3211-3237.

Singhal, S.K., Srivastava, A.K., Pant, R.P., Halder, S.K., Singh, B.P. and Gupta, A.K., 2008. Synthesis of boron nitride nanotubes employing mechanothermal process and its characterization. Journal of materials science, 43(15), pp.5243-5250.

Soeder, D., 2021. The History of Oil & Gas Development in the US. Fracking and the Environment, pp. 37-61.

Soma, T., Sawaoka, A. and Saito, S., 1974. Characterization of wurtzite type boron nitride synthesized by shock compression. Materials Research Bulletin, 9(6), pp.755-762.

Song, C., 2002. New approaches to deep desulfurization for ultra-clean gasoline and diesel fuels: an overview. Prepr Pap Am Chem Soc Div Fuel Chem, 47(2), pp.438-444.

Song, J., Zhao, L., Wang, Y., Xue, Y., Deng, Y., Zhao, X. and Li, Q., 2018. Carbon quantum dots prepared with chitosan for synthesis of CQDs/AuNPs for iodine ions detection. Nanomaterials, 8(12), p.1043.

Song, X., Hu, J. and Zeng, H., 2013. Two-dimensional semiconductors: recent progress and future perspectives. Journal of Materials Chemistry C, 1(17), pp.2952-2969.

Srivastava, V.C., 2012. An evaluation of desulfurization technologies for sulfur removal from liquid fuels. Rsc Advances, 2(3), pp.759-783.

Stafie, N., Stamatialis, D.F. and Wessling, M., 2005. Effect of PDMS cross-linking degree on the permeation performance of PAN/PDMS composite nanofiltration membranes. Separation and purification technology, 45(3), pp.220-231.

Stratas Advisors, 2021. Insights 2019 - 2021, s.l.: Stratas Advisors.

Su, C., Huang, S., Qin, M. and Umar, M., 2021. Does crude oil price stimulate economic policy uncertainty in BRICS?. Pacific-Basin Finance Journal, Volume 66, p. 101519.

Subramanian, C., 2021. Corrosion prevention of crude and vacuum distillation column overheads in a petroleum refinery: A field monitoring study. Process Safety Progress, 40(2), p. e12213.

Sudeep, P.M., Vinod, S., Ozden, S., Sruthi, R., Kukovecz, A., Konya, Z., Vajtai, R., Anantharaman, M.R., Ajayan, P.M. and Narayanan, T.N., 2015. Functionalized boron nitride porous solids. RSC advances, 5(114), pp.93964-93968.

Takahashi, A., Yang, F.H. and Yang, R.T., 2002. Desulfurization of gasoline by extraction with N-alkyl-pyridinium-based ionic liquids. Ind. Eng. Chem. Res, 41, pp.2487-2496.

Tang, C., Bando, Y., Huang, Y., Zhi, C. and Golberg, D., 2008. Synthetic routes and formation mechanisms of spherical boron nitride nanoparticles. Advanced Functional Materials, 18(22), pp.3653-3661.

Tian, Y., Xu, B., Yu, D., Ma, Y., Wang, Y., Jiang, Y., Hu, W., Tang, C., Gao, Y., Luo, K. and Zhao, Z., 2013. Ultrahard nanotwinned cubic boron nitride. Nature, 493(7432), pp.385-388.

Titirici, M.M., Antonietti, M. and Baccile, N., 2008. Hydrothermal carbon from biomass: a comparison of the local structure from poly-to monosaccharides and pentoses/hexoses. Green Chemistry, 10(11), pp.1204-1212.

Torres, M., Morales, A., Peralta, A. and Kroneck, P., 2020. 2. Sulfur, the Versatile Non-metal. Transition Metals and Sulfur–A Strong Relationship for Life, pp. 19-50.

Tseng, H.H., Itta, A.K., Weng, T.H. and Li, Y.L., 2013. SBA-15/CMS composite membrane for H2 purification and CO2 capture: Effect of pore size, pore volume, and loading weight on separation performance. Microporous and mesoporous materials, 180, pp.270-279.

Vattipalli, V., Qi, X., Dauenhauer, P.J. and Fan, W., 2016. Long walks in hierarchical porous materials due to combined surface and configurational diffusion. Chemistry of Materials, 28(21), pp.7852-7863.

Velu, S., Ma, X. and Song, C., 2003. Selective adsorption for removing sulfur from jet fuel over zeolite-based adsorbents. Industrial & engineering chemistry research, 42(21), pp.5293-5304.

Venna, S.R., Lartey, M., Li, T., Spore, A., Kumar, S., Nulwala, H.B., Luebke, D.R., Rosi, N.L. and Albenze, E., 2015. Fabrication of MMMs with improved gas separation properties using

externally-functionalized MOF particles. Journal of Materials Chemistry A, 3(9), pp.5014-5022.

Vinh-Thang, H. and Kaliaguine, S., 2013. Predictive models for mixed-matrix membrane performance: a review. Chemical reviews, 113(7), pp.4980-5028.

Wang, H., Wang, F., Li, X., Peng, X., Ci, Z. and Wang, Z., 2018. Preparation and performance investigation of polydimethylsiloxane microsphere/polyvinyl alcohol composite hydrogel. Materials Letters, 228, pp.399-402.

Wang, L., Zhao, Z., Li, J. and Chen, C., 2006. Synthesis and characterization of fluorinated polyimides for pervaporation of n-heptane/thiophene mixtures. European polymer journal, 42(6), pp.1266-1272.

Wang, Q., Zheng, H., Long, Y., Zhang, L., Gao, M. and Bai, W., 2011. Microwave–hydrothermal synthesis of fluorescent carbon dots from graphite oxide. Carbon, 49(9), pp.3134-3140.

Wang, W., Bando, Y., Zhi, C., Fu, W., Wang, E. and Golberg, D., 2008. Aqueous noncovalent functionalization and controlled near-surface carbon doping of multiwalled boron nitride nanotubes. Journal of the American Chemical Society, 130(26), pp.8144-8145.

Wang, X., Cao, L., Lu, F., Meziani, M.J., Li, H., Qi, G., Zhou, B., Harruff, B.A., Kermarrec, F. and Sun, Y.P., 2009. Photoinduced electron transfers with carbon dots. Chemical Communications, (25), pp.3774-3776.

Wang, X., Zhi, C., Weng, Q., Bando, Y. and Golberg, D., 2013, November. Boron nitride nanosheets: novel syntheses and applications in polymeric composites. In Journal of Physics: Conference Series (Vol. 471, No. 1, p. 012003). IOP Publishing.

Wang, Y., Yang, R.T. and Heinzel, J.M., 2008. Desulfurization of jet fuel by π-complexation adsorption with metal halides supported on MCM-41 and SBA-15 mesoporous materials. Chemical Engineering Science, 63(2), pp.356-365.

Wang, Y., Yang, R.T. and Heinzel, J.M., 2009. Desulfurization of jet fuel JP-5 light fraction by MCM-41 and SBA-15 supported cuprous oxide for fuel cell applications. Industrial & Engineering Chemistry Research, 48(1), pp.142-147.

Weber, T.W. and Chakravorti, R.K., 1974. Pore and solid diffusion models for fixed-bed adsorbers. AIChE Journal, 20(2), pp.228-238.

Weber, W.J. and Smith, E.H., 1987. Simulation and design models for adsorption processes. Environmental science & technology, 21(11), pp.1040-1050.

Weng, Q., Wang, X., Wang, X., Bando, Y. and Golberg, D., 2016. Functionalized hexagonal boron nitride nanomaterials: emerging properties and applications. Chemical Society Reviews, 45(14), pp.3989-4012.

World Oil Projections, 2021. WorldOMeters. [Online] Available at: https://www.worldometers.info/oil/.

World Population Projections, 2021. WorldOMeters. [Online] Available at: https://www.worldometers.info/world-population/world-population-projections.

Wu, J. and Yin, L., 2011. Platinum nanoparticle modified polyaniline-functionalized boron nitride nanotubes for amperometric glucose enzyme biosensor. ACS applied materials & interfaces, 3(11), pp.4354-4362.

Wu, P., Zhu, W., Chao, Y., Zhang, J., Zhang, P., Zhu, H., Li, C., Chen, Z., Li, H. and Dai, S., 2016. A template-free solvent-mediated synthesis of high surface area boron nitride nanosheets for aerobic oxidative desulfurization. Chemical Communications, 52(1), pp.144-147.

Xiao, J., Li, Z., Liu, B., Xia, Q. and Yu, M., 2008. Adsorption of benzothiophene and dibenzothiophene on ion-impregnated activated carbons and ion-exchanged Y zeolites. Energy & Fuels, 22(6), pp.3858-3863.

Xiao, J., Song, C., Ma, X. and Li, Z., 2012. Effects of aromatics, diesel additives, nitrogen compounds, and moisture on adsorptive desulfurization of diesel fuel over activated carbon. Industrial & Engineering Chemistry Research, 51(8), pp.3436-3443.

Yan, Z., Lin, J., Yuan, X., Song, T., Yu, C., Liu, Z., He, X., Liang, J., Tang, C. and Huang, Y., 2017. Desulfurization of model oil by selective adsorption over porous boron nitride fibers with tailored microstructures. Scientific reports, 7(1), pp.1-8.

Yang, D., Yang, S., Jiang, Z., Yu, S., Zhang, J., Pan, F., Cao, X., Wang, B. and Yang, J., 2015. Polydimethyl siloxane–graphene nanosheets hybrid membranes with enhanced pervaporative desulfurization performance. Journal of Membrane Science, 487, pp.152-161.

Yang, R.T., Hernández-Maldonado, A.J. and Yang, F.H., 2003. Desulfurization of transportation fuels with zeolites under ambient conditions. Science, 301(5629), pp.79-81.

Yang, Z., Zhang, W., Wang, T. and Li, J., 2014. Improved thiophene solution selectivity by Cu^{2+}, Pb^{2+} and Mn^{2+} ions in pervaporative poly [bis (p-methyl phenyl) phosphazene] desulfurization membrane. Journal of Membrane Science, 454, pp.463-469.

Yang, Z.J., Wang, Z.Q., Li, J. and Chen, J.X., 2013. Enhancing FCC gasoline desulfurization performance in a polyphosphazene pervaporative membrane. Separation and Purification Technology, 109, pp.48-54.

Yin, Y., Jiang, W.J., Liu, X.Q., Li, Y.H. and Sun, L.B., 2012. Dispersion of copper species in a confined space and their application in thiophene capture. Journal of Materials Chemistry, 22(35), pp.18514-18521

Yong, H.H., Park, H.C., Kang, Y.S., Won, J. and Kim, W.N., 2001. Zeolite-filled polyimide membrane containing 2, 4, 6-triaminopyrimidine. Journal of Membrane Science, 188(2), pp.151-163.

Yu, S., Jiang, Z., Li, W., Mayta, J.Q., Ding, H., Song, Y., Li, Z., Dong, Z., Pan, F., Wang, B. and Zhang, P., 2018. Elevated performance of hybrid membranes by incorporating metal organic framework CuBTC for pervaporative desulfurization of gasoline. Chemical Engineering and Processing-Process Intensification, 123, pp.12-19.

Yu, S., Jiang, Z., Yang, S., Ding, H., Zhou, B., Gu, K., Yang, D., Pan, F., Wang, B., Wang, S. and Cao, X., 2016. Highly swelling resistant membranes for model gasoline desulfurization. Journal of Membrane Science, 514, pp.440-449.

Yuen, S.M., Ma, C.C.M., Chiang, C.L., Lin, Y.Y. and Teng, C.C., 2007. Preparation and morphological, electrical, and mechanical properties of polyimide-grafted MWCNT/polyimide composite. Journal of Polymer Science Part A: Polymer Chemistry, 45(15), pp.3349-3358.

Zehra, S., Mobin, M. and Aslam, R., 2022. Corrosion inhibitors: an introduction. Environmentally Sustainable Corrosion Inhibitors, pp. 47-67.

Zhai, M. and Wolff, H., 2021. Air pollution and urban road transport: evidence from the world's largest low-emission zone in London. Environmental Economics and Policy Studies, pp. 1-28.

Zhang, Y., Song, J., Mayta, J.Q., Pan, F., Gao, X., Li, M., Song, Y., Wang, M., Cao, X. and Jiang, Z., 2020. Enhanced desulfurization performance of hybrid membranes using embedded hierarchical porous SBA-15. Frontiers of Chemical Science and Engineering, 14(4), pp.661-672.

Zhao, X., Krishnaiah, G. and Cartwright, T., 2004. S-Brane technology brings flexibility to refiners' clean fuel solutions. In NPRA annual meeting, San Antonio, TX.

Zheng, Z., Cox, M. and Li, B., 2018. Surface modification of hexagonal boron nitride nanomaterials: a review. Journal of Materials Science, 53(1), pp.66-99.

Zhi, C., Bando, Y., Tang, C. and Golberg, D., 2005. Immobilization of proteins on boron nitride nanotubes. Journal of the American Chemical Society, 127(49), pp.17144-17145.

Zhu, Y., Ji, X., Pan, C., Sun, Q., Song, W., Fang, L., Chen, Q. and Banks, C.E., 2013. A carbon quantum dot decorated RuO_2 network: outstanding supercapacitances under ultrafast charge and discharge. Energy & Environmental Science, 6(12), pp.3665-3675.

3. CHAPTER THREE: DEVELOPMENT OF BORON NITRIDE AND CARBON DOT SYSTEM

3.1 Introduction

This chapter elaborates on the development of hexagonbal boron nitride (h-BN) and carbon dot (C-dot) system and their charecterization with reference to the methodology graphically depicted in section 3.2.

3.2 Graphical representation of Methodology

This section describes graphically the materials used, as well as the experimental and analysis techniques employed in this study. Each following Figure provides the process flow of activities and materials used in the research work, providing details about the methods which included characterization as well.

The following includes graphical representation of the flow diagram of the following research activities:

- Overview of h-BN synthesis
- Overview of C-dot synthesis
- Overview of C-dot doped on h-BN

3.2.1 Overview of h-BN synthesis

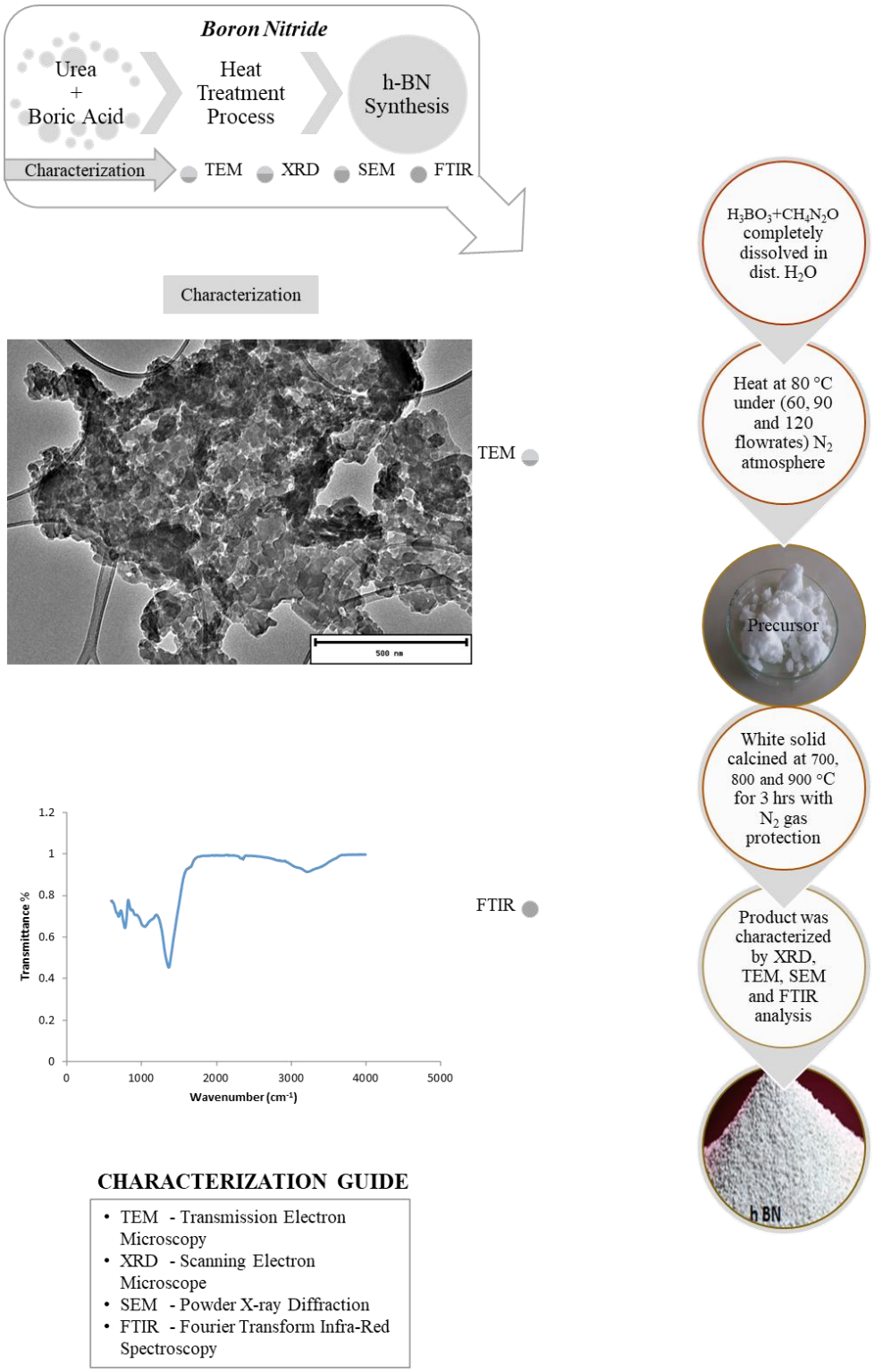


Figure 3.1 The flow diagram of h-BN synthesis and its characterization

3.2.2 Overview of C-dot synthesis

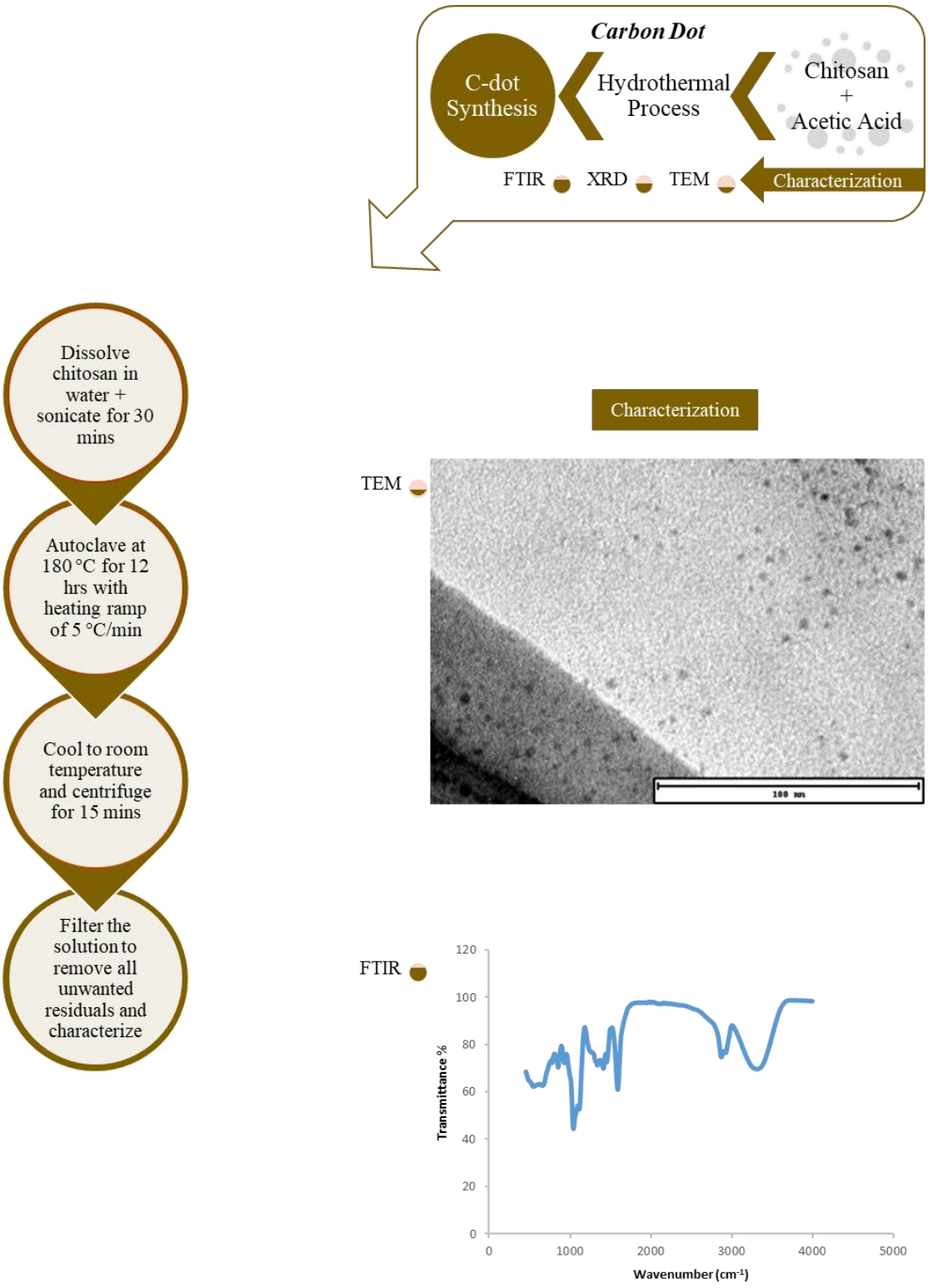


Figure 3.2 The flow diagram of C-dot synthesis and its characterization

3.2.3 Overview of C-dot doped on h-BN

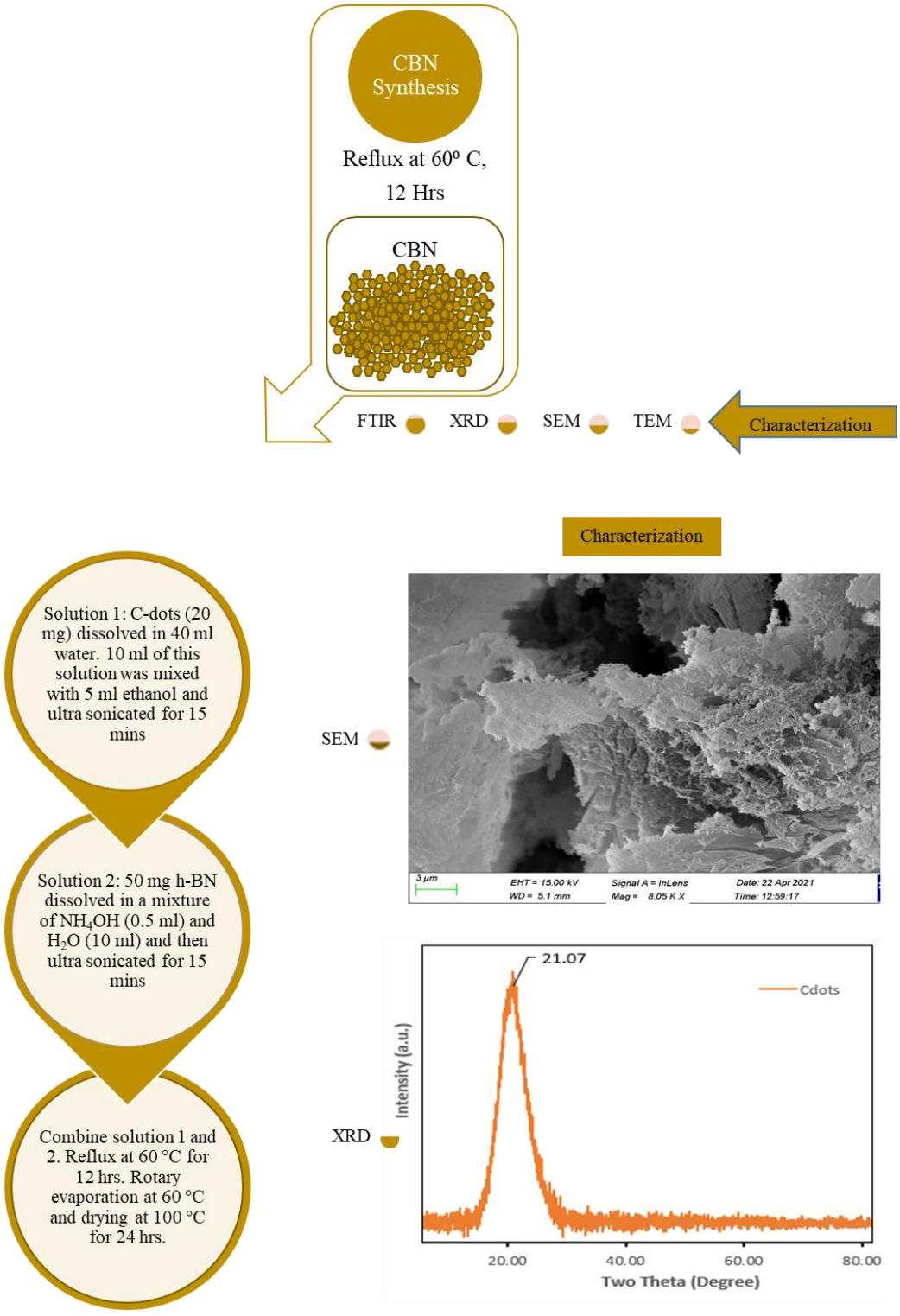


Figure 3.3 The flow diagram of C-dot doped on h-BN and its characterization

3.3 Methods

The literature review in chapter two assisted in adopting the methods and analytical techniques used in this investigation. The presentation of the methods was split in three sections namely, hexagonal boron nitride (h-BN), carbon dots and doping synthesis. Figure 3.4 shows the method used for the synthesis of the adsorptive material system used prior to embedding into the polymeric membrane.

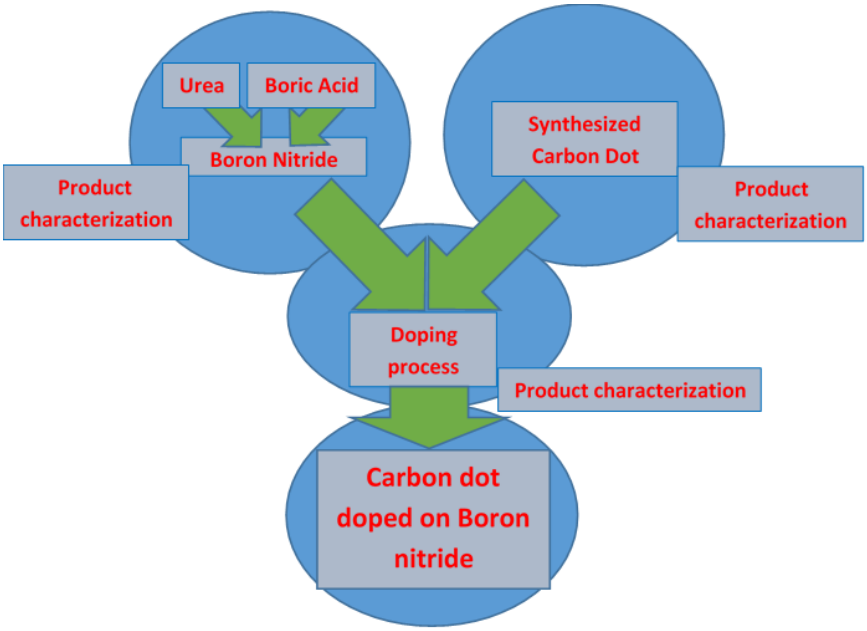


Figure 3.4 Methods used for the development of adsorptive materials

3.3.1 Synthesis of Boron Nitride

The raw materials and synthesis pathways used to generate h-BN are critical since the quality and properties of the developed h-BN will be determined by them. Hard templates, such as mesoporous silica (Rushton and Mokaya, 2008), carbonaceous materials (Dibandjo et al., 2005), or structure-directing chemicals (Li et al.,2013) are commonly used as sacrificial material to maintain better control over BN pore structure in template synthesis (Schlienger et

al., 2012). However, there are a number of drawbacks to templating techniques, such as the removal of solid templates after synthesis or the presence of various impurities in the final product. Alternative template-free approaches that nevertheless allow for tailorable structures are being researched to try to overcome these drawbacks. The heat-treatment of solid nitrogen and boron precursors in either an inert, an ammonia, or a nitrogen/hydrogen environment is frequently used in the template-free synthesis of porous BN. Even though the ease of this synthesis approach has advantages over template procedures, little is known about how to manage the structure and chemistry of porous BN, which is necessary to modify the materials characteristics for specific applications. As a result, it is necessary to look into the impact of different synthesis conditions on the structure and chemistry of porous BN materials. Variable synthesis parameters have been shown to be critical in managing the porous BN structure in several exploratory investigations.

Nag et al., (2010), found that increasing the urea to boric acid molar ratio increased the surface area of BN by up to three times. The implications of dissolving the nitrogen and boron precursors in a solvent before the synthesis step were neglected until recently, when Wu et al., (2016), revealed that this had a major impact on BN formation. The surface area of BN might be adjusted by recrystallizing urea and boric acid from different solvents with different boiling temperatures. This re-crystallization phase created intermediates with varying crystalline structures, which influenced their disintegration following heat treatment, resulting in BN structures that varied. As a result, this experiment explored the introduction of N_2 gas at initial stage of precursor preparation for h-BN synthesis in order to acquire a better inert environment and have better knowledge of BN production in template-free method and the effect it has on the adsorption performance. It was hypothesized that by gaining a better understanding of template-free synthesis processes, a path to enhanced control over the synthesis of porous BN structures may be found.

The current study develops h-BN from low-cost B and N-containing precursors such as boric acid (H_3BO_3) and urea (NH_2CONH_2) which are widely used in h-BN production. The two raw materials were purchased from Sigma Aldrich (Pty) Ltd., South Africa and were utilized as received. There were two steps in the synthesis route in this investigation: synthesis of the precursor, and development of h-BN.

Step 1: Synthesis of the h-BN precursor

This experiment explores a method of introducing N_2 gas at initial stage of precursor preparation. The continuous supply of N_2 ensures that the reaction proceeds as intended and also serves as a protective gas during the synthesis process. For this purpose, three flowmeters of N_2 with different flowrates (60, 90 and 120 ml/min) were employed into the reaction mixtures in a water bath with a fixed temperature.

Boron (boric acid) and nitrogen (urea) containing reactants were added in 10 ml of distilled water. The solutions were stirred continuously at a certain temperature to investigate the effect N_2 flow rate on the development of h-BN. The ratio of boric acid to urea was fixed at 1:24. Boric acid and urea mixture solutions were introduced into a water bath set with specific temperature and connected to different flowmeters with 60, 90 and 120ml/min flowrates of N_2 gas. The reactions were carried out at 80 ^oC till a white solid is formed and no liquid remained in the mixture. The solid precursors were dried in an oven at 75 ^oC till a firm white solid is formed. Figure 3.5 shows the precursor preparation with N_2 inflow used in this research.



Figure 3.5 Water bath set up for precursor preparation

Step 2: Development of the h-BN

Two calcination methods were used for the development of h-BN from the precursor, namely Heat Treatment Furnace (HTF) and Chemical Vapour Deposition (CVD) methods. Both methods used inert gas to avoid oxidation of the developed product.

Method 1: Heat Treatment Furnace (HTF)

The dried powder precursor was heated at 3 different furnace temperatures of 700, 800 and 900 ^{o}C to have 3 samples prepared at different furnace temperatures. The heating was carried out for 3 hours in the presence of N_2 atmosphere. The product was cooled down and removed from

furnace to obtain a white product. All the obtained products were characterized to confirm the formation of h-BN.

Method 2: Chemical Vapour Deposition (CVD)

The fourier transform infrared spectroscopy (FTIR) of h-BN samples generated from precursors prepared with different nitrogen flowrates showed no significant differences. Therefore, the dried powder precursor from N2 with 120ml/min flowrate was selected for CVD calcination. A horizontal CVD tube with an electrical wire resistance was employed for this purpose (Camurlu, 2011). The furnace was secured with gas-tight fittings and a trap for outlet gases from furnace was arranged to restrict air from getting into the system and to dissolve the released gases.

The samples were transferred to a crucible and further heated in a CVD for 3 hours under Argon atmosphere at a constant flowrate. Three samples were prepared in CVD at 3 different temperatures of 700, 800 and 900 °C. The developed h-BN was removed from the CVD, and was characterized. Figure 3.6 illustrates horizonatal CVD method for h-BN synthesis from the precursor.

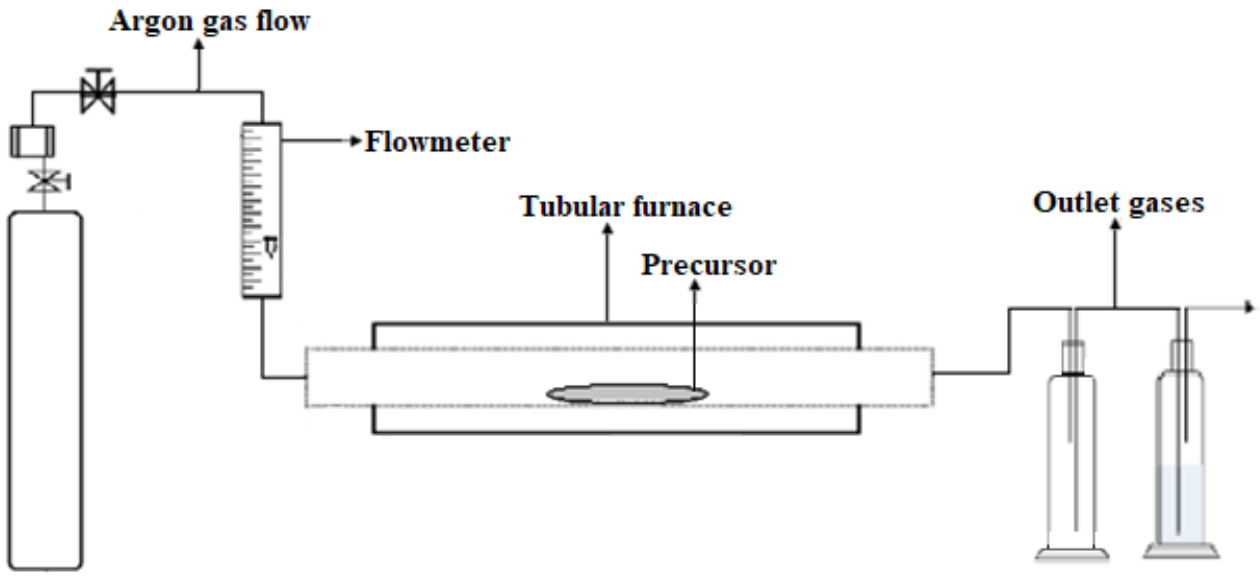


Figure 3.6 Horizontal CVD method for h-BN synthesis

3.3.2 Carbon Dot (C-dots)

The C-dots were produced using chitosan as carbon source, which was carbonized using hydrothermal process. 0.5g of chitosan was added to 100 ml of 1% acetic acid solution and mixed for 20 minutes with an ultrasonicator. The solution was shifted into a stainless steel teflon autoclave and was heated in a muffle furnace for hydrothermal treatment. The autoclave undergoes a thermal treatment, at 180 ^{o}C temperature for 12 hours with a heating rate of 5 ^{o}C/min. The autoclave was left to cool down to room temperature after the reaction. The solution was transformed from a colourless liquid to a dark brown solution, signalling the development of the C-dots. The resulting solution obtained was centrifuged at a speed of 10 000 rpm for 15 minutes and filtered to eliminate unwanted particles (Song et al., 2018). The produced C-dots were characterised with FTIR and transmission electron microscopy (TEM) analysis. Figure 3.7 describes the hydrothermal synthesis of C-dots from chitosan.

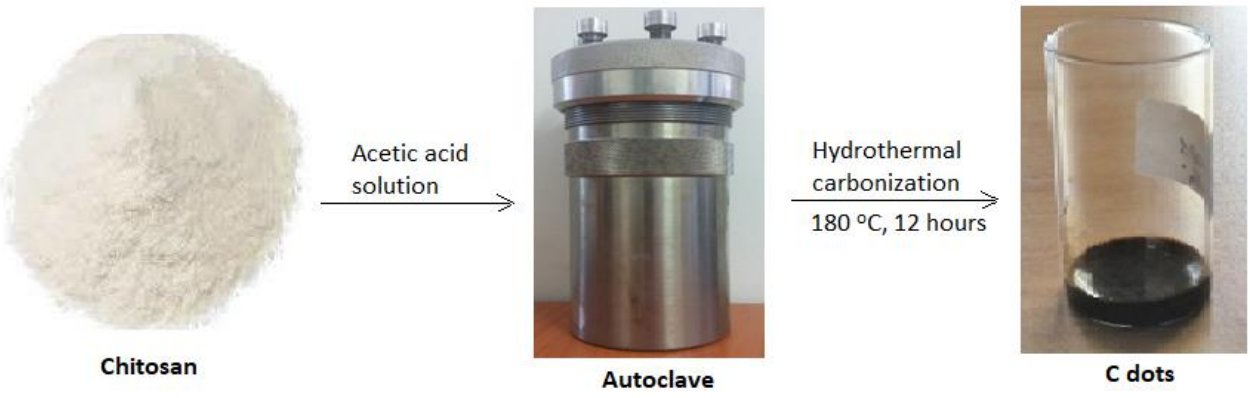


Figure 3.7 Hydrothermal synthesis of Carbon dots

3.3.3 Carbon dot doped on h-Boron nitride (CBN)

The synthesis of C-dot doped BN (CBN) was adopted from the method used by Zhao et al., (2011). Two solutions were prepared to dope C-dot into h-BN.

Solution 1: 20 mg C-dots were dispered in 40 ml distilled water. 10 ml of this solution was mixed with 5 ml of ethyl alcohol and was ultra-sonicated in a water bath for 15 minutes at room temperature.

Solution 2: 50 mg h-BN was added to 10 ml distilled water and 0.5 ml liquid ammonia mixture. This solution was ultra-sonicated in a water bath for 15 minutes at room temperature.

The prepared solutions (1 and 2) were combined together and subjected to a 12 hour reflux at 60 °C. Thereafter, the solvent from the resultant mixture was evaporated at 60 °C using rotary evaporator. The final mixture was dried in an oven at 100 °C for 24 hours for the remaining solvent to evaporate.

3.4 Analytical Techniques

The synthesized products were analysed with transmission electron microscopy (TEM), scanning electron microscope (SEM), powder X-ray diffraction (XRD), fourier transform infrared (FTIR) for morphology, crystal structure and functional groups respectively.

Fourier transform infrared spectroscopy (FTIR)

The chemical composition of the produced products were analysed with FTIR. Bruker Tensor 27 model with Opus software was used to record the IR spectra ranging between 500 and 4000 cm^{-1} to detect the functional groups of the materials. A small amount of material was placed on the instrument for scanning to generate the IR spectra. The peaks were compared with the literature to determine the specific functional groups.

Transmission electron microscope (TEM)

TEM analysis was performed by using FEI Tecnai TEM instrument. TEM samples for examination were arranged by firstly adding a small quantity of sample in ethanol and sonicating in water bath for about 10 minutes for even distribution of sample particles in the solvent. Secondly, a small droplet of the dispersion was carefully applied on a 200 mesh carbon grid with lacy carbon film and left for few minutes to dry. The grid was finally introduced into the TEM instrument to analyse the sample at different magnifications to record images of interest.

Scanning Electron Microscopy (SEM)

SEM was additionally used to inspect the microstructure of the samples using FEI Quanta 200 SEM model. The samples were placed onto the carbon resins and then mounted onto spuds using a dual sided tape. Gold palladium (Au/Pd) coating was used on the samples prior scanning, to make the material surface conductive.

X-ray diffraction spectroscopy (XRD)

XRD is a non-destructive bulk method used to interpret the crystal structures of substances. XRD, furnished with a Cu Kα (λ = 1.5418 Å) source on a Bruker D2 X-ray diffractometer was used to analyse the crystalline structure of the samples synthesized. The 2θ measurements range from 20 to 100 °. The data obtained was interpreted using an EVA software with PLU2018-pdf-4-2018RDB database. The material is finely ground in powder XRD, and each set of crystallographic planes diffracts X-rays constructively at particular angles (θ). Crystalline patterns plot the intensity of X-rays diffracted at various angles and can be used to identify the type of crystalline structure formed, as well as the spacing between various planes (d-spacing), the crystalline size and their orientation. The d-spacing is calculated by using Bragg's law.

Bragg's Law:

$$n\lambda = 2d\sin\theta \qquad (3.0)$$

Where, θ = angle between incident X-rays and crystal lattice; n = integer; d = spacing between planes;and λ = wavelength

3.5 Results and Discussion

3.5.1 Hexagonal Boron Nitride

This section provides with the results and discussion aspects of h-BN. Figure 3.8a shows the precursor formed from the reaction mixture with N_2 inlet and, h-BN formed from CVD and HTF processes.

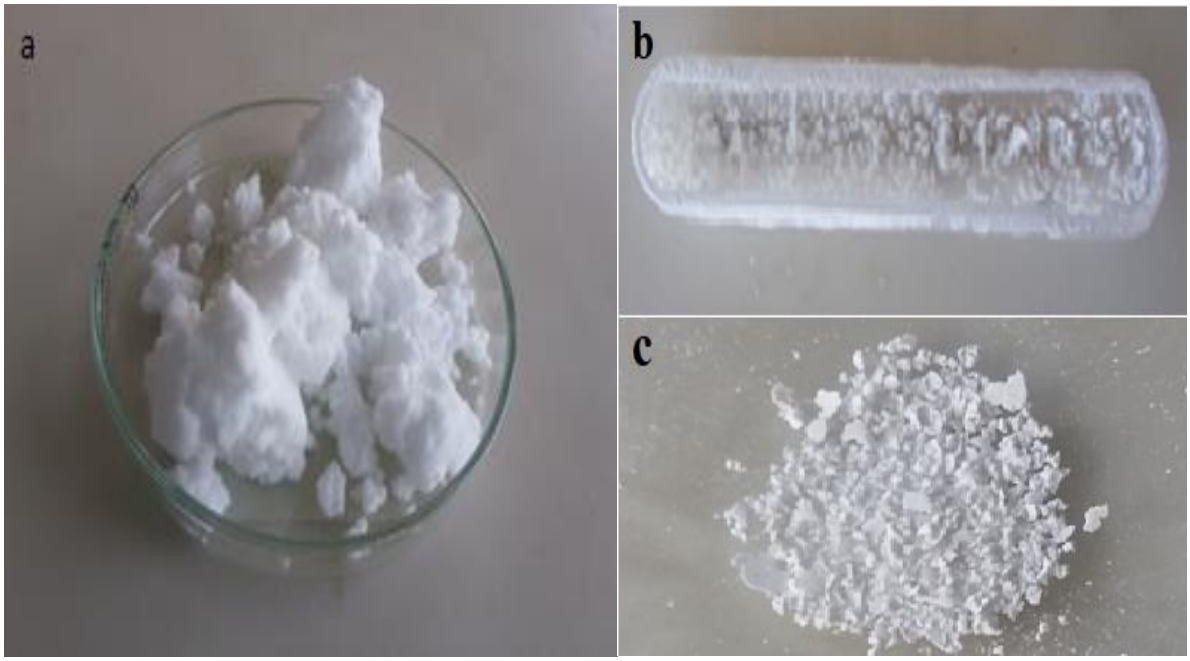


Figure 3.8 (a) Precursor formed from Boric acid and urea reaction mixture, (b) h-BN product after heating in a CVD reactor, and (c) h-BN from HTF

The reaction in CVD was carried out in argon atmosphere, which is inert and no N_2 source was introduced into the CVD system. It can be assumed that nitrogen and boron present in the precursor/intermediate (HNBOH) reacts to produce h-BN along with other gaseous by-products that exit from the reactor while heating. For HTF, N_2 gas was introduced to avoid air

contact with the precursor. The following reactions take place during the formation of h-BN according to Hubacek and Ueki, (1996):

$$2H3BO3 + CO(NH2)\,2 = 2\,H(NB)OH + CO2 + 3H2O \quad (3.1)$$

A complex HNBOH (precursor) is formed by reacting urea with boric acid along with the release of CO2 and H2O in equation 3.1.

$$3H(NB)OH = BN + B2O3 + N2 + 3H2 \quad (3.2)$$

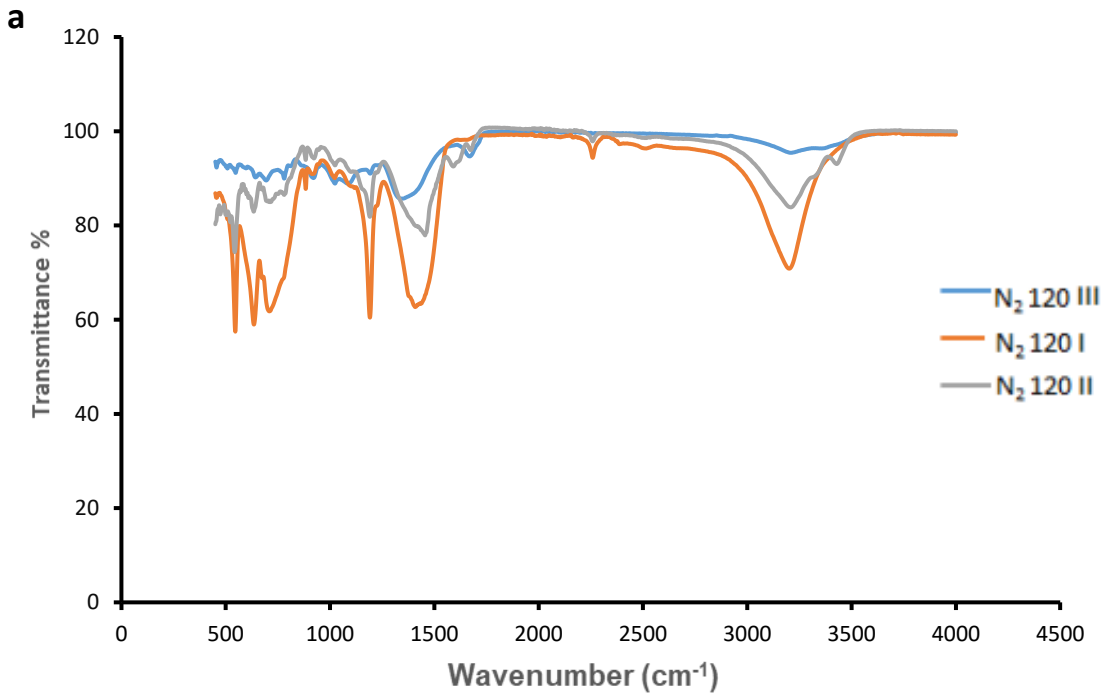
h-BN was formed from the precursor by the release of B_2O_3, H_2 andN_2 as can be seen from equation 3.2. To maintain the stoichiometric coefficients simple in the equations quantifying the hydrolysis process, the constitutional water was ignored in the calculation for boron nitride on the side of the reaction products. H-BN grows during the heating process while liberating hydrogen and hydroxyl groups. Hydrogen and nitrogen gases are formed by thermal decomposition process. Hydrogen released during the reaction may get used in the reduction of boron oxide to elemental boron which then reacts with nitrogen to form h-BN (Bartnitskaya et al., 1998). In a study by Nag et al., (2010), relative proportions of urea and boric acid were varied to investigate its effect on the development of h-BN. They proposed the following reactions from their study:

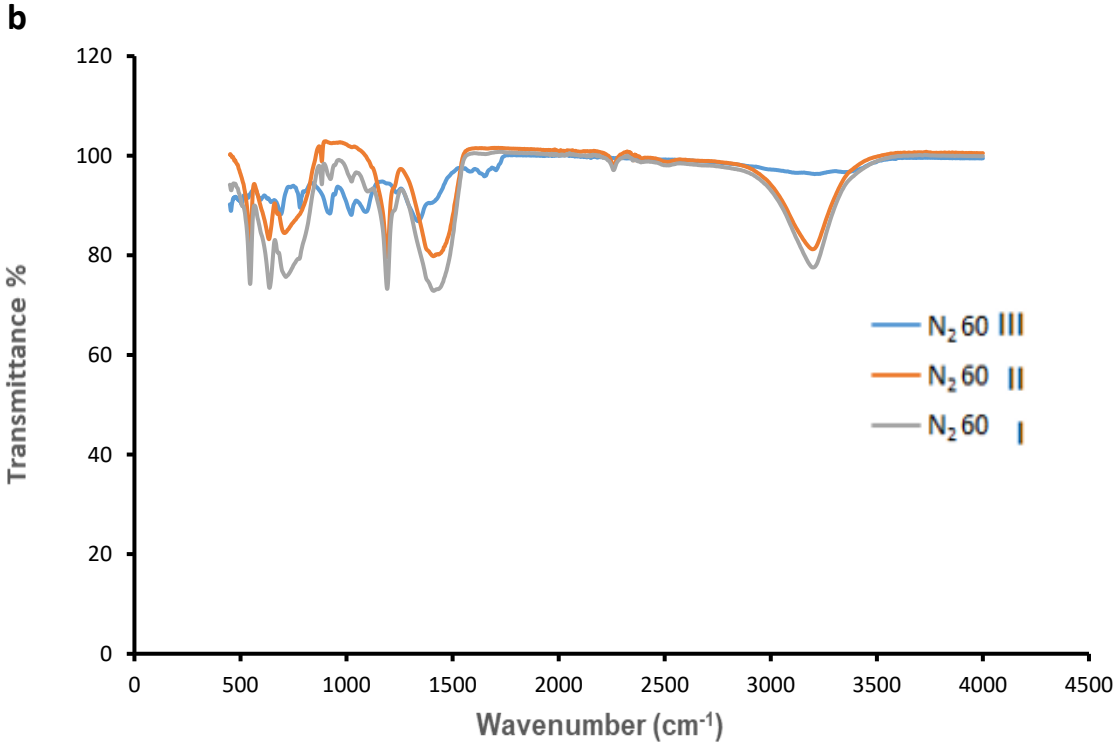
The equations 3.3, 3.4 and 3.5 explains the simultaneous reactions taking place during the h-BN synthesis process. Boron oxide and ammonia released during the reation would react under thermal heating process to produce boron nitride and water molecules.

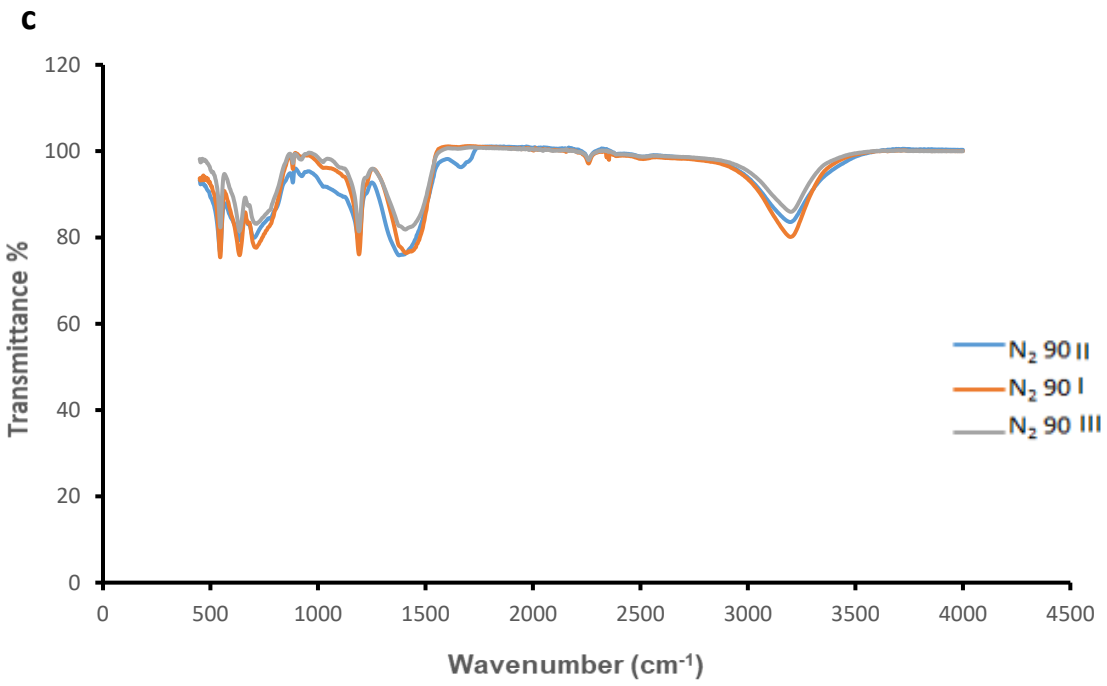
$$2H_3BO_3 \xrightarrow{\triangle} B_2O_3 + 3H_2O \quad (3.3)$$

$$NH_2CONH_2 \xrightarrow{\triangle} NH_3 + HNCO \quad (3.4)$$

$$B_2O_3 + 2NH_3 \xrightarrow{\triangle} 2BN + 3H_2O \qquad (3.5)$$







HTF Calcination at I=700 ºC, II= 800ºC and III=900ºC

Figure 3.9 (a) FTIR spectra of h-BN from the precursors prepared at (a) 120 N_2 flowrate, (b) 60 N_2 flowrate and (c) 90 N_2 flowrate

Figure 3.9 a, b and c shows FTIR spectra for h-BN samples developed from precursors prepared at different N_2 flowrate**s** after calcination using HTF method. All the h-BN FTIR spectra show peaks conforming the B–N–O vibration at ~1190 cm^{-1} (Sudeep et al., 2015). There are also various broad peaks ranging between 540-720 cm^{-1} and 1190-1445 cm^{-1} which can be attributed to the unreacted precursor material present in the final products. It has been stated that finding the functional peaks in the FTIR range of h-BN is challenging due to the high intensity of B–N peaks at ~ 785 cm^{-1} and ~1370 cm^{-1}, which may interfere with other vibrations (Nazarov et al., 2012).

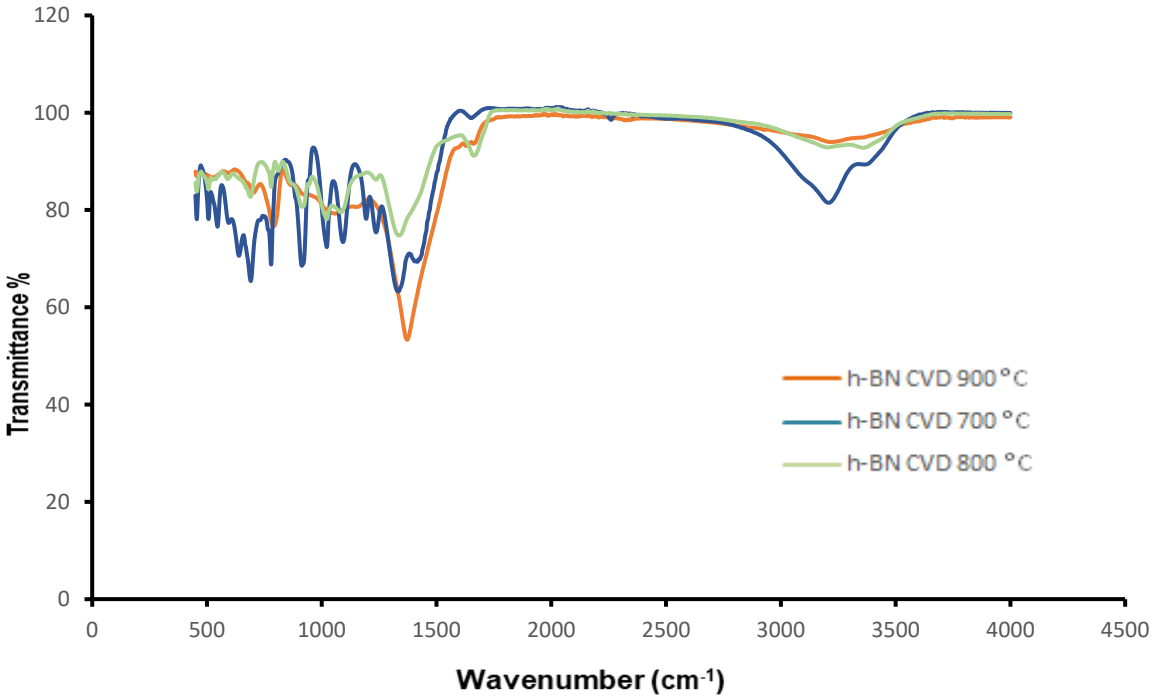


Figure 3.10 FTIR spectra of h-BN synthesized using CVD method at different temperatures

Figure 3.10 reveals the FTIR spectra of CVD h-BN synthesized at different temperatures. A trend was observed when the calcination temperature was increased from 700 °C to 900 °C with the FTIR Figure 3.9 (a, b and c) and Figure 3.10 of h-BN showing the presence of –OH at ~3210 cm^{-1} that indicate the presence of additional functional group in h-BN. The -OH peak intensity was seen to be decreasing when the calcination temperature increases, as can be understood from the FTIR spectra of different h-BN products produced at 3 different calcination temperatures (Camurlu, 2011). The additional peak intensities between 540 and 1350 cm^{-1} are also seen to be reducing with increased temperature which can be hypothesised that the increase in calcination temperature increases the removal of volatile substances during the synthesis process.

The FTIR spectra of the final products produced using the HTF method of precursors with various nitrogen inert gas flowrates exhibited no significant pattern. There were no major

changes observed between the samples synthesized with varied nitrogen flowrates. However, the calcination temperatures and method used had a considerable impact on the final products. Therefore, h-BN prepared by CVD method at 900 ºC was utilized in the study to prepare the final adsorptive material as it had much less impurities when compared to other samples.

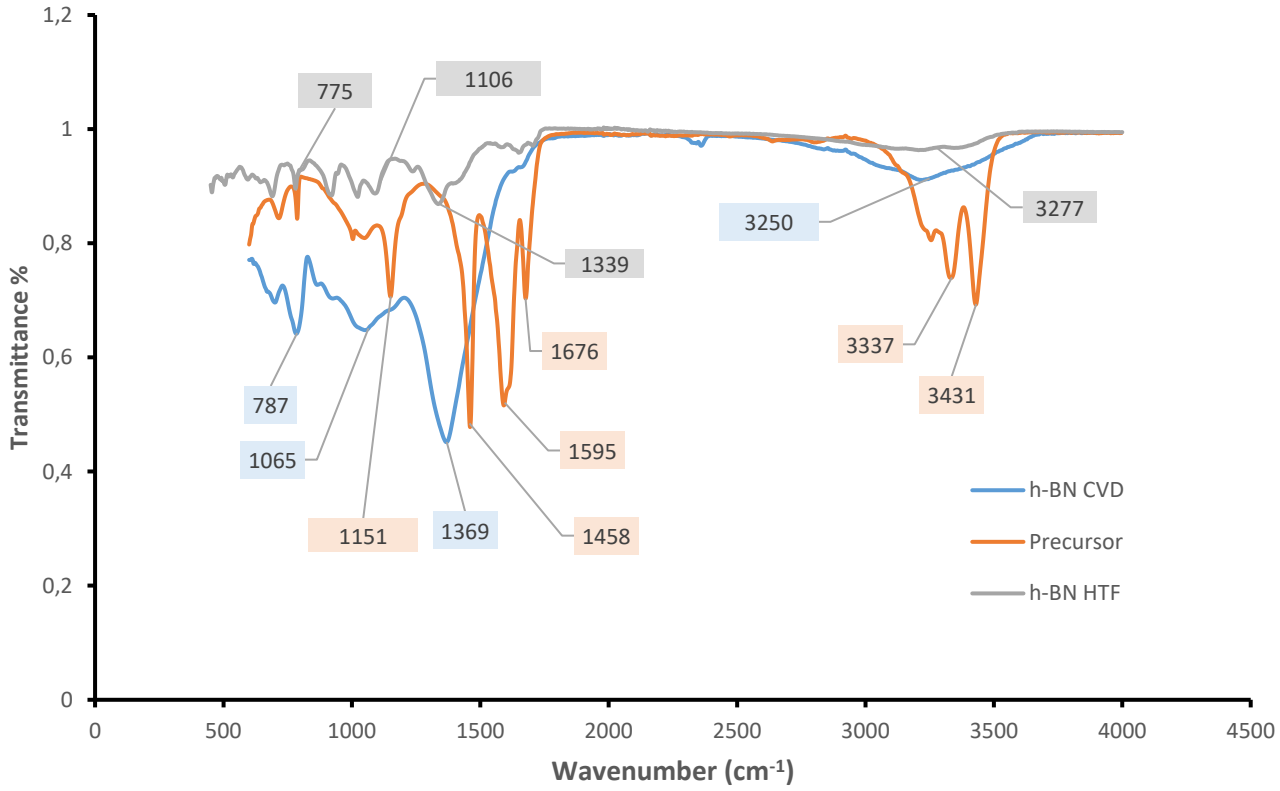


Figure 3.11 The FTIR spectra of precursor formed from urea, boric acid before heat treatment and final h-BN product from CVD and HTF methods heated at 900 ºC

Figure 3.11 compares the FTIR spectra of the precursor, h-BN prepared from CVD and HTF methods. The Figure showed that h-BN formed at 900 ºC from CVD favours the development of ~~pure~~ h-BN with less impurities compared to h-BN from HTF at 900 ºC. The h-BN from

CVD shows two distinctive peaks at 1369 cm^{-1} and 787 cm^{-1} representing the in-plane B-N stretching vibrations and out of plane B-N-B bending vibrations, respectively whereas, the precursor lacks these two main peaks (Xiong et al., 2015; Yan et al., 2017; Besisa et al., 2016). Besides the two significant peaks, another broad peak at 1065 cm^{-1} was recorded for h-BN CVD, which is believed to be indicating the presence of surface bonds containing boron and/or nitrogen or it might be due to a C-B bond . This formation might be an impurity formed in very low quantity (Besisa et al., 2016).

h-BN has a polymer like structure with hexagons consisting of B and N. The presence of -OH and -H groups on periphery of h-BN was suggested to be found as a result of H_2O release during h-BN crystal unification process (Hubacek and Ueki, 1996). The peak at ~ 3250 cm^{-1} for h-BN CVD 900 ^oC designates the -OH vibration, ~~peak~~ indicating the presence of -OH on h-BN (Nazarov et al., 2012). The presence of oxygen bearing functional groups is evident from all the h-BN FTIR spectra. The existence of oxygen-containing functional groups in the product is assumed to increase hydrophilicity which are advantageous for adsorption effect (Shen et al., 2019).

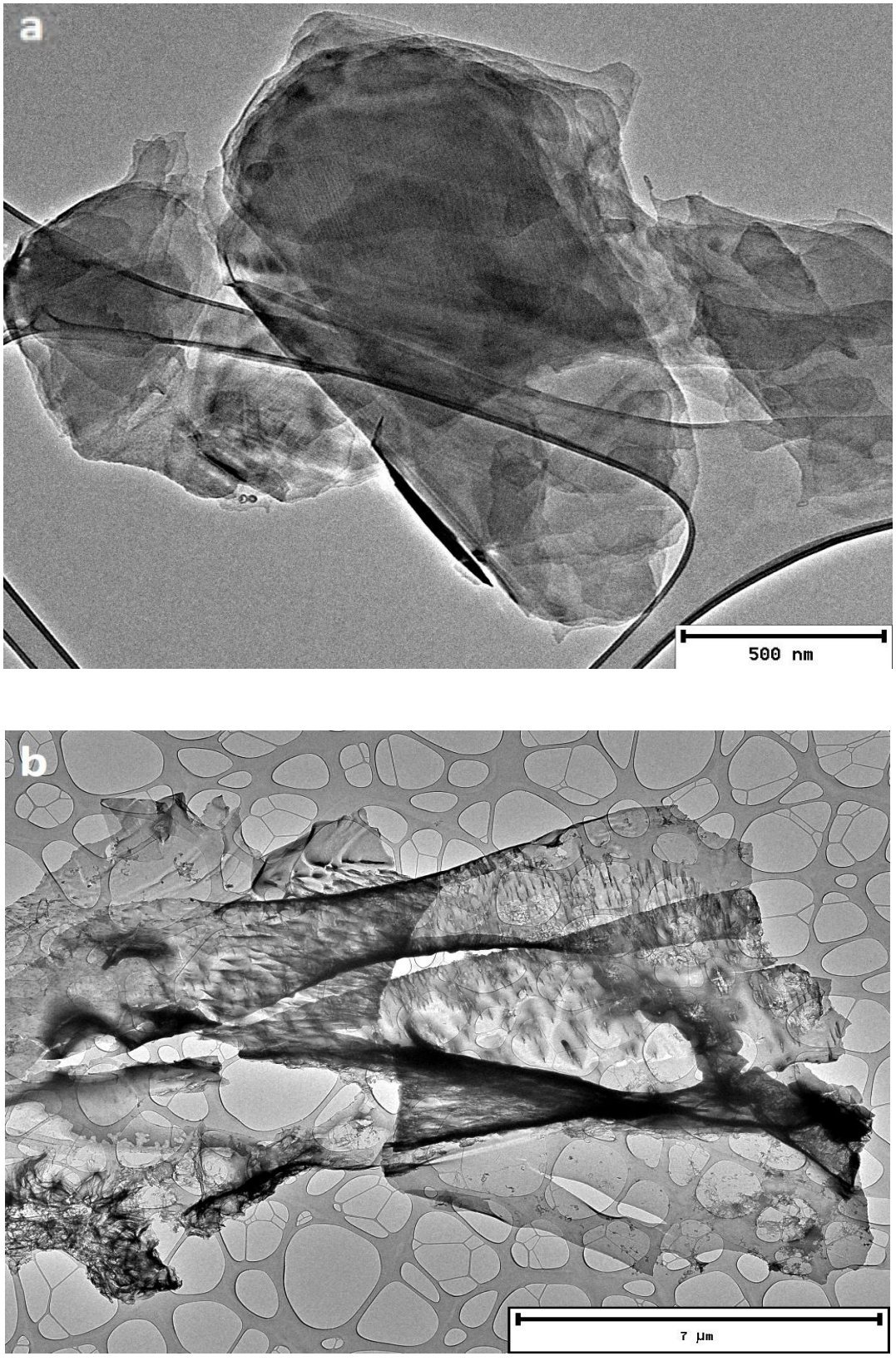


Figure 3.12 TEM images of h-BN CVD (900 ºC) (a) showing stacked layer like structures, and (b) h-BN with multiple crippled layers

TEM analysis shows the morphology of h-BN taken at different magnifications. The image in Figure 3.12a reveals several stacked layers with the upper layer showing straight line like structures arranged parallel to each other. The distance between each line in the surface layer appears to be equal (Besisa et al., 2016; Hidalgo et al., 2013). The TEM image in Figure 3.12b clearly revealed almost transparent crippled surfaces with pores and protruding edges of h-BN indicating their ultra-thin thickness (Xiong et al., 2018). All the images from TEM analysis observed have multiple layered disordered structures of h-BN flakes.



Figure 3.13 SEM image showing h-BN aggregates from CVD (900 ^{o}C)

The aggregate assembly of h-BN was observed using a SEM image as shown in the Figure 3.13. The image of the h-BN displays an irregular and unevenly distributed grained crystal like

structures. Due to the clustering over a large area, the picture represents an unequal distribution of large faceted particles with tiny incrustations on the surface. The retention of moisture may be the reason for the presence of large faceted particles and aggregation (Berchmans et al., 2009).

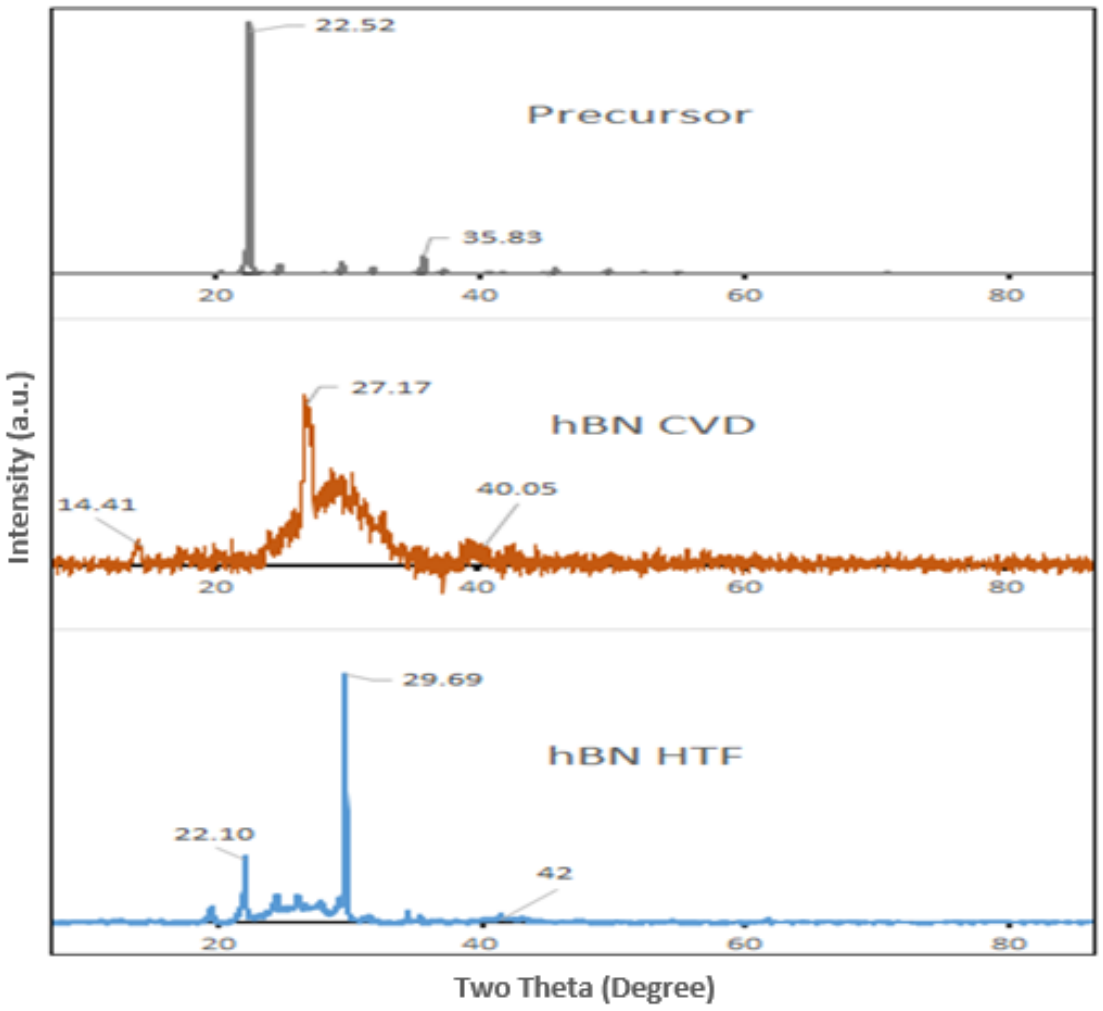


Figure 3.14 Image showing XRD peaks of precursor, synthesized h-BN by CVD (900 ^{o}C) method and HTF (900 ^{o}C) method

Figure 3.14 presents the XRD patterns of the precursor and h-BN formed by CVD under argon atmosphere and HTF methods. XRD peaks of h-BN HTF reveals a strong peak of the

crystallographic (002) plane at 2θ = 29.69° for h-BN which indicates the crystalline structure of h-BN. Bragg's law is used to calculate d (interplanar spacing values) indicating the distance between BN layers which can be deduced to be ~ 0.30nm of the produced h-BN (Camurlu, 2011). Another classical peak (100), was noticed but is very weak at about 42 °. The peak at 22.10 ° and other broad peaks indicate that the h-BN produced might have unreacted precursor and some impurities (Xiong et al., 2018). An extra peak at 22.10 ° indicates the presence of impurity which agrees with the FTIR data. The XRD result of the precursor shows two distinctive peaks at 22.52 ° and 35.83 ° which are completely different from the peaks observed for h-BN. The h-BN synthesized using CVD at 900 ºC has a sharp peak at 27.17 º and some of it spreading over a wide range indicating h-BN powder may be of low crystallinity. Two peaks at 40.05 ° (100) and 14.41 ° (001) are similar to the BN peaks observed in the study by Huang et al., (2013).

3.5.2 Carbon Dot

This section provides with the results and discussion of C-dots produced by hydrothermal process.

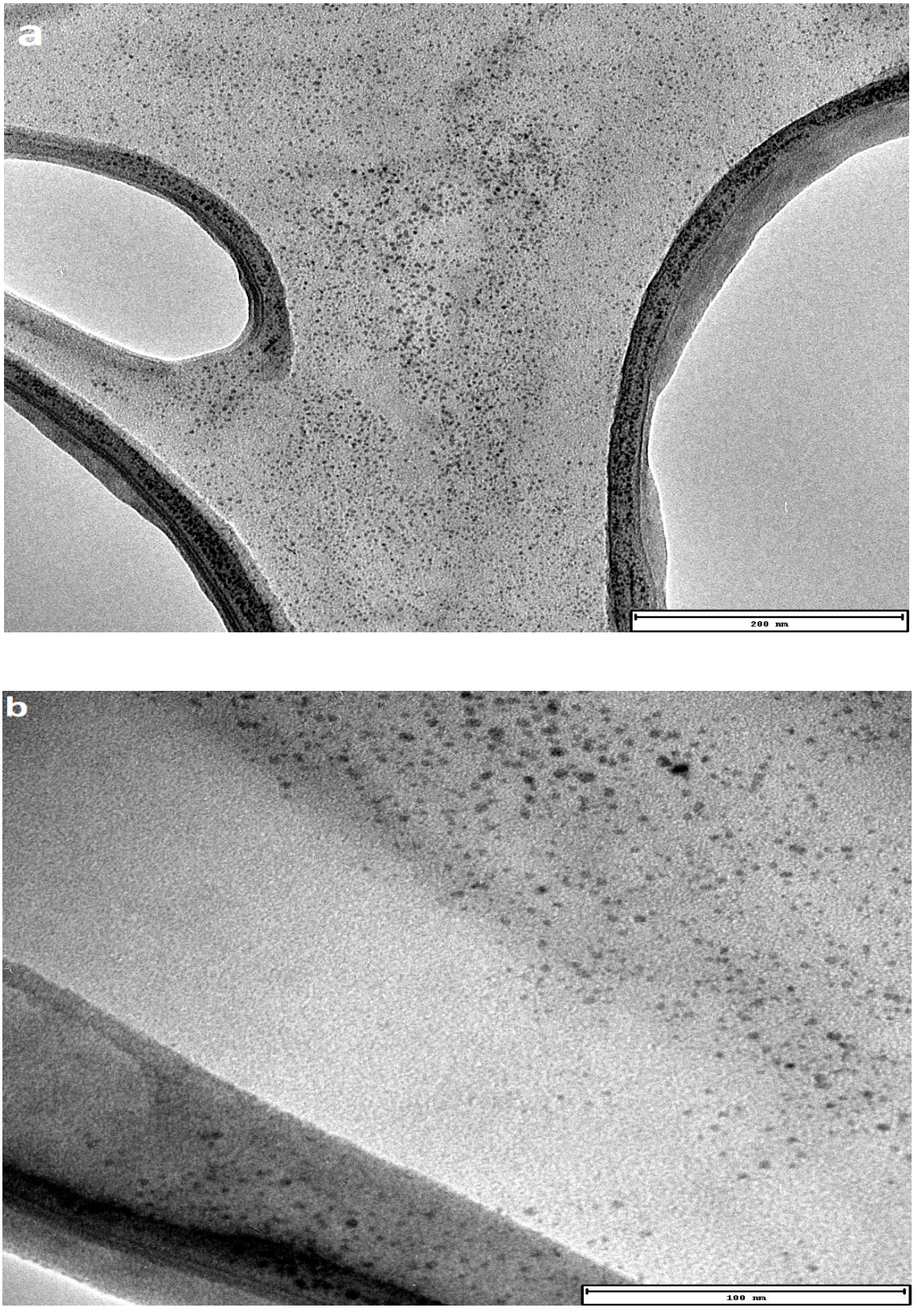


Figure 3.15 TEM images (a) C-dots (200nm) and (b) C-dots (100nm)

Figure 3.15 displays the TEM results of C-dots images taken at different magnifications. The C-dot images from Figure 3.15a and b are clearly observed to have a nearly spherical shape with a nano size range of around 5-10 nm in diameter (Jahanbakhshi and Habibi, 2016). Figure 3.15 b also reveals some C-dots that are agglomerated.

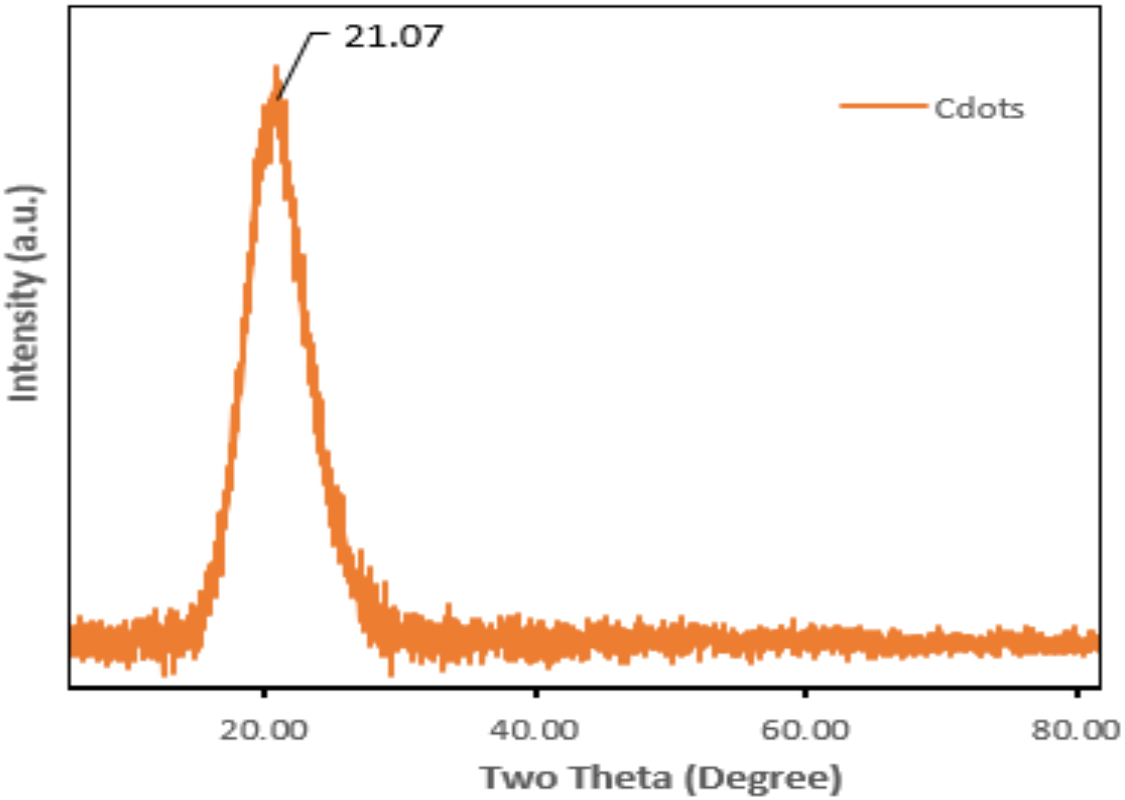


Figure 3.16 XRD spectra of C-dots

Figure 3.16 shows the XRD spectra of C-dots synthesized from hydrothermal process. A broad, low-intensity diffraction peak centred at $2\theta = 21.07$ ° was evident in the XRD spectrum figure, confirming the presence of amorphous carbon (Liu et al., 2017). The XRD patterns revealed

no sharp peaks other than 2θ = 21.07 °, reflecting the amorphous nature of the synthesized C-dots (Bajpai et al., 2019).

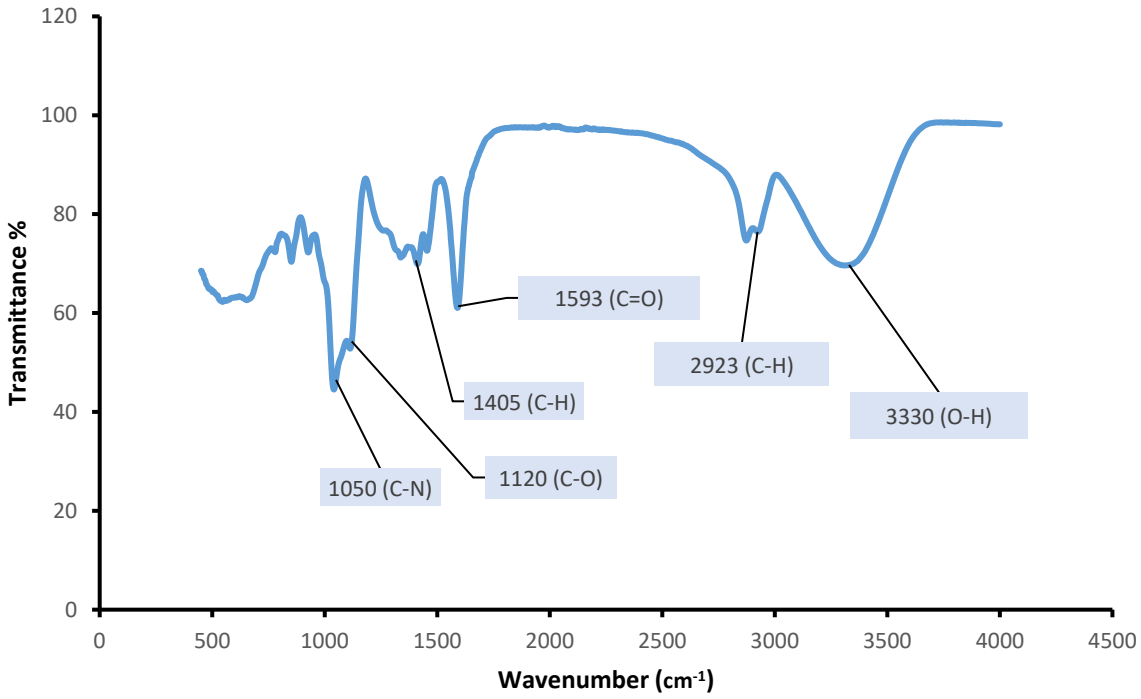


Figure 3.17 FTIR of synthesized C-dots

The existence of various functional groups in each sample is confirmed by FTIR spectroscopy of the produced C-dots as illustrated in the graph of Figure 3.17. The O–H vibrational stretching and C–H bending peaks of C-dots are positioned at 3330 cm^{-1} and 2923 cm^{-1}, respectively. The vibrational stretching peaks of C=O, C–H, C–O, and C–N can be found at 1593 cm^{-1}, 1405 cm^{-1}, 1120 cm^{-1}, and 1050 cm^{-1} respectively (Vasimalai et al., 2018)

3.5.3 Carbon dot doped on Boron nitride (CBN)

This section discusses the results of C-dots obtained from various analytical techniques.

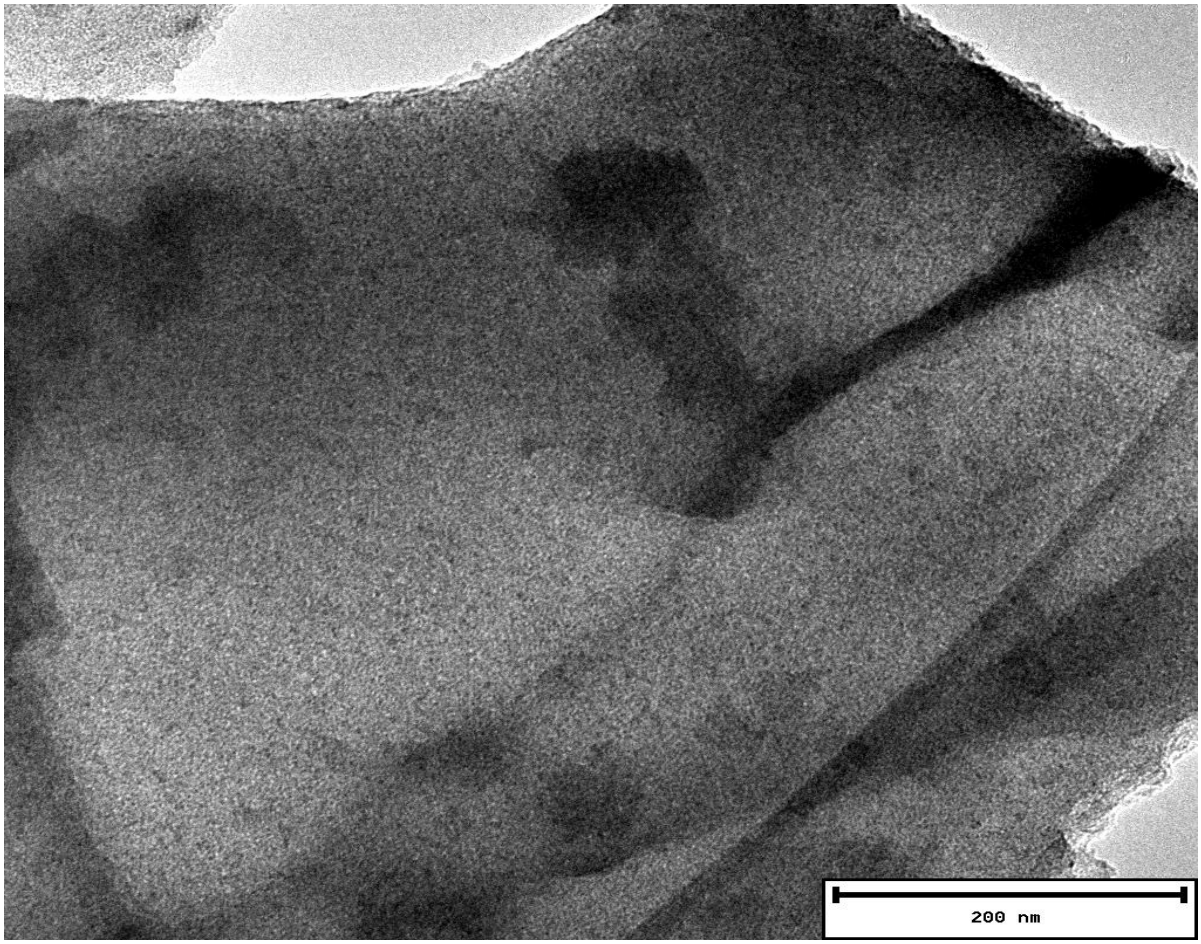
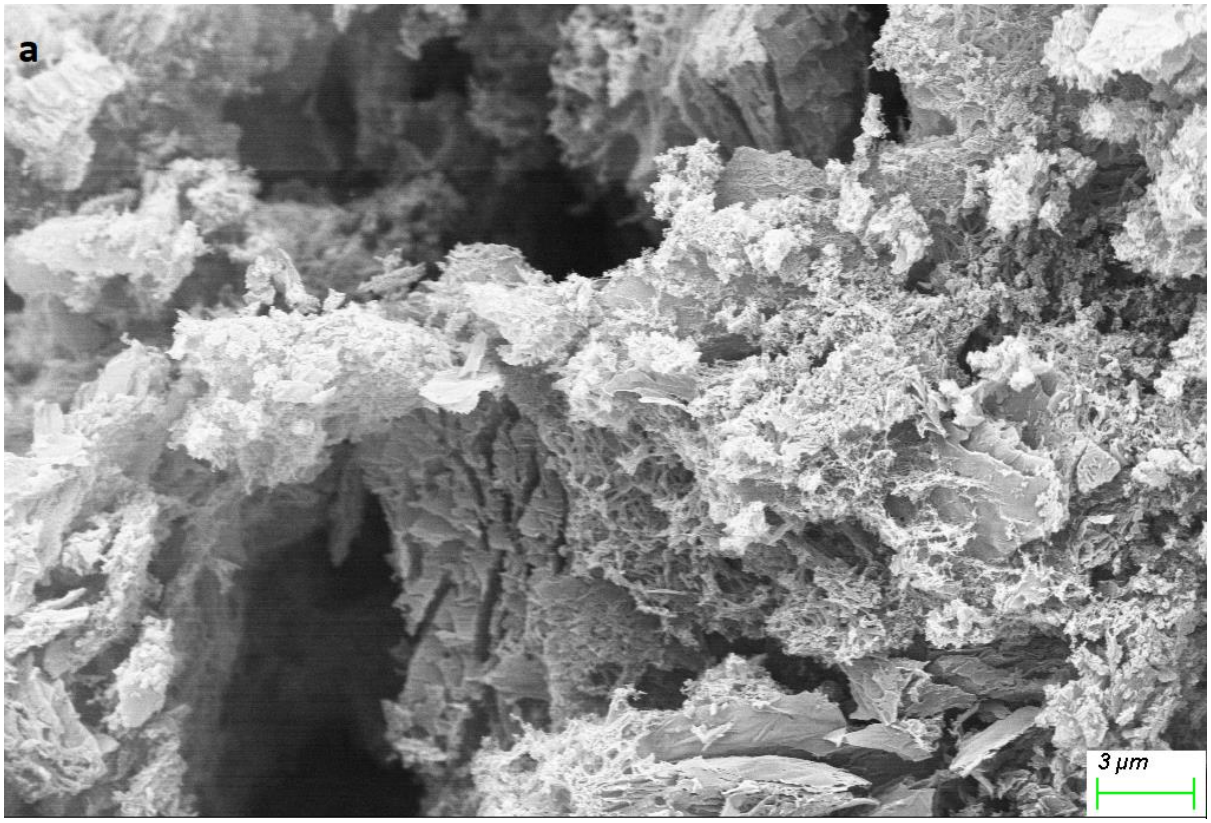


Figure 3.18 TEM image of C-dots doped onto h-BN

Figure 3.18 exhibits a low resolution TEM image of CBN showing nano sized C-dots doped onto the h-BN. Whereas, h-BN image from Figure 3.12 a, presents a structure with thin nano sheets having smooth surfaces (Ouyang and Long, 2021).


a
3 µm

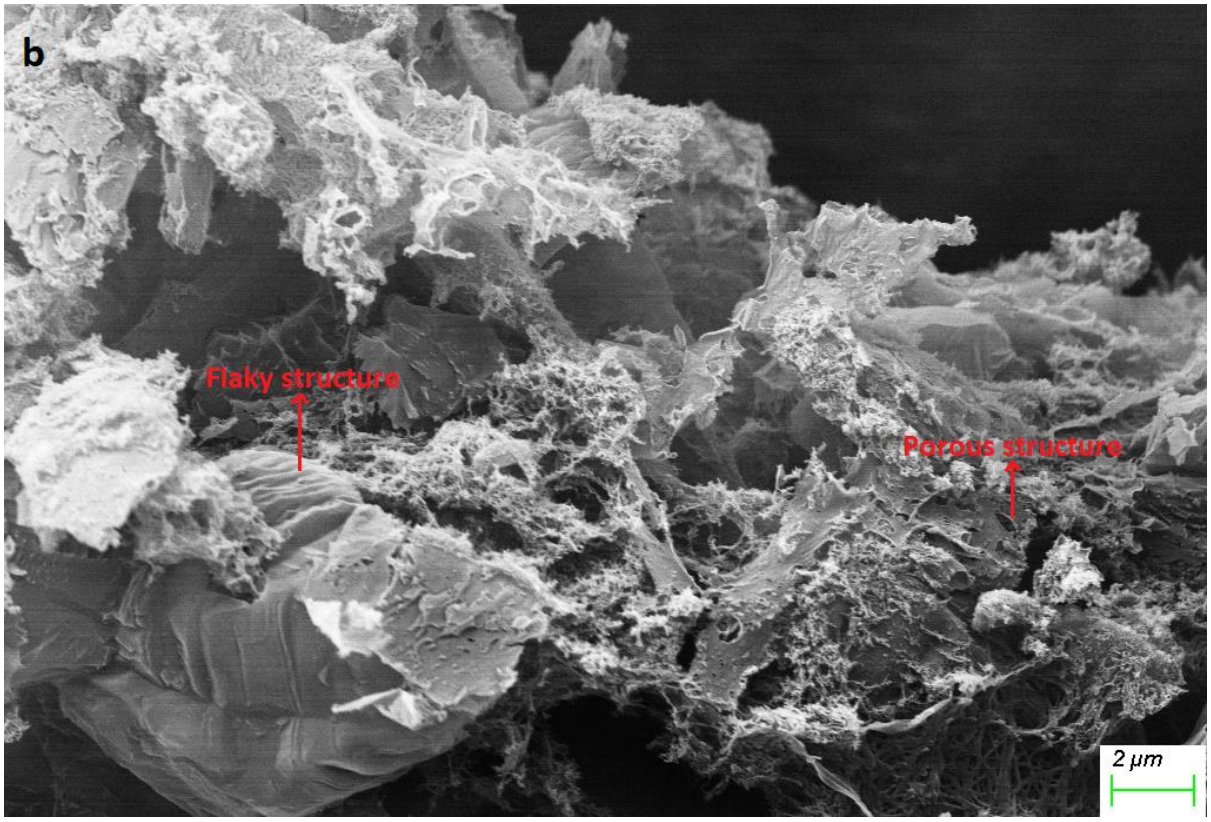

b
Flaky structure
Porous structure
2 µm

Figure 3.19 SEM images of (a) CBN porous microstructure, and (b) Porous bulk solids and some flakes of hexagonal layers

The image in the Figure 3.19 a illustrates the intertwined porous microstructure of the CBN nanomaterial. The doping of C-dots is believed to induce some structural defects into the h-BN that resulted in decreasing the crystallinity of CBN and becoming more porous in nature. It is well understood from XRD results that C-dots are amorphous while h-BN showed sharp peaks indicating some crystalline nature. The image in Figure 3.19 b discloses some amorphous solids of porous bulk solids of CBN and others showing flakes of hexagonal layers indicating the C-dots did not alter the structure of the h-BN completely. It is significant to note that the porous structure of the h-BN compound may be the consequence when C-dots were used as an additive (Li et al., 2014).

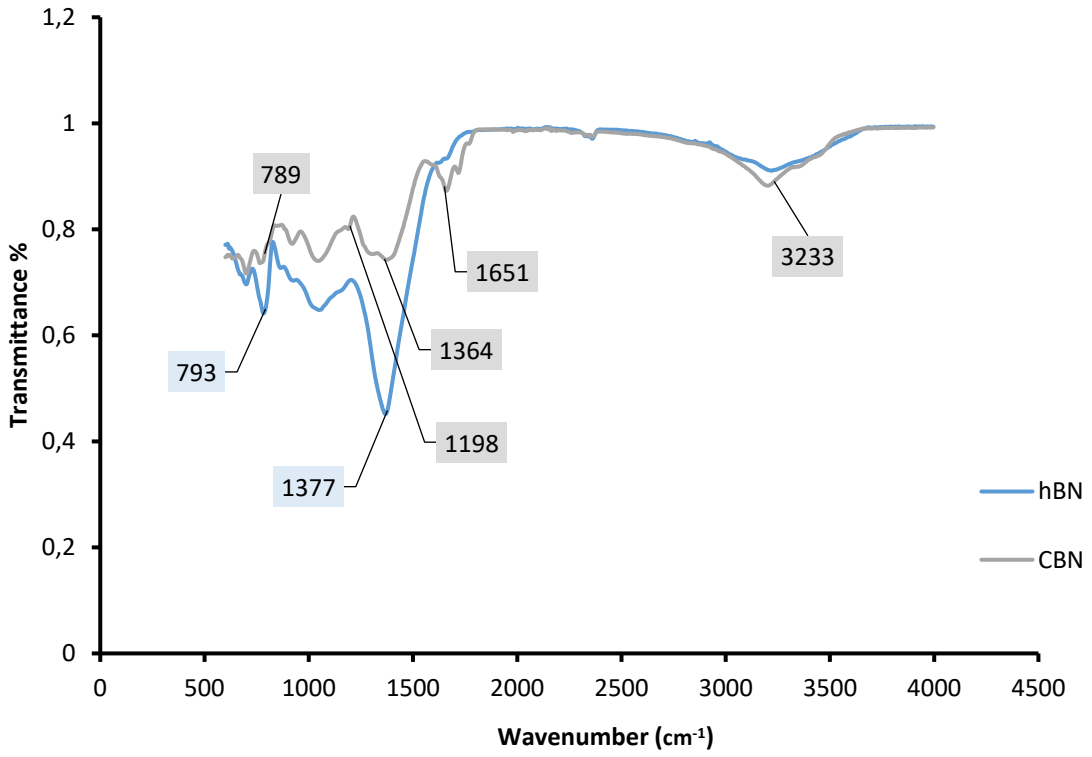


Figure 3.20 Comparison of FTIR spectra of h-BN CVD (900°C) and CBN

The FTIR spectra of CBN and h-BN CVD are shown in Figure 3.20. The presence of absorption bands at 1364 cm^{-1} and 789 cm^{-1}, of CBN correlates to the stretching and bending vibrations of B-N and B-N-B, respectively, confirming the original hexagonal BN structure, remained nearly unchanged (Liu et al., 2020). In contrast to pure h-BN, the CBN showed many additional absorption peaks. It can be observed that there is an increase in the 3233 cm^{-1} peak intensity corresponding to the O-H vibration, resulted from the doping of C-dots. The peaks at 1651 cm^{-1} and 1198 cm^{-1} indicate the formation of C-O-N bond and C-N bond indicating the doping of C-dots into h-BN (Ouyang and Long, 2021).

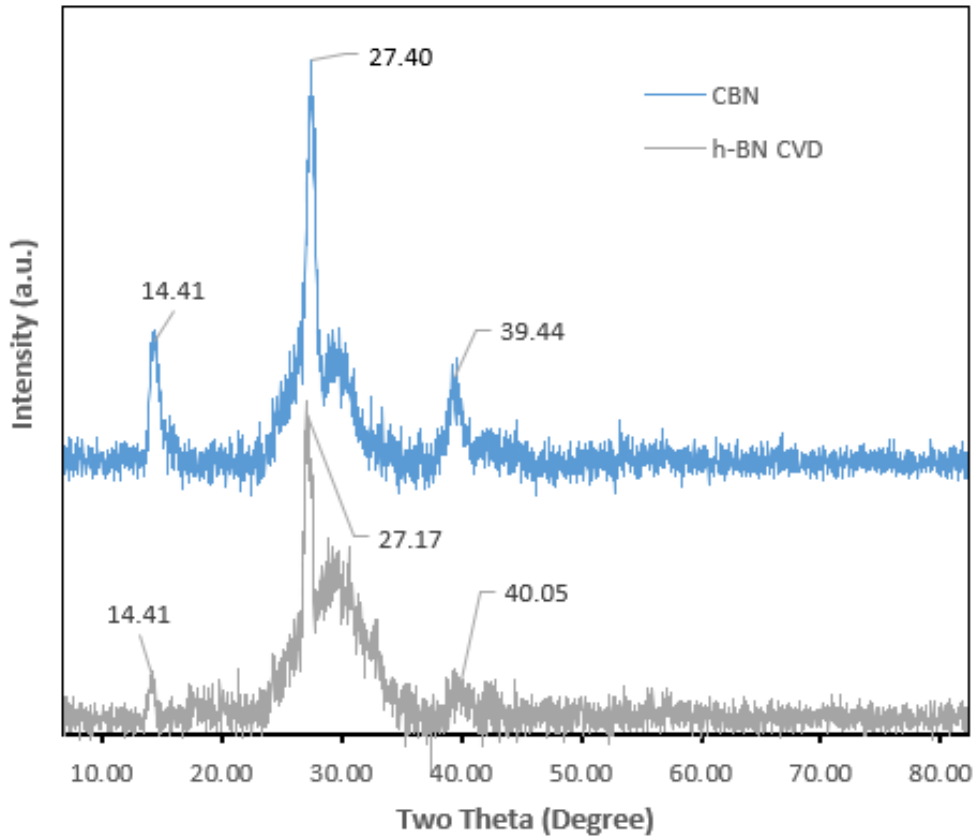


Figure 3.21 XRD image of CBN and h-BN CVD

XRD spectra have been used to determine the structure of CBN prepared from C-dots doped into h-BN CVD (900 ^{o}C) . Figure 3.21 shows XRD peaks of the synthesized C-dots and C-dot doped h-BN (CBN). The XRD result of CBN demonstrates two main peaks at 27.40 ^{o} and 39.44°, which might relate to the C-BN (002) and (100) planes, respectively, as shown in Figure 3.21. The XRD peak positions 14.41 ^{o}, 27.40 ^{o} and 39.44 ^{o} of the CBN as synthesized were almost identical to those of the h-BN CVD. This indicates that the crystalline nature of h-BN was only slightly changed after doping with C-dots.

3.6 Conclusion

This chapter provided a detailed insight on the materials and methods used and developed in synthesizing the h-BN, C-dots and CBN system this research study. The synthesized products were analysed by FTIR, XRD, SEM and TEM analytical techniques to confirm the production of the synthesis of h-BN, C-dots and CBN.

3.7 References

Bajpai, S.K., D'Souza, A. and Suhail, B., 2019. Blue light-emitting carbon dots (CDs) from a milk protein and their interaction with Spinacia oleracea leaf cells. International Nano Letters, 9(3), pp.203-212.

Bartnitskaya, T.S., Kurdyumov, A.V., Lyashenko, V.I. and Ostrovskaya, N.F., 1998. Structural-chemical aspects of the catalytic synthesis of graphite-like boron nitride. Powder metallurgy and metal ceramics, 37(1-2), pp.26-32.

Berchmans, L.J., Bharathi, B., Amalajyothi, K. and Subramanian, K., 2009. Synthesis of nanocrystalline boron nitride by combustion process. International Journal of Self-Propagating High-Temperature Synthesis, 18(1), pp.34-37.

Besisa, D.H., Hagras, M.A., Ewais, E.M., Ahmed, Y.M., Zaki, Z.I. and Ahmed, A., 2016. Low temperature synthesis of nano-crystalline h-boron nitride from boric acid/urea precursors. J. Ceram. Process. Res., 17(12), pp.1219-1225.

Camurlu, H.E., 2011. Effect of Na2CO3 on hexagonal boron nitride prepared from urea and boric acid. Ceramics International, 37(6), pp.1993-1999.

Dibandjo, P., Chassagneux, F., Bois, L., Sigala, C. and Miele, P., 2005. Comparison between SBA-15 silica and CMK-3 carbon nanocasting for mesoporous boron nitride synthesis. Journal of Materials Chemistry, 15(19), pp.1917-1923.

Hidalgo, A., Makarov, V., Morell, G. and Weiner, B.R., 2013. High-yield synthesis of cubic and hexagonal boron nitride nanoparticles by laser chemical vapor decomposition of borazine. Dataset Papers in Nanotechnology, 2013.

Huang, C., Chen, C., Ye, X., Ye, W., Hu, J., Xu, C. and Qiu, X., 2013. Stable colloidal boron nitride nanosheet dispersion and its potential application in catalysis. Journal of Materials Chemistry A, 1(39), pp.12192-12197.

Hubacek, M. and Ueki, M., 1996. Chemical reactions in hexagonal boron nitride system. Journal of Solid State Chemistry, 123(2), pp.215-222.

Jahanbakhshi, M. and Habibi, B., 2016. A novel and facile synthesis of carbon quantum dots via salep hydrothermal treatment as the silver nanoparticles support: Application to electroanalytical determination of H2O2 in fetal bovine serum. Biosensors and Bioelectronics, 81, pp.143-150.

Li, J., Xiao, X., Xu, X., Lin, J., Huang, Y., Xue, Y., Jin, P., Zou, J. and Tang, C., 2013. Activated boron nitride as an effective adsorbent for metal ions and organic pollutants. Scientific reports, 3(1), pp.1-7.

Li, L.H., Glushenkov, A.M., Hait, S.K., Hodgson, P. and Chen, Y., 2014. High-efficient production of boron nitride nanosheets via an optimized ball milling process for lubrication in oil. Scientific reports, 4(1), pp.1-6.

Liu, Y., Zhou, Q., Yuan, Y. and Wu, Y., 2017. Hydrothermal synthesis of fluorescent carbon dots from sodium citrate and polyacrylamide and their highly selective detection of lead and pyrophosphate. Carbon, 115, pp.550-560.

Liu, Z., Zhang, M., Wang, H., Cang, D., Ji, X., Liu, B., Yang, W., Li, D. and Liu, J., 2020. Defective carbon-doped boron nitride nanosheets for highly efficient electrocatalytic conversion of N2 to NH3. ACS Sustainable Chemistry & Engineering, 8(13), pp.5278-5286.

Nag, A., Raidongia, K., Hembram, K.P., Datta, R., Waghmare, U.V. and Rao, C.N.R., 2010. Graphene analogues of BN: novel synthesis and properties. ACS nano, 4(3), pp.1539-1544.

Nazarov, A.S., Demin, V.N., Grayfer, E.D., Bulavchenko, A.I., Arymbaeva, A.T., Shin, H.J., Choi, J.Y. and Fedorov, V.E., 2012. Functionalization and Dispersion of Hexagonal Boron Nitride (h-BN) Nanosheets Treated with Inorganic Reagents. Chemistry–An Asian Journal, 7(3), pp.554-560.

Ouyang, H., Li, W. and Long, Y., 2021. Carbon-doped h-BN for the enhanced electrochemical determination of dopamine. Electrochimica Acta, 369, p.137682.

Rushton, B. and Mokaya, R., 2008. Mesoporous boron nitride and boron-nitride-carbon materials from mesoporous silica templates. Journal of materials chemistry, 18(2), pp.235-241.

Schlienger, S., Alauzun, J., Michaux, F., Vidal, L., Parmentier, J., Gervais, C., Babonneau, F., Bernard, S., Miele, P. and Parra, J.B., 2012. Micro-, mesoporous boron nitride-based materials templated from zeolites. Chemistry of Materials, 24(1), pp.88-96.

Shen, T., Liu, S., Yan, W. and Wang, J., 2019. Highly efficient preparation of hexagonal boron nitride by direct microwave heating for dye removal. Journal of Materials Science, 54(12), pp.8852-8859.

Song, J., Zhao, L., Wang, Y., Xue, Y., Deng, Y., Zhao, X. and Li, Q., 2018. Carbon quantum dots prepared with chitosan for synthesis of CQDs/AuNPs for iodine ions detection. Nanomaterials, 8(12), p.1043.

Sudeep, P.M., Vinod, S., Ozden, S., Sruthi, R., Kukovecz, A., Konya, Z., Vajtai, R., Anantharaman, M.R., Ajayan, P.M. and Narayanan, T.N., 2015. Functionalized boron nitride porous solids. RSC advances, 5(114), pp.93964-93968.

Vasimalai, N., Vilas-Boas, V., Gallo, J., de Fátima Cerqueira, M., Menéndez-Miranda, M., Costa-Fernández, J.M., Diéguez, L., Espiña, B. and Fernández-Argüelles, M.T., 2018. Green synthesis of fluorescent carbon dots from spices for in vitro imaging and tumour cell growth inhibition. Beilstein journal of nanotechnology, 9(1), pp.530-544.

Wu, P., Zhu, W., Chao, Y., Zhang, J., Zhang, P., Zhu, H., Li, C., Chen, Z., Li, H. and Dai, S., 2016. A template-free solvent-mediated synthesis of high surface area boron nitride nanosheets for aerobic oxidative desulfurization. Chemical Communications, 52(1), pp.144-147.

Xiong, J., Luo, J., Yang, L., Pang, J., Zhu, W. and Li, H., 2018. Boron defect engineering in boron nitride nanosheets with improved adsorptive desulfurization performance. Journal of Industrial and Engineering Chemistry, 64, pp.383-389.

Xiong, J., Zhu, W., Li, H., Ding, W., Chao, Y., Wu, P., Xun, S., Zhang, M. and Li, H., 2015. Few-layered graphene-like boron nitride induced a remarkable adsorption capacity for dibenzothiophene in fuels. Green Chemistry, 17(3), pp.1647-1656.

Yan, Z., Lin, J., Yuan, X., Song, T., Yu, C., Liu, Z., He, X., Liang, J., Tang, C. and Huang, Y., 2017. Desulfurization of Model Oil by Selective Adsorption over Porous Boron Nitride Fibers with Tailored Microstructures. Scientific Reports, 7.

Zhao, L., Wu, R.A., Han, G., Zhou, H., Ren, L., Tian, R. and Zou, H., 2011. The highly selective capture of phosphopeptides by zirconium phosphonate-modified magnetic nanoparticles for phosphoproteome analysis. Journal of the American Society for Mass Spectrometry, 19(8), pp.1176-1186.

4. CHAPTER FOUR: DEVELOPMENT OF PPSU MEMBRANES EMBEDDED WITH H-BN AND CBN

4.1 Introduction

This chapter describes the development and the charecterization of polyphenyl sulfone (PPSU) membranes embedded with hexagonal boron nitride (h-BN) and carbon dot doped (CBN) nanoparticles.

4.2 Methods

Polyphenyl sulfone (PPSU) (Radel R-5000) was obtained from Solvay Polymers and Chemicals (Pretoria, South Africa). N-Methyl-2-pyrrolidone (NMP) solvent of analytical grade was purchased from Sigma Aldrich (Pty) Ltd, South Africa. The chemicals were used as received. PPSU was dried in an oven at 100 ^{o}C overnight before use. H-BN and CBN nanoparticles synthesized in this study were used to develop PPSU embedded with h-BN and CBN composite membranes by phase-inversion process.

4.2.1 PPSU membrane preparation

PPSU was dissolved in pure NMP solvent to produce 14 wt. % of the dope solution (pristine PPSU membrane). The PPSU-NMP mixture was stirred at a constant speed for 24 hours at room temperature in a round bottomed flask closed with a tight lid for complete dissolution of PPSU, until a homogenous solution was formed. The produced dope solution was degassed by sonication for up to 20 minutes to get rid of the air bubbles. The PPSU-NMP solution was then cast onto a glass plate using a casting knife of 100 μm-gap thickness to form thin films. The membrane was submerged in deionized water at room temperature for 15 minutes, to complete

phase separation and removal of solvent. The developed membrane was peeled off from the glass plate and preserved in deionised water until use.

4.2.2 Synthesis of PPSU Mixed Matrix Membranes (MMM) embedded with h-BN and CBN nanofillers

The process of developing MMM follows the same procedure of synthesizing pristine PPSU membrane, additionally by adding different weight ratios of h-BN and CBN into the PPSU dope solution. Different wt. % of h-BN and CBN nanoparticles selected (0, 0.2, 0.4, 0.6, 0.8, 1.0, 1.2, and 1.4 wt. %) were added to the NMP solvent and sonicated with an ultrasonicater probe for 10 minutes. Thereafter, the nanoparticle solution was added to the PPSU solution to produce 14 wt. % (PPSU) dope solution and casted to produce the MMMs. Figure 4.1 illustrates the graphical representation of the synthesis and charecterization of the MMM incorporated with CBN particles.

4.2.3 Overview of the membrane development

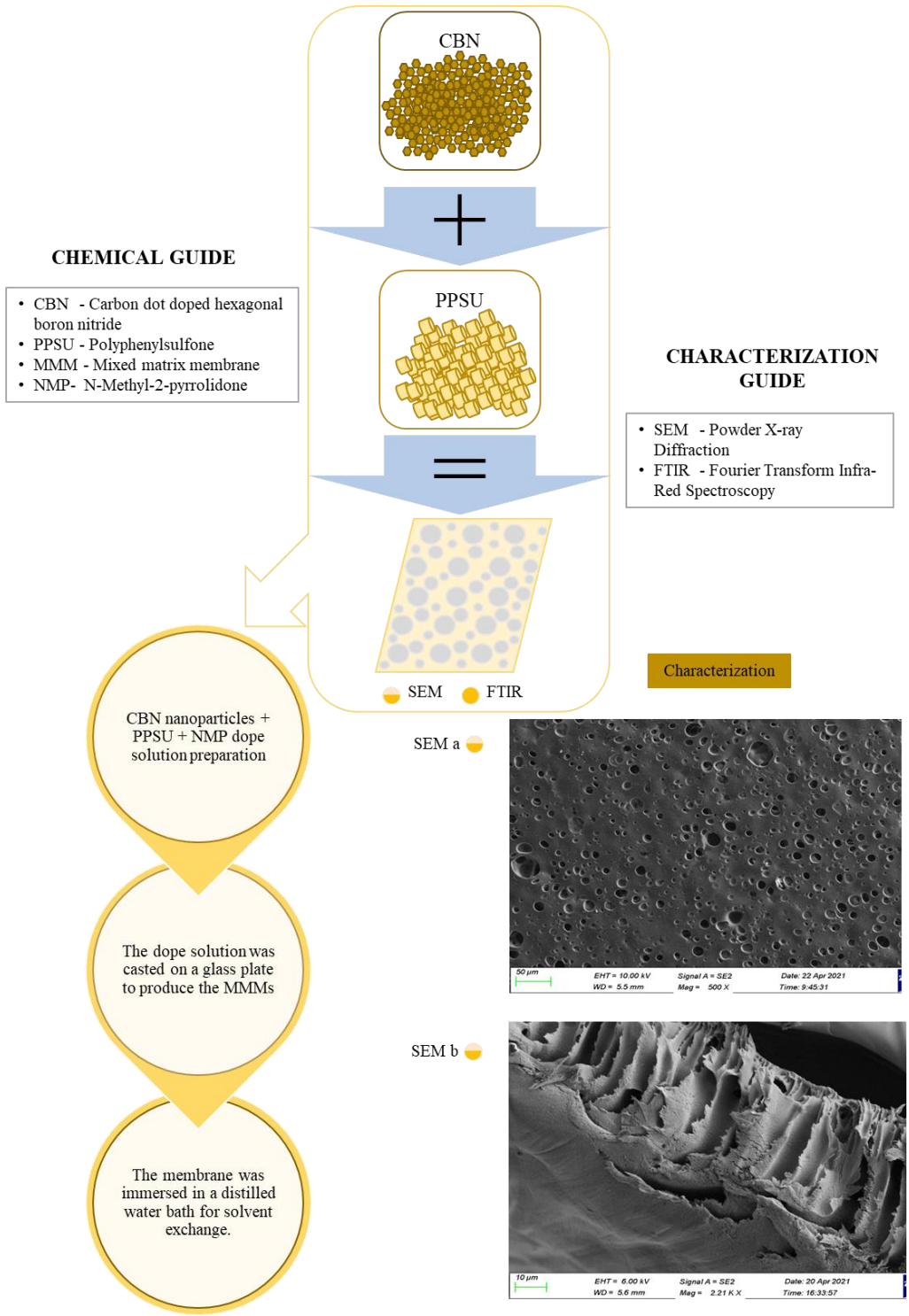


Figure 4.1 Development ofPPSU MMM with CBN nanoparticles

4.3 Membrane desulfurization process

The developed membranes were tested in dibenzothiophene (DBT)/ hexane model fuel containing 0.1g refractory sulfur DBT in 100 ml hexane for desulfurization efficiency. Each test was performed by taking 20 ml of model oil and a measured amount of membrane (MMM) in a conical flask, stirred at a constant speed. A detailed process of desulfurization using membrane is discussed in chapter five. The membrane sample was filtered and removed, and the fuel sample was collected and analysed for % sulfur removal.

4.4 Analytical Techniques

The developed membranes were characterized with FTIR for specific functional groups, SEM for morphology (membrane thickness, porous nature, distribution of nanoparticles).

4.5 Results and Discussions

This section provides with the FTIR and SEM results and discussion of the PPSU membranes developed.

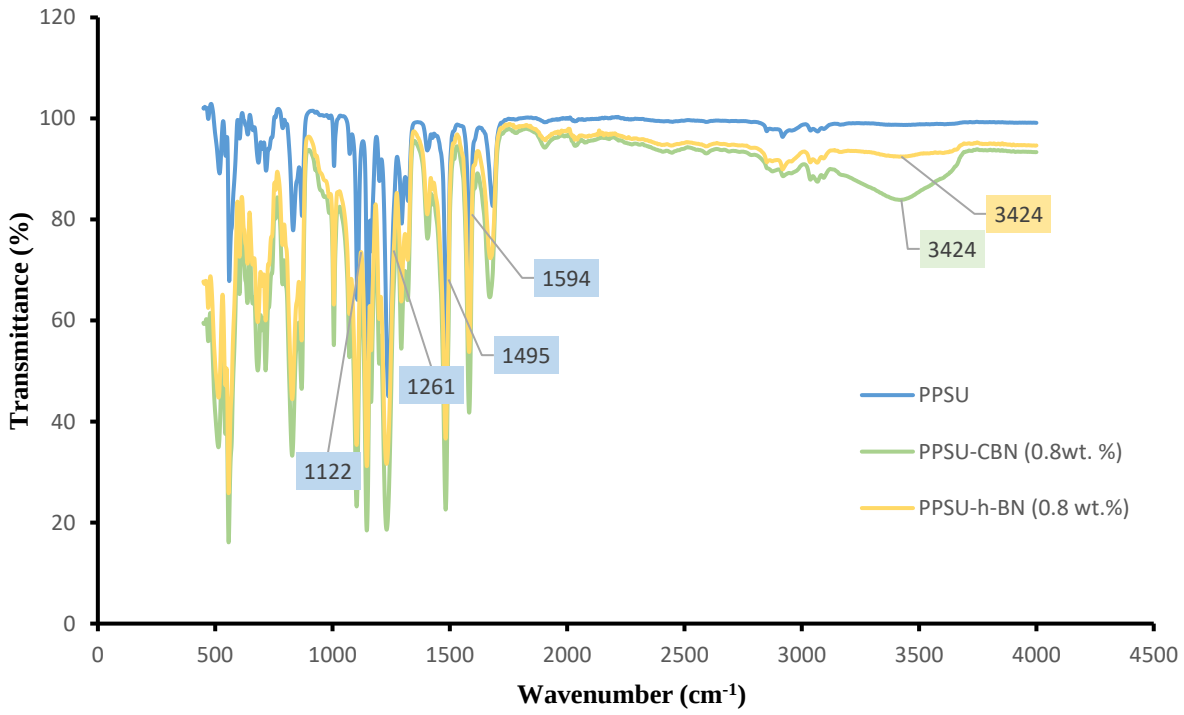


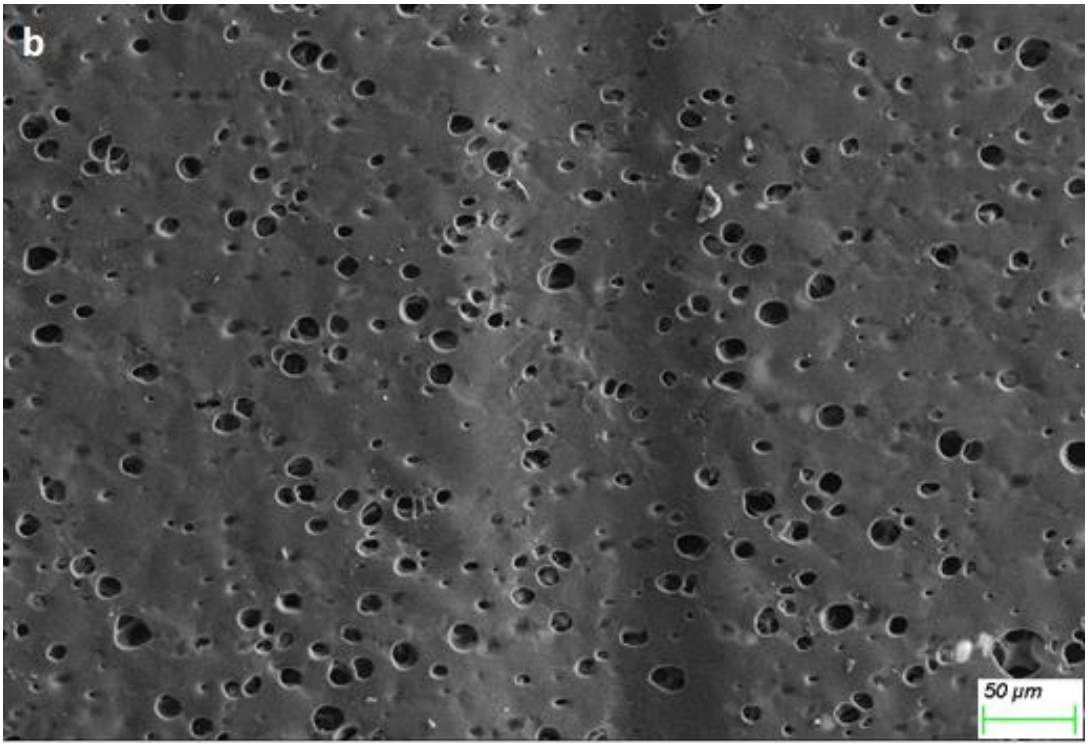
Figure 4.2 FTIR spectra of PPSU, PPSU-CBN and PPSU-h-BN membranes

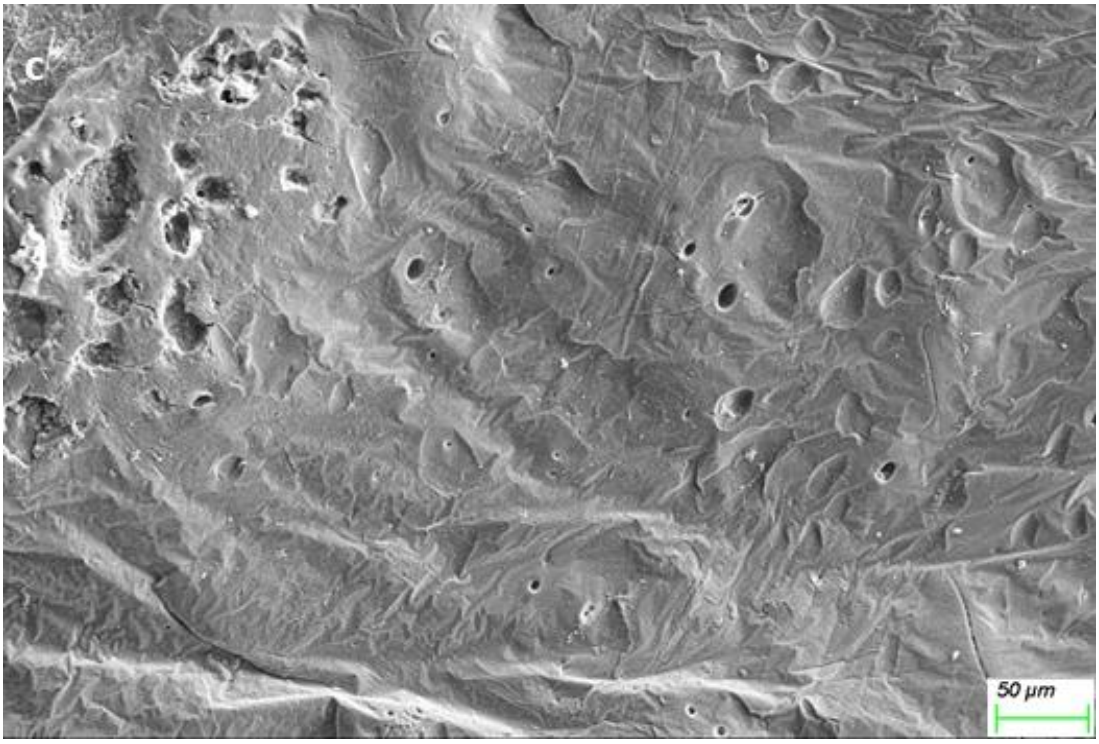
Figure 4.2 displays the infrared spectra of pristine PPSU membranes, PPSU-CBN and PPSU-h-BN mixed matrix membranes at 0.8 wt%. The PPSU peaks at 1122 cm^{-1} and 1261 cm^{-1} are indicative of the symmetric stretching of O=S= and antisymmetric contraction of O=S=O bond groups respectively. The C=C stretching vibration of the benzene ring has clear peaks representing at 1495 cm-1 and 1594 cm-1 (Kiani et al., 2015).

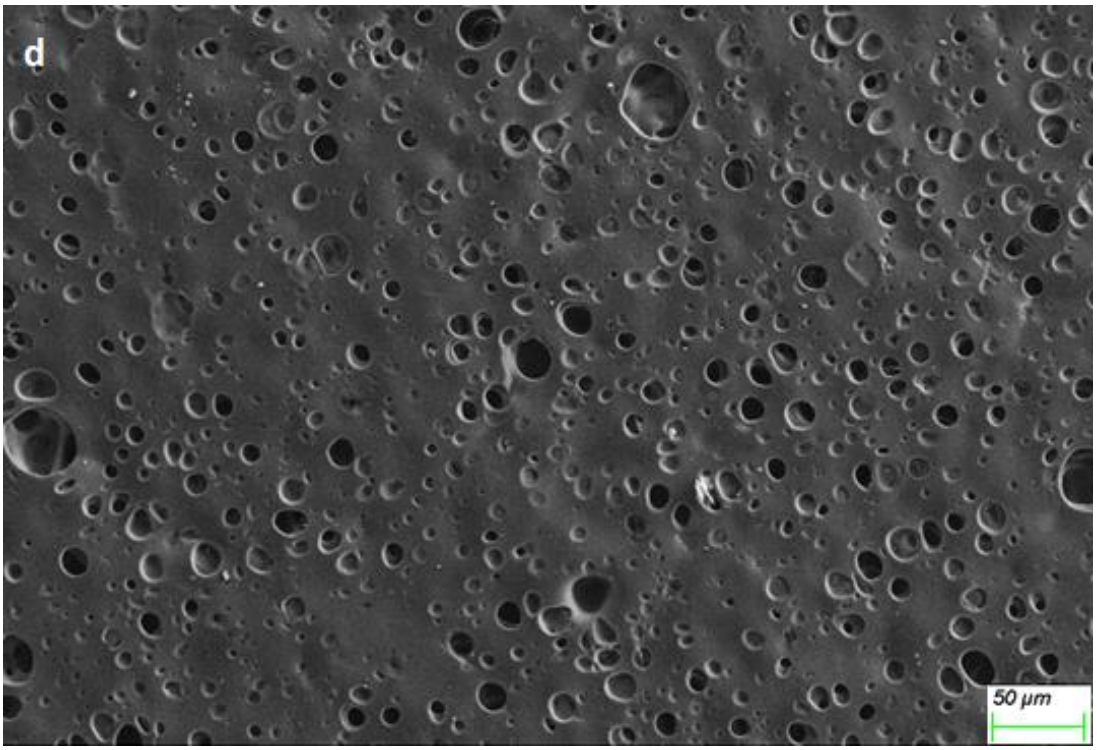
The FTIR peaks of PPSU-CBN and PPSU-h-BN do not have any additional peaks other than the peaks at 3424 cm^{-1} for both CBN and h-BN embedded membranes. The peaks indicate the the presence of -OH groups which can enhance the hydrophilicity of the MMMs, and be beneficial to improve the permeability of the membrane (Xiao et al., 2017). The -OH peak of h-BN filled PPSU

is not significant as the the one with PPSU-CBN indicating that CBN nanoparticles might have more interactions with PPSU membrane matrix compared to the h-BN particles.






c
50 µm


d
50 µm

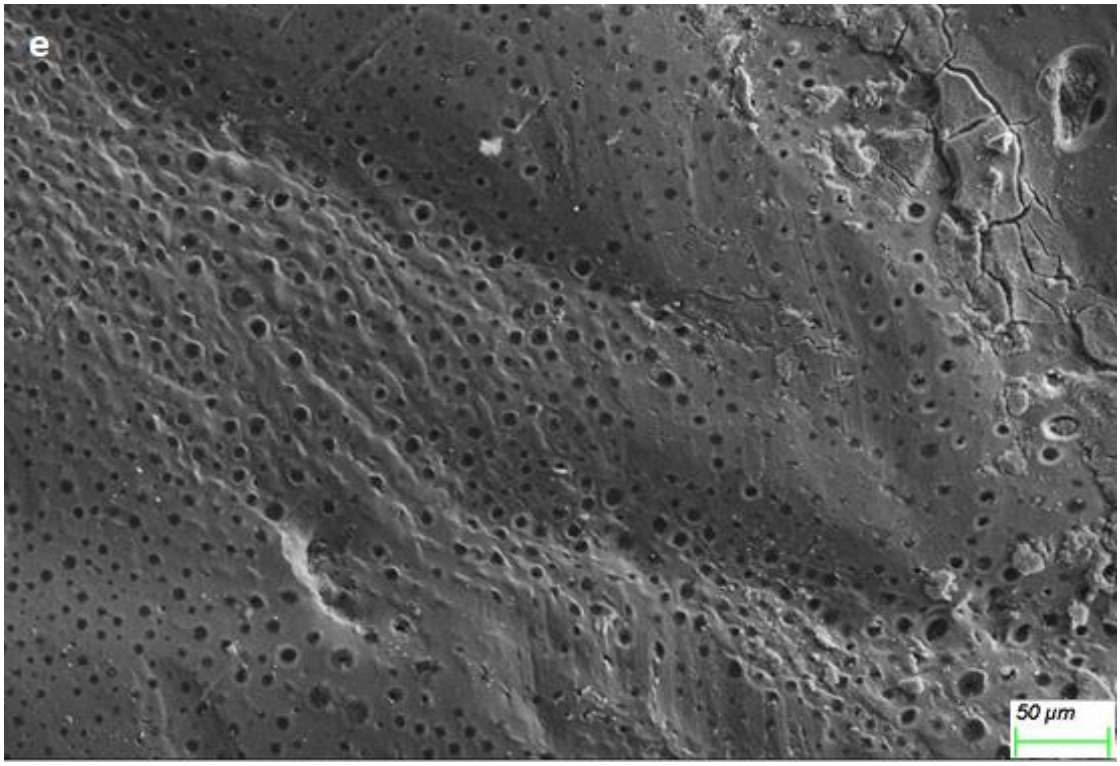
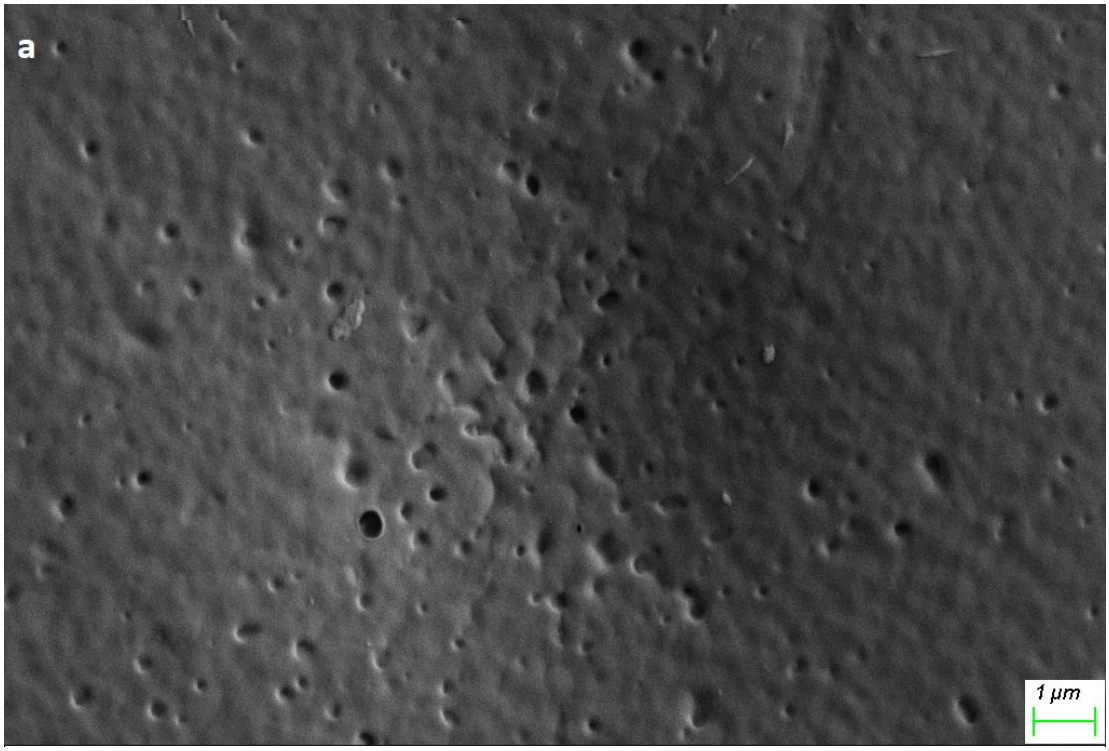


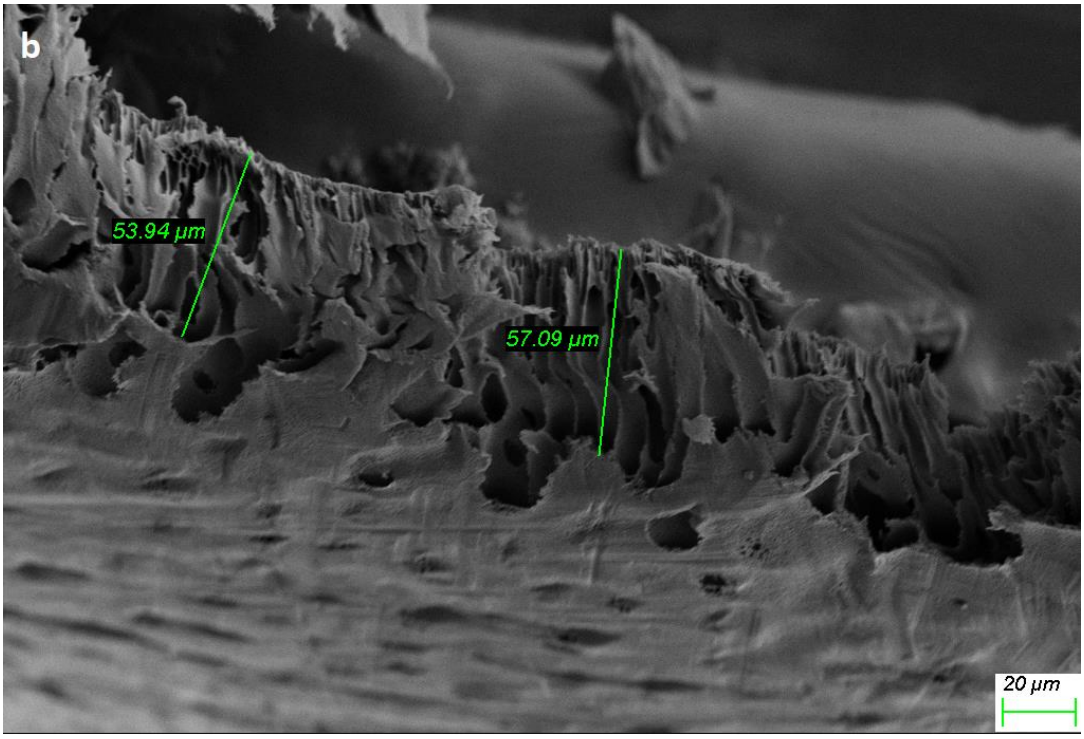
Figure 4.3 SEM images of (a) PPSU membrane with surface layer and inner pores (b) PPSU-CBN (0.2wt.%) membrane, (c) PPSU-h-BN (0.2wt.%) membrane, (d), PPSU-CBN (0.4wt.%) membrane and (e) PPSU-h-BN (0.4 wt.%) membrane

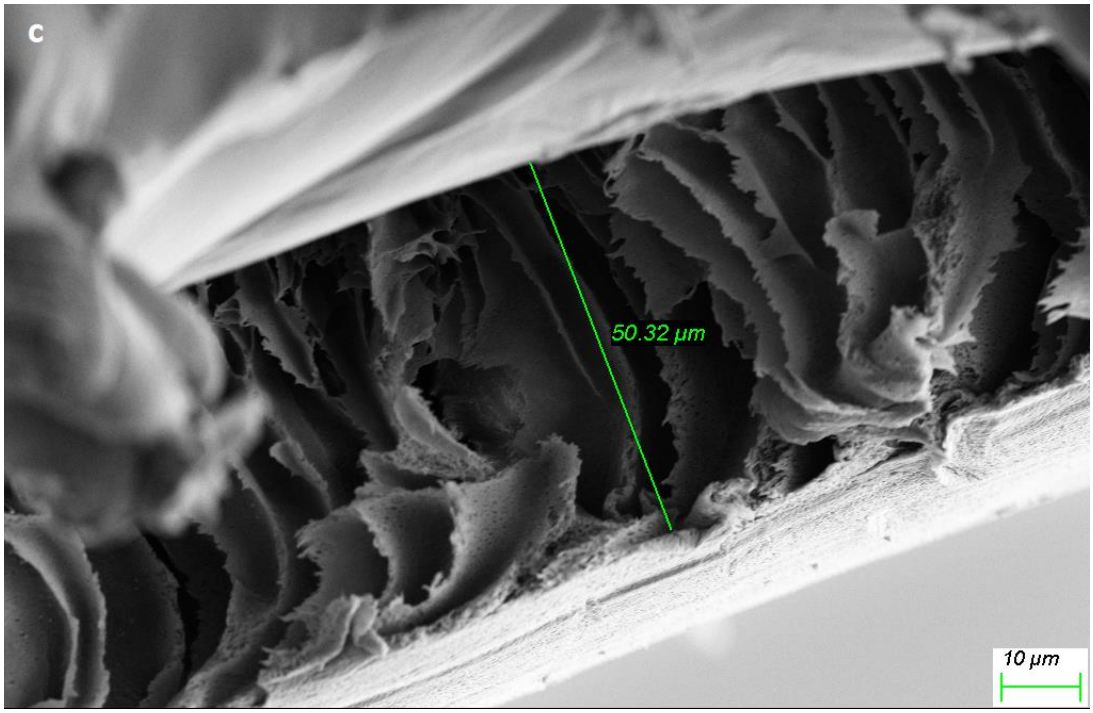
The SEM images in Figure 4.3 show that the PPSU membranes with and without the nanoparticles revealed a porous structure. The surface morphology of the PPSU membrane (Figure 4.3 a) appears to be smooth whereas, the PPSU-CBN (0.2wt.%) membrane surfaces (Figure 4.3 b and d) show an evenly and highly porous structure of the matrix. However, the PPSU-h-BN surface images (Figure 4.3 c and e) show an uneven structure indicating the agglomeration of h-BN particles in the PPSU matrix.

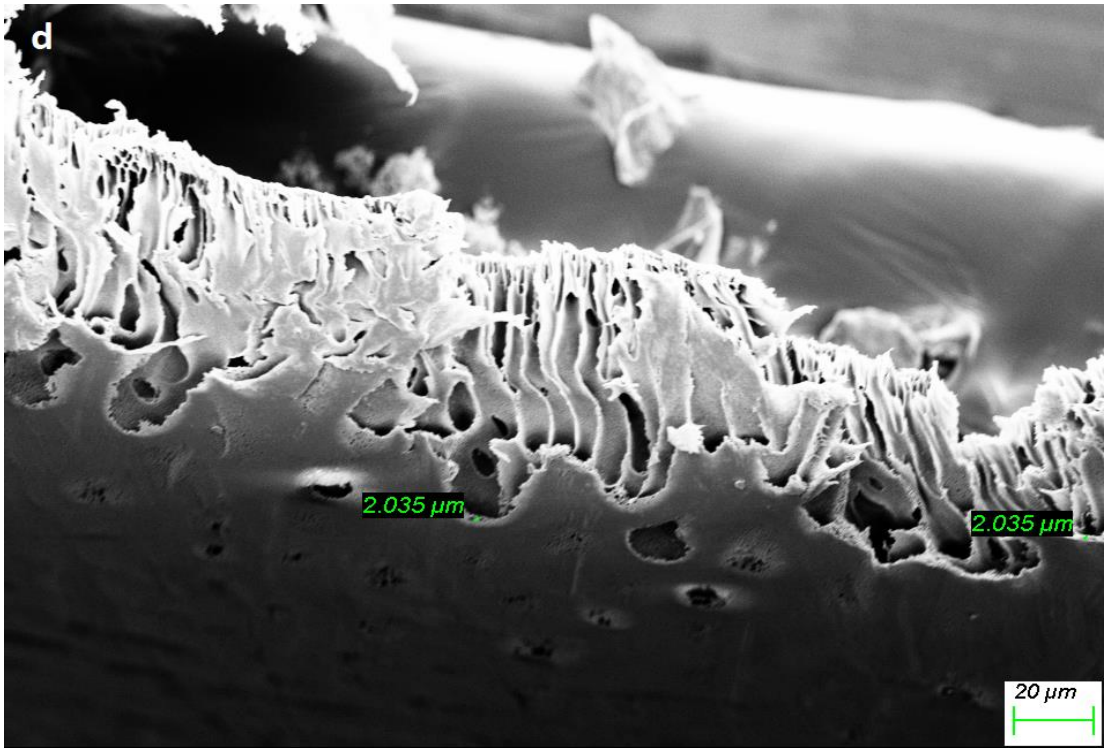
The synthesis process of CBN particles might have resulted in having better structure which resulted in enhanced distribution of the CBN particles in the PPSU matric while

ultrasonication. It can be assumed that CBN particles have better interactions with PPSU membranes which improved the membrane forming properties.






c
50.32 µm
10 µm


d
2.035 µm
2.035 µm
20 µm

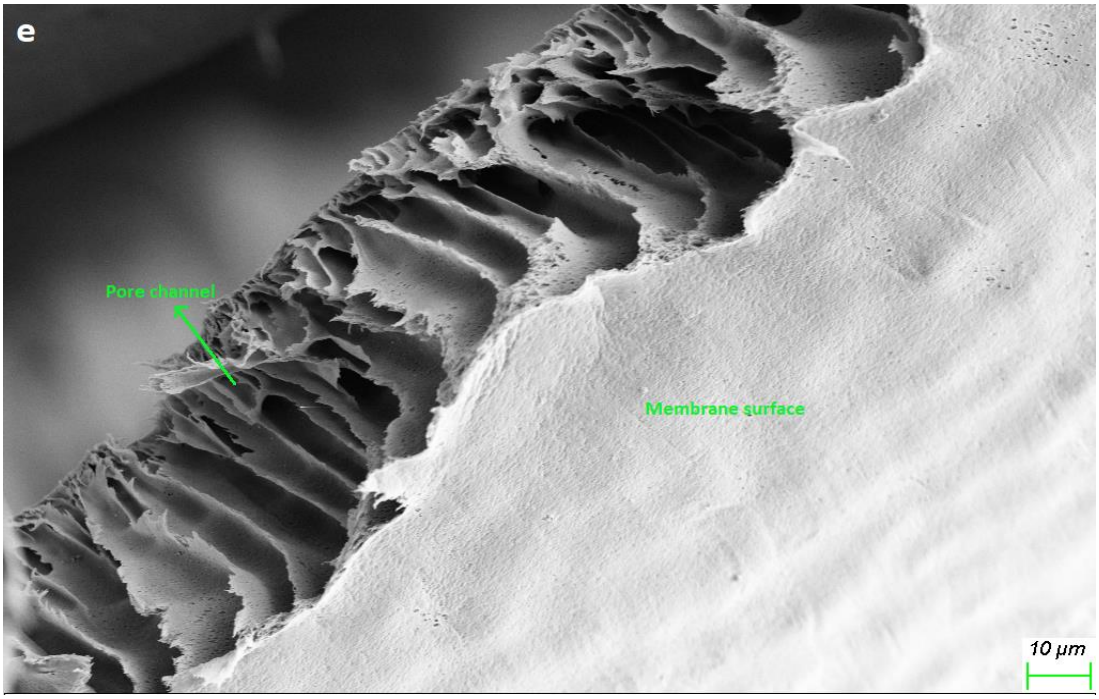


Figure 4.4 (a) PPSU membrane surface (b) cross section of PPSU membrnae, (c) cross section of PPSU-CBN (1.2 wt.%) membrane, (d), PPSU-CBN (1.2 wt.%) membrane surface showing surface layer thickness and (e) porous network channels of PPSU-CBN (0.8 wt.%) membrane

The presence and dispersion of h-BN and CBN in PPSU matrix may be examined using SEM images. The SEM image in FigureFigure 4.4 a shows the surface of pristine PPSU membrane exhibiting pores that are concentrated at certain places indicating an uneven distribution of pores in the membrane without adding fillers. The Figure 4.4 b shows the cross section of the pristine PPSU membrane prepared by fracturing of membrane sample in liquid N_2. The membrane thickness is 53.94 µm and 57.09 µm as shown, indicating the formation of an asymmetric membrane. Figure 4.4 c shows the cross section of PPSU-CBN (1.2 wt.%) membrane with 50.32 µm thickness. It can be expected that the membranes developed have a

thickness ranging between 50 μm to 60 μm. The surface layer formed for PPSU-CBN membrane has a thickness of 2.035 μm as can be seen from Figure 4.4 d.

Image in Figure 4.4 e clearly reveals a number of sponge like pores of different diameters forming channel like structures suggesting a good mechanism to ensure contact between the integrated fillers and liquid fuel flowing through them which are essential for the sulfur removal process. This shows that there is no requirement of an additional pore forming agent in the membrane development. This is because the PPSU-NMP dope solution, by using phase inversion method has induced pore formation into the membrane.

4.6 Conclusion

Mixed matrix membranes with different ratios of synthesized nano particles such as h-BN and CBN incorporated into the PPSU polymer matrix were prepared. The FTIR analysis shows thereare no chemical bonds formed between PPSU and nanoparticles, however, a significant peak at 3434 cm^{-1} was observed for PPSU-CBN membrane indicating a strong CBN interatction with PPSU. The SEM analysis revealed the microstructure of the PPSU-CBN membranes synthesized to be highly porous. The FTIR and SEM analysis show that the CBN fillers have enhanced the membrane forming properties as a result of the superior interaction of CBN with PPSU polymer.

4.7 References

Kiani, S., Mousavi, S.M., Shahtahmassebi, N. and Saljoughi, E., 2015. Hydrophilicity improvement in polyphenylsulfone nanofibrous filtration membranes through addition of polyethylene glycol. Applied Surface Science, 359, pp.252-258.

Xiao, S., Yu, S., Yan, L., Liu, Y. and Tan, X., 2017. Preparation and properties of PPSU/GO mixed matrix membrane. Chinese Journal of Chemical Engineering, 25(4), pp.408-414.

5. CHAPTER FIVE: DESULPHURISATION PROCESS OF MIXED MATRIX MEMBRANES

5.1 Introduction

This chapter presents the adsorption performance of the synthesized polyphenylsulfone (PPSU) membranes with h-BN and CBN nano materials for dibenzothiophene (DBT) removal from a model fuel (DBT in hexane). The adsorbent materials are analysed with varying amounts of nano materials, time and temperature, to evaluate the effectiveness of membranes in separating DBT from the model fuel.

5.2 Methods

The research of the desulfurization of model compounds including DBT has dominated because of the refractory molecules such as DBT and substituted DBTs account for up to 70% of the sulfur in fuels (Monticello, 2000). DBT is found in nearly all crude oils, nevertheless, because of steric hindrance, benzothiophene (BT) and DBT derivatives are significantly more resistant to the traditional hydrodesulfurization method and pose a major hindrance to obtaining very low sulfur levels in fuels. Hence, DBT is selected as a model refractory sulfur compound in modern desulfurization methods. Therefore, this study has focused on removal of DBT as it is the major proportion of thiophenic sulfur found in most fuels.

The influence of operating variables on the adsorption efficiency of the mixed matrix membranes (MMM) for the DBT removal from the model oil was investigated to better understand the performance of hexagonal boron nitride (h-BN) and carbon dot doped boron nitride (CBN)

embedded PPSU membranes during desulfurization of DBT. The batch adsorption process is the technique used.

DBT, hexane-98 % were purchased from Sigma Aldrich (Pty) Ltd, South Africa. All other products were of analytical grade, and were used as received.

Adsorption performances of the MMM were estimated by using a model diesel prepared in the laboratory by dissolving 0.1 g DBT in 100 ml hexane.

Study of operating conditions is essential in evaluation of the membrane performance. The effect of operating conditions such as temperature (K), time (min), and the amount of adsorbents in membranes (wt. %) on the performance of the MMM were studies in batch mode experiments. The operating variables such as; time (0-240 minutes), temperature (290 to 320 K), amount of adsorbents (0 -1.4 wt.%) were varied.

The following equation calculates the amount of sulfur compounds adsorbed (q_t) (Xiong et al., 2018):

$$q_t = \frac{(Co - Ct)V}{m} \quad (5.1)$$

Where, C_o and C_t (mg L^{-1}) are initial and final sulfur concentrations respectively, t=time, V (L) = volume of the fuel, and m (g) = mass of the adsorbent

$$SR = \frac{(Co - Ce)}{Co} \times 100 \quad (5.2)$$

Where, SR (%) is the percentage DBT removal, C_o and C_e are the initial and final concentration of DBT in the model oil in mg L^{-1}, respectively (Kiran and Kaushik, 2008).

5.3 Desulfurization process

The developed membranes were tested in DBT/n-hexane model fuel. The following procedure describes the desulfurization experimental process. The Figure 5.1 shows the desulfurization experimental set up.

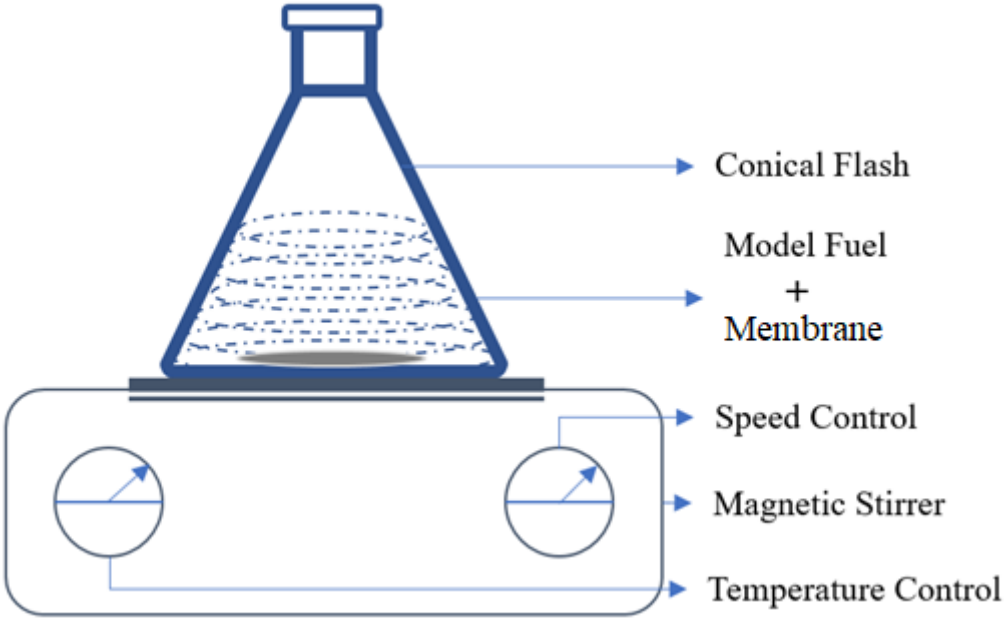


Figure 5.1 Batch adsorption process set-up for sulfur removal using MMM embedded with h-BN and CBN

5.3.1 Effect of contact time

20 ml model fuel with a known amount of each adsorbent sample were taken in a conical flask and stirred at a constant speed with varying contact times (0, 30, 60, 90, 120, 150, 180, 210, and 240 minutes). The temperature and adsorbent amount were kept constant at 26 ^{o}C (299.15K) and 0.8 wt. % respectively. The samples were collected after every 30 minutes and were filtered to recover the resulting membrane. The fuel samples were then taken for analysis to determine % removal of sulfur.

5.3.2 Effect of amount of adsorbent

In this experiment, the adsorbent amount is varied (0, 0.2, 0.4, 0.6, 0.8, 1.0, 1.2, and 1.4 wt. %) and a similar method discussed for effect of contact time was used except for the varied amounts of adsorbents, constant temperature of 26 ^{o}C (299.15K) and contact time of 150 minutes. Separate flasks were used for each adsorbent amount. The fuel sample from each flask was collected after the experiment and analysed for % removal of sulfur.

5.3.3 Effect of temperature

The procedure is similar to section 5.3.1, with the contact time and adsorbent volume fixed at 150 minutes and 1.2 wt. % respectively, while the temperature was varied at 290 , 300, 310 and 320 minutes. Samples from each flask with different temperatures were collected and analysed.

5.4 Analytical Techniques

The adsorption experiments using MMM with h-BN and CBN nanoparticles were carried out by varying different parameters: temperature (290-320K) and the time (0-240 minutes) and adsorbent amount (0-1.4 wt.%). The samples were taken at several intervals and tested for DBT removal. The adsorption capacity and % DBT removal were calculated using equations in section 5.2. The analysis of desulfurized model fuel samples was performed with an agilent high performance liquid chromatography (HPLC) fitted with an eclipse C-18 column. For the mobile phase, acetonitrile was used. HPLC was operated 10 mins at 234 nm wavelength, 1.0 µl/ min flow rate, and 10 µl injection volume.

5.5 Results and Discussion

The influence of the operating factors such as contact time, amount of adsorbent and temperature on membrane performance were studied and the experimental data result was used to plot graphs. This section used heat treated h-BN precursor, calcined at 900 ^{o}C in a CVD furnace to synthesize h-BN product, CBN and to develop MMMs. The experiments used single component adsorption involving the adsorption of one adsorbate (DBT) from a liquid model fuel system.

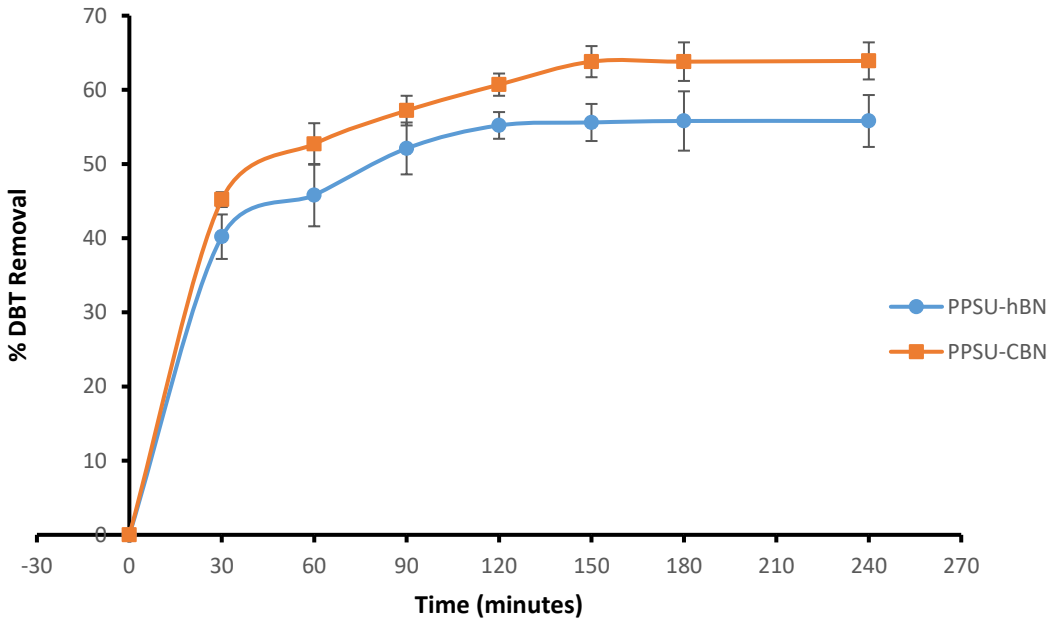


Figure 5.2 Desulfurisation behaviour with time

The impact of contact time on removal of DBT from model fuel was investigated in this experiment, by keeping the variables such as, adsorbent amount (0.8 wt. %), and temperature (26 ^{o}C) constant.

The samples were collected after every 30 minutes starting from 0 to 240 minutes contact time. From Figure 5.2, it can be perceived that the sulfur removal efficiency of both PPSU-h-BN and PPSU-CBN increased rapidly at the start of the reaction with 40.2 and 45.2 % removal of DBT with PPSU-h-BN and PPSU-CBN systems respectively, from 0 to 30 minutes contact time.

This is most likely because of the significant amount of sites available on the adsorbent surface at the start of each reaction. The sulfur reduction efficiency of both adsorbents increased slightly with 55.2 % (PPSU-h-BN system) and 60.7 % (PPSU-CBN system) at 120 minutes before reaching equilibrium at 150 minutes. This small improvement after 150 minutes in removal percentage may be attributed to the available adsorbent's vacant sites being completely filled to capacity with sulfur compounds. There was no significant change after equilibrium was reached for both PPSU-h-BN and PPSU-CBN systems. This is most likely due to the adsorbent's poor reactivity to sulfur compounds in high sulfur fuels (Fadhel, 2010).

Although, PPSU-h-BN and PPSU-CBN membranes showed a similar trend in DBT removal, PPSU-CBN system was remarkably showing a better performance in DBT adsorption. This indicates that the addition of C-dots in h-BN can drastically improve the desulfurization process, raising the overall sulfur removal efficiency. Other variables were adjusted to establish the optimal operating conditions and the adsorbents' potential to attain ultra-deep desulfurization.

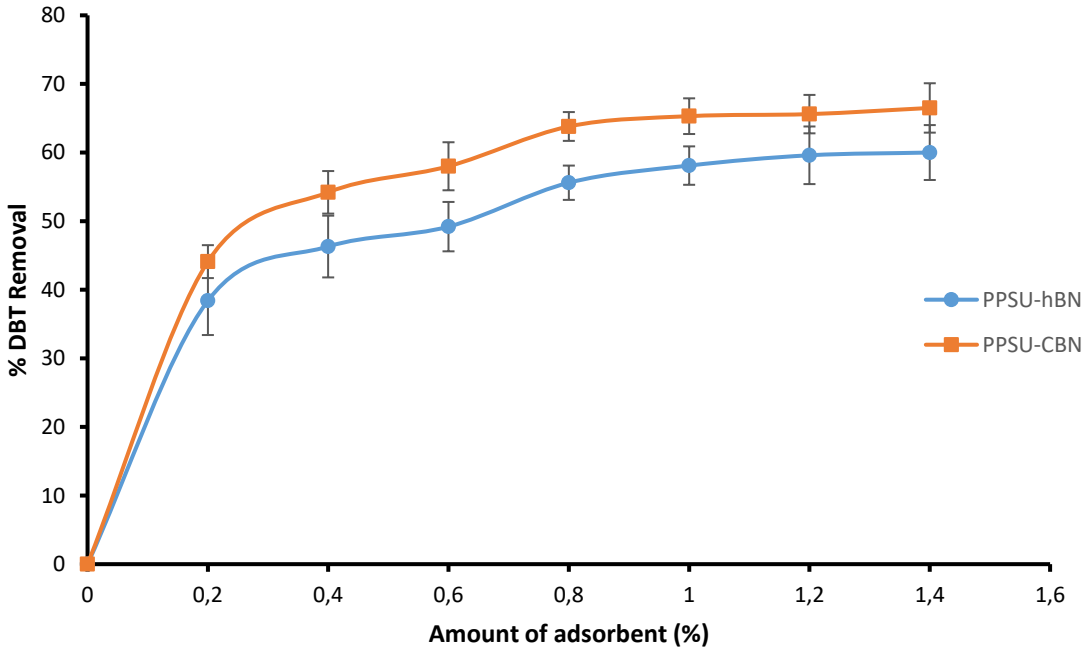


Figure 5.3 Desulfurisation behaviour with adsorbent amount

The effect of adsorbent amount on sulfur removal was studied by maintaining a constant time of 150 minutes and temperature of 26^{o}C throughout the experiment. Figure 5.3 shows the desulfurization behaviour of the adsorbents by varying the amounts of h-BN and CBN amounts from 0.2 to 1.6 wt. % in the membranes. It is evident from the graph that, the increase in the amount of adsorbent from 0 to 0.8 wt. %, has considerably increased the wt. % removal of DBT from the model fuel. This may be as a result of availability of more surface area due to increased adsorbent volume for DBT adsorption (Srivastav and Srivastava, 2009). In some studies, it was found that increasing the adsorbent volume speeds up the desulfurization mechanism, as more number of adsorption sites will be available for DBT (Fadhel, 2010).

PPSU-h-BN and PPSU-CBN systems followed the same trend in DBT removal with the highest DBT removal efficiency of 60% and 66.5% respectively at 1.4 wt. % of both the adsorbents. Additionally, PPSU-CBN system showed greater removal efficiency for DBT for the reason

mentioned in discussion for Figure 5.2. However, the DBT removal performance after 0.8 wt. % of adsorbent volume dropped significantly as it can be observed with very small increase in % DBT removal which was still low. It can be inferred that beyond a certain concentration of adsorbent amount, the removal efficiency does not change due to the overlapping of adsorption sites (Kumar and Kirthika, 2009). Hence, at 0.8 wt. %, both systems can be credited with the optimum sulfur removal efficiency.

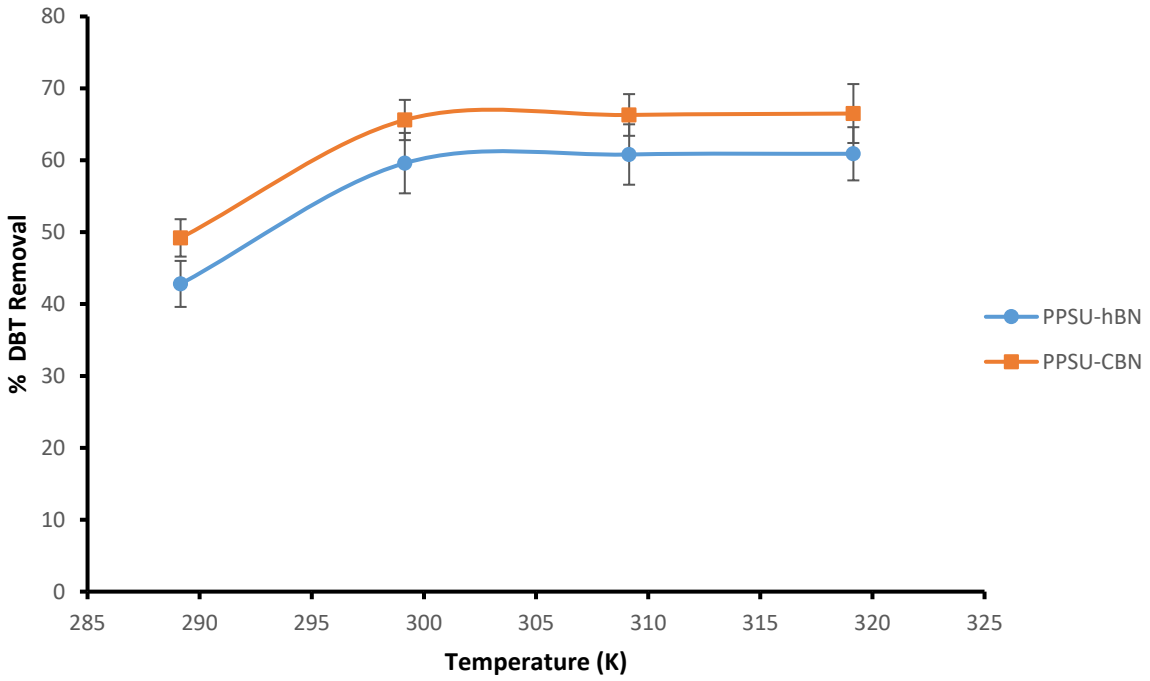


Figure 5.4 Desulfurisation behaviour with temperature

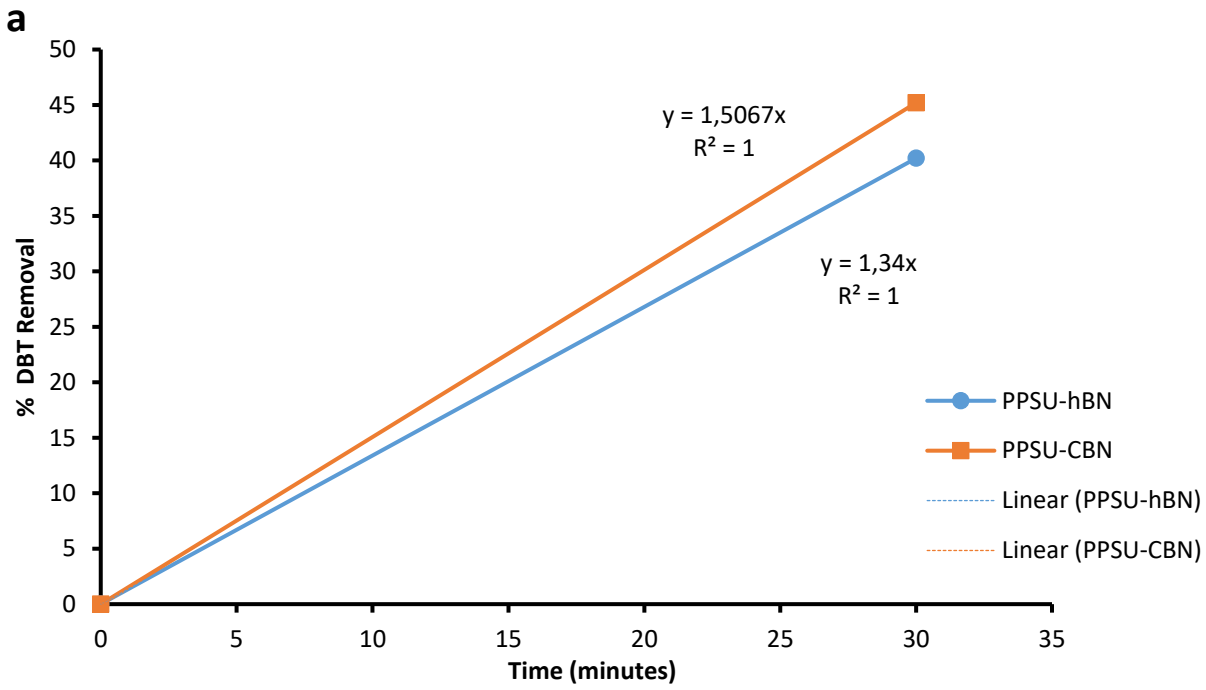
The effect of different operating temperatures on the desulfurization efficiency of the adsorbents was studied in the range of temperature from 290 to 320K, with 150 minutes time and 1.2 wt. % adsorbent amounts. As observed in FigureFigure 5.4, the graphs show a steady rise in sulfur removal efficiency at low temperatures from 49.2% (PPSU-CBN), 42.8% (PPSU-h-BN) DBT removal at

290K to 65.6% (PPSU-CBN), 59.6% (PPSU-h-BN) at 300K. This effect may mainly emerge from the enlargement of adsorbent pores and forming of additional active sites on the surface of the adsorbent due to cleavage of the bond at higher temperature (Bettermann and Staudt, 2009). It can also be assumed that the initial rise in temperature acted as a driving force for the diffusion of the penetrant molecule (DBT) into the adsorbent vacant sites (Ishaq et al., 2017). The equilibrium was reached at 310K with 66.3% and 60.8% DBT removal for PPSU-CBN and PPSU-h-BN respectively. Thereafter, the increase was negligible.

The results from Figure 5.4 suggest that the adsorption mechanism is profoundly preferred at temperatures below 310K (36.85 °C) for both the adsorbent systems. It was shown that there was a remarkable drop in the removal efficiency at higher temperatures, which may be because of the decomposition of the sulfonium salts (Shiraishi et al., 2001). Based on the findings, it is recommended that the desulfurization process be carried out at lower to room temperature and not beyond 35 ^{o}C. Since, this is a lab scale experiment with a model fuel, further research is needed for varied temperatures. Furthermore, since the variation in removal efficiencies is not substantial, after the equilibrium the optimal working temperature for both PPSU-h-BN and PPSU-CBN systems can be maintained at is 310K (36.85°C). As carbon nano materials are shown to be highly stable at higher temperature, this proves that the addition of C-dots to h-BN has an advantage of enhancing the overall efficiency of the sulfur removal.

The FigureFigures 5.2, 5.3 and 5.4 show a typical behaviour where three phases can be identified, namely, rapid phase, slow phase and stationary phase. The adsorption of both PPSU-h-BN and PPSU-CBN systems in all three Figures has a similar pattern where PPSU-CBN system was shown to have higher DBT removal than PPSU-h-BN for all the three varying parameters. The rapid phase has a linear slope where the adsorption was very fast while in the slow phase, there was a sluggish and gradual increase in the % sulfur compound removal. The

graph reaches a stationary phase where no more adsorption of DBT takes place. The equilibrium is reached at this point where no more adsorption sites are available for the sulfur molecules (Yu et al., 2017).



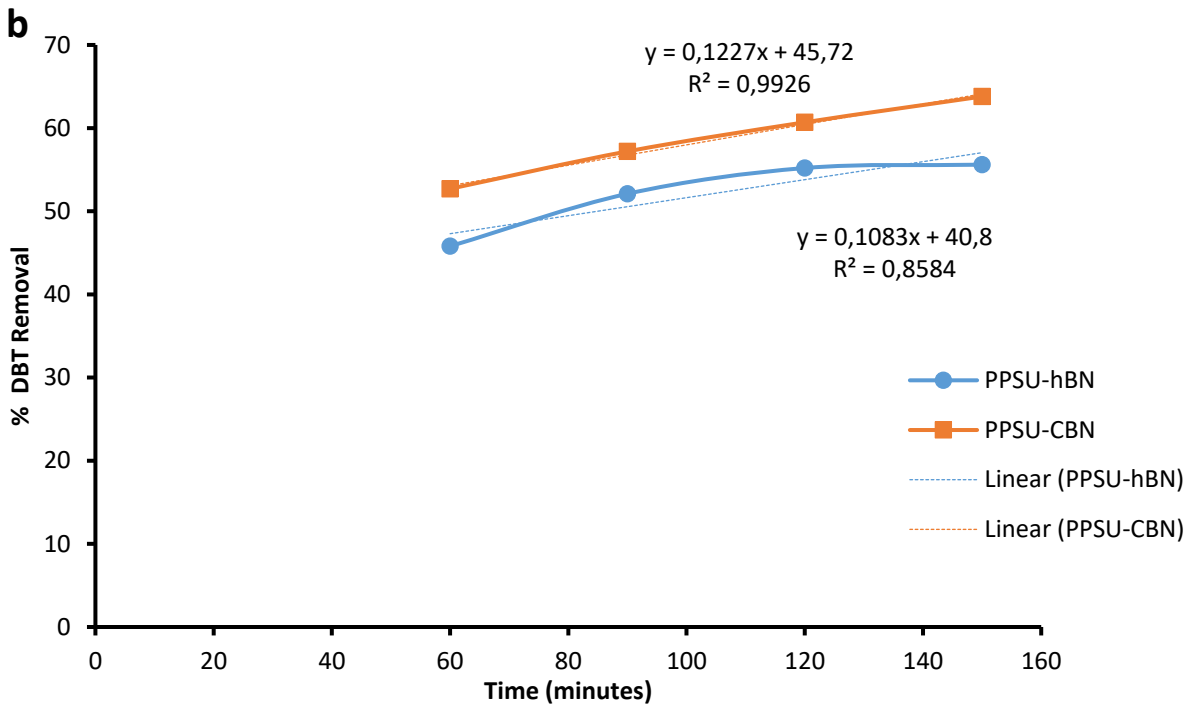


Figure 5.5 Graphs showing adsorption behaviour for varying contact time at (a) rapid phase and (b) slow phase

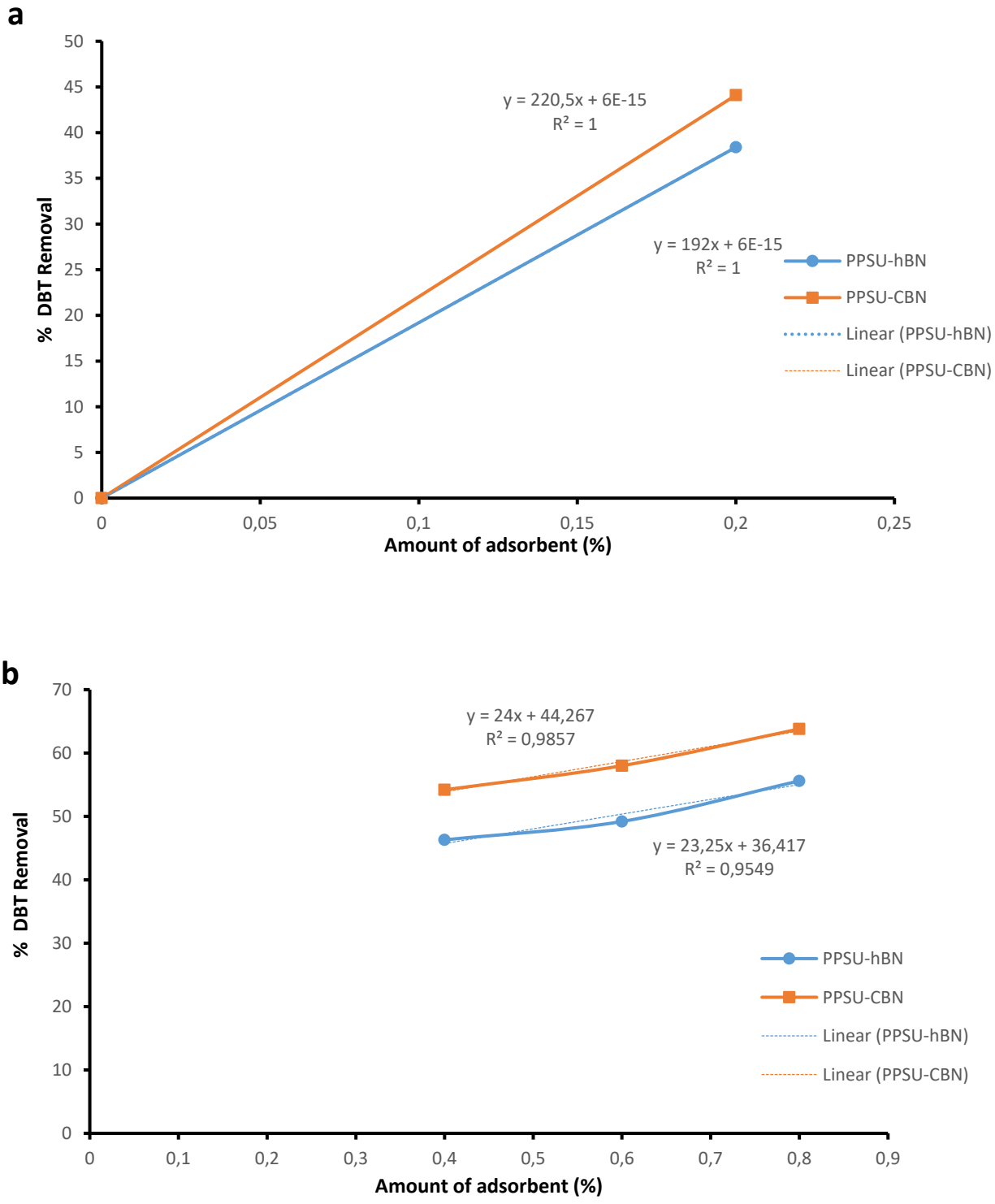


Figure 5.6 Graphs showing adsorption behaviour for varying adsorbent amount at (a) rapid phase and (b) slow phase

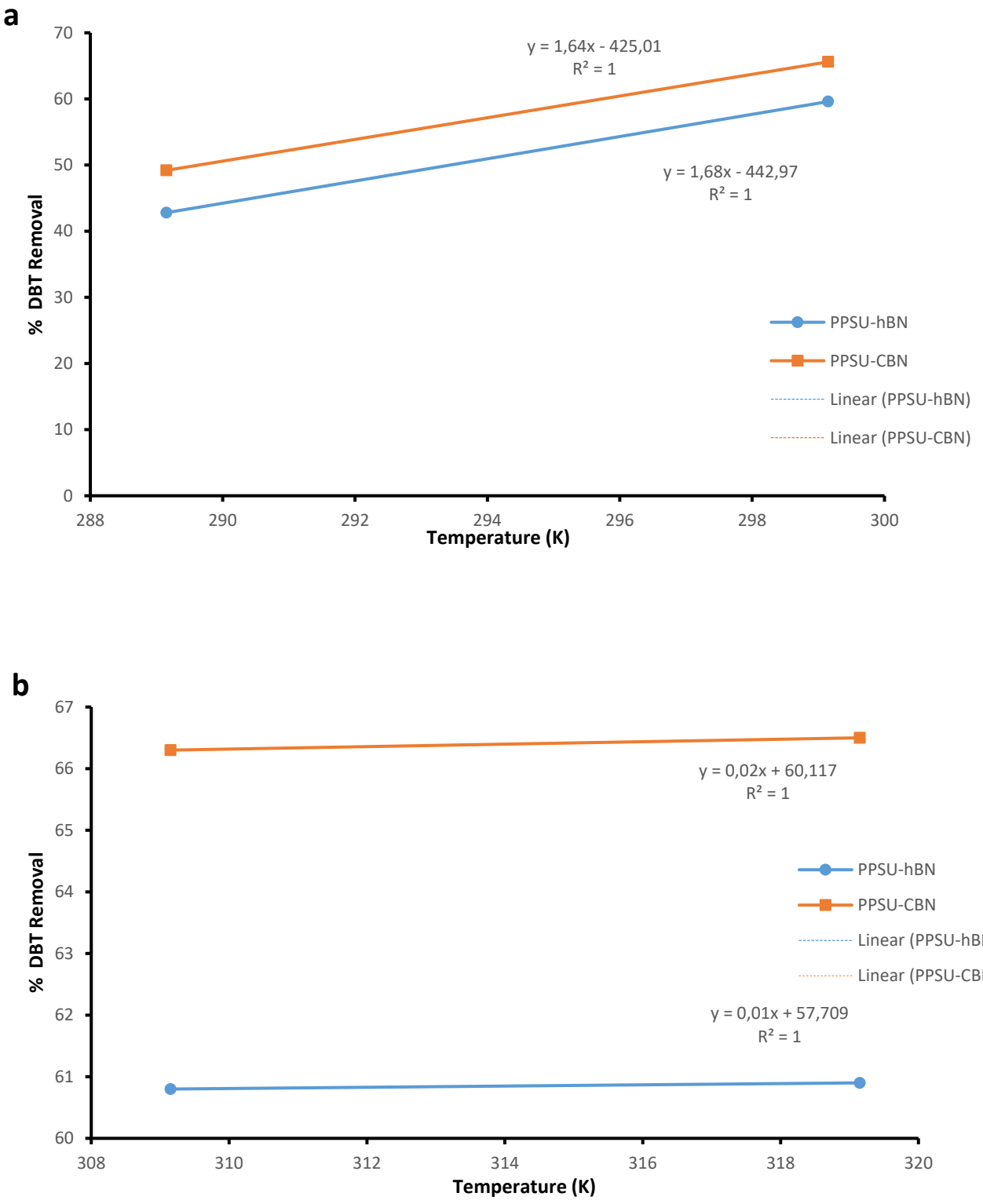


Figure 5.7 Graphs showing adsorption behaviour for varying temperature at (a) rapid phase and (b) slow phase

The linear adsorption behaviour of PPSU-h-BN and PPSU-CBN systems at different operating parameters is shown in Figures 5.5, 5.6 and 5.7. At all the parameters, the adsorbents showed a linear behaviour with R^2 values closer to unity. The slow phase is important as most of the adsorption takes place and the slope values are compared to identify the optimum conditions. The plot from Figure 5.5 b shows a significant difference in R^2 (distribution coefficient) values of PPSU-h-BN (R^2=0.8584). PPSU-CBN system shows more linear adsorption behaviour with higher R^2 values, which might be attributed to the combined properties of C-dots and h-BN.

Table 5.3 R^2 values of h-BN and CBN systems at different parameters at slow phase

Adsorbent	**Contact Time (Fig. 5.5)**	**Adsorbent amount (Fig. 5.6)**	**Temperature (Fig. 5.7)**
h-BN (R^2)	0.8584	0.9549	1
CBN (R^2)	0.9926	0.9857	1

5.5.1 Adsorption capacity behaviour

Linear Adsorption Isotherm: The most basic and extensively used method of adsorption isotherm is the linear isotherm which reflects the affinity of the binding sites. The equation is expressed as:

$$q_e = K_d C_e \qquad (5.3)$$

Where, q_e is the concentration of solute adsorbed onto the solid phase; K_d is the distribution coefficient and C_e is the concentration of the solute in solution. It usually adopts the distribution coefficient as a constant and forms the basis of the general retardation factor (Goldberg et al., 2007).

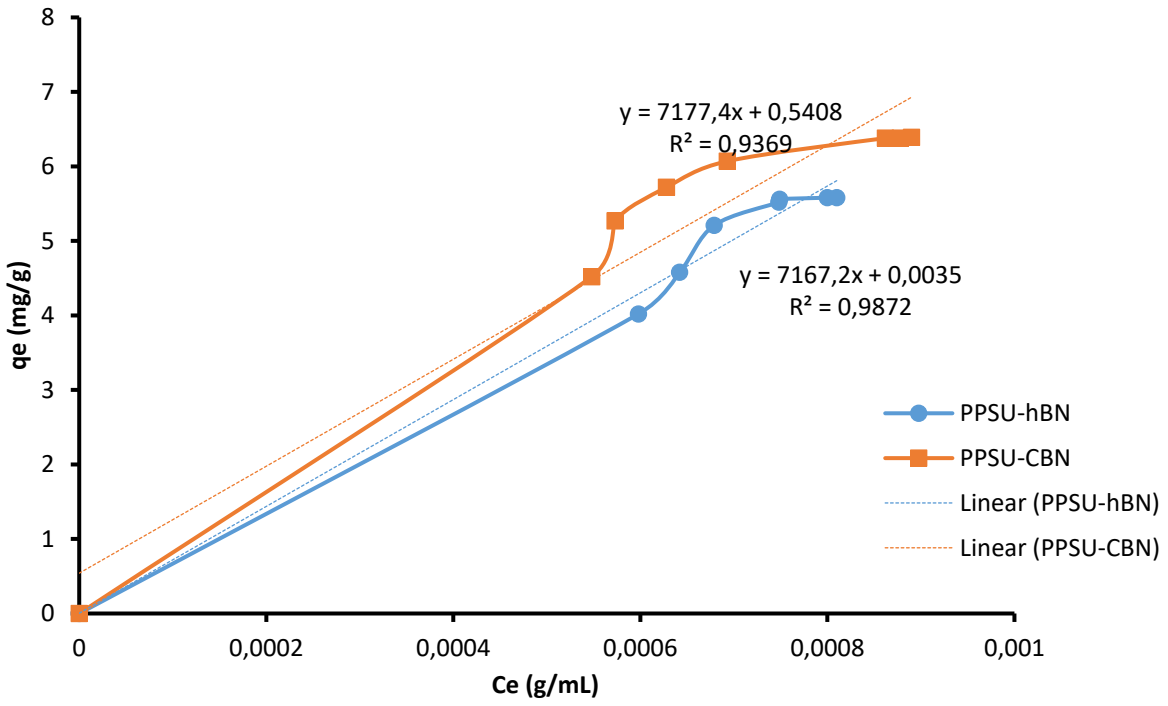


Figure 5.8 Linear adsorption isotherm (for effect of varying contact time) of PPSU-h-BN and PPSU-CBN membranes

The effect of the varying contact time can be shown using the linear adsorption isotherm by plotting *q* against C_e of PPSU-h-BN and PPSU-CBN membranes.

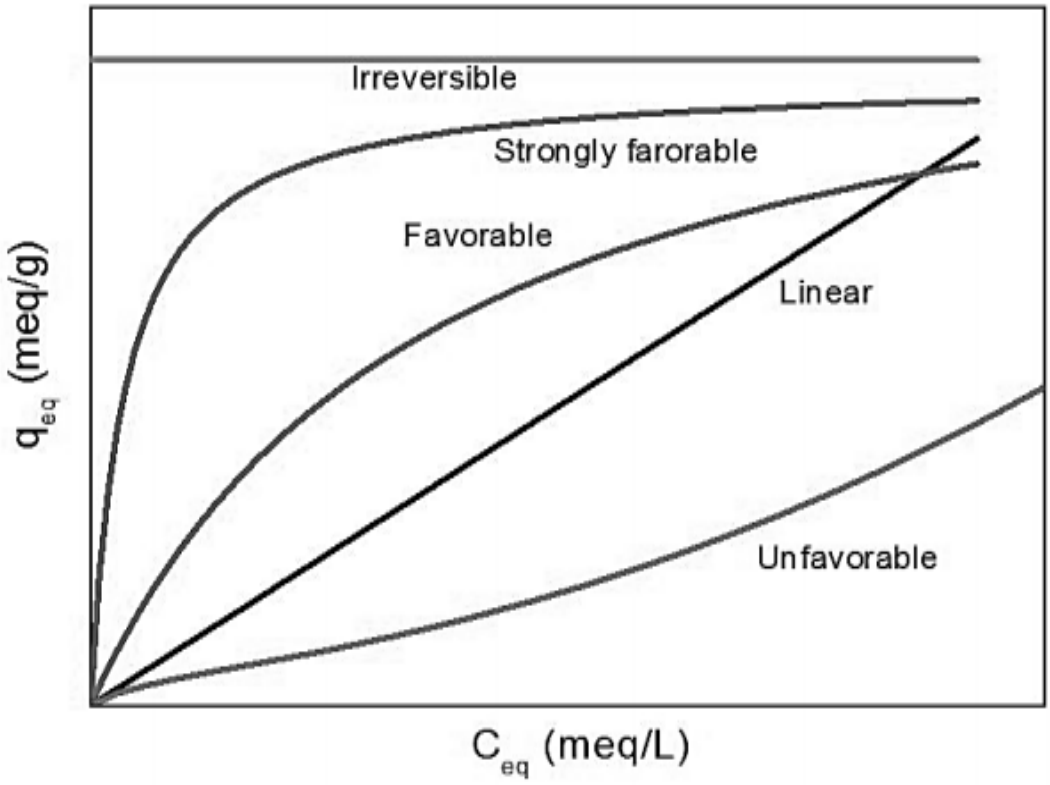
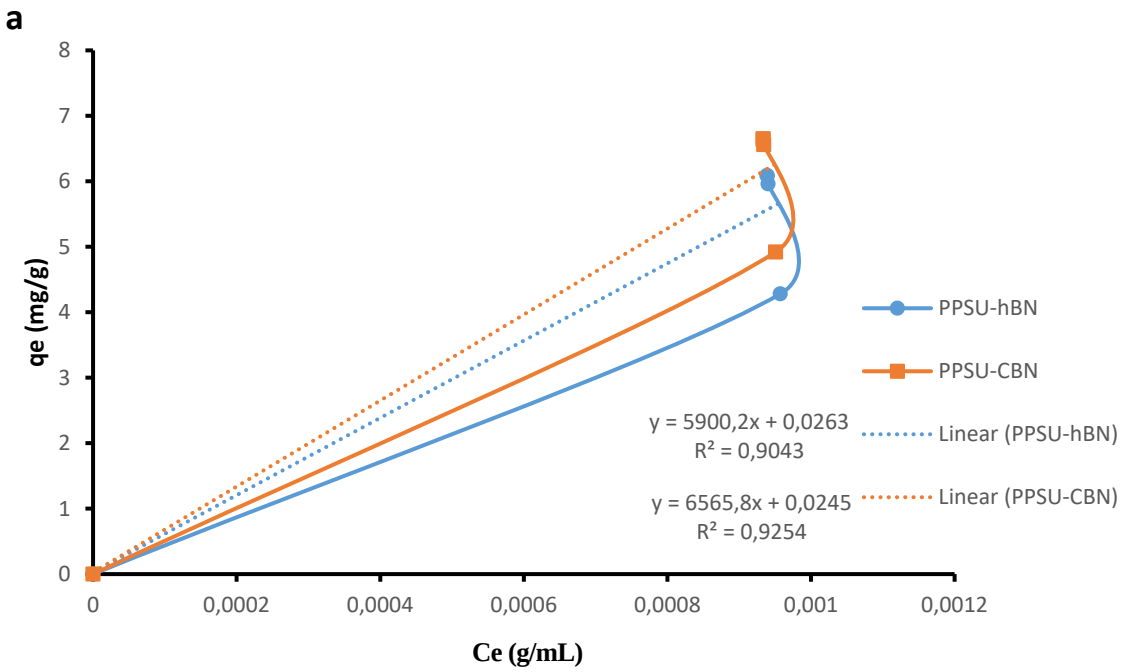


Figure 5.9 Adsorption isotherms (Barros et al., 2013)

Adsorption capacity behaviour as shown in Figure 5.9 can be generally characterized by various shapes such as linear and curved, which can be favourable, strongly favourable, irreversible and unfavourable as per the investigation of Barros et al., (2013). Figure 5.8 shows a curve indicating the favourable behaviour of both the membrane systems. The investigated adsorptive capacity for varying contact time was favoured and had a general linear behaviour with $q_e = 7177.4C_e + 0.5408$ ($R^2 = 0.9369$) for PPSU-h-BN and $q_e = 7167.2C_e + 0.0035$ ($R^2 = 0.9872$) for PPSU-CBN. The favarouble behaviour of PPSU-h-BN system and PPSU-CBN

system showed that the used material have higher potential for sulfur removal. The R^2 values support the above discussed behaviour as the values are close to 1.

The R^2 value for PPSU-h-BN was observed to be higher than PPSU-CBN indicating a more favoured nature. The reason may be due to the boron atoms in h-BN are sp^2 hybridized, and have virtual orbitals (Song et al., 2013). As an outcome, Lewis bases will pair with the electron deficient boron atoms on h-BN. DBT acts a Lewis base as it has lone pair of electrons in the sulfur atoms that can result in the Lewis acid–base interactions between h-BN and DBT (Nag et al., 2010). The higher increase in the favourable region may have been due to the pore size of h-BN and their chemical interactions with sulfur compounds. More investigations on the removal mechanism is required to understand the type of interaction and improve the selectivity of used materials in the future.



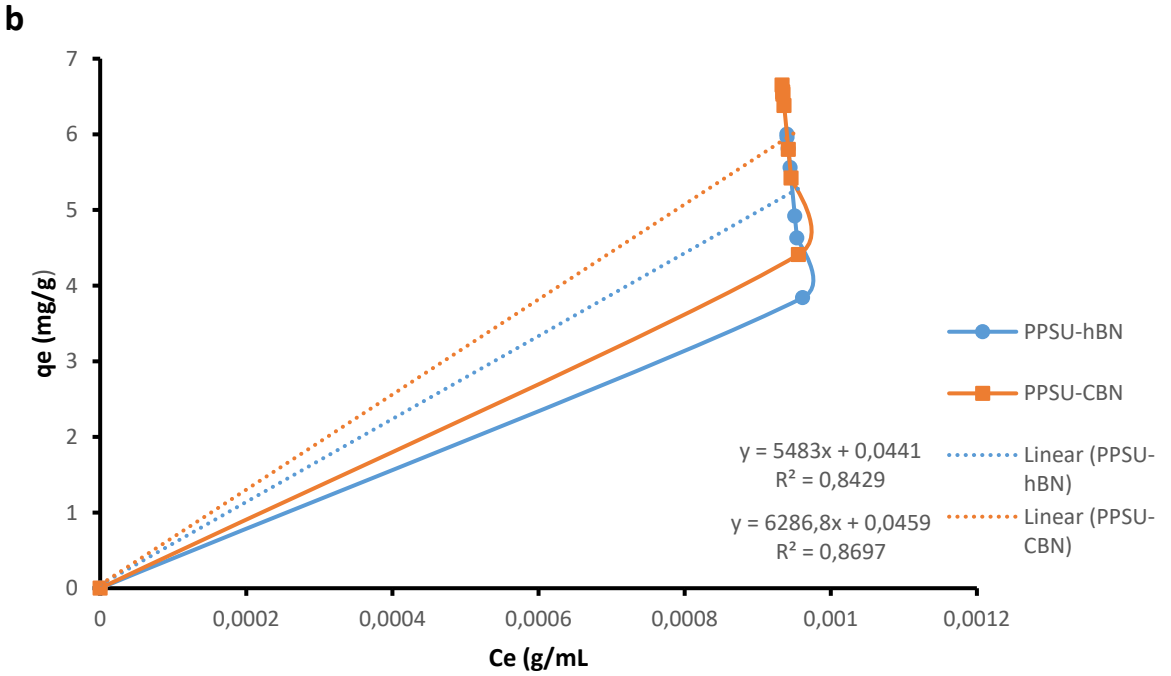


Figure 5.10 Linear adsorption isotherms of PPSU-h-BN and PPSU-CBN membranes for varying (a) temperature and (b) amount of adsorbents

Figure 5.10 shows the linear graph of q_e against C_e for varying temperature (Figure 5.10 a) and varying amount of adsorbent (5.10 b) in membrane which show distribution coefficients (R^2) values for both PPSU-h-BN (Figure 5.10 a, R^2 = 0.9043; b, R^2 = 0.8429) and PPSU-CBN (Figure 5.10 a, R^2 = 0.9254; b, R^2 = 0.8697). PPSU-CBN system in Figure 5.10 is showing higher R^2 values when compared to PPSU-h-BN system. The reasons for this behaviour could be the increase in specific area due to the presence of C-dots and also the nano carbon materials were showed to have superior adsorption properties. As a result, PPSU-CBN are assumed to have a stronger interaction with sulfur compounds than PPSU-h-BN and might have support sites due to the presence of C-dots.

The Figure 5.10 (a and b) also follows a linear pattern as Figure 5.8 and showed an opposite behaviour compared to Figure 5.8. The increase in temprerature and amount of adsorbents have shown unfavoured behaviour on the adsorption process based on the investigation of Barros et al (2013).

The adsorption performance of PPSU-CBN membrane has shown to be superior in all the varying parameters and also fits the adsorption isotherm well. It was previously demonstrated that h-BN with more exposed surface atoms could have better adsorption efficiency. But, the developed porous structure in CBN system could result in a significantly greater amount of exposed atoms along the pores edges, and these exposed surface atoms may serve as additional adsorption sites. The C atoms are assumed to enter N site when doped into the h-BN structure, which will reduce the outer surface electron cloud density of CBN materials and increase the electro positivity of boron atom's virtual empty orbitals. The increased adsorption capacity is assumed to be due to the more exposed atoms around the edges of the pores and the greater Lewis acid–base association formed between porous CBN materials and DBT (Xiong et al., 2015).

5.5.2 Effect of temperature on the adsorption capacity of PPSU-CBN membrane

The investigated temperature did not affect the adsorption capacity pattern of PPSU_CBN system, but increased the ability to adsorb more targeted solute, DBT. This could be explained by removal of volatile materials that occupied the adsorbent pore during the synthesis process. Figure 5.11 presents the q_e behaviour with time (minutes), and it could be observed that the PPSU membrane embedded with CBN (CBN produced from h-BN) calcined at temperature of 299.15 K gave better removal of DBT. The adsorption models in the next chapter explored the

behaviour of MMM developed with CBN developed from h-BN calcinated at 900 ^{o}C using CVD method.

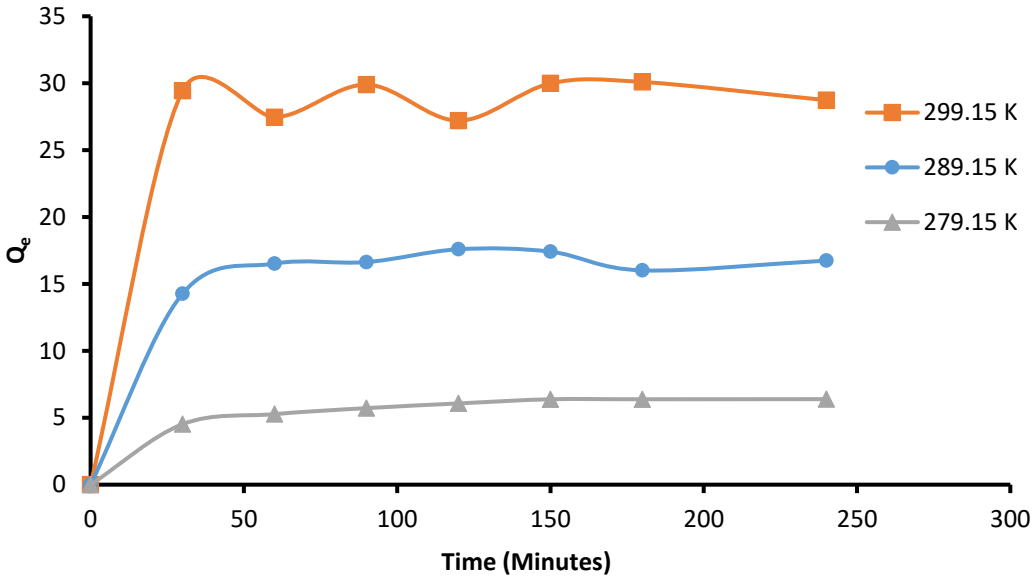


Figure 5.11 Effect of temperature on PPSU-CBN membrane adsorption capacity

5.6 Conclusion

The adsorption of PPSU-h-BN and PPSU-CBN membrane system was performed in this chapter. The R^2 values for linear adsorption isotherms of varying contact time for PPSU-h-BN is 0.8584 and PPSU-CBN is 0.9926; R^2 of varying adsorbent amount for PPSU-h-BN is 0.9549 and PPSU-CBN is 0.9857 and R^2 of varying temperature for both PPSU-h-BN and PPSU-CBN is 1. The linear isotherms show that the adsorption of both the systems favour the increase in contact time and showed an unfavourable behaviour for increase in adsorbent amount and temperature. The results from all the varying parameters such as contact time, temperature and

adsorbent concentration show that PPSU-CBN system was superior in all the parameters as a result of increase in adsorption sites due to C-dot doping in h-BN. This increased the overall performance of the PPSU-CBN system showing significant increase in % sulfur removal.

5.7 References

Barros, M. A. S. D., Arroyo, P. A., & Silva, E. A. (2013). General Aspects of Aqueous Sorption Process in Fixed Beds. Mass Transfer—Advances in Sustainable Energy and Environment Oriented Numerical Modeling, InTech, Rijeka: 361-3.

Bettermann, I. and Staudt, C., 2009. Desulphurization of kerosene: Pervaporation of benzothiophene/n-dodecane mixtures. Journal of Membrane Science, 343(1-2), pp.119-127.

Fadhel, Z.S., 2010. Desulfurization of Light Diesel Fuel Using Chloramine T and Polymer Supported Imidation Agent. University of Technology, Iraq.

Goldberg, S., Criscenti, L.J., Turner, D.R., Davis, J.A. and Cantrell, K.J., 2007. Adsorption–desorption processes in subsurface reactive transport modeling. Vadose Zone Journal, 6(3), pp.407-435.

Ishaq, M., Sultan, S., Ahmad, I., Ullah, H., Yaseen, M. and Amir, A., 2017. Adsorptive desulfurization of model oil using untreated, acid activated and magnetite nanoparticle loaded bentonite as adsorbent. Journal of Saudi Chemical Society, 21(2), pp.143-151.

Kiran, B. and Kaushik, A., 2008. Cyanobacterial biosorption of Cr (VI): Application of two parameter and Bohart Adams models for batch and column studies. Chemical Engineering Journal, 144(3), pp.391-399.

Kumar, P.S. and Kirthika, K., 2009. Equilibrium and kinetic study of adsorption of nickel from aqueous solution onto bael tree leaf powder. Journal of Engineering Science and Technology, 4(4), pp.351-363.

Monticello, D.J., 2000. Biodesulfurization and the upgrading of petroleum distillates. Current Opinion in Biotechnology, 11(6), pp.540-546.

Nag, A., Raidongia, K., Hembram, K.P., Datta, R., Waghmare, U.V. and Rao, C.N.R., 2010. Graphene analogues of BN: novel synthesis and properties. ACS nano, 4(3), pp.1539-1544.
Xiong, J., Zhu, W., Li, H., Yang, L., Chao, Y., Wu, P., Xun, S., Jiang, W., Zhang, M. and Li, H., 2015. Carbon-doped porous boron nitride: metal-free adsorbents for sulfur removal from fuels. Journal of Materials Chemistry A, 3(24), pp.12738-12747.

Shiraishi, Y., Taki, Y., Hirai, T. and Komasawa, I., 2001. A novel desulfurization process for fuel oils based on the formation and subsequent precipitation of S-alkylsulfonium salts. 1. Light oil feedstocks. Industrial & engineering chemistry research, 40(4), pp.1213-1224.

Song, X., Hu, J. and Zeng, H., 2013. Two-dimensional semiconductors: recent progress and future perspectives. Journal of Materials Chemistry C, 1(17), pp.2952-2969.

Srivastav, A. and Srivastava, V.C., 2009. Adsorptive desulfurization by activated alumina. Journal of hazardous materials, 170(2-3), pp.1133-1140.

Xiong, J., Luo, J., Yang, L., Pang, J., Zhu, W. and Li, H., 2018. Boron defect engineering in boron nitride nanosheets with improved adsorptive desulfurization performance. Journal of Industrial and Engineering Chemistry, 64, pp.383-389

Xiong, J., Zhu, W., Li, H., Yang, L., Chao, Y., Wu, P., Xun, S., Jiang, W., Zhang, M. and Li, H., 2015. Carbon-doped porous boron nitride: metal-free adsorbents for sulfur removal from fuels. Journal of Materials Chemistry A, 3(24), pp.12738-12747.

Yu, J., Xie, L.H., Li, J.R., Ma, Y., Seminario, J.M. and Balbuena, P.B., 2017. CO2 capture and separations using MOFs: computational and experimental studies. Chemical reviews, 117(14), pp.9674-9754.

6. CHAPTER SIX: ADSORPTION BEHAVIOUR AND KINETIC MODELS

6.1 Introduction

This chapter elaborates on adsorption behaviour and kinetic models as well as provides the base of this research with reference to the methodology.

6.2 Adsorption isotherms for single component equilibria

Adsorption process allows targeted molecules to occupy the pores of the adsorption system, while the non-targeted substances escape through the removal system. The C-dot doped with h-BN embedded in the membrane can adsorb sulfur molecules and its ability can be well discussed using the isotherms' models. Foo and Hameed, (2010) and Sanyangare, (2016) describe how the use of isotherm models assists in understanding the mechanism of controlling the adsorption process. The adsorption isotherms were focussed on the adsorption capacity q_e, which was presented in various mathematical equations to understand the adsorbability of materials for adsorption module design (Sanyangare, 2016; Worch, 2021).

6.2.1 Linear adsorption isotherm equation

As discussed in chapter five, the graph of q_e against C_e is an indication of the favourable or unfavourable behaviour of the adsorption process. Figure 6.1 showed that the adsorption of sulfur using CBN embedded PPSU membrane is not reversible (q_e = constant). The

investigation showed that $q_e = k_d C_e + b$, with the distribution coefficient k_d equals to 18.6, 17.95, 20.2, and 18.1 at 289.15, 299.15, 309.15 and 319.15 K, respectively. It was seen that at 299.15 K, the adsorption capacity was higher compared to 289.15, 309.15 and 319.15 K. However, there was a larger range of adsorption capacity at 309.15 K. These results showed the potential of CBN on controlling the removal of sulfur compounds. The temperature became a factor in the removal range of the adsorbate. The R^2 value showed that the adsorption isotherm is more linear at 309.15 K, with higher distribution coefficient. More investigation should be done in order to understand the effect of time on the large range of adsorbability of sulfur on PPSU-CBN, and investigate factors that can increase the range of adsorbability at 299.15 K. The diffusion of adsorbate into the pore of the adsorbent and the interaction of adsorbate-adsorbent are favoured at room temperature.

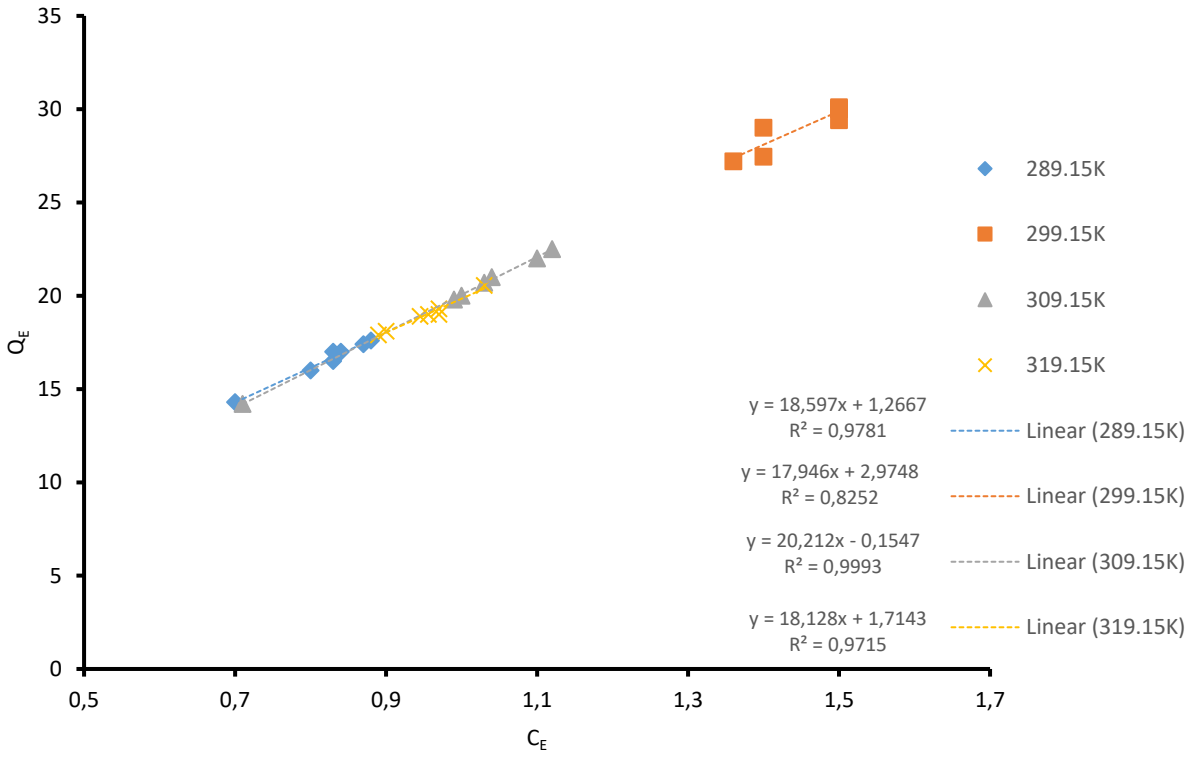


Figure 6.1 Linear adsorption isotherm

6.2.2 Freundlich adsorption equation

Sanyangare, (2016), stated that the Freundlich isotherm can be used for homogeneous and heterogeneous systems, and for both physical and chemical adsorption processes. This was a motivation to investigate the Freundlich isotherm behaviour for sulfur using PPSU-CBN membrane in organic environment as stated by Xu et al. (2013) and Sanyangare, (2016). Freundlich isotherm equation is given by ln q_e = ln K_F + (1/n) ln C_e. The indicator of adsorption capacity is given by k_F, which are 19.83, 20.75, 20.055 and 19.8 at 289.15, 299.15, 309.15 and 319.15 K, respectively as seen in Figure 6.2. As discussed above, the adsorption capacity at 299.15 K was higher compared to 289.15, 309.15 and 319.15 K. The numerical values of n were 1.087, 1.11, 0.99 and 1.108 at 289.15, 299.15, 309.15 and 319.15 K, respectively. These results confirmed that the adsorption capacity with C_e has a linear behaviour as discussed above. The behaviour at 299.15 and 309.15 K are the same for both graphs (Figures 6.1 and 6.2). If n = 1, ln q_e = ln K_F + (1/n) ln C_e = ln K_F + ln C_e = ln K_F + ln C_e = ln K_F + ln C_e = ln (K_F x C_e); and q_e = K_F x C_e.

The findings of Sanyangare (2016), Muzic et al. (2010a); Muzic et al. (2010b) and Adeyi and Aberuagba (2012) confirmed that the Freundlich isotherm model was found to describe the desulfurization behaviour of various adsorbents from petroleum fuels.

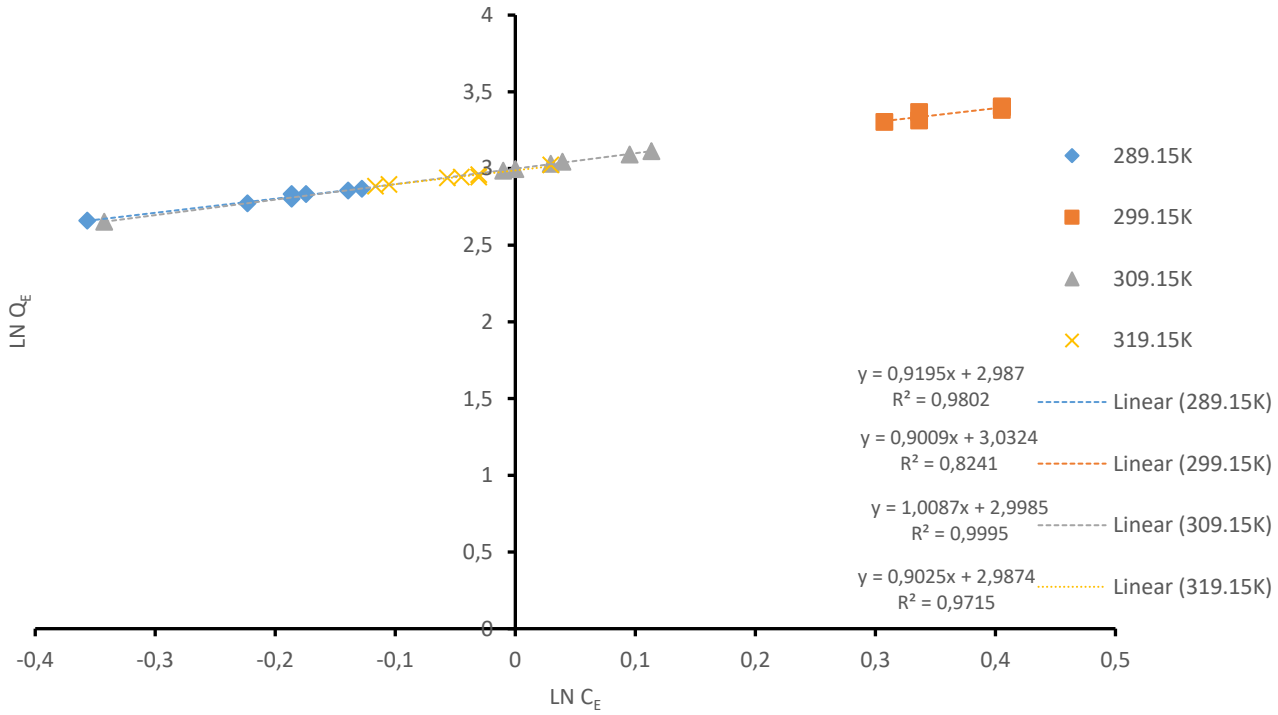


Figure 6.2 Freundlich adsorption isotherm

6.2.3 Langmuir adsorption Equation

As per the investigations of Sanyangare (2016), Vijayaraghavan et al. (2006), Foo and Hameed, (2010) and Worch (2021b), the adsorption fits intio the Langmuir model only if the interaction is possible between adsorbate and adsorbent where chemical adsorption is promoted. Figure 6.3 showed that at 299.15 K, the adsorption capacity was too low compared to the other investigated temperatures. 309.15 K showed higher range and higher adsorption capacity. The behaviour seen in Figure 6.3 was opposed to the behaviour in Figures 6.1 and 6.2. The linear form of Langmuir equation given by $(1/q_e) = (1/Q_m K)(1/C_e) + (1/Q_m)$ assists in determining the maximum amount of the adsorbate per unit mass of sorbent (Q_m) and the affinity of the binding sites K (L/mg). The maximum amount of sulfur per unit mass of PPSU-CBN were 192.3, 303, 2000 and 181.8 at 289.15, 299.15, 309.15 and 319.15 K, respectively. These results

showed that the maximum amount of the adsorbate was more pronounced at 309.15 K. The affinities of the binding sites K were 4235.85, 6704.2, 39682.5 and 4049.4 L/ mg. The affinity and the linear behaviour were higher at 309.15 K as discussed above. The amount of sulfur adsorbed and the affinity at 309.15 K were almost 10 times of the amount and affinity at 289.15, 299.15 and 319.15 K.

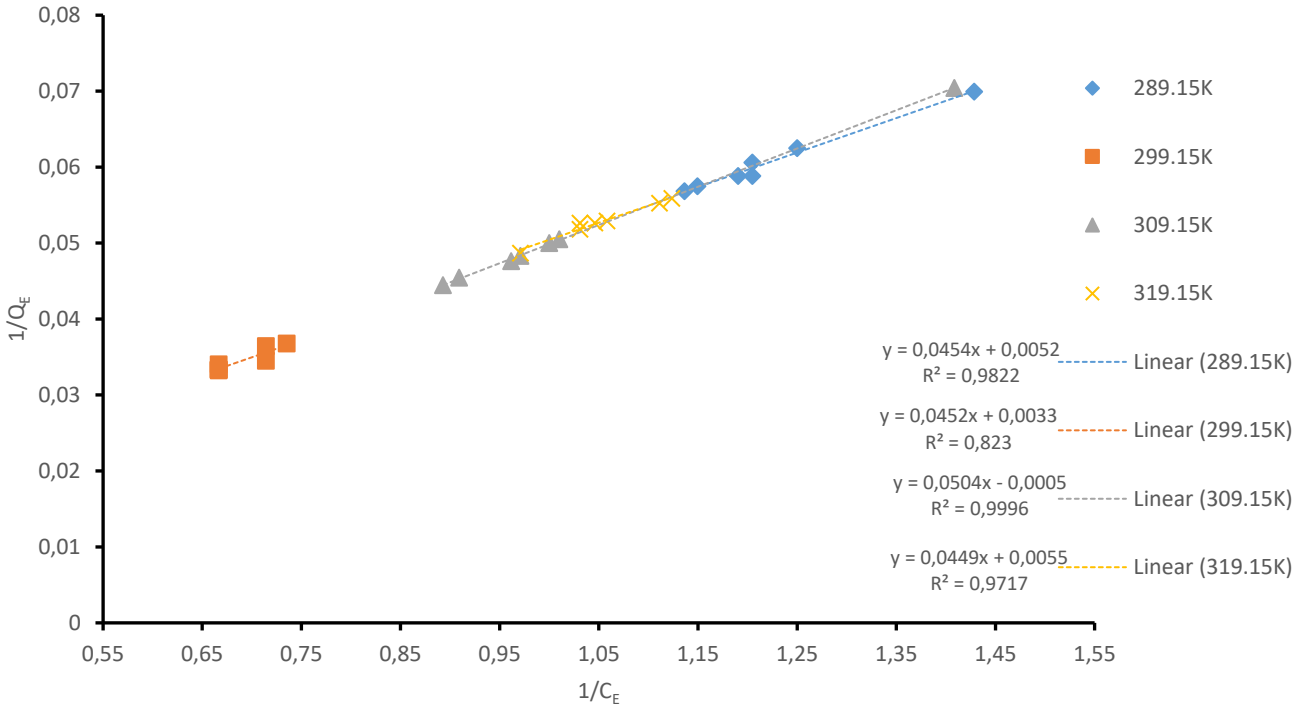


Figure 6.3 Langmuir adsorption isotherm

6.2.4 Temkin Adsorption Equation

Temkin adsorption equation describes the relationship between the adsorption and the heat of sorption. The Temkin adsorption equation is given by $q_e = BlnA + BlnC_e$, with B = RT/b and A. The Temkin constant related to the heat of sorption b (J/mol) and the Temkin isotherm

constant A (L/g) were determined from the graph. The adsorption constants are given in table 6.1.

Table 6.4 Temkin adsorption constants

T	**B**	**b** (J/mol)	**A** (L/g)
289.15 K	14.56	165.11	3.801144
299.15 K	25.825	96.31	2.121288
309.15 K	17.912	143.49	3.092278
319.15 K	17.248	153.84	3.158889

Table 6.1 showed low heat involved in the adsorption process at 299.15 K, while at 289.15 K, the heat was too high (165.11 J/mol). The same behaviours seen in Figures 6.1 to 6.2 were observed in Figure 6.4 (higher adsorption capacity at 299.15 K and higher range at 309.15 K).

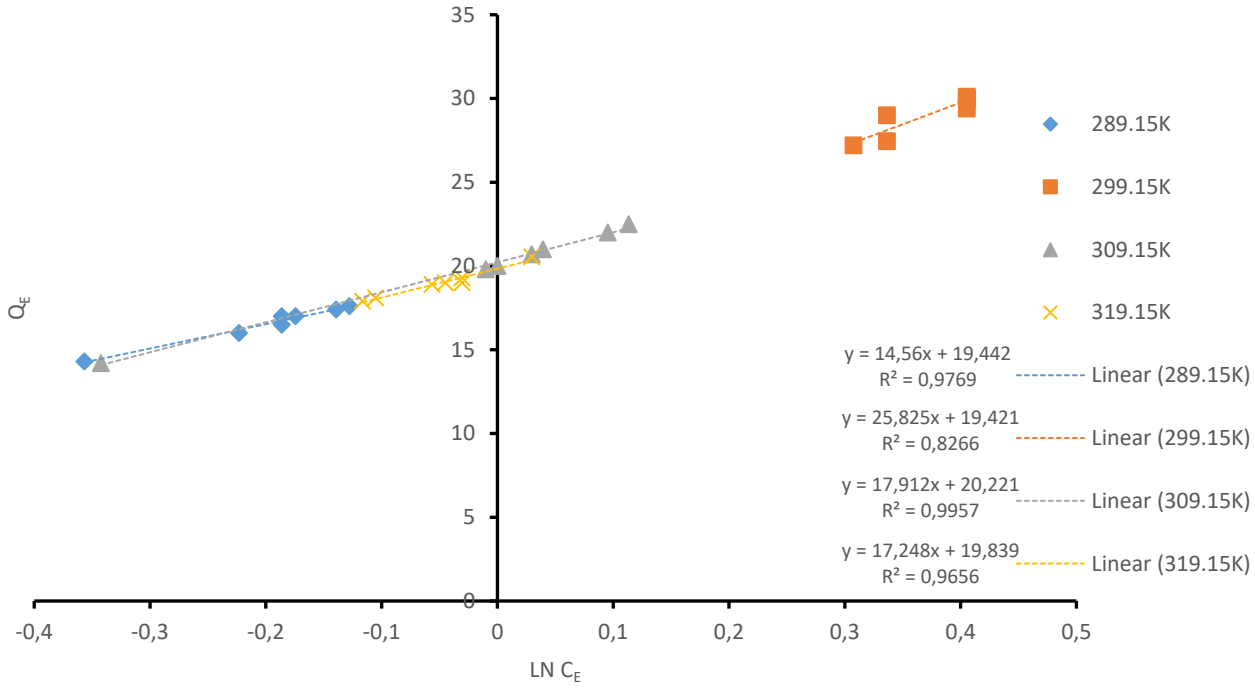


Figure 6.4 Temkin adsorption isotherm

6.2.5 Multi-isotherms behaviour

Table 6.2 showed that higher R^2 values were seen at 309.15 K for all investigated adsorption isotherms. The multi-isotherms behaviour can be understood by multi-mechanism of adsorption of sulfur on PPSU-CBN membrane. Temkin isotherm showed that the favourable temperature (299.15 – 309.15 K) releases moderate heat of sorption, while 289.15 and 319.15 K, involved higher heat of sorption. The kinetic analysis can confirm these findings, and future optimization study should assist to identify the range of temperatures that removes more sulfur material.

Table 6.5 Coefficient of determination (R^2)

	289.15K	299.15K	309.15K	319.15K
Linear Adsorption Isotherm	R^2 = 0,9781	R^2 = 0,8252	R^2 = 0,9993	R^2 = 0,9715
Freundlich Adsorption Equation	R^2 = 0,9802	R^2 = 0,8241	R^2 = 0,9995	R^2 = 0,9715
Langmuir adsorption Equation	R^2 = 0,9822	R^2 = 0,823	R^2 = 0,9996	R^2 = 0,9717
Temkin Adsorption Equation	R^2 = 0,9769	R^2 = 0,8266	R^2 = 0,9957	R^2 = 0,9656

6.3 Adsorption Kinetics

The understanding of the adsorption kinetic behaviour is a key step for the design of the adsorption system, and provide detailed information for the process management and mechanism at which the adsorbate interacts with the adsorption system. The kinetic analysis was required to determine the type of reaction and diffusion mechanism (bulk diffusion, external mass transfer (film diffusion) and intra-particle diffusion (pore diffusion)) and PPSU-CBN removeal process of sulfur materials. The diffusion of adsorbate occurs at three steps, namely external diffusion around the membrane (between the solution and the removal system), internal diffusion or intra-particle diffusion (within the membrane system), and the

diffusion within the CBN pores of PPSU-CBN system (active site) (Sanyangare, 2016). The strength of the interaction between adsorbate and CBN determines the stability of the adsorption and desorption processes. Higher strength reduces the number of re-uses of the membrane, as this will require energy and/or chemicals for washing the membrane.

The diffusion of the adsorbate in the solution – module system can be understood by the following, which determines the rate-controlling factor:

a) Transport of sulfur materials from the solution to the membrane system;
b) Transport of adsorbate around the membrane before reaching the CBN pores;
c) Transport of adsorbate within the CBN pores;
d) The equilibrium state of the adsorbate (adsorption and desorption) within the CBN pores of PPSU-CBN system.

6.3.1 Adsorption Reaction Models

The adsorption reaction models assist in determining the rate constant, the order of reaction and the heat involved in the adsorption process. There are several reaction models, but the following were investigated in this study.

6.3.1.1 Pseudo First Order Reaction model

The pseudo first order reaction model can be presented by Rate = k ($q_e - q_t$) with q_e, q_t and k the adsorption capacities at equilibrium, time t and rate constant, respectively. The rate constant can be determined from the slope of the graph by plotting Ln q against time as seen in Figure

6.5. The R^2 value (0.5653) at 309.15 K was higher compared to the other investigated temperatures, which agreed with the above discussion.

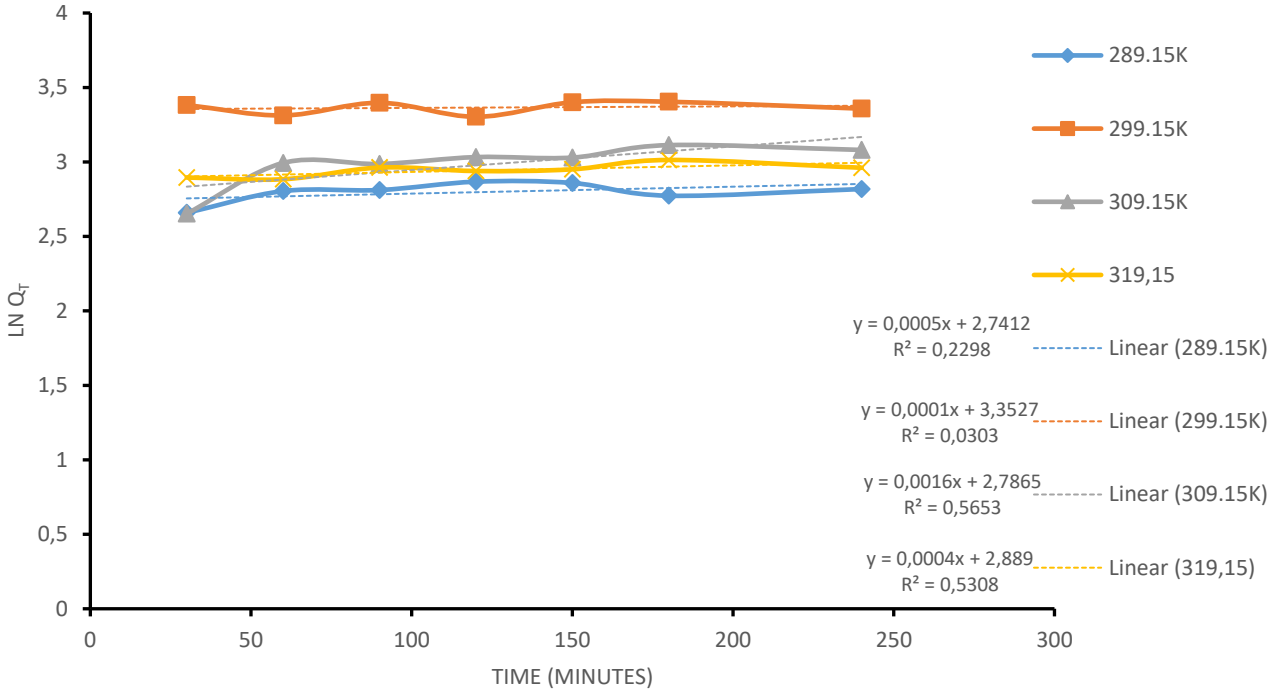


Figure 6.5 Pseudo First Order reaction

6.3.1.2 Pseudo Second Order Reaction model

The pseudo second order reaction model can be presented by Rate = k $(q_e - q_t)^2$. The integrated expression of this model can be written as $(t/ q_t) = (1/ k q_e^{\ 2}) + (t/ q_e)$. q_e and the rate constant were determined from the graph of (t/ q_t) against time. The R^2 values (0.9963, 0.9977, 0.9962 and 0.9960 at 289.15, 299.15, 309.15 and 319.15 K, respectively) showed that the removal of sulfur materials using PPSU-CBN fits the pseudo second order reaction model. The rate constant at 309.15 K was higher compared to the other temperatures, which showed that the

rate diffusion-controlled at 309.15 K was higher. As stated by Sanyangare (2016), k strongly depends on the process temperature as the initial concentration, and the driving forces toward the membrane were kept constant. It was observed that q_e increased with the temperature. The behaviour of the graph on Figure 6.6 confirmed the above discussion concerning 299.15 and 309.15 K.

Table 6.6 Pseudo second order reaction constants

	Rate constant	**q_e**	**R^2**
289.15 K	0.00326	16.835 mg/g	0.9963
299.15 K	0.01349	20.080 mg/g	0.9977
309.15 K	0.02293	22.990 mg/g	0.9962
319.15 K	0.00404	29.760 mg/g	0.9960

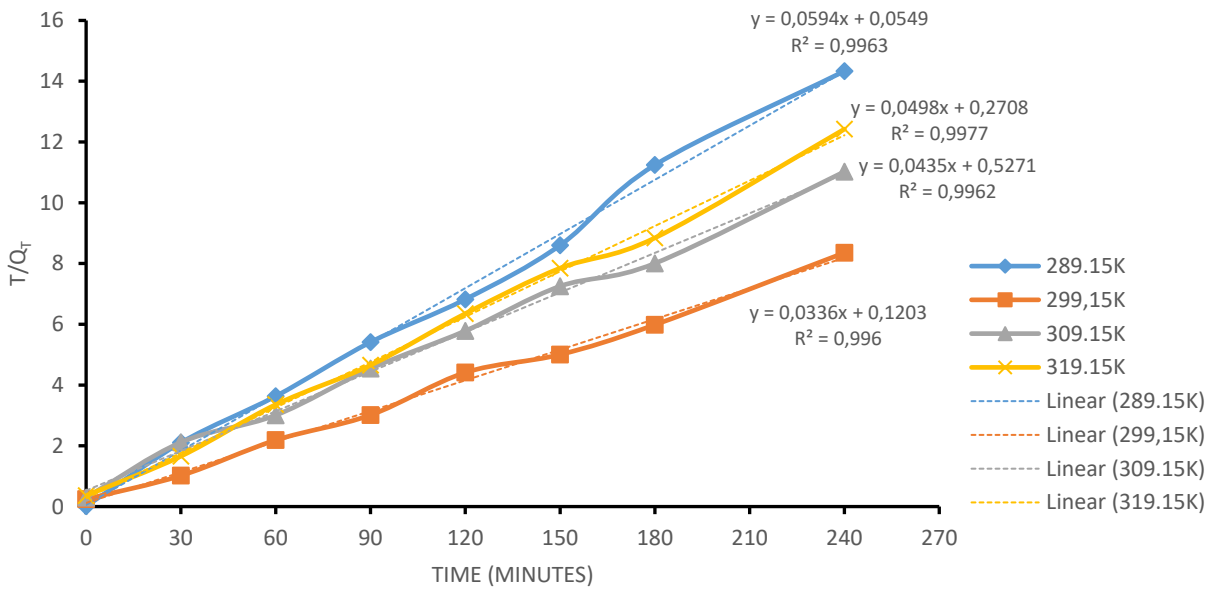


Figure 6.6 Pseudo Second Order reaction

6.3.1.3 Elovich's equation

The Elovich equation is mostly used for heterogeneous system describing the chemisorption process of adsorption. The rate of reaction is given by $ae^{-\propto q}$. The reaction constants were determined by the graph of q against LN time as seen in Figure 6.7. The R^2 value at 309.15 K was 0.8227 (closer to 1), which showed that at this temperature the active sites interacted strongly with the adsorbate.

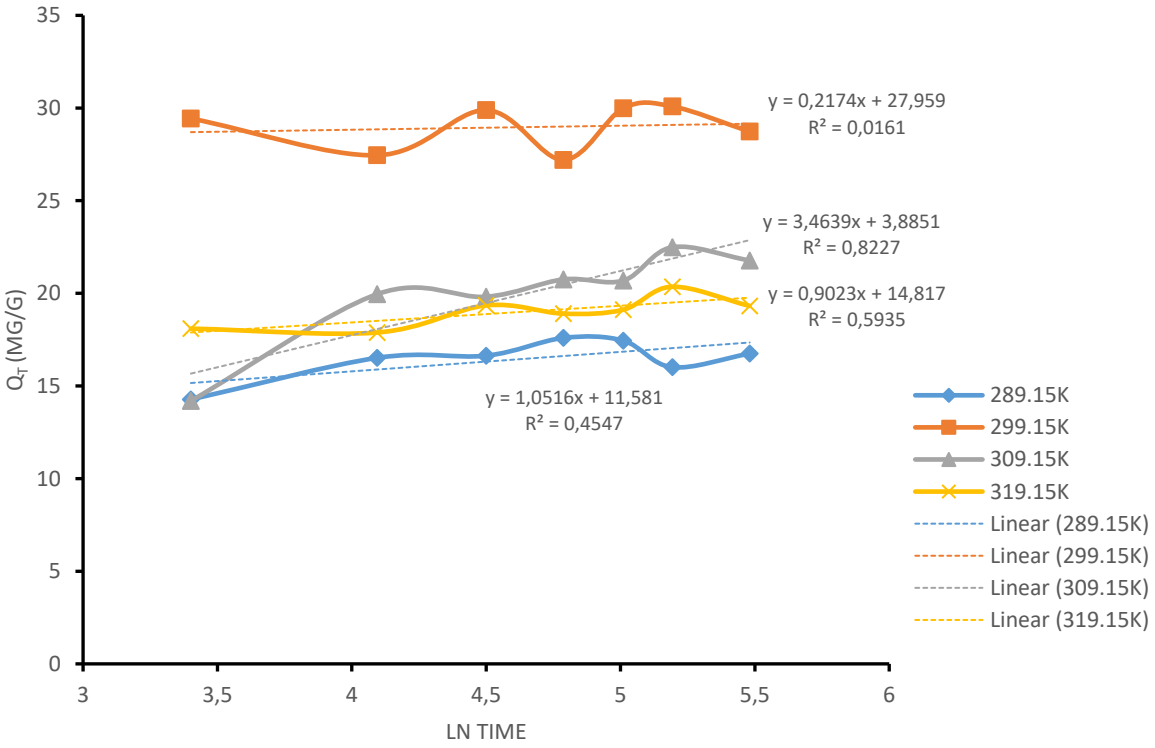


Figure 6.7 Elovich's kinetic model

6.3.1.4 Langmuir-Hinshelwood Kinetics

The Langmuir-Hinshelwood kinetic model is mostly used for heterogeneous reactions where the rate of reaction is controlling factor. The reaction constants were determined by the graph of LN $C_o/C_t)/ (C_o - C_t$ against t/ (Co - Ct) as seen in Figure 6.8. The R^2 value at 309.15 K was 0,6347, which showed that at this temperature the ability to accommodate the sulfur materials on the adsorbent surface was higher compared to other investigated temperature.

The analysis of the adsorption reaction models showed that 309.15 K had multi behaviour, and promotes various controlling factors. Future investigations are required to understand factors that differentiate the level of different mechanisms at 309.15 K. In general, the adsorption of sulfur material on CBN using PPSU membrane had a pseudo second order behaviour.

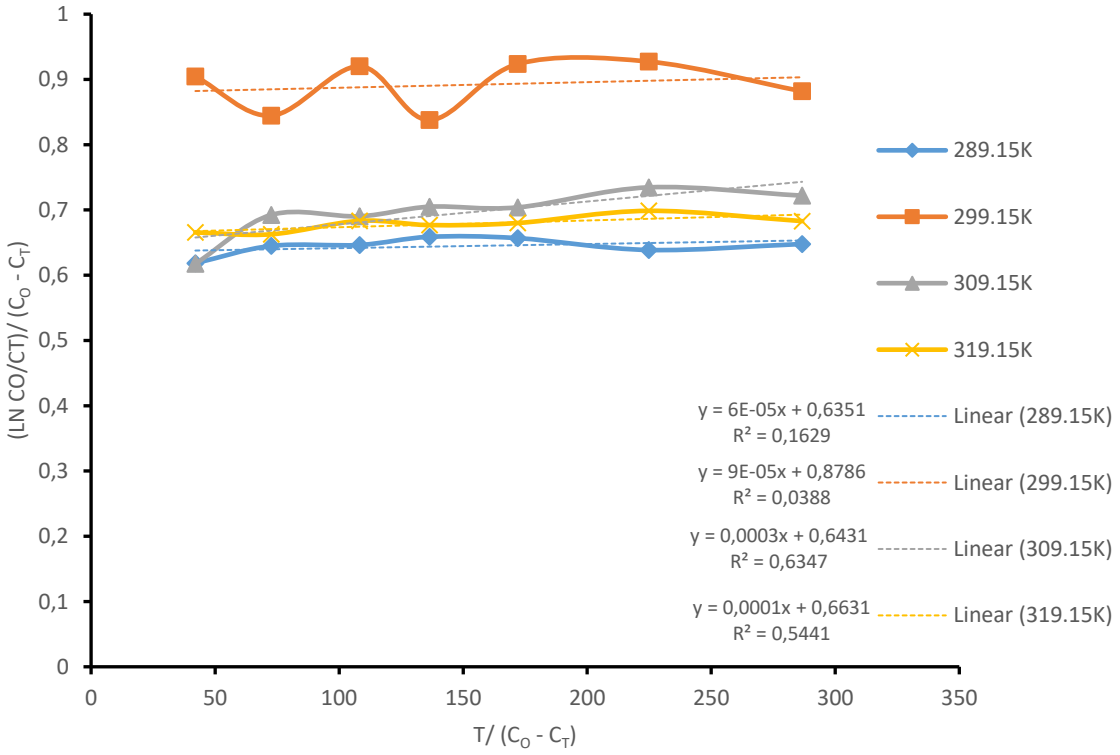


Figure 6.8 Langmuir-Hinshelwood Kinetic model

6.3.2 Adsorption Diffusion Models

Sanyangare (2016), stated that the kinetics of the adsorption process is controlled by film or intraparticle diffusions. The adsorption diffusion models can assist in understanding the mechanism at which the adsorbate diffuse in the adsorption system. There are several adsorption diffusion models but the following sections are focussed on the selected models.

6.3.2.1 Linear driving force diffusion model

The Linear driving force diffusion model showed the linear behaviour of the rate of solute accumulation in the solid phase against the change in concentration ($\Delta q/\Delta t = k_f\, a\, (C_0 - C_t)$ with

k_f, the external mass coefficient). The plotted graph can be used to determine the particle surface area per unit particle volume (Sanyangare, 2016). Figure 6.9 showed that at 309.15 K, the rate become linearly proportional to the change in concentration. Figures 6.9 and 6.10 showed that the R^2 values at 299.15 K were 0.6736 and 0.7345 for the linear and polynomial behaviours, respectively. The R^2 values varied between 0.7749 and 0.7345 from the polynomial equation with power 5 to 3. The Linear driving force diffusion model at 309.15 K showed that the diffusion mechanism considered single adsorbate diffusion into the adsorbent system. Therefore, multi mechanism occurs at 309.15 K as discussed for the reaction rate as controlling factor.

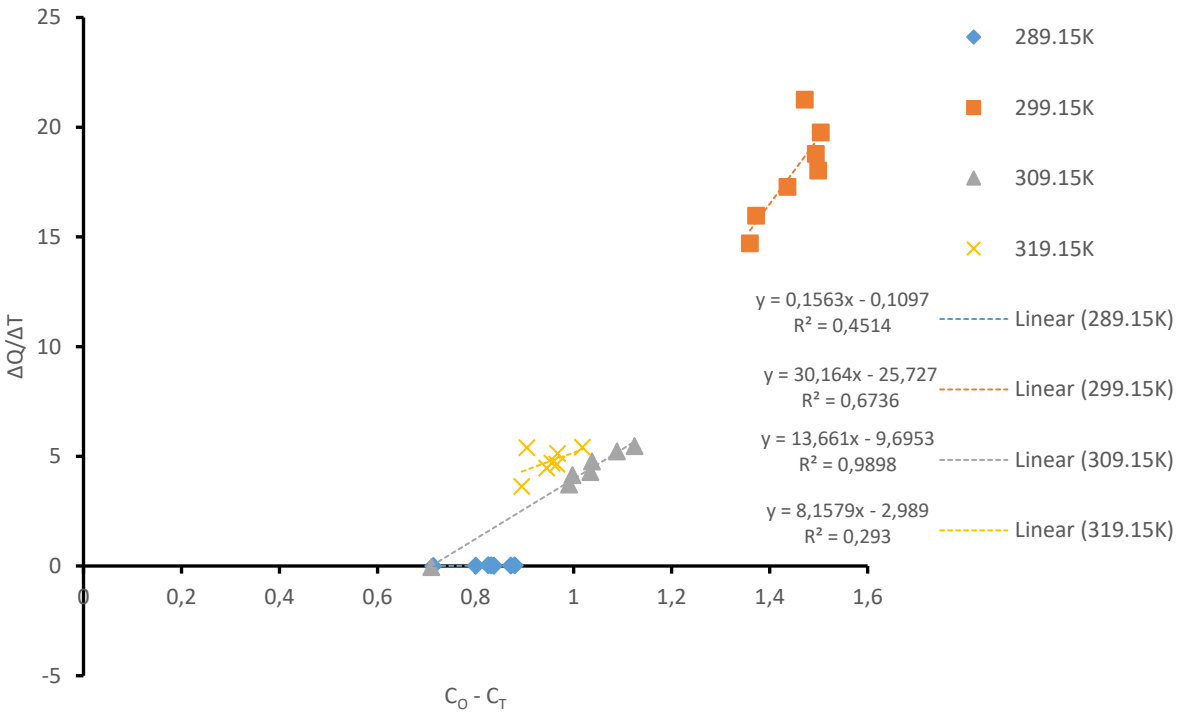


Figure 6.9 Linear driving force diffusion model

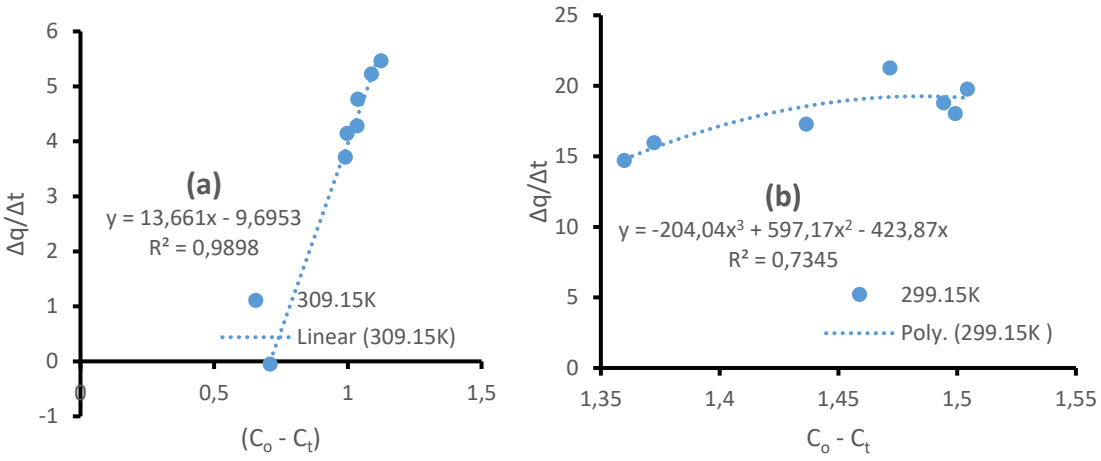


Figure 6.10 Linear driving force diffusion behaviour (a) at 309.15K and (b) 299.15K

6.3.2.2 Film diffusion model

The external surface, which can be represented by the membrane becomes a key factor for the diffusion process (Sanyangare 2016). The film diffusion constant was determined from the graph of LN(1 - q_t/q_e) against time. As per above discussion, 309.15 K was the only temperature that fits the linear form of the film diffusion model with R^2 value equal to 0.6686.

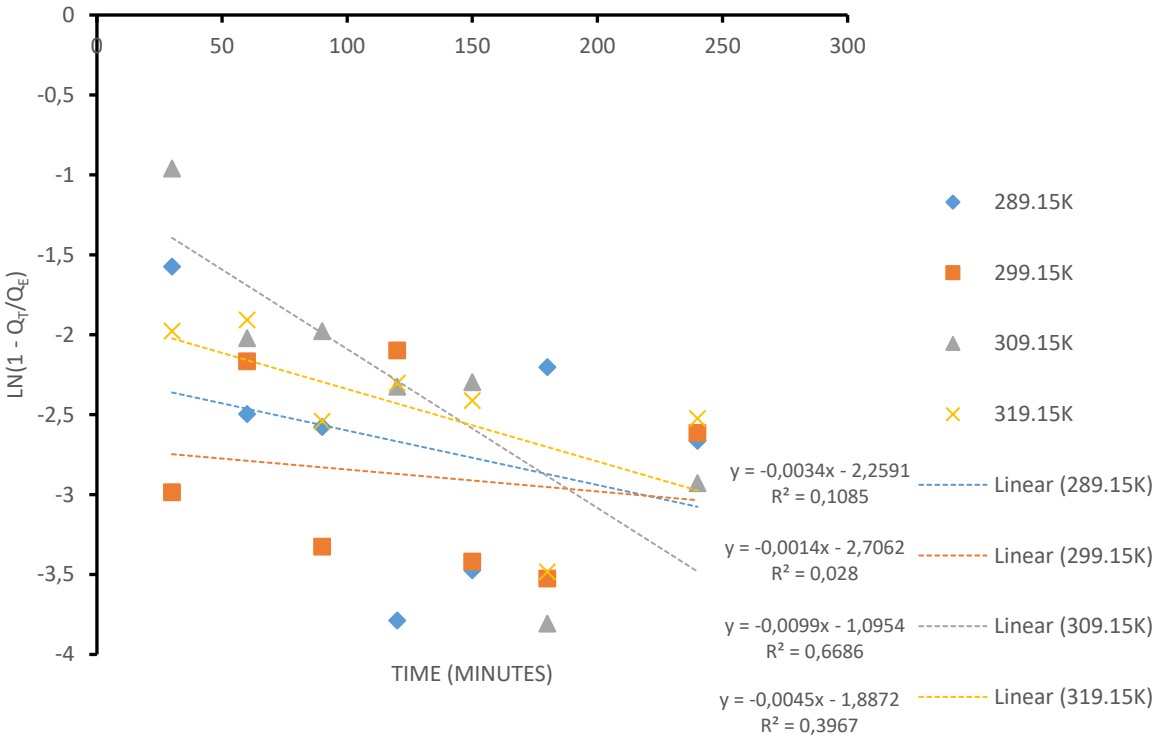


Figure 6.11 Film diffusion model

6.3.2.3 Spahn and Schlunder film diffusion model

The Spahn and Schlunder film diffusion model as seen in Figure 6.12, showed that at 309.15 K the film–pore diffusion mechanism controlled the adsorption process. This was confirmed with the above diffusion film models.

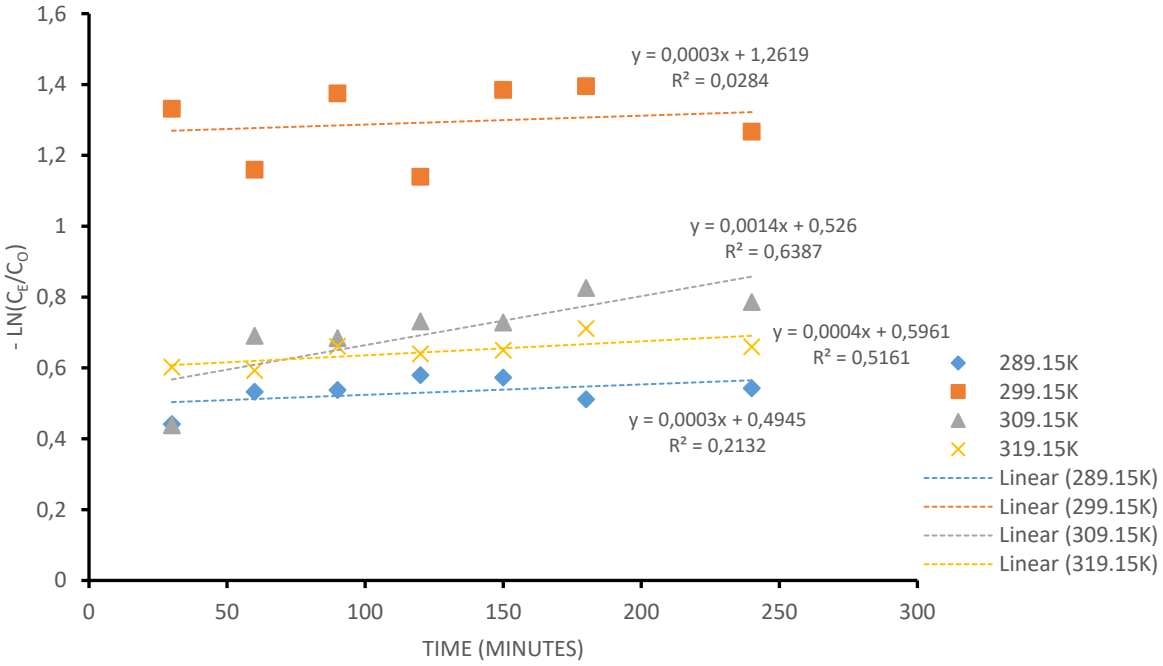


Figure 6.12 Spahn and Schlunder film diffusion model

6.3.2.4 Weber-Morris model

The Weber-Morris model is based on the intra-particle diffusion as the controlling process. It can be ssen from Figure 6.13 that at 309.15 K, the adsorption fits the linear form of the Weber-Morris model with R^2 value equal to 0.7184.

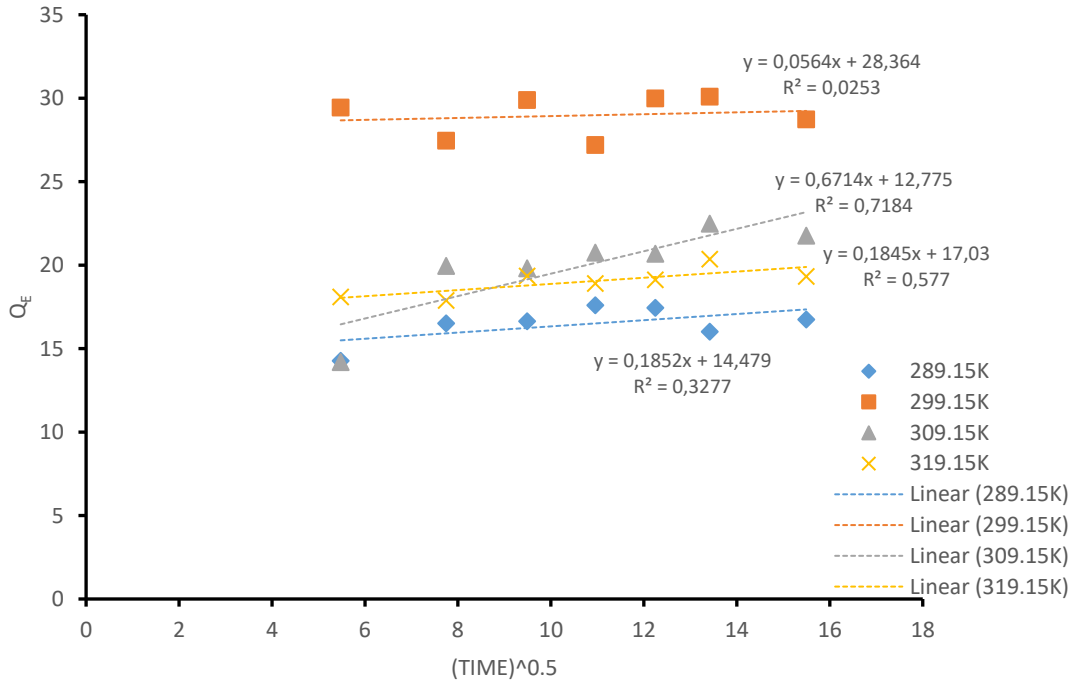


Figure 6.13 Weber-Morris model

Based on the R^2 values, It can be concluded that the removal of sulfur materials using a polymeric membrane embedded with CBN involved various mechanisms. It was also observed that the film and intraparticle diffusions are both controlling the removal process at 309.15 K. Future investigations should highlight the level at each diffusion mechanism tocontrol the adsorption process.

6.4 Conclusion

The adsorption study kinetic models are thoroughly discussed to fit the best model for the study of PPSU-CBN membrane system . Isotherm models were used to investigate the ability of CBN incorporated into the membrane to adsorb sulfur molecules. The adsorption potential was found to be higher at 299.15 K than at other temperatures. At 309.15 K, however, there was a wider range of adsorption power. These findings established CBN's ability to monitor the removal of sulfur-containing materials. The temperature played a role in the adsorbate's removal process with room temperature being favoured for the interaction between adsorbent and adsorbate. The R^2 value revealed a more linear adsorption isotherm for the system. The diffusion models shown that the adsorption process was majorly controlled by film-pore diffusion model.

6.5 References

Adeyi, A.A. and Aberuagba, F., 2012. Comparative analysis of adsorptive desulphurization of crude oil by manganese dioxide and zinc oxide. Research Journal of Chemical Sciences

Foo, K.Y. and Hameed, B.H., 2010. Insights into the modeling of adsorption isotherm systems. Chemical engineering journal, 156(1), pp.2-10.

a. Muzic, M., Gomzi, Z. and Sertic-Bionda, K., 2010. Modeling of the Adsorptive Desulfurization of Diesel Fuel in a Fixed-Bed Column. Chemical engineering & technology, 33(7), pp.1137-1145.
b. Muzic, M., Sertic-Bionda, K., Gomzi, Z., Podolski, S. and Telen, S., 2010. Study of diesel fuel desulfurization by adsorption. Chemical engineering research and design, 88(4), pp.487-495.

Sanyangare, F., 2016. Simulation of the Adsorptive Desulphurisation of Diesel Fuel (Doctoral dissertation, University of the Witwatersrand, Faculty of Engineering and the Built Environment, School of Chemical and Metallurgical Engineering).

Vijayaraghavan, K., Palanivelu, K. and Velan, M., 2006. Biosorption of copper (II) and cobalt (II) from aqueous solutions by crab shell particles. Bioresource technology, 97(12), pp.1411-1419.

a. Worch, E., 2021. 3 Adsorption equilibrium I: General aspects and single-solute adsorption. In Adsorption Technology in Water Treatment (pp. 49-88). De Gruyter.
b. Worch, E., 2021. Adsorption technology in water treatment. Book. de Gruyter.

Xu, Z., Cai, J.G. and Pan, B.C., 2013. Mathematically modeling fixed-bed adsorption in aqueous systems. Journal of Zhejiang University SCIENCE A, 14(3), pp.155-176.

7. CHAPTER SEVEN: CONCLUSION AND RECOMMENDATIONS

7.1 Conclusion

The recent regulations on sulfur emissions has motivated the academia to focus on alternative, cost effective and efficient technologies in order to reduce emissions and improve air quality. The membrane technology is an efficient and economical alternative to traditional hydrodesulfurization method. The introduction and literature review chapters give an overview of current sulfur regulations along with existing technologies. A brief description of MMMs in desulfurization looks into the research advancements in using new materials to enhance the efficiency with minimal time consumption and in a profitable manner. Therefore, the objectives of this study in developing mixed matrix membranes for desulfurization is achieved by the following:

The synthesis of h-BN to develop a new material system of C-dot doped h-BN was investigated. The effect of Nitrogen on precursor formation and the calcination temperature on the formation of h-BN from the precursor was studied. Two methods, CVD and HTF methods were used to synthesize the h-BN to compare the efficient calcination method in producing pure h-BN. The FTIR and XRD results of the produced products confirms the formation of h-BN. CVD method at 900 ^{o}C produced better h-BN product. The calcined precursors through HTF synthesized h-BN with impurities such as unreacted precursor. The increase in HTF and CVD temperatures decreased the impurities in h-BN which can be confirmed from the FTIR spectra. SEM and TEM analysis showed the microstructure of the synthesized h-BN, that showed the crystal grain structure, the size and several layered h-BN confirming the successful synthesis. Synthesis of C-dots through hydrothermal carbonization of chitosan produces high

purity C-dots of less than 10nm size. The hydrothermal process introduced several functional groups into the Carbon core, confirmed from the FTIR analysis, which can be applied in multiple applications. The TEM analysis shows the size of C-dots to be below 10 nm in size. These C-dots were utilized in synthesizing C-dot doped h-BN system to use as nano filler in the membrane synthesis for sulfur removal application. A simple method adopted for CBN synthesis was applied and FTIR, SEM and TEM analysis confirmed the successful doping of C-dots on h-BN. C-dots have induced highly porous structure to the h-BN which increased the adsorption ability of PPSU-CBN membranes and showed superior adsorption to PPSU-h-BN membranes.

MMM based on PPSU polymer embedded with h-BN and CBN adsorbent materials were developed for the desulfurization of DBT-hexane model fuel. SEM analysis of the developed membranes indicates the porous structure forming channels that can efficiently remove sulfur from model fuel. The FTIR analysis showed an extra peak of –OH group after PPSU incorporated with CBN. The adsorption study for membrane desulfurization was investigated with varying operating parameters. The results showed that the PPSU-CBN system performed better than the PPSU-h-BN system as a result of doping C-dots onto h-BN. This proved to be efficient as extra adsorptive sites were induced by the c-dots in PPSU-CBN membrane system. The effect of temperature showed significant impact on the adsorption as can be seen from the adsorption isotherms. This study has successfully synthesized CBN and developed a membrane system with CBN that showed higher desulfurization efficiency. CBN nano particle synthesis is a step closure to the industrial applications in desulfurization, with further research in this field to refine and optimize the CBN synthesis process.

7.2 Recommendation

The h-BN synthesized via both the synthesis methods produced very little product which is not adequate for large scale industrial applications. More research into h-BN synthesis needs to be explored to realise its full potential. The waste raw materials can be reused and explored in the production of C-dot synthesis for energy efficiency and waste reduction. The future study on optimization of CBN synthesis parameters would help to understand the reaction kinetics and produce CBN in large scale.

The adsorption was performed in model fuels at laboratory scale with 3 operating parameters. It would be better to analyse as many parameters as possible to optimize the adsorption capacity. To resolve real world emission problems, testing the adsorptions for fuels like diesel, gasoline etc., with the synthesized materials is essential.

Appendix A: Development of hexagonal boron nitride (h-BN) and carbon dot system

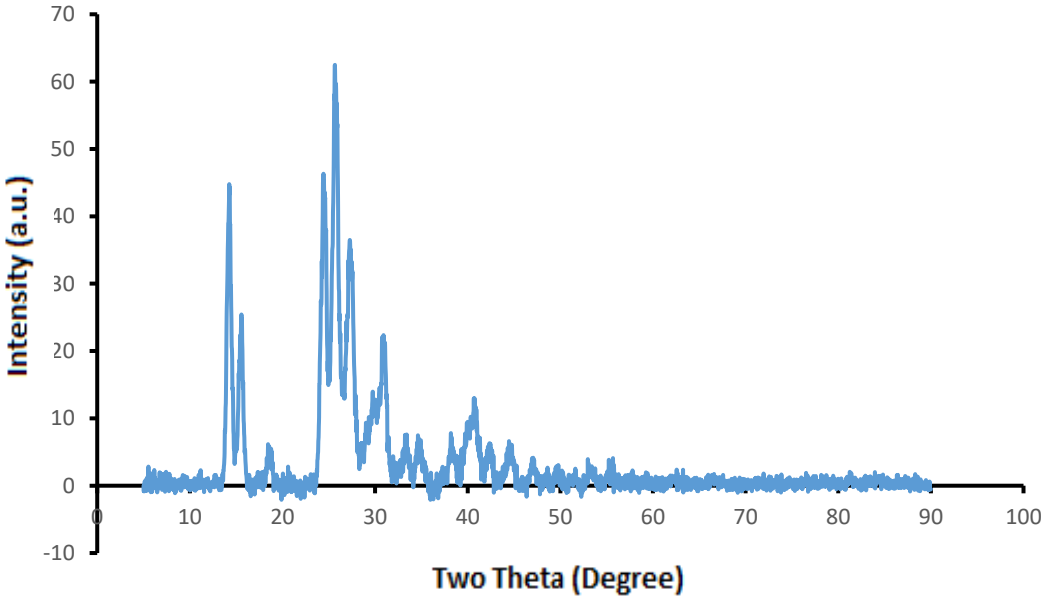


Figure A.1 XRD of h-BN synthesized by HTF method calcined at 700 ºC

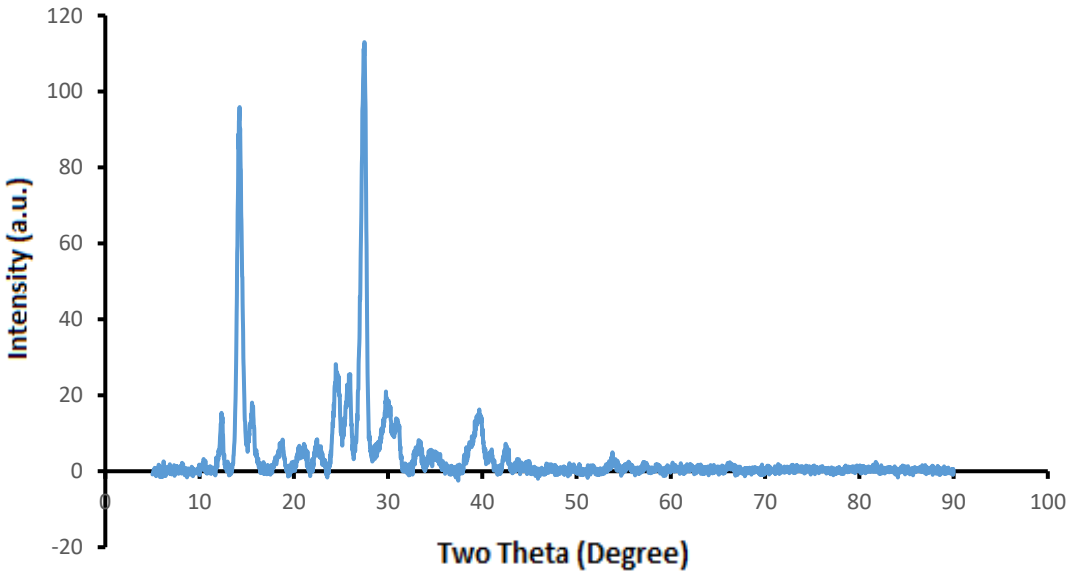


Figure A.2 XRD of h-BN synthesized by HTF method calcined at 800 ºC

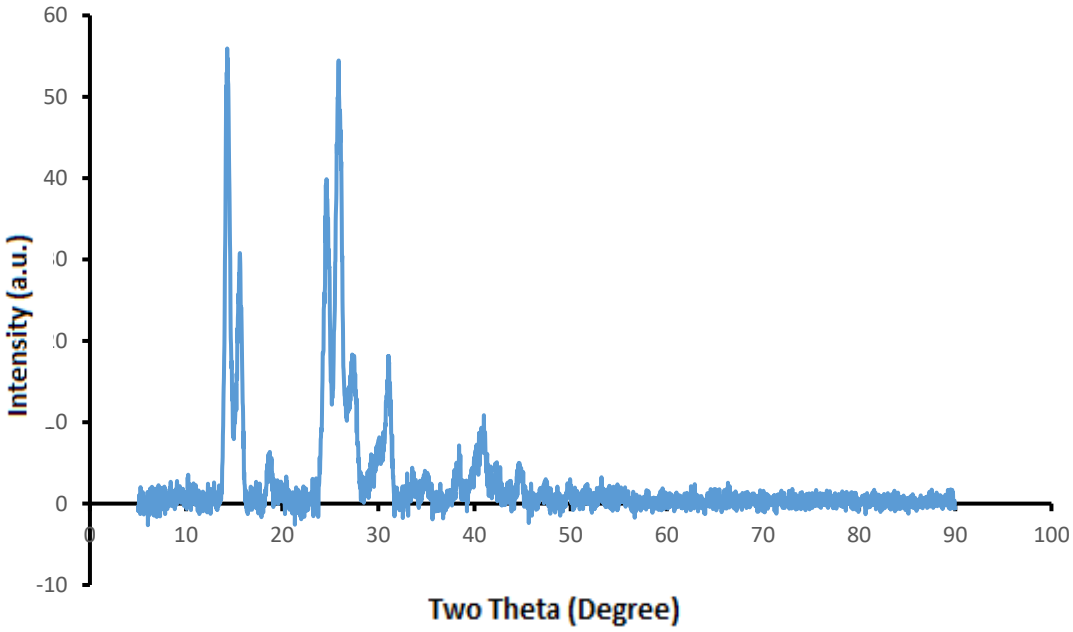


Figure A.3 XRD of h-BN synthesized by CVD method calcined at 700 ºC

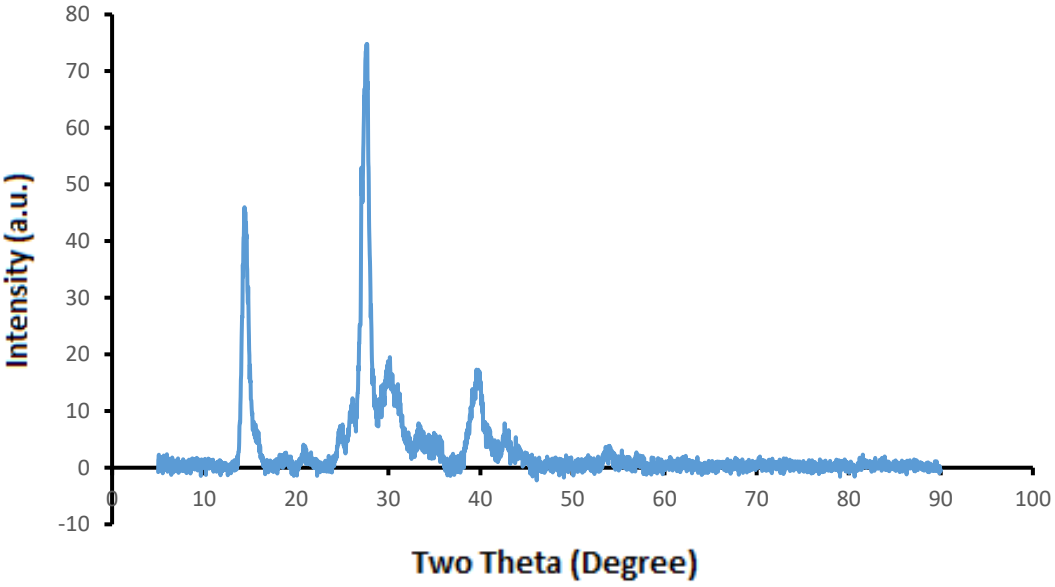


Figure A.4 XRD of h-BN synthesized by CVD calcined at 800 ºC

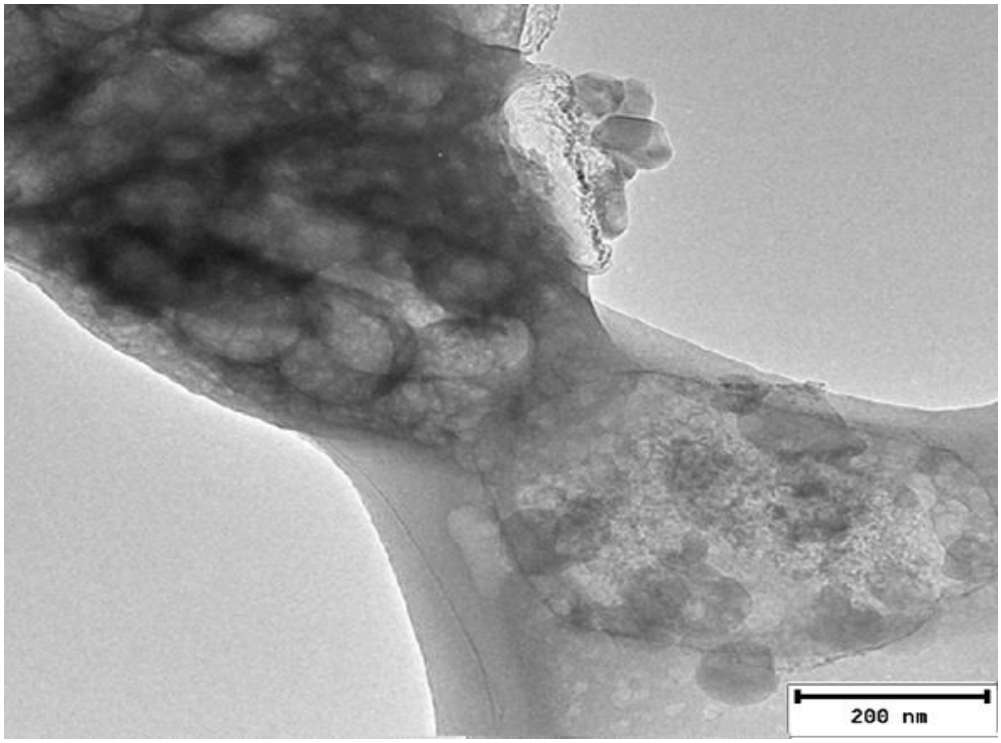


Figure A.5 TEM image of h-BN calcined by HTF (800 ºC)

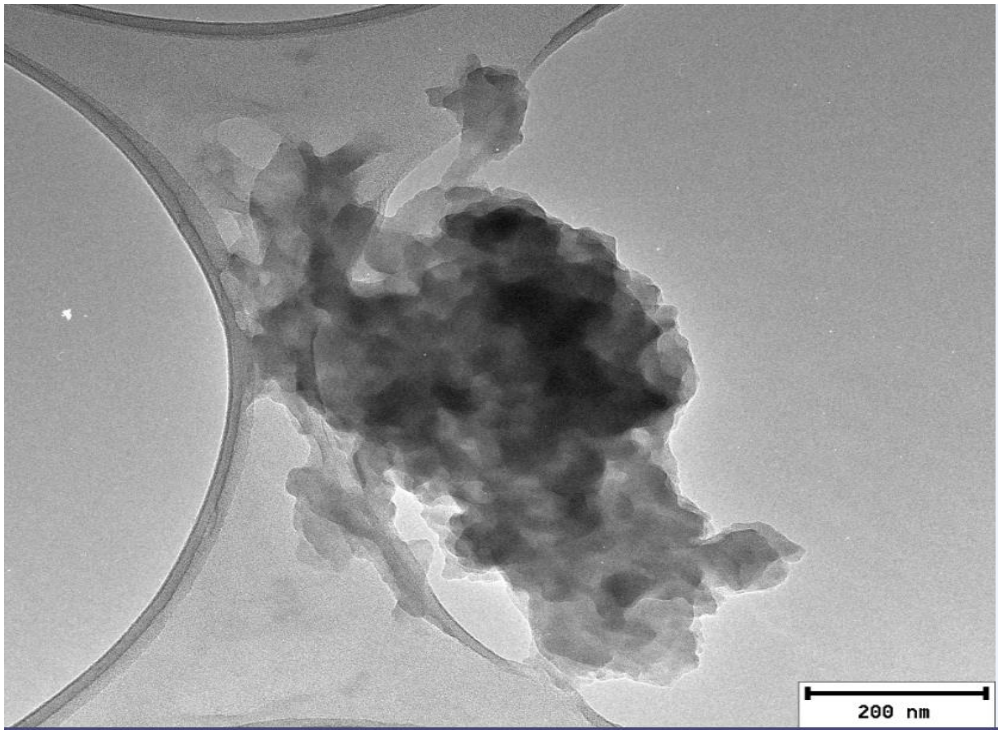


Figure A.6 TEM image of h-BN calcined by CVD (800 ºC)

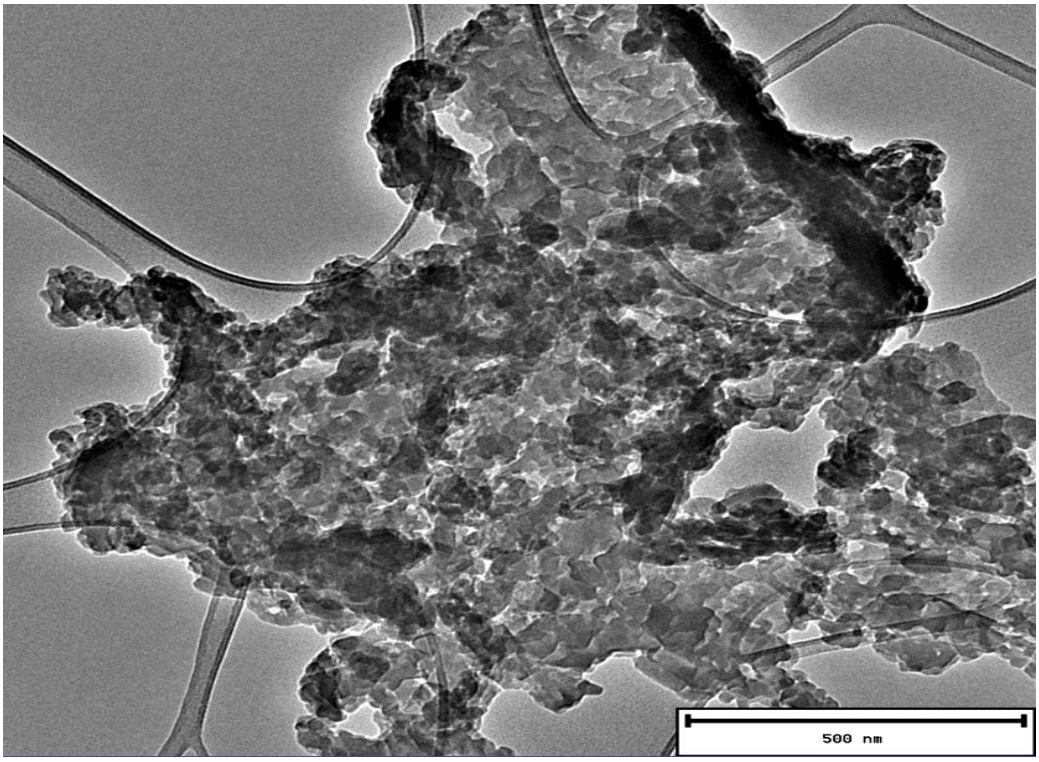


Figure A.7 TEM image of h-BN calcined by CVD (900 ºC)

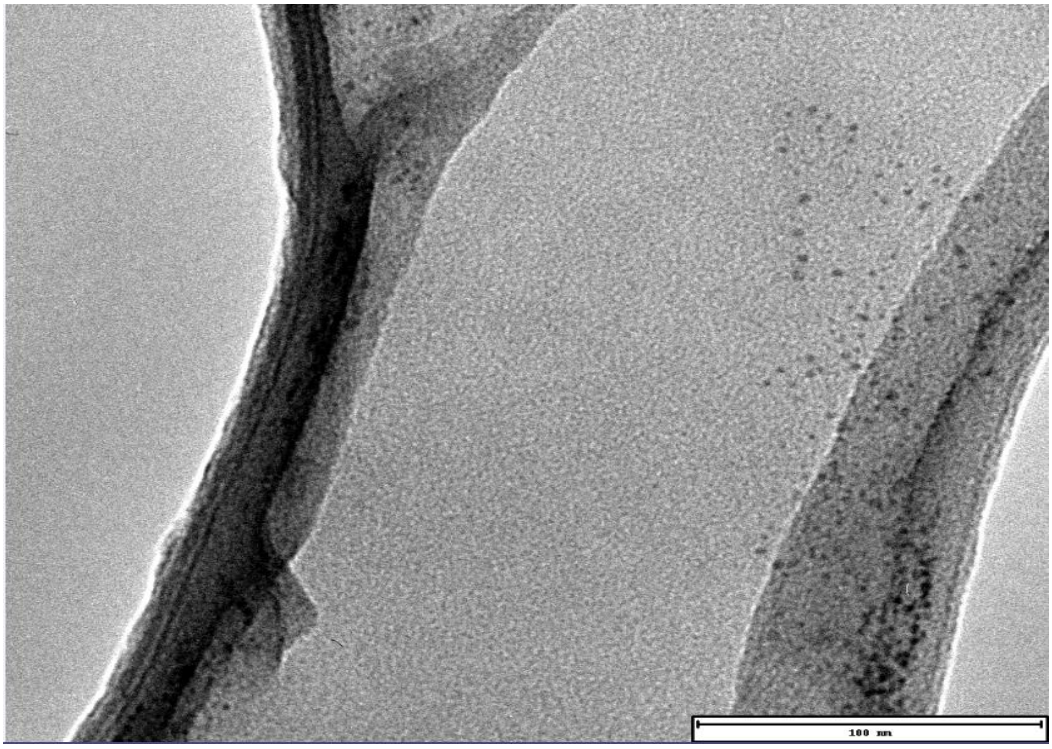


Figure A.8 TEM image of C-dots

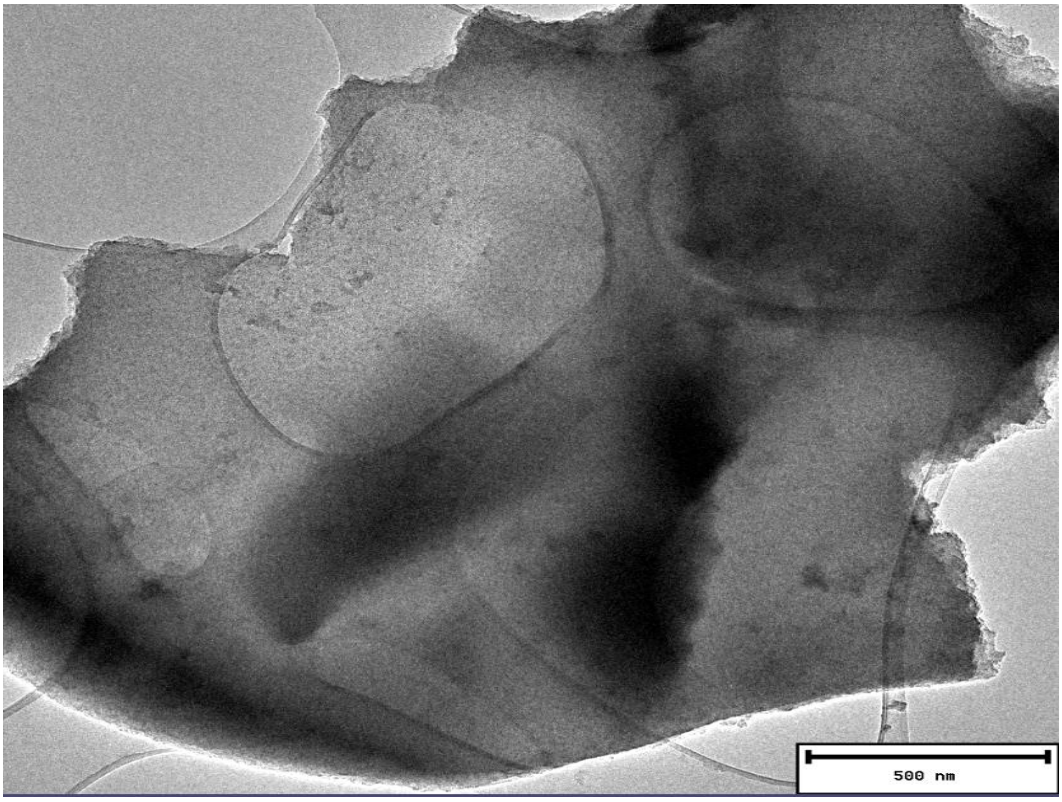


Figure A.9 TEM image of CBN

Appendix B: Development of PPSU MMM

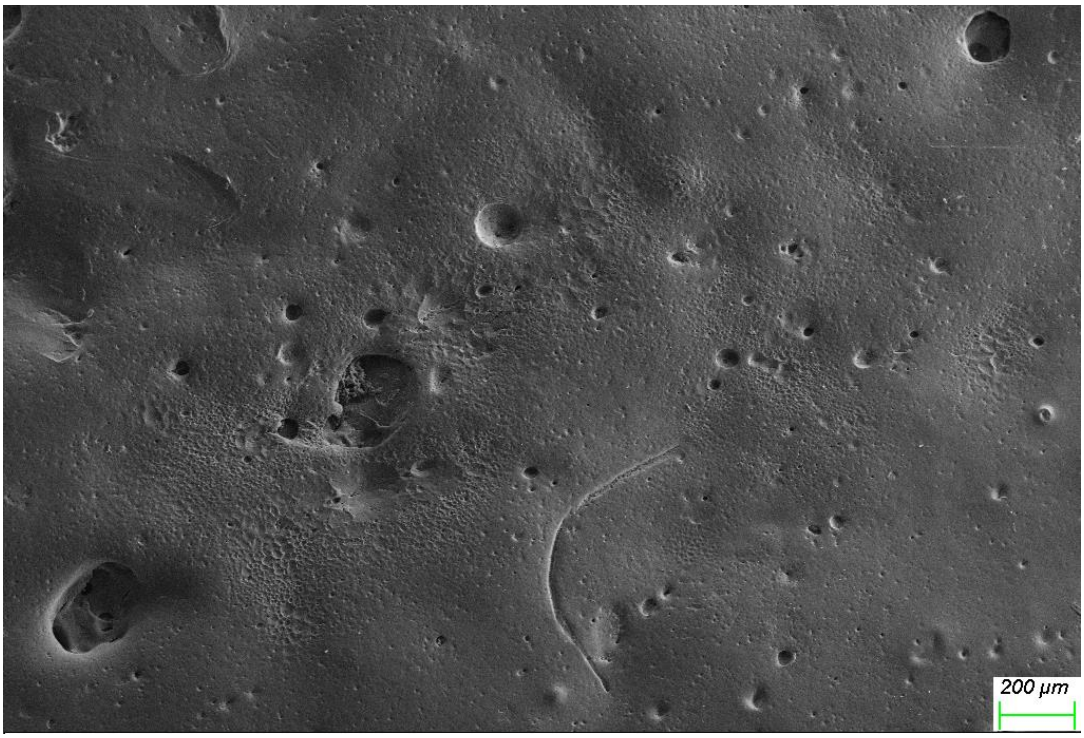


Figure B.1 SEM image of PPSU membrane

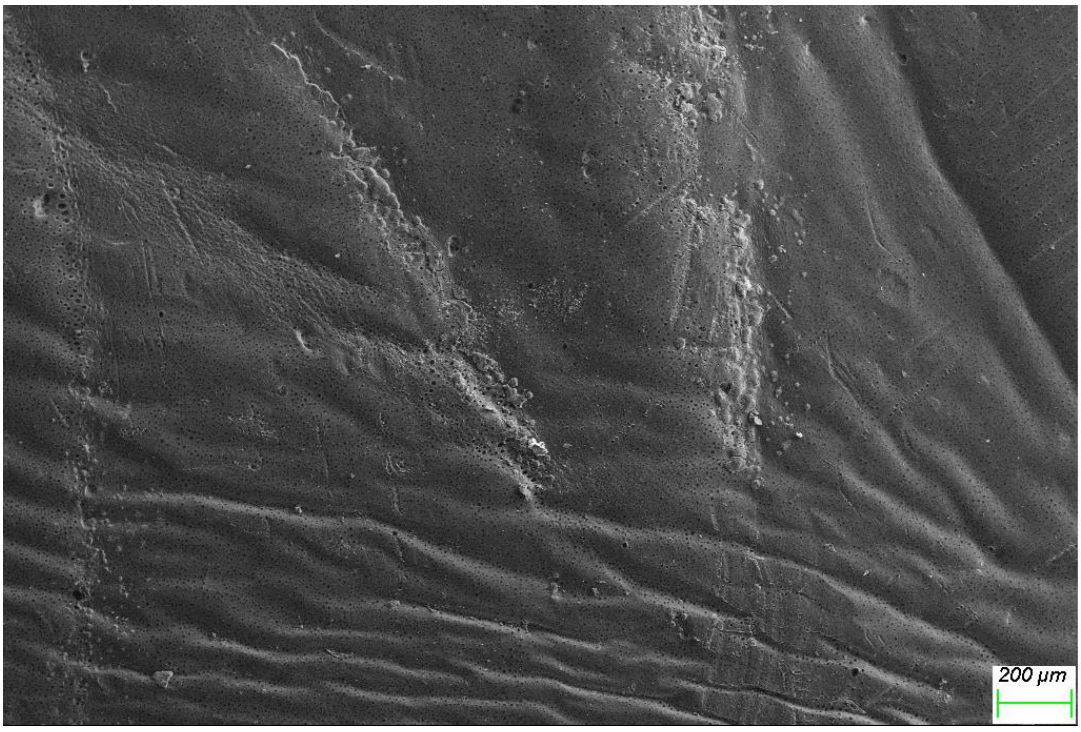


Figure B.2 SEM image of PPSU-h-BN (0.6wt.%) membrane

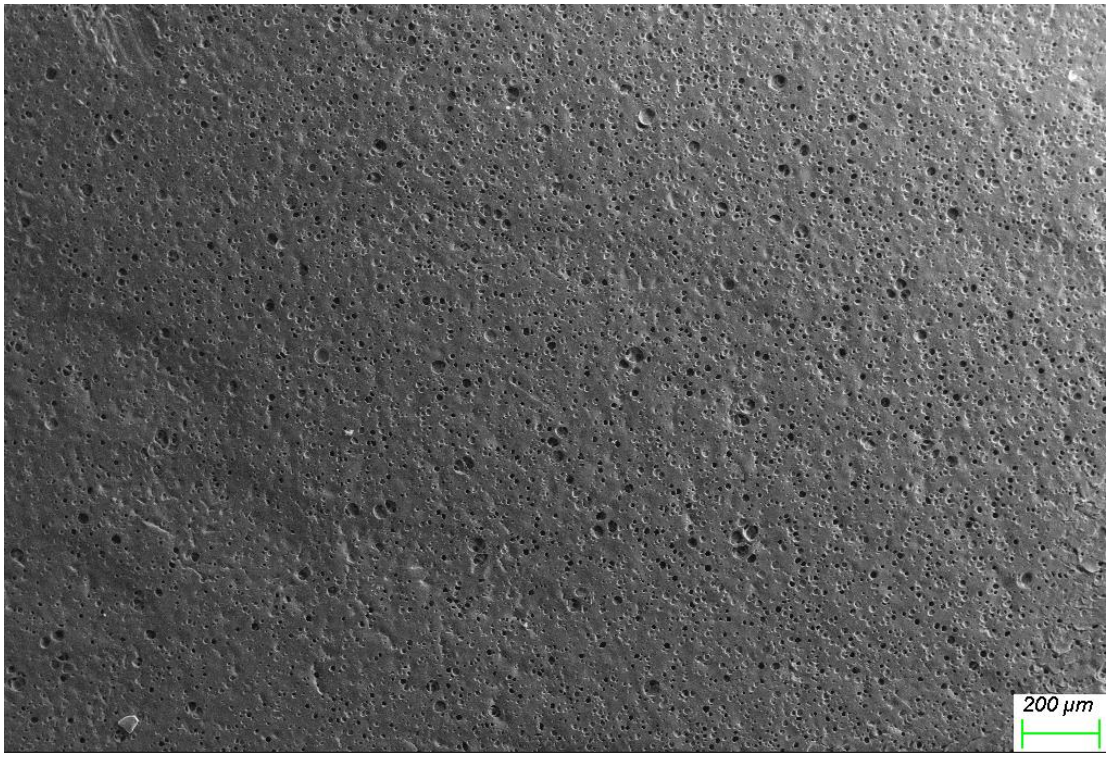


Figure B.3 SEM image of PPSU-CBN (0.6wt.%) membrane

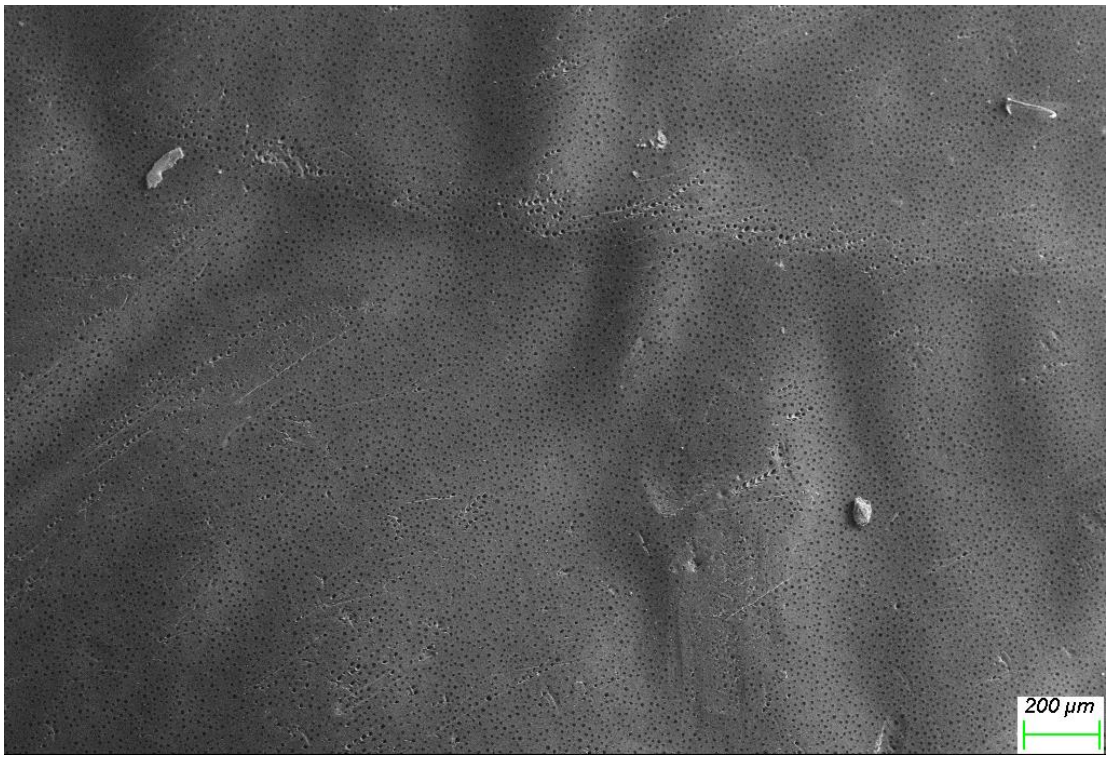


Figure B.4 SEM image of PPSU-h-BN (0.8wt.%) membrane



Figure B.5 SEM image of PPSU-CBN (0.8wt.%) membrane

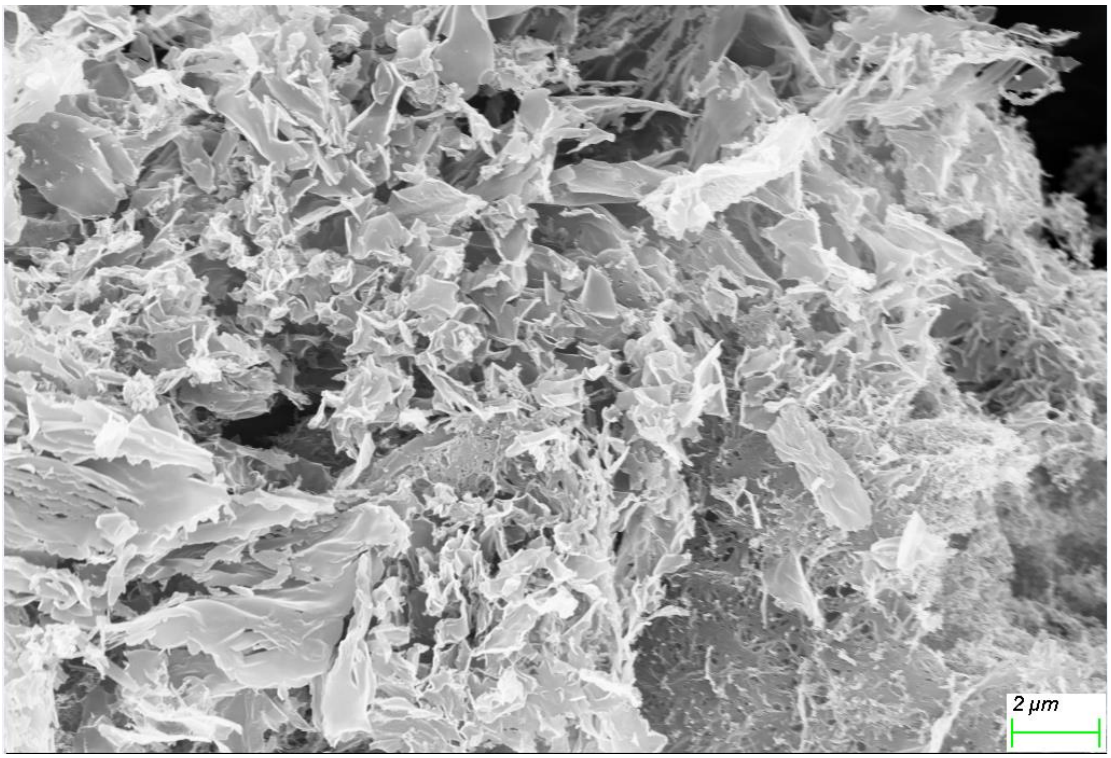


Figure B.6 SEM image of CBN material

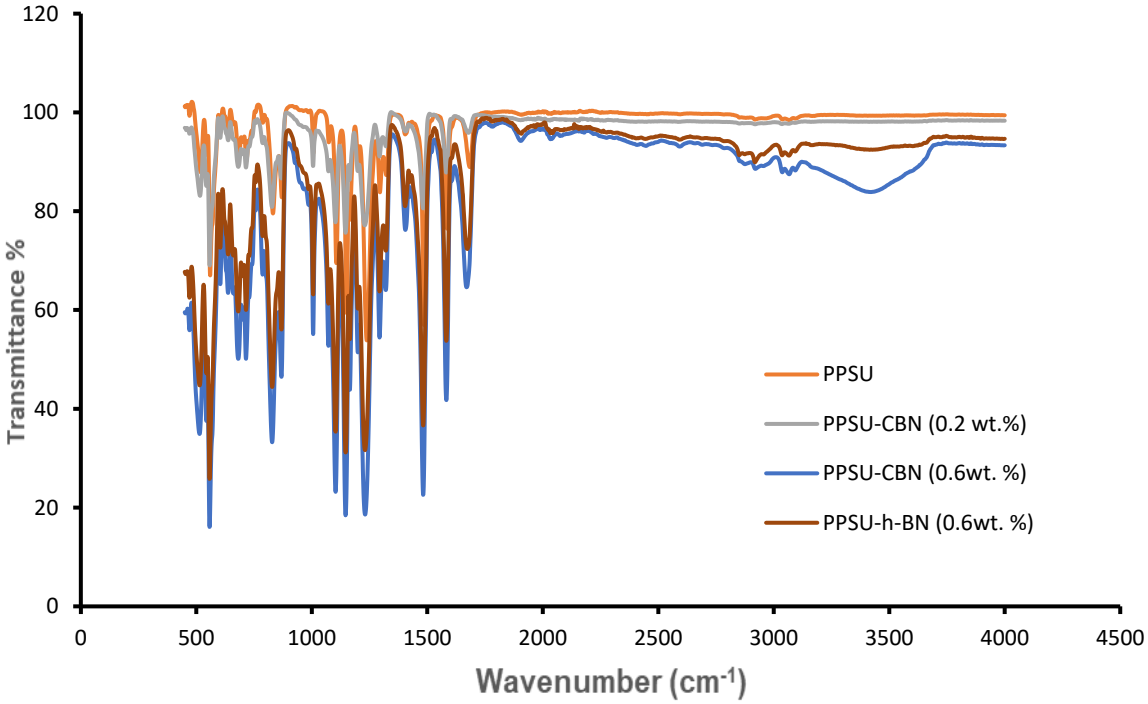


Figure B.7 FTIR spectra of PPSU, PPSU-h-BN and PPSU-CBN membranes

Appendix C: Adsorption studies

Table C.7 Sulfur removal capacity of PPSU-h-BN and PPSU-CBN membranes with varying time

Time (min)	PPSU-h-BN	PPSU-CBN
0	0	0
30	40.2	45.2
60	45.8	52.7
90	52.1	57.2
120	55.2	60.7
150	55.6	63.8
180	55.8	63.8
240	55.8	63.9

Table C.8 Sulfur removal capacity of PPSU-h-BN and PPSU-CBN membranes with varying amount od adsorbent material in PPSU

Amount	PPSU-h-BN	PPSU-CBN
0	0	0
0.2	38.4	44.1
0.4	46.3	54.2
0.6	49.2	58
0.8	55.6	63.8
1	58.1	65.3
1.2	59.6	65.6
1.4	60	66.5

Table C.9 Sulfur removal capacity of PPSU-h-BN and PPSU-CBN membranes with varying temperature

Temperature	PPSU-h-BN	PPSU-CBN
289.15	42.8	49.2
299.15	59.6	65.6
309.15	60.8	66.3
319.15	60.9	66.5